TRANSITIONAL AND TURBULENT FLOW OF NON-NEWTONIAN SLURRIES IN PIPES

by

PAUL THOMAS SLATTER
B Sc (Civ Eng)(Natal), M Sc (Civ Eng)(UCT)

Thesis presented for the Degree of
DOCTOR OF PHILOSOPHY
in the Department of Civil Engineering
UNIVERSITY OF CAPE TOWN

January, 1995

LUT 620 SLAT

95/10/12.

ABSTRACT

TRANSITIONAL AND TURBULENT FLOW OF NON-NEWTONIAN SLURRIES IN PIPES

PAUL THOMAS SLATTER

Department of Civil Engineering, University of Cape Town,
Private Bag, RONDEBOSCH 7700, Republic of South Africa.

January, 1995.

The only reliable approach open to designers of pipeline systems conveying non-Newtonian slurries in the turbulent flow regime has been large scale pipe tests. This thesis addresses this design problem, with particular emphasis on the theoretical modelling of the laminar/turbulent transition and turbulent flow behaviour of these slurries in pipes.

The literature and theory pertinent to the flow of slurries in pipes is examined. The development of non-Newtonian Reynolds numbers and laminar/turbulent transition criteria are presented and existing theoretical models for predicting turbulent flow are reviewed.

Three test facilities were built for the establishment of a data base of non-Newtonian slurry behaviour - a tube viscometer and two pumped recirculating pipe test rigs. The experimental investigation covered wide ranges of diameter (5mm to 200mm nominal bore), mean pipe velocity (0,1m/s to 10m/s), slurry relative density (1,02 to 1,65), volumetric concentration (2% to 37%), solids relative density (2,4 to 2,8) and particle size range (d_{85} = 24 to 120μm).

The experimental results are analysed using theoretical models from the literature. Rheological characterisation was successfully performed using the approach of Lazarus & Slatter (1988) and the yield pseudoplastic rheological model. The laminar/turbulent analyses showed that the Metzner & Reed (1955) Reynolds number and the intersection method (Xu *et al*, 1993) gave the best results. However, the intersection method cannot explain flow behaviour. An increasing trend in the value of the stability criterion (Ryan & Johnson, 1959) with increasing Hedström number is evident - this value was previously believed to be constant. The turbulent flow predictions of the Torrance (1963) and Wilson & Thomas (1985) models are similar and produce good results in the early turbulent region but diverge from the data as the shear stress increases. These models are also shown to be sensitive to changes in rheology. Predicted thicknesses of the laminar sub-layer are less than the size of the larger particles showing that the continuum approximation is being compromised in the wall region.

New models for the prediction of the laminar/turbulent transition and turbulent flow are developed from widely accepted fundamentals. The laminar/turbulent transition is modelled using a new Reynolds number formulation which takes into account the full viscous force and the unsheared plug caused by the presence of a yield stress. A particle roughness effect has been observed and turbulent flow is modelled using a new roughness Reynolds number to correlate the roughness function.

A new pipe Reynolds number is developed and found to be a reliable predictor of the laminar/turbulent transition and the increase in the value of the stability criterion can be predicted using this new Reynolds number. Turbulent flow predictions using the new turbulent model are accurate and better than previous models, particularly in the rough wall region. The new analysis is based on physical behaviour and contributes to the understanding of the mechanisms involved.

Declaration

I, Paul Thomas Slatter, hereby declare that this thesis is essentially my own work and has not been submitted for a degree at another university.

Signed by candidate

Signature Removed

P T Slatter

January, 1995

DEDICATION

To Lesley,
Sarah, Stuart and Timothy.

"My help cometh from the Lord,
who hath made Heaven and Earth."
Psalm 121

ACKNOWLEDGEMENTS

I would like to thank the following persons and organisations:-

Dr John Lazarus and Dr Robert Cooke for leadership, help, guidance, encouragement and supervision, but most of all for creating the milieu in which this thesis was possible.

My wife and children for their love, support and many sacrifices.

The directors and staff of Paterson and Cooke Consultants for technical expertise and moral support.

Mr J Bosman, Dr J Clifford, Assoc Prof M de Kock, Prof G Ekama, Assoc Prof A Kilner and Dr A Paterson for support, helpful discussions and advice.

The Civil Engineering Laboratory and Workshop staff for practical assistance.

Mr Gary Thorvaldsen for assistance with the data processing.

The Council of the Cape Technikon for study leave and financial support.

P T Slatter

January, 1995

CONTENTS

PREAMBLE
Title page i
ABSTRACT ii
DECLARATION iii
DEDICATION iv
ACKNOWLEDGEMENTS v
CONTENTS vi
NOMENCLATURE xv

CHAPTER 1
INTRODUCTION 1.1
1.1 STATEMENT OF THE PROBLEM 1.1
1.1.1 Laminar Flow 1.2
1.1.2 Laminar/Turbulent Transition 1.2
1.1.3 Turbulent Flow 1.2
1.1.4 Engineering Implications 1.4
1.2 OBJECTIVE 1.4
1.3 METHODOLOGY 1.5
1.3.1 Literature Review 1.5
1.3.2 Experimental Work 1.5
1.3.3 Analysis of Data Using Models from the Literature 1.5
1.3.4 New Model 1.6

CHAPTER 2
THEORY AND LITERATURE REVIEW 2.1
2.1 INTRODUCTION 2.1
2.2 ENERGY LOSS IN PIPE FLOW 2.1
2.3 SHEAR STRESS DISTRIBUTION IN A PIPE 2.3
2.4 HOMOGENEOUS SLURRIES 2.4

2.5 RHEOLOGY 2.4
2.6 CHOICE OF RHEOLOGICAL MODEL 2.6
2.7 LAMINAR FLOW 2.7
2.7.1 The yield pseudoplastic model 2.7
2.7.2 Boundary Conditions 2.8
2.7.3 Laminar Pipe Flow 2.8
2.7.4 The Rabinowitsch-Mooney Relation 2.10
2.7.5 The Metzner & Reed generalised approach 2.11
2.8 VISCOMETRY 2.12
2.9 THE RHEOLOGICAL CHARACTERISATION OF TUBE VISCOMETER DATA 2.13
2.10 LAMINAR/TURBULENT TRANSITION 2.15
2.10.1 Reynolds number and flow regimes 2.15
2.10.2 Newtonian approximation 2.16
2.10.3 Metzner & Reed Generalised Reynolds Number 2.17
2.10.4 Torrance approach 2.18
2.10.5 Bingham Plastic Reynolds Number 2.19
2.10.6 Stability criteria 2.20
2.10.7 Intersection Method 2.23
2.11 NEWTONIAN TURBULENT FLOW IN PIPES 2.23
2.11.1 The Laminar Sub-layer 2.23
2.11.2 Surface Roughness 2.25
2.11.3 Analysis of Turbulent Flow of Newtonian Fluids in Smooth Pipes 2.26
2.11.4 Analysis of Turbulent Flow of Newtonian Fluids in Rough Pipes 2.29
2.11.5 Partially Rough Wall Turbulent Flow 2.31
2.11.6 Moody Diagram 2.31
2.12 NON-NEWTONIAN TURBULENT FLOW MODELS 2.33
2.12.1 The Torrance Model 2.33
2.12.2 The Wilson & Thomas Model 2.34
2.12.3 The Dodge & Metzner Model 2.36

2.12.4 The Kemblowski & Kolodziejski Model 2.37
2.12.5 The Bowen Correlation 2.38
2.13 ASPECTS OF NON-NEWTONIAN TURBULENT FLOW 2.40
2.13.1 Importance of rheology in turbulent flow 2.40
2.13.2 Partially Rough Wall Turbulent Flow 2.40
2.13.3 Similarity between Newtonian and non-Newtonian turbulent flow 2.41
2.13.4 Von Karman constant 2.43
2.13.5 Unsheared Core 2.44
2.13.6 Particle Size Effect 2.44
2.13.7 The Continuum Approximation 2.44
2.13.8 Turbulent Flow Predictions from Rheological Data 2.44
2.13.9 The work of Park *et al* (1989) 2.45
2.13.10 The work of Xu *et al* (1993) 2.45
2.13.11 Fluid/Particle Interactions 2.46
2.13.12 Particle Reynolds Number 2.48
2.13.13 Experimental Work 2.48
2.14 CONCLUSIONS 2.49
2.14.1 Laminar Flow 2.49
2.14.2 Laminar/Turbulent Transition 2.49
2.14.3 Turbulent Flow 2.50
2.15 RESEARCH ASPECTS IDENTIFIED 2.51
2.15.1 Laminar Flow 2.51
2.15.2 Laminar/Turbulent Transition 2.51
2.15.3 Turbulent Flow 2.51
2.15.4 Experimental Work 2.52

CHAPTER 3
EXPERIMENTAL WORK 3.1
3.1 INTRODUCTION 3.1
3.2 APPARATUS 3.2
3.2.1 The Balanced Beam Tube Viscometer 3.2

3.2.2 The Mini Rig 3.4
3.2.3 The East Rig 3.6
3.2.4 Pressure tappings 3.8
3.2.5 Weigh tank 3.9
3.2.6 The manometer board (East and Mini Rigs) 3.9
3.2.7 BBTV Manometer 3.10
3.3 MEASURED VARIABLES AND CALIBRATION 3.12
3.3.1 Linear Regression 3.12
3.3.2 Load Cell 3.13
3.3.3 Magnetic flow meters 3.13
3.3.4 Differential pressure transducer (BBTV) 3.15
3.3.5 Differential pressure transducer (East and Mini Rigs) 3.16
3.4 OTHER MEASURED VARIABLES 3.16
3.4.1 Slurry Density 3.16
3.4.2 Solids Relative Density 3.17
3.4.3 Internal Pipe Diameter 3.17
3.4.4 Slurry Temperature 3.17
3.4.5 Particle Size Distributions 3.18
3.5 DERIVED VARIABLES 3.18
3.5.1 Average Slurry Velocity 3.18
3.5.2 Wall Shear Stress 3.18
3.5.3 Pipe Roughness 3.19
3.6 EXPERIMENTAL ERRORS 3.19
3.6.1 Differential Pressure Transducer (DPT) 3.19
3.6.2 Density and Relative Density Measurements 3.19
3.6.3 Slurry Temperature 3.20
3.6.4 Particle Size Distributions 3.20
3.7 COMBINED ERRORS 3.20
3.7.1 Pipe Diameter 3.21
3.7.2 Wall Shear Stress Errors 3.22
3.7.3 Pseudo-Shear Rate Errors 3.23
3.7.4 Pipe Roughness 3.25

3.7.5 BBTV Errors 3.26
3.8 EXPERIMENTAL PROCEDURE 3.26
3.8.1 The Balanced Beam Tube Viscometer. (Slatter, 1986 and Neill, 1988) 3.26
3.8.2 The East Rig 3.27
3.8.3 The Mini Rig 3.28
3.9 MATERIAL 3.29
3.9.1 Kaolin 3.29
3.9.2 Uranium Tailings 3.29
3.9.3 Gold Slimes Tailings 3.29
3.9.4 Tap Water 3.30
3.10 RESULTS AND DISCUSSION 3.30
3.10.1 Pipeline Tests 3.31
3.10.2 The Influence of Diameter 3.32
3.10.3 The influence of concentration 3.32
3.10.4 Settling and Homogeneity 3.33
3.10.5 Particle Size Distributions 3.33
3.11 CONCLUSIONS 3.34

CHAPTER 4
ANALYSIS OF RESULTS USING MODELS FROM THE LITERATURE 4.1
4.1 INTRODUCTION 4.1
4.2 RHEOLOGICAL CHARACTERISATION 4.1
4.2.1 Sensitivity 4.1
4.2.2 Forced Fits 4.3
4.3 LAMINAR/TURBULENT TRANSITION 4.6
4.3.1 Results of Analysis Using Models from the Literature 4.6
4.3.2 Graphical Comparison of Models with Data 4.7
4.4 TURBULENT FLOW 4.11
4.4.1 Turbulent Model Performance 4.12
4.4.2 Laminar Sub-layer Thickness 4.13
4.4.3 Velocity Profiles 4.14

4.4.4 Torrance Rough Wall Model 4.15
4.4.5 Sensitivity of the Newtonian Model 4.16
4.4.6 Sensitivity of the Torrance Model 4.17
4.4.7 Sensitivity of the Wilson & Thomas Model 4.18
4.4.8 Discussion of the sensitivity of the models 4.21
4.5 CONCLUSIONS 4.22
4.5.1 Rheological Characterisation 4.22
4.5.2 Laminar/Turbulent Transition 4.22
4.5.3 Turbulent Flow 4.23

CHAPTER 5
NEW ANALYSIS 5.1
5.1 INTRODUCTION 5.1
5.2 LAMINAR/TURBULENT TRANSITION 5.1
5.2.1 First approach 5.2
5.2.2 Second approach 5.2
5.2.3 Third Approach 5.4
5.2.4 Dimensional Analysis 5.6
5.3 NEW ANALYSIS OF NON-NEWTONIAN SLURRY TURBULENT FLOW IN PIPES 5.7
5.3.1 Velocity distribution 5.7
5.3.2 The effect of solid particles 5.7
5.3.3 Partially Rough Wall Turbulent Flow 5.9
5.3.4 Fully Developed Rough Wall Turbulent Flow 5.9
5.3.5 Plug flow 5.9
5.3.6 Reversion to the Newtonian Model 5.10
5.3.7 New analysis 5.10
5.3.8 The von Karman constant 5.11
5.3.9 Formulation of the roughness Reynolds number 5.11
5.3.10 Correlation of the Roughness Function 5.14
5.3.11 Sensitivity Analysis of the Representative Particle Size 5.16
5.4 CONCLUSION 5.18

5.4.1 Laminar/Turbulent Transition 5.18
5.4.2 Turbulent Flow 5.18

CHAPTER 6
EVALUATION AND DISCUSSION OF THE NEW ANALYSIS 6.1
6.1 INTRODUCTION 6.1
6.2 LAMINAR/TURBULENT TRANSITION 6.1
6.2.1 Results 6.1
6.2.2 Effect of Velocity 6.2
6.2.3 Effect of Diameter 6.3
6.2.4 Hedström Number Trend 6.5
6.2.5 Sensitivity 6.6
6.2.6 Roughness Reynolds Number 6.7
6.2.7 Reversion to the Newtonian Model 6.7
6.2.8 Use of the new Reynolds Numbers 6.7
6.3 TURBULENT FLOW 6.10
6.3.1 Sensitivity of the New Model 6.11
6.3.2 Laminar Sub-layer Thickness 6.15
6.3.3 Smooth wall turbulent flow 6.15
6.3.4 Fully developed or rough wall turbulent flow 6.16
6.3.5 Partially rough wall turbulent flow 6.16
6.3.6 Friction Factor/Reynolds Number Diagrams 6.17
6.3.7 Pipe Roughness 6.19
6.3.8 Analysis of the Particle Roughness Effect 6.20
6.4 CONCLUSIONS - LAMINAR/TURBULENT TRANSITION MODEL 6.21
6.5 CONCLUSIONS - TURBULENT FLOW MODEL 6.21
6.5.1 Rheological Characterisation 6.21
6.5.2 The effect of solid particles 6.21
6.5.3 Particle Roughness Effect 6.22
6.5.4 Velocity Distribution 6.22
6.5.5 Energy Gradient Prediction 6.22
6.5.6 Fully Developed Rough Turbulent Flow 6.23

6.5.7 Sensitivity 6.23
6.5.8 Reversion to the Newtonian Model 6.23
6.6 FINAL CONCLUSIONS 6.24

CHAPTER 7
SUMMARY, SIGNIFICANT CONTRIBUTIONS AND RECOMMENDATIONS . 7.1
7.1 INTRODUCTION 7.1
7.2 SUMMARY 7.1
7.3 SIGNIFICANT CONTRIBUTIONS 7.3
7.3.1 Laminar Flow 7.4
7.3.2 Laminar/Turbulent Transition 7.4
7.3.3 Turbulent Flow 7.4
7.3.4 Experimental Work 7.6
7.4 FUTURE RESEARCH RECOMMENDATIONS 7.6
7.5 CONCLUSION 7.7

REFERENCES

APPENDIX A
EXPERIMENTAL RESULTS
A.1 TEST DATA SUMMARY A.2
A.2 LAMINAR/TURBULENT TRANSITION RESULTS A.4
A.3 SUMMARY OF TURBULENT MODEL PERFORMANCE RESULTS A.11
A.4 DETAILED PIPE TEST RESULTS I A.16
A.5 BBTV TEST RESULTS A.40
A.6 DETAILED PIPE TEST RESULTS II A.76
A.7 TESTS FROM THE LITERATURE A.89

APPENDIX B
DIMENSIONAL ANALYSIS OF THE YIELD PSEUDOPLASTIC MODEL

APPENDIX C

CASE STUDY C.1
C.1 INTRODUCTION C.1
C.2 METHODOLOGY C.1
C.3 EXPERIMENTAL TEST RESULTS AND ANALYSIS C.2
C.4 DISCUSSION AND CONCLUSIONS C.4

APPENDIX D
RECOMMENDED DESIGN PROCEDURE - HEAD LOSS FOR STEADY FLOW OF NON-NEWTONIAN SLURRIES IN STRAIGHT CIRCULAR PIPES D.1
D.1 INTRODUCTION D.1
D.2 DETERMINATION OF SLURRY PROPERTIES D.1
D.3 INITIAL VALUES D.1
D.4 REGIME DETERMINATION D.2
D.5 LAMINAR FLOW HEAD LOSS D.3
D.6 TURBULENT FLOW HEAD LOSS D.3
D.7 ITERATION AND OPTIMISATION D.4
D.8 NUMERICAL EXAMPLE D.6
D.8.1 Slurry Properties D.6
D.8.2 Pipeline Conditions D.8
D.8.3 Regime Determination D.8
D.8.4 Turbulent flow headloss D.8
D.9 GRAPHICAL PRESENTATION OF NEW MODEL D.9

NOMENCLATURE

Symbol	Description	Unit
A	constant	
	cross sectional area	m^2
A_r	area ratio	
b	constant	
B	constant	
	roughness function	
c	constant	
C	concentration	
d	particle diameter	μm
D	internal pipe diameter	m
E	error function	
	rheological parameter	
E_τ	shear stress prediction error	
f	Fanning friction factor	
g	gravitational acceleration	m/s^2
G	pseudo shear rate	1/s
H	head	m
He	Hedström number	
i	hydraulic gradient	m(water)/m(pipe)
k	constant	
	hydraulic roughness	μm
K	fluid consistency index	Pa s^n
K′	apparent fluid consistency index	
$\mathscr{L}$	Prandtl mixing length	m
L	pipe length	m
m	slope	
	rheological parameter	
M	mass	kg
n	flow behaviour index	

n'	apparent flow behaviour index	
N	number of items	
p	pressure	Pa
Q	volumetric flow rate of slurry	m^3/s
r	radius at a point in the pipe	m
	correlation coefficient	
R	radius of the pipe	m
Re	Reynolds number	
S	relative density	
t	time	
u	point velocity	m/s
u^+	dimensionless velocity	
V	average slurry velocity	m/s
V_*	shear velocity	m/s
V_s	particle settling velocity	m/s
X	unknown quantity	
	abscissa value	
y	distance from the pipe wall	m
y^+	dimensionless wall distance	
Y	ordinate value	
Z	stability function	
α	shear stress ratio	
	proportional to	
δ	laminar sub-layer thickness	μm
Δ	increment	
κ	stability function	
μ	dynamic viscosity	Pa s
μ'	apparent dynamic viscosity	Pa s
ρ	slurry or fluid density	kg/m^3
τ	shear stress	Pa
τ_y	yield stress	Pa

Φ	function of rheological parameter
χ	von Karman constant
Ω	velocity function

Subscripts

0	at the pipe wall
85	85^{th} percentile of the particles passing
ann	refers to the annulus
c	critical
calc	calculated
l	loss
m	mixture (slurry)
max	maximum
N	Newtonian
NN	non-Newtonian
obs	observed (experimental)
p	particle
plug	of the plug
r	roughness
res	residual
s	solids
shear	zone over which shear occurs
v	volumetric
visc	viscous
w	water
x	representative size

CHAPTER 1

CHAPTER 1

INTRODUCTION

The hydraulic transportation of solids in pipes is an established technology, with vast tonnages of solids pumped each year in many different industries. The theory used in the design of hydrotransport systems is developing and techniques are refined as fundamental and applied research continue to improve our understanding of these systems.

Slurries can be classified according to the velocity at which solid particles settle in the mixture. For example, coarse sand particles that settle rapidly in water form heterogeneous slurries whereas fine clay particles that settle very slowly in water form homogeneous slurries. Mixtures comprising a range of particles from slow settling to rapid settling are termed mixed regime slurries.

The presence of fine particles in a fluid changes the viscous nature of the mixture. Most homogeneous slurries do not obey Newton's law of viscosity (Govier & Aziz, 1972) and these slurries are described as non-Newtonian slurries.

This thesis deals with the flow of homogeneous non-Newtonian slurries in pipelines. In particular, the following aspects are examined:

(i) the transition from laminar to turbulent flow,

(ii) smooth wall, partially rough wall and fully rough wall turbulent flow.

1.1 STATEMENT OF THE PROBLEM

The flow of non-Newtonian slurries can be divided into three sections: laminar flow, the laminar/turbulent transition and turbulent flow.

1.1.1 Laminar Flow

The laminar pipe flow behaviour of non-Newtonian slurries can be understood and predicted using theoretical models from the literature, provided that the freely settled solids concentration is not exceeded (Paterson, 1991). There is however no consensus in the literature as to which rheological model should be used for the rheological characterisation of a slurry. The correct rheological characterisation is particularly important for subsequent turbulent flow predictions (Hanks & Ricks, 1975).

1.1.2 Laminar/Turbulent Transition

Although there are several different methods in the literature for the identification of the transition, there are no conclusive guidelines as to which method is more accurate. This means that there are times when a designer is not sure in which regime a given pipeline will operate.

1.1.3 Turbulent Flow

The turbulent pipe flow of these slurries is not well understood, despite the large amount of research interest in this area (Mun, 1988). Slurries having similar viscous properties are known to have dissimilar turbulent properties (Harris & Quader, 1971). According to Shook & Roco (1991), the predictions of the various theories in the literature differ significantly.

1.1.4 Illustration of the Problem

Aspects of the problem can be illustrated by examining two practical examples.

(i) Recent attempts to predict the pipe flow energy requirements for these slurries in terms of their viscous characteristics have met with limited success (Xu *et al*, 1993). Figure 1.1 shows that the turbulent model predictions of Wilson & Thomas (1985) are too high for the measured slurry data. Extrapolation of the

Wilson & Thomas model will give errors of 50% in the velocity range 2,5-3m/s.

The Bingham Plastic rheological model was used by Xu *et al* for this analysis, even though the rheogram was curved, indicating that other models could have been used.

Turning to the laminar/turbulent transition, theoretical predictions using models from the literature give values of critical velocity for this slurry varying from 0,67m/s to 2,1m/s, while the actual critical velocity of 2,0m/s can clearly be seen in Figure 1.1 giving an error of 70%.

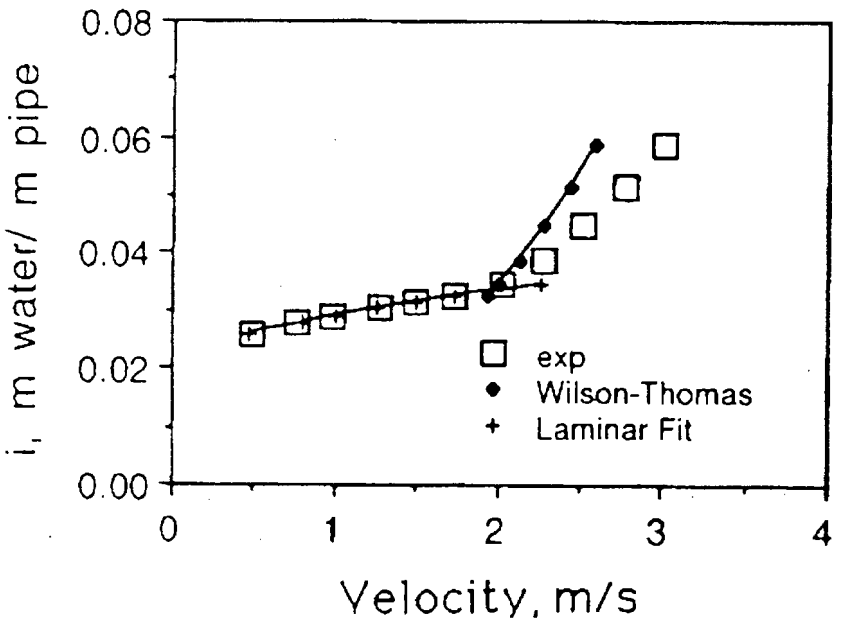

Figure 1.1 : Turbulent flow predictions using the Wilson & Thomas model. Kaolin slurry C_V = 17% D = 158mm. (Taken from Xu *et al*, 1993.)

(ii) An investigation conducted by the Author to determine design parameters for a pipeline conveying kaolin slurry further highlighted deficiencies in existing models for the turbulent flow of non-Newtonian slurries. Figure 1.2 shows that the turbulent flow predictions of Torrance (1963) and Wilson & Thomas (1985) under predict the wall shear stress for the kaolin slurry by 30%. The investigation is presented in more detail in Appendix C.

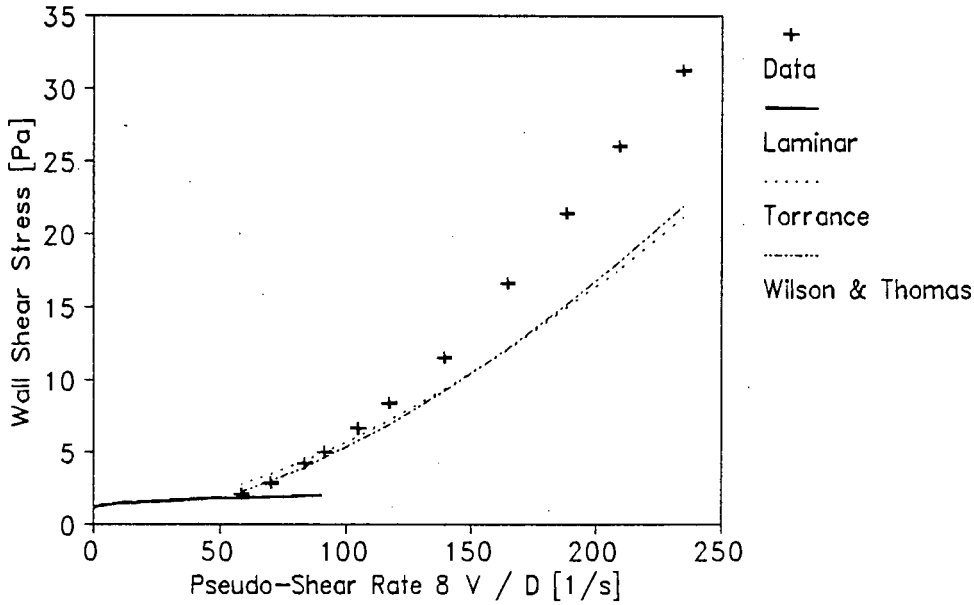

Figure 1.2 : Test KERM1501 : S_m = 1,05 : D = 141mm : Kaolin.

1.1.5 Engineering Implications

Figures 1.1 and 1.2 indicate errors in head loss predictions of between 30% to 50% in the velocity range 2,5 to 3m/s. Furthermore, these predictions could be either too high or too low. Any problems associated with the rheological characterisation of a slurry would increase the uncertainty of the results. The implications of errors of this magnitude could be that the wrong size pump or pipe diameter are specified and that the system will not operate at the required throughput.

Apart from the incorrect calculation of head loss, the engineering implications of inaccurate laminar/turbulent predictions are that over a long transit time, the slurry could begin to settle due to lack of turbulence and block the pipe. Conversely, wear rates could be significantly higher than expected, due to unpredicted turbulent conditions.

Errors which can result in incorrect throughput, pipe blockage and unexpectedly high wear rates are unacceptable. The errors pointed out here are general and other types of error may arise as each hydrotransport application is different. From a practical, engineering point of view, existing theoretical design methods for non-Newtonian

slurries are inaccurate and the results lack confidence.

The only reliable approaches open to designers of pipeline systems conveying non-Newtonian slurries are either full scale pipeline tests, or scale up of tests over wide ranges of laminar and turbulent flow for the slurry under consideration (Wilson *et al*, 1992). Design procedures are therefore costly and inefficient.

1.2 OBJECTIVE

The objective of this thesis is to develop a more reliable theoretical analysis for the flow of non-Newtonian slurries in pipelines. The analysis should be based on widely accepted fundamentals and incorporate the following aspects:

(i) The laminar flow regime.

(ii) The point at which laminar flow breaks down into turbulent flow.

(iii) Turbulent flow in smooth, partially rough and fully rough wall pipes.

1.3 METHODOLOGY

In order to achieve this objective, the research proceeded as follows.

1.3.1 Literature Review (Chapter 2)

The fundamentals of pipeline flow and the general yield pseudoplastic and Metzner & Reed laminar flow models are reviewed. Critical flow models pertinent to the slurries are presented. The Newtonian turbulent flow model and the non-Newtonian turbulent flow models of Torrance (1963) and Wilson & Thomas (1985) are discussed, as well as other important contributions in the literature.

1.3.2 Experimental Work (Chapter 3)

The Balanced Beam Tube Viscometer was developed and used by the Author to obtain non-Newtonian slurry test results (Slatter, 1986) as well as test work performed by Neill (1988) which was supervised by the Author. Pumped pipeline apparatus was specially constructed and test work performed over a wide range of laminar and turbulent flow in pipe sizes from 5mm to 200mm nominal bore.

1.3.3 Analysis of Data Using Models from the Literature (Chapter 4)

The data obtained in the test work was analysed using the models presented in the literature and the results of these analyses are discussed.

1.3.4 New Analysis (Chapters 5 and 6)

A new theoretical analysis which covers the laminar/turbulent transition and turbulent flow is developed from widely accepted fundamentals.

This analysis is shown to predict the test data more reliably than previous models.

CHAPTER 2

CHAPTER 2

THEORY AND LITERATURE REVIEW

2.1 INTRODUCTION

The theory and literature relevant to the pipe flow of time independent non-Newtonian slurries is presented.

Because of its strong historical influence, the Newtonian model is presented. This model has served as the starting point for many of the other models. Indeed, it is even recommended by some researchers for use in non-Newtonian slurry turbulent design, without modification (see Section 2.13.3).

The most general rheological models applicable to time independent non-Newtonian slurries, namely the Herschel-Bulkley or yield pseudoplastic model and the approach of Metzner & Reed, are reviewed.

Non-Newtonian Reynolds numbers and transition criteria, and turbulent flow models are discussed and other pertinent literature on non-Newtonian slurry turbulent flow is examined.

2.2 ENERGY LOSS IN PIPE FLOW

When a fluid flows through a pipe, there is a dissipation of energy. Energy is expended in overcoming viscous friction or in causing turbulent mixing to occur. When flow occurs in a horizontal straight pipe of uniform diameter, this energy loss manifests itself as a head loss ΔH, that can be detected by appropriately connected manometer tubes as shown in Figure 2.1.

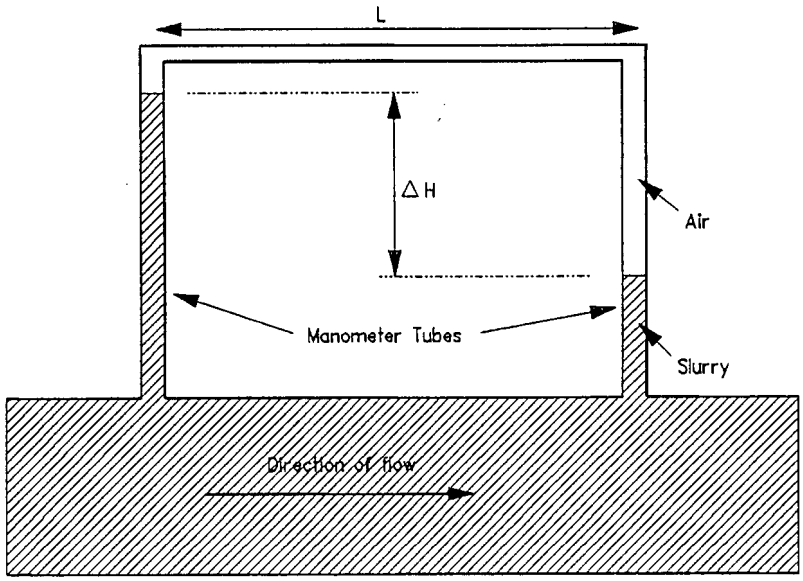

Figure 2.1 : Head loss in a pipe

The pressure loss can be calculated from

$$\Delta p = \rho \, g \, \Delta H \, . \tag{2.1}$$

The head loss, or loss of energy per unit weight, is given directly by the head difference, ΔH, measured in metres of slurry, which can be calculated using the Darcy formula (Massey, 1970)

$$\Delta H = \frac{4 \, f \, L}{D} \cdot \left[\frac{V^2}{2 \, g} \right] , \tag{2.2}$$

where f is the Fanning friction factor defined as (Massey, 1970),

$$f = \frac{2 \, \tau_0}{\rho \, V^2} \, . \tag{2.3}$$

2.3 SHEAR STRESS DISTRIBUTION IN A PIPE

The shear stress distribution in a pipe can be found by considering a coaxial cylindrical element of length L and radius r in a pipe of radius R over which a pressure difference Δp exists. The shear stress, τ, acts uniformly on the curved surface of this cylinder to provide the retarding force. A force balance over the cylinder will yield the shear stress within the pipe at radius r

$$\tau = \frac{\Delta p \; r}{2 \; L} \; , \tag{2.4}$$

and also the shear stress at the pipe wall

$$\tau_0 = \frac{D \; \Delta p}{4 \; L} \; . \tag{2.5}$$

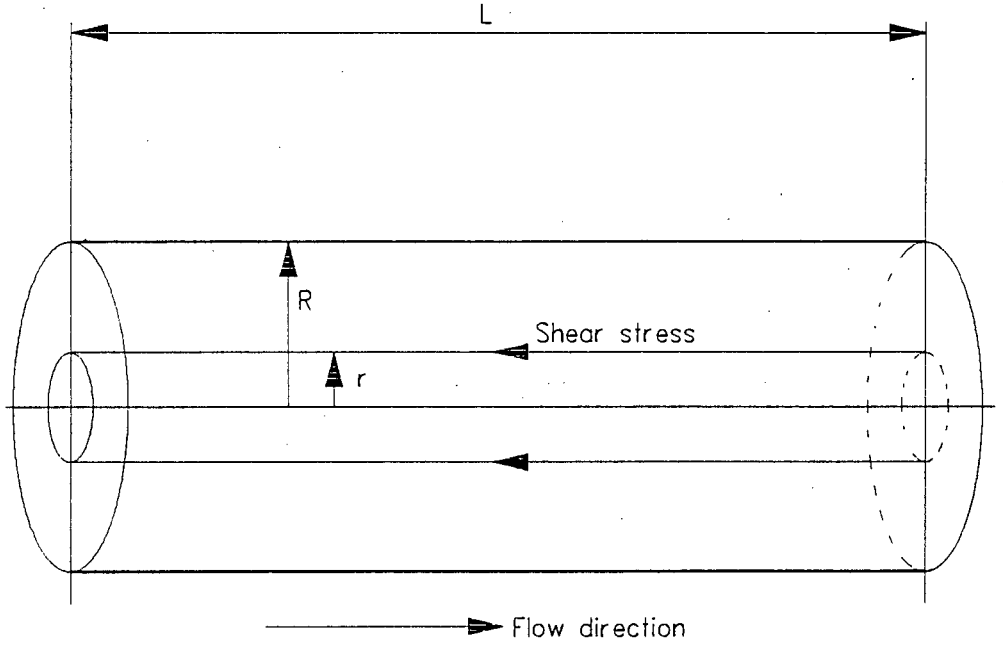

Figure 2.2 : Cylindrical element for shear stress distribution

Note that these fundamental relationships are based only on a force balance and the assumption that the fluid is homogeneous. They do not rely on any assumptions regarding the viscous nature of the fluid or the type of flow.

2.4 HOMOGENEOUS SLURRIES

The use of the term homogeneous is problematic (Shook & Roco, 1991) - no slurry is truly homogenous because it consists of two distinct phases. However, the name is used to imply a uniform spatial distribution of the solid particles and uniform concentration of solids (Wilson *et al*, 1992). The term non-settling has also been used and this is useful because it includes the circumstances as well as the properties of the mixture. Unfortunately this introduces a further problem because real slurries often show a small but finite tendency to settle (Shook & Roco, 1991).

Govier & Aziz (1972) and Hanks (1981) refer to these slurries as pseudo-homogeneous mixtures, provided that the solids are uniformly distributed.

Homogeneity can be regarded as a limiting condition to which real slurries approach (Shook & Roco, 1991). The important point on which all these authors agree is that under these asymptotic conditions, fine particle slow settling slurries can be treated as homogeneous, and continuum models can be used to describe their behaviour. The fact that the slurry is a solid/liquid mixture and not a true continuum can be ignored for fluid flow modelling purposes.

2.5 RHEOLOGY

Rheology (from the Greek "rheos" - flow and "logos" - knowledge) is the science of flow phenomena. Within the context of this thesis, rheology is defined as the viscous characteristics of a fluid or homogeneous solid-liquid mixture.

The science of rheology as it is known today owes its origin to Sir Isaac Newton who postulated the relationship between the shear stress and shear rate in a fluid as follows (in Barr, 1931):-

> *"The resistance which arises from the lack of slipperiness originating in a fluid - other things being equal - is proportional*

to the velocity by which the parts of the fluid are being separated from each other."

Mathematically formulated, Newton's hypothesis is

$$\tau \alpha \frac{du}{dy} \quad \text{or} \quad \tau = \mu \frac{du}{dy} , \tag{2.6}$$

where τ is the shear stress parallel to the direction of motion and du/dy is the shear rate or the rate at which the velocity u is increasing in the y direction, normal to the direction of motion. The constant of proportionality, μ, is known as the coefficient of dynamic viscosity. In terms of the axially symmetric flow of fluid in a pipe, the relationship then becomes

$$\tau = \mu \left[- \frac{du}{dr} \right] . \tag{2.7}$$

Any fluid which obeys this linear relationship in laminar flow is said to be a Newtonian fluid and any fluid which does not is said to be a non-Newtonian fluid. The definition of a non-Newtonian fluid is therefore a negative one and an infinite number of possible relationships between shear stress and shear rate exist.

A plot of shear stress versus shear rate is called a rheogram and some of these relationships are shown graphically in Figure 2.3.

As will be shown later, all of these rheological relationships can be accommodated in the yield pseudoplastic rheological model. This model has been referred to by several names in the literature ; Herschel-Bulkley (Herschel & Bulkley, 1926, Skelland, 1967, Al-Fariss & Pinder, 1987 and Jacobs, 1993), yield power law (Torrance, 1963, Hanks & Ricks, 1974, Hanks, 1978 and Park *et al* 1989), yield pseudoplastic (Govier & Aziz, 1972, and Slatter, 1986) and generalised Bingham (Cheng, 1970) rheological model. The term "yield pseudoplastic" will be used in this thesis to describe this model.

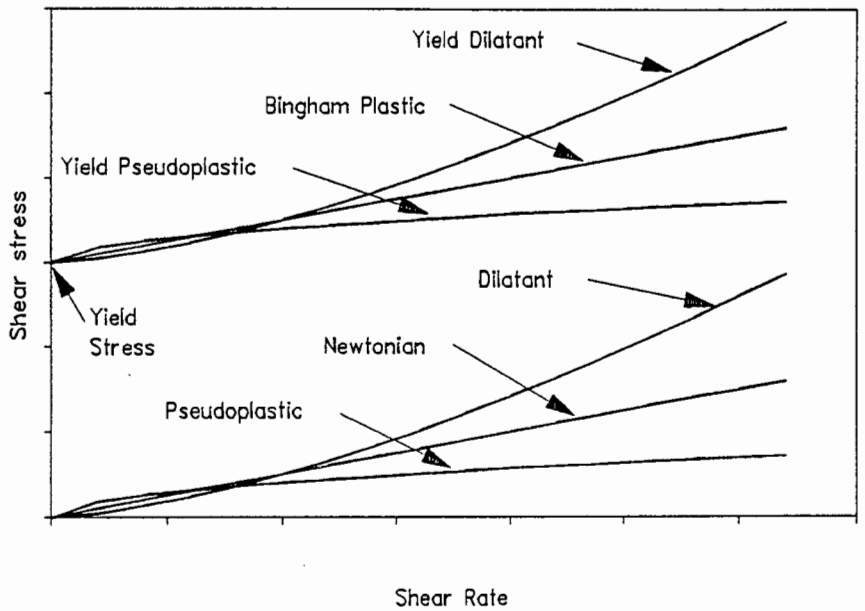

Figure 2.3 : Rheological Models (Linear Axes)

It should be noted that the above relationships are only valid within the regime of laminar or streamline flow. As soon as velocity components exist which are perpendicular to the streamlines or flow direction, turbulent flow has begun and the above relationships are no longer valid.

2.6 CHOICE OF RHEOLOGICAL MODEL

Several rheological models can be used and there are divided opinions in the literature as to which rheological model should be used to model the laminar flow of non-Newtonian slurries. The choice of model is in fact extremely important not only for the rheological characterisation in laminar flow, but even more important for turbulent flow predictions (Hanks & Ricks, 1975). The reason for this is that the data is usually extrapolated (Thomas & Wilson, 1987) to much higher shear stresses for turbulent flow predictions than can be measured in laminar flow, even in small diameter tubes (Shook & Roco, 1991).

The pseudoplastic model is favoured by researchers such as Kemblowski & Kolodziejski (1973), Chhabra & Richardson (1985) and Heywood *et al* (1993a) and the Bingham plastic model by Xu *et al* (1993) and Duckworth *et al* (1986). These two models appear to be the most popular (Wilson, 1986). The yield pseudoplastic model incorporates the features of the pseudoplastic model (rheogram curvature) and the Bingham plastic model (yield stress). The

advantages of this model for laminar and turbulent flow predictions of head loss have also been pointed out by Thomas & Wilson (1987).

There are two problems associated with the practical use of the yield pseudoplastic model. The first problem is that it is extremely sensitive to small changes in the rheological parameters (or conversely, small errors in experimental data) when the model is fitted to experimental data (Johnson, 1982). This aspect has been investigated by Al-Fariss & Pinder (1987) and they conclude that although the model is sensitive, the reproducibility of the data fit is good. Provided that the rheological parameters are determined by analysing laminar flow data from a number of small tube diameters, there is no need to reject the model on grounds of sensitivity.

The second problem is that this model predicts a constantly diminishing apparent viscosity at increasing shear rates, which appears to contradict experimental data (Wilson, 1986). Newtonian asymptotes can be expected at very low and very high shear rates (Hanks, 1981). However, this aspect has not become problematic for the slurries tested and the analyses used in this thesis.

2.7 LAMINAR FLOW

2.7.1 The yield pseudoplastic model

Non-Newtonian slurries are often best modelled as yield pseudoplastics (Govier & Aziz, 1972 and Hanks, 1979) and the laminar flow of all the slurries tested in the Hydrotransport Research facilities at the University of Cape Town (UCT) have been successfully characterised using the yield pseudoplastic rheological model. The constitutive rheological equation is

$$\tau = \tau_y + K \left[-\frac{du}{dr} \right]^n , \qquad (2.8)$$

where τ_y is the yield stress

K is the fluid consistency index

n is the flow behaviour index.

The yield stress provides the ordinate offset, and the fluid consistency index and the flow behaviour index together control the rheogram curvature.

2.7.2 Boundary Conditions

There are normally two boundary conditions which are applied to pipe flow (Janna, 1983):

1. At r=R, u=0. This is known as the no slip at the wall condition.

2. At r=0, du/dr=0. This states that the slope of the velocity distribution is zero at the pipe centre line.

2.7.3 Laminar Pipe Flow

The equations for laminar pipe flow can be derived as follows (Govier & Aziz, 1972). The velocity gradient is given by :

$$-\frac{du}{dr} = \left(\frac{1}{K}\right)^{\frac{1}{n}} \left[\frac{r}{2}\frac{\Delta p}{L} - \tau_y\right]^{\frac{1}{n}} . \qquad (2.9)$$

In this case we observe that, when $\tau = r\Delta p/2L \leq \tau_y$, the fluid does not shear and adjacent laminae are stationary relative to one another. This occurs for values of $r \leq r_{plug}$ where

$$r_{plug} = \frac{R\,\tau_y}{\tau_0} . \qquad (2.10)$$

This situation is shown graphically in Figure 2.4.

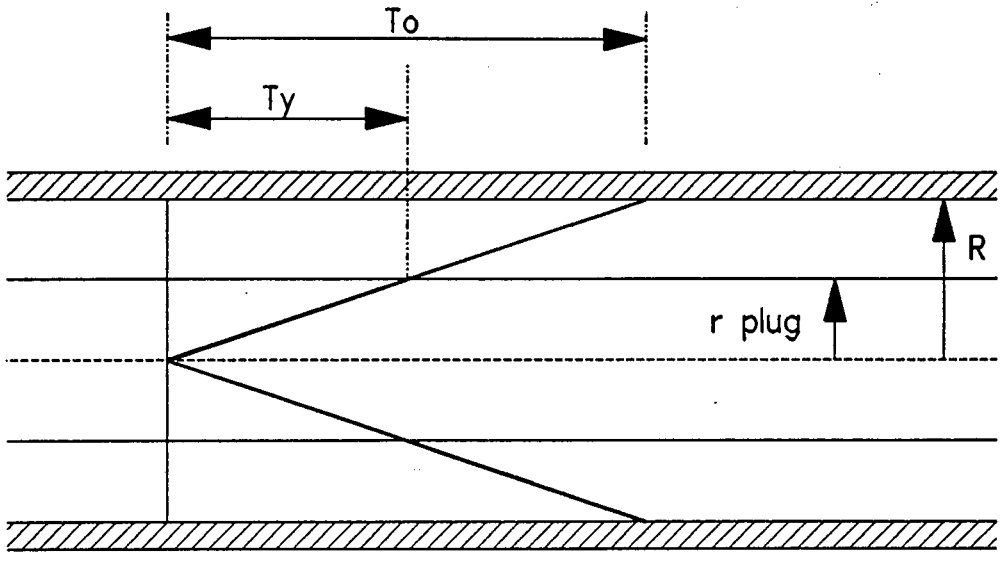

Figure 2.4 Shear stress distribution in a pipe showing unsheared plug radius.

For $R > r > r_{plug}$ the fluid shears and Equation (2.9) can be integrated to yield

$$u = \frac{\left[\frac{1}{K}\right]^{\frac{1}{n}}}{\left[\frac{\Delta p}{2\,L}\right]} \frac{n}{n+1} \left[(\tau_0 - \tau_y)^{\frac{n+1}{n}} - (\tau - \tau_y)^{\frac{n+1}{n}} \right] . \qquad (2.11)$$

When $0 < r < r_{plug}$ the fluid moves as a plug at a uniform plug velocity u_{plug}. The discharge is the sum of the flow through the sheared region ($R > r > r_{plug}$) and the plug ($r < r_{plug}$) as follows :

$$Q = \left[2\pi \int_{r_{plug}}^{R} u.r.dr \right] + \left(\pi\, r_{plug}^2\, u_{plug} \right) . \qquad (2.12)$$

Equation (2.12) is integrated to obtain the volumetric discharge, Q, and average velocity, V ;

$$\frac{32Q}{\pi D^3} = \frac{8V}{D} = \frac{4n}{K^{\frac{1}{n}}\,\tau_0^3}\left(\tau_0 - \tau_y\right)^{\frac{1+n}{n}}\left[\frac{(\tau_0-\tau_y)^2}{1+3n}+\frac{2\tau_y(\tau_0-\tau_y)}{1+2n}+\frac{\tau_y^2}{1+n}\right], \qquad (2.13)$$

where $\tau_0 = D\Delta p/4L$ and $V=Q/A$.

Referring to Figure 2.3, the following rheological relationships can be accommodated in the yield pseudoplastic model:-

Yield dilatant	$\{\tau_y>0$ and $n>1\}$
Bingham plastic	$\{\tau_y>0$ and $n=1\}$
Yield pseudoplastic	$\{\tau_y>0$ and $n<1\}$
Dilatant	$\{\tau_y=0$ and $n>1\}$
Newtonian	$\{\tau_y=0$ and $n=1\}$
Pseudoplastic	$\{\tau_y=0$ and $n<1\}$

For the Newtonian case ($\tau_y=0$ and $n=1$) and setting $K=\mu$ in Equation (2.13) yields

$$\tau_0 = \mu\,\frac{8V}{D}\,. \qquad (2.14)$$

Comparing Equation (2.14) with Equation (2.7) shows that the shear rate at the pipe wall for Newtonian fluids is 8V/D. For non-Newtonian flow, this is not the case (Wilson *et al*, 1992) and the quantity 8V/D is called the pseudo shear rate, flow characteristic or bulk shear rate. The plot of τ_0 vs 8V/D is called a pseudo shear diagram. The pseudo shear rate is of great importance in non-Newtonian flow, and can be related to the true shear rate by the Rabinowitsch-Mooney relation.

2.7.4 The Rabinowitsch-Mooney Relation

The relation attributed to Rabinowitsch (1929) and Mooney relates the true wall shear rate $(-du/dr)_0$ to the pseudo shear rate 8V/D

$$\left[-\frac{du}{dr}\right]_0 = \frac{8V}{D}\left[\frac{3n' + 1}{4n'}\right], \tag{2.15}$$

where

$$n' = \frac{d\,(\ln \tau_0)}{d\left[\ln \frac{8V}{D}\right]}. \tag{2.16}$$

The coefficient n′ is obtained as the slope of a double logarithmic plot of τ_0 versus 8V/D .

2.7.5 The Metzner & Reed generalised approach

Metzner & Reed (1955) developed a generalised approach applicable to the laminar pipe flow of any time-independent fluid, based on the Rabinowitsch-Mooney relation. The double logarithmic plot itself characterises the rheological properties of the non-Newtonian fluid and may be used directly for pipe scale up or design purposes (in laminar flow) if data is available over the required range of shear rates and stresses.

Metzner & Reed carry the approach further by setting :

$$\tau_0 = \frac{D\Delta p}{4L} = K'\left[\frac{8V}{D}\right]^{n'}, \tag{2.17}$$

which represents the tangent to the double logarithmic plot of τ_0 versus 8V/D at any particular value of τ_0 or 8V/D. This relationship can be used directly for design purposes in laminar flow. Their approach is shown graphically in Figure 2.5. Note that if K′ and n′ are constant then a pseudoplastic rheology ensues.

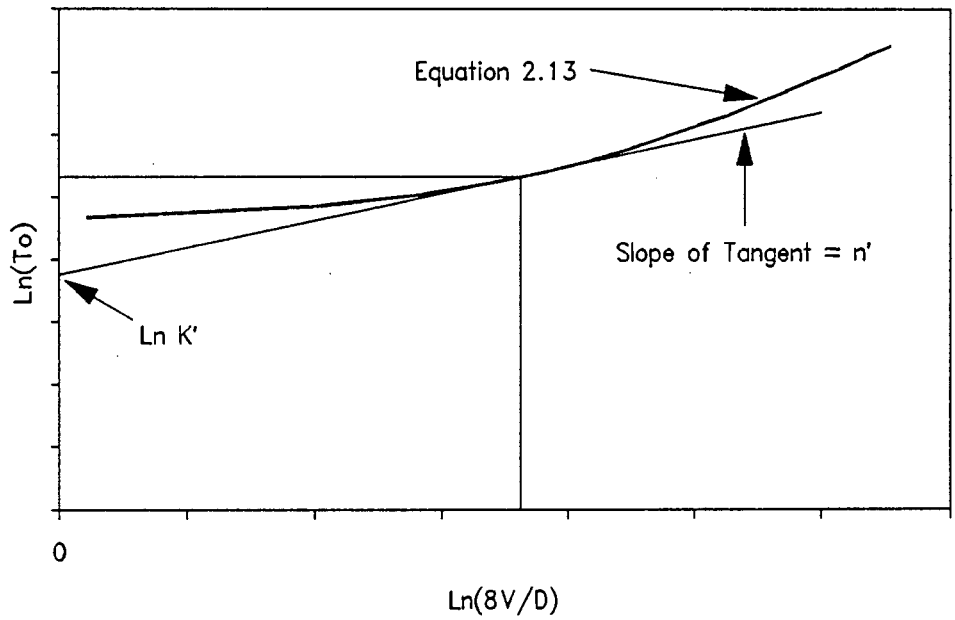

Figure 2.5 : Metzner-Reed approach shown graphically

2.8 VISCOMETRY

Viscometry encompasses the collection of physical data from tests on a sample of the fluid under investigation for the purpose of establishing the relationship between shear stress and shear rate both qualitatively (identification of the applicable rheological model) and quantitatively (the actual values of the rheological constants in the model eg τ_y, K and n).

The instrument used to measure viscous properties is called a viscometer. There are two main types of viscometer - rotational and tube. The rotational viscometer usually consists of a concentric bob and cup, one of which is rotated to produce shear in the test fluid which is in the gap between the bob and cup. The shear stress is determined by measuring the torque on one of the elements. A tube viscometer is essentially a small diameter pipeline. The test fluid flows at a controlled, measured rate through the tube and the pressure drop over a known length of the tube is measured.

Although there are many advantages to using the rotational type, for non-Newtonian slurries the tube type of viscometer is preferred (Wilson *et al*, 1992). The main difficulties associated with the rotational type is that relatively low shear rates are achieved and centrifuge action

can occur in the measuring gap (Johnson, 1982; Slatter, 1986 and Shook & Roco, 1991). On the other hand, the tube viscometer is geometrically similar to a pipe, and is in fact a miniature pipeline (Slatter & Lazarus, 1988). The data from a tube viscometer can be analysed using the Rabinowitsch-Mooney relation. However, this method contains inherent practical problems associated with the accurate determination of the value of n′ and the method of Lazarus & Slatter (1988) is preferred. This method determines the values of τ_y, K and n directly from the tube data using the laminar pipe flow equation, Equation (2.13).

Ideally, test work for the prediction of turbulent energy gradients from rheology should be performed so that the wall shear stress in laminar flow for the tests is the same as the wall shear stress in the prototype in turbulent flow. This is usually not possible as the flow becomes turbulent at these higher shear stresses and flow rates, even in small diameter tube viscometers (Shook & Roco, 1991). Therefore, the rheology obtained is extrapolated, sometimes by several orders of magnitude, to arrive at the required shear stress. The accuracy of the rheological measurements and characterisation is therefore of utmost importance.

2.9 THE RHEOLOGICAL CHARACTERISATION OF TUBE VISCOMETER DATA

Rheological characterisation involves choosing a rheological model which best fits the data (the yield pseudoplastic model is used in this thesis), and then determining the values of τ_y, K and n for a particular slurry.

The output of a tube viscometer is a set of co-ordinates of (V;Δp). These data are plotted as DΔp/4L vs 8V/D on a pseudo-shear diagram. The viscous flow data in the laminar region is coincident for the different tube diameters and the rheological constants (τ_y, K and n) are determined from the data in the laminar region and Equation (2.13) (Lazarus & Slatter, 1988). Typical test data are shown in Figure 2.6.

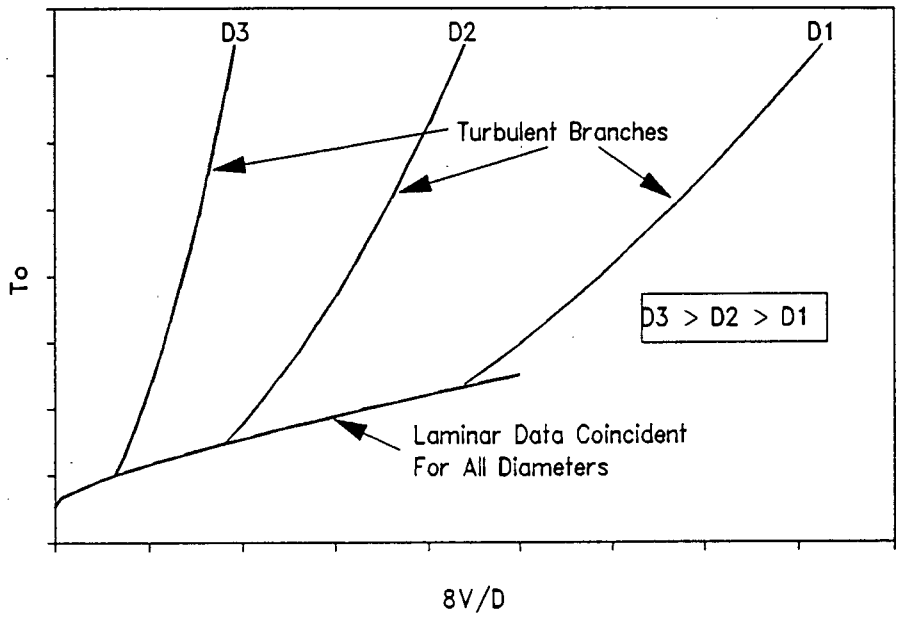

Figure 2.6 Typical tube viscometer test data loci for three tube diameters.

For a series of N data points in the laminar flow region and fixed values of τ_y, K and n, a root mean square error of fit function E can be defined (Neill, 1988),

$$E = \sqrt{\frac{\sum_{i=1}^{N} \left[\left(\frac{8V}{D} \right)_{i\,obs} - \left(\frac{8V}{D} \right)_{i\,calc} \right]^2}{N - 1}} \quad . \tag{2.18}$$

For a fixed value of τ_y and n, the K value for minimum error K_{min} can be found by setting dE/dK=0, yielding

$$K_{min} = 1 \Big/ \left[\frac{2 \sum_{i=1}^{N} \left(\frac{8V}{D} \right)_i \Big/ 8}{n \sum_{i=1}^{N} (\tau_{0\,i} - \tau_y)^{\frac{1+n}{n}} \left[\frac{(\tau_{0\,i} - \tau_y)^2}{1+3n} + \frac{2\tau_y(\tau_{0\,i} - \tau_y)}{1+2n} + \frac{\tau_y^2}{1+n} \right]} \right]^n \quad . \tag{2.19}$$

The τ_y and n values are then optimized to give a global minimum for E.

2.10 LAMINAR/TURBULENT TRANSITION

2.10.1 Reynolds number and flow regimes

For a given pipeline and Newtonian fluid, when the velocity is below a certain critical value, the flow in the pipe is found to be laminar and when the velocity is above a second higher critical value, the flow is found to be turbulent. This is shown in Figure 2.7.

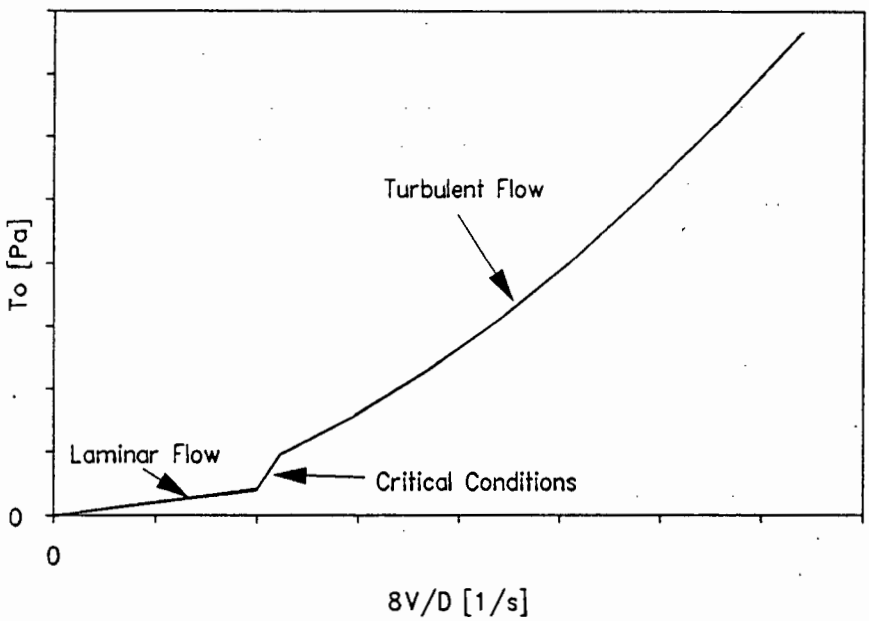

Figure 2.7 : Newtonian Pipe Flow for fixed values of diameter and viscosity.

The change from the laminar to the turbulent flow regime results in a large increase in the flow resistance and also in a change in the way energy loss varies with mean velocity. The functional relationships and physical flow patterns are fundamentally different for the two regimes.

Non-Newtonian fluids behave in a similar fashion. At a certain critical velocity, the relationship between energy loss and velocity changes fundamentally. At this point observations in transparent conduits show that turbulence begins, and a transition from the laminar to the turbulent flow regime occurs.

Experimental work has shown that the transition from laminar to turbulent flow for

a Newtonian fluid occurs at some fixed value of a dimensionless group called the Reynolds number. The Reynolds number is the ratio of the inertial to viscous forces and is calculated using:

$$Re = \frac{\rho V D}{\mu} \quad . \tag{2.20}$$

The generally accepted value of the Reynolds number at the lower bound of the laminar/turbulent transition is 2100 (Govier & Aziz, 1972), although this can occur at much higher values in the absence of mechanical vibration (Schlichting, 1960).

One of the objectives of this thesis is to provide a simple, single criterion for the determination of the flow regime in non-Newtonian flow. To this end existing non-Newtonian Reynolds numbers and stability criteria are presented below.

2.10.2 Newtonian approximation

In order to make use of standard Newtonian theory, a value for the viscosity of the fluid is required. Usually the term viscosity is meaningless once a non-Newtonian approach has been adopted. However, an apparent or secant viscosity (Holland, 1973 & Wilson, 1986) can be defined as (see Figure 2.8);

$$\mu' = \frac{\tau_0}{\left[-\frac{du}{dr}\right]_0} \quad . \tag{2.21}$$

The Reynolds number may now be calculated using

$$Re_{Newt} = \frac{\rho V D}{\mu'} \quad . \tag{2.22}$$

Note that μ' is not a constant for a given fluid and pipe diameter, but must be evaluated at a given value for τ_0.

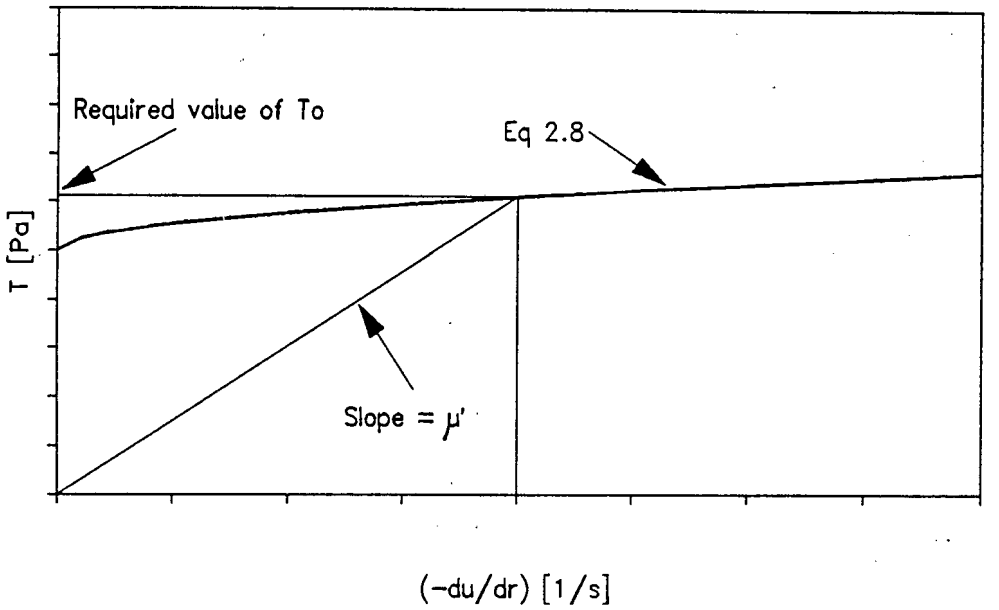

Figure 2.8 : Illustration of Secant Viscosity μ'

Note that $\mu' \rightarrow \infty$ as (-du/dr)$\rightarrow$0 for any fluid with a yield stress. However, this is usually not a problem as the region of interest is at relatively high values of (-du/dr).

2.10.3 Metzner & Reed Generalised Reynolds Number

Metzner & Reed (1955) developed a generalised Reynolds number for the correlation of non-Newtonian pipe flow data. Continuing from their approach presented in Section 2.7.5, since

$$f = \frac{D\ \Delta p}{2\rho\ V^2\ L}\ , \tag{2.23}$$

they define a non-Newtonian Reynolds number Re_{MR} as

$$f = \frac{16}{Re_{MR}}\ . \tag{2.24}$$

These equations may be combined to obtain the following solution for Re_{MR}

$$Re_{MR} = \frac{8\ \rho\ V^2}{K' \left(\frac{8V}{D} \right)^{n'}}\ . \tag{2.25}$$

One of the main reasons which Metzner & Reed give for the motivation of their approach is that K′ and n′ are often constant for a given fluid. Unfortunately K′ and n′ are not constant for fluids which can be characterised using the yield pseudoplastic model (Lazarus & Slatter, 1988). Thus K′ and n′ must be evaluated for each value of τ_0 considered. This leads to a significant complication in the use of this model.

2.10.4 Torrance approach

Torrance (1963) based his work on the pseudoplastic model work of Clapp (1961) and investigated the turbulent flow of yield pseudoplastic fluids. He used the following formulation for a Reynolds number, also known as the Clapp Reynolds number (Govier & Aziz, 1972) :

$$Re_{nn} = \frac{8\,\rho\,V^2}{K\left(\frac{8V}{D}\right)^n} . \qquad (2.26)$$

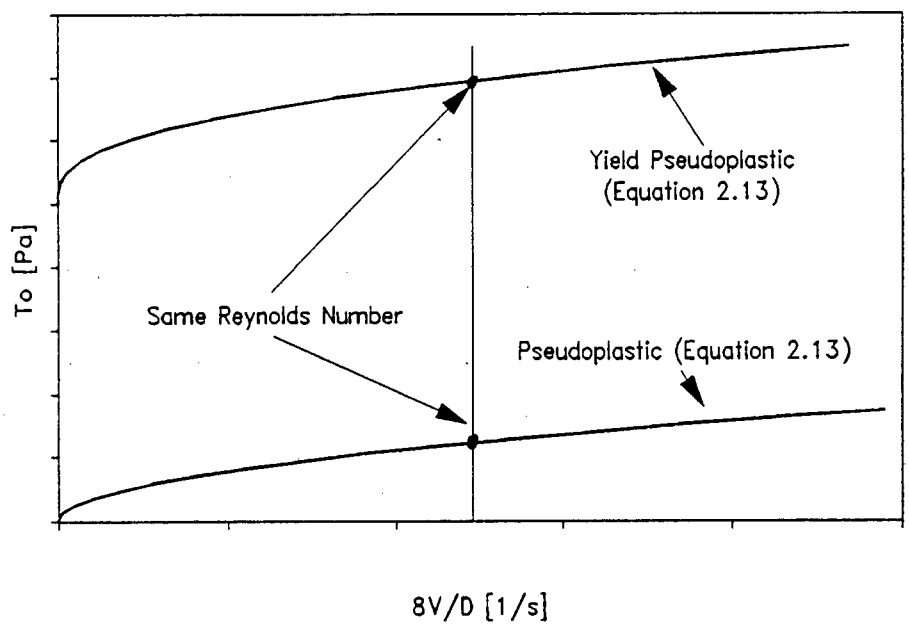

Figure 2.9 : Illustration of Torrance Reynolds Number

Figure 2.9 shows that for the same K and n values this Reynolds number is the same value for a Pseudoplastic and a Yield Pseudoplastic fluid. It can clearly be seen that the yield stress is totally ignored. It should be noted that there is no direct claim in

the literature that this Reynolds number should obtain the value 2100 at the transition point. However, it is included in this thesis to show the effect of neglecting τ_y and also because of its close association with the turbulent flow of yield pseudoplastic fluids.

2.10.5 Bingham Plastic Reynolds Number

A Reynolds number which does take the yield stress into account has been formulated for the Bingham plastic rheological model, for which the flow behaviour index, n, is unity (Govier & Aziz, 1972; Thomas, 1979 and Wilson *et al*, 1992).

Substituting n=1 and combining Equations (2.3) and (2.13) gives

$$f = \frac{16\ K}{D\ V\ \rho} \left[\frac{1}{1 - \frac{4\ \alpha}{3} + \frac{\alpha^4}{3}} \right] , \qquad (2.27)$$

where $\alpha = \tau_y/\tau_0$.

A Bingham plastic Reynolds number, Re_{BP}, can now be derived by analogy to Newtonian fluids, ie assuming that the Reynolds number will be equivalent to 16/f, and also by neglecting the fourth-power term;

$$Re_{BP} = \frac{D\ V\ \rho}{K \left[1 + \frac{\tau_y\ D}{6\ K\ V} \right]} . \qquad (2.28)$$

Furthermore, it is assumed that the transition from laminar to turbulent flow will occur when $Re_{BP} = 2100$. Taking this approach further (Govier & Aziz, 1972), noting that the term $\tau_y D/6KV$ becomes significantly greater than unity for pipes more than 25mm in diameter and then solving for the critical velocity,

$$V_c \approx 19 \sqrt{\frac{\tau_y}{\rho}} . \qquad (2.29)$$

An important implication of Equation (2.29) is that the yield stress can cause the

critical velocity to become independent of the pipe diameter at larger diameters. This is in sharp contrast to the Newtonian condition where the product $V_c D$ is a constant.

This approach has not been extended to the yield pseudoplastic rheological model.

Skelland (1967) has shown that the Metzner Reed Reynolds number is valid for a Bingham plastic, and that the laminar/turbulent transition should occur when $Re_{MR}=2100$.

Note that $Re_{BP} \approx Re_{MR}$ since both are derived from Re=f/16.

2.10.6 Stability criteria

Ryan & Johnson (1959) and Hanks (1981) have derived stability functions for laminar flow velocity vector fields. For axially symmetrical pipe flow the two functions differ by a factor of 2.

The Hanks stability function is :

$$\kappa = \frac{R\,\rho}{4\,\tau_0}\left[-\frac{d(u^2)}{dr}\right] = \frac{R\,u\,\rho}{2\,\tau_0}\left[-\frac{du}{dr}\right] \qquad (2.30)$$

The Ryan & Johnson stability function is :

$$Z = \frac{R\,u\,\rho}{\tau_0}\left[-\frac{du}{dr}\right] . \qquad (2.31)$$

Thus $Z = 2\,\kappa$. For fixed values of R, ρ and τ_0 the Ryan & Johnson function can be regarded as

$$Z = \text{constant} \cdot u \left[-\frac{du}{dr} \right] , \qquad (2.32)$$

and takes the shape of the product of u and (-du/dr), as shown for a typical yield pseudoplastic rheology in Figure 2.10.

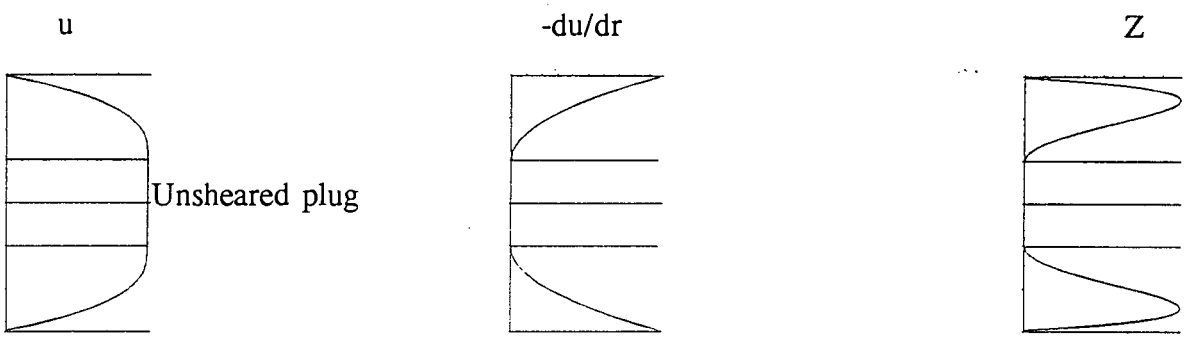

Figure 2.10 : Velocity, shear rate and the Ryan & Johnson Z function distributions across a pipe section.

The maximum value of this function Z_{max} across a given laminar velocity vector field is taken as the stability criterion. For Newtonian flow, Z_{max} = 808 for Re = 2100 & **it is assumed that all fluids will obtain this value of Z_{max} = 808 at the transition limit.** The equations given in Section 2.7.3 on laminar pipe flow are used to evaluate Z_{max}.

Hanks extended this approach and developed a critical Reynolds number based on the generalised Hedström number (Hanks, 1963 and Hanks & Ricks, 1974) after the method of Hedström (1952)

$$He = \frac{D^2 \rho}{\tau_y} \left(\frac{\tau_y}{K} \right)^{\frac{2}{n}} . \qquad (2.33)$$

Since this approach is based on the stability criterion, only the stability criterion will be investigated in this thesis, and not the Reynolds number itself, which is derived from the stability criterion. A puzzling aspect of this method is that it predicts

laminar/turbulent transitions at high Hedström numbers without any discernible change in the relationship between friction factor and Reynolds number. This effect can be seen clearly on the friction factor-Reynolds number plots shown in papers by Hanks & Dadia (1971) and Hanks (1978).

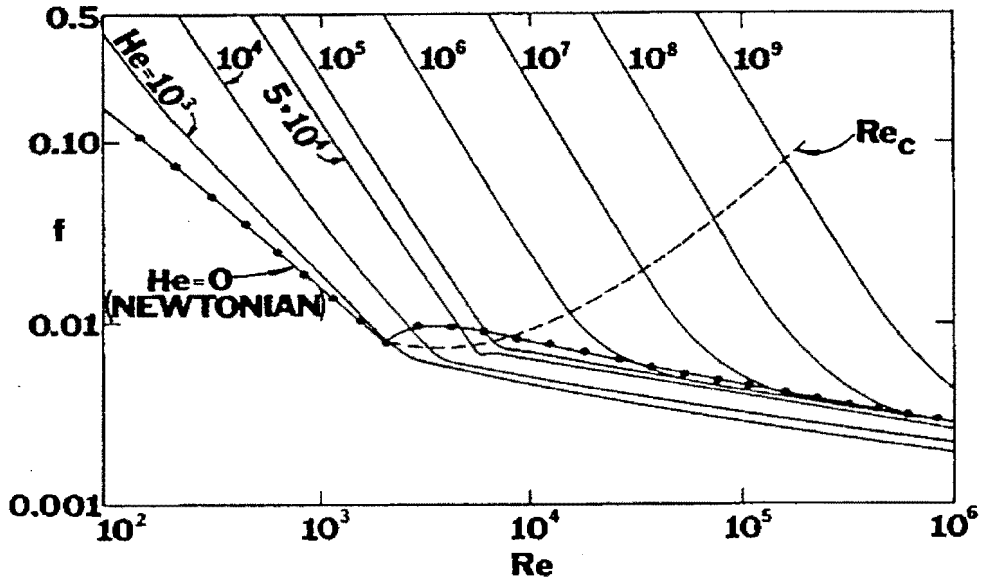

Figure 2.11 : Friction factor/Reynolds number diagram showing the critical Reynolds number Re_c. (Taken from Hanks, 1978.)

Figure 2.11 shows no change in the relationship between friction factor and Reynolds number as the graph crosses the locus of critical Reynolds numbers. Since there is a fundamental change in the behaviour at this point, this change in behaviour should be reflected on the diagram. A possible conclusion is that the real change of regime does not occur at a constant value of the stability criterion, Z_{max}.

An important point of interest which can be seen in the data plotted by Hanks (1963) is that the data at high Hedström numbers falls below the theoretical line. This means that the actual critical velocity is occurring at progressively higher velocity values than the theoretical predictions. Once again, one could conclude that the real change of regime does not occur at a constant value of the stability criterion, Z_{max}, but rather that the value will increase with an increase in Hedström number.

Another important point of interest which can clearly be seen in Figure 2.10 is that

the criterion technique takes into account the presence of the unsheared plug at the pipe axis caused by the yield stress (*op cit*).

2.10.7 Intersection Method

This practical approach uses the intersection of the laminar and turbulent flow theoretical lines as the critical point (Shook & Roco, 1991). The degree of success of this method is entirely dependent on the accuracy of the turbulent model used. The Wilson & Thomas model has been used here, as this model has given good results as reported by Xu *et al* (1993).

It should be emphasised that this approach is purely practical and cannot explain the flow behaviour as does the Newtonian Reynolds number approach, which works from fundamental assumptions regarding inertial and viscous forces. This method is also incompatible with Newtonian behaviour, where the critical point is not the intersection of the laminar and turbulent theoretical lines (see Figure 2.7).

2.11 NEWTONIAN TURBULENT FLOW IN PIPES

Turbulent flow is characterised by large, random swirling or eddy motions. Particle paths cross and velocity (both direction and magnitude) and pressure fluctuate on a continuous and random basis. The flow behaviour becomes extremely complex and full rigorous analysis becomes impossible (Tennekes & Lumley, 1972). The equations of motion must be time-averaged to yield meaningful practical results and analysis and measurements are based on these temporal means (Janna, 1983).

2.11.1 The Laminar Sub-layer

Velocity components normal to the pipe axis cannot exist at the pipe wall, and turbulence is suppressed in this region. Viscous forces are dominant and a laminar sub-layer exists for some finite thickness δ. Since $\delta << R$, shear stress and therefore shear rate can be considered constant and u increases linearly with y. There are

therefore two zones of particular interest - the laminar sub-layer and the turbulent core (Wilson, 1992).

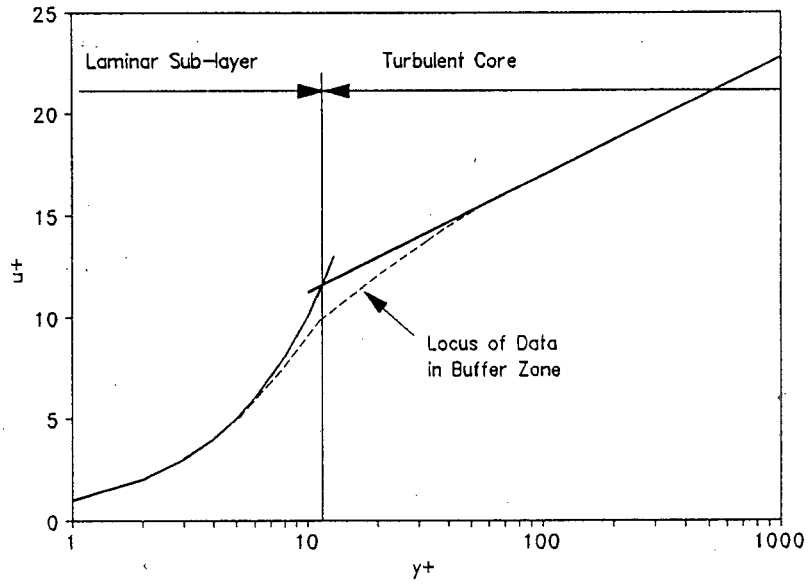

Figure 2.12 : Velocity profile in turbulent flow.

The two zones are shown in Figure 2.12, where $y^+ = \rho V_* y/\mu$ is dimensionless position and $u^+ = u/V_*$ is dimensionless velocity.

The name "laminar sub-layer" can be misleading and the term "viscous sub-layer" is often used. Although the flow is not steady in the laminar sub-layer, the velocity fluctuations are not significant and are damped by the overwhelming viscous forces (Tennekes & Lumley, 1972).

The thickness of the laminar sub-layer is given by the point of intersection of the two zones (Ireland, 1971). The dimensionless position variable y^+ has a value of 11,6 at this point (Wilson, 1986). The thickness of the laminar sub-layer for Newtonian turbulent flow in pipes can therefore be expressed by

$$\delta = \frac{11{,}6\ \mu}{\sqrt{\rho\ \tau_0}} \ . \qquad (2.34)$$

2.11.2 Surface Roughness

The thickness of the laminar sub-layer is important in the modelling of rough wall turbulent flow. The microscopic surface of a pipe contains surface roughnesses or asperities which are usually random in both height and position as in Figure 2.13. If the laminar sub-layer is thicker than the height of the largest asperities (δ_1), then the flow is considered to be smooth wall turbulent. If the laminar sub-layer thickness is smaller than the small asperities (δ_3), and they protrude into the turbulent core, they generate a wake of eddies, causing resistance to the flow known as form drag (Massey, 1970). This form drag energy loss is proportional to the square of the velocity and in turn leads to a constant friction factor. This situation is termed rough wall turbulent flow. Between these two extremes (δ_2), some of the asperities pierce the laminar sub-layer and some remain hidden, and the flow is termed partially rough wall turbulent.

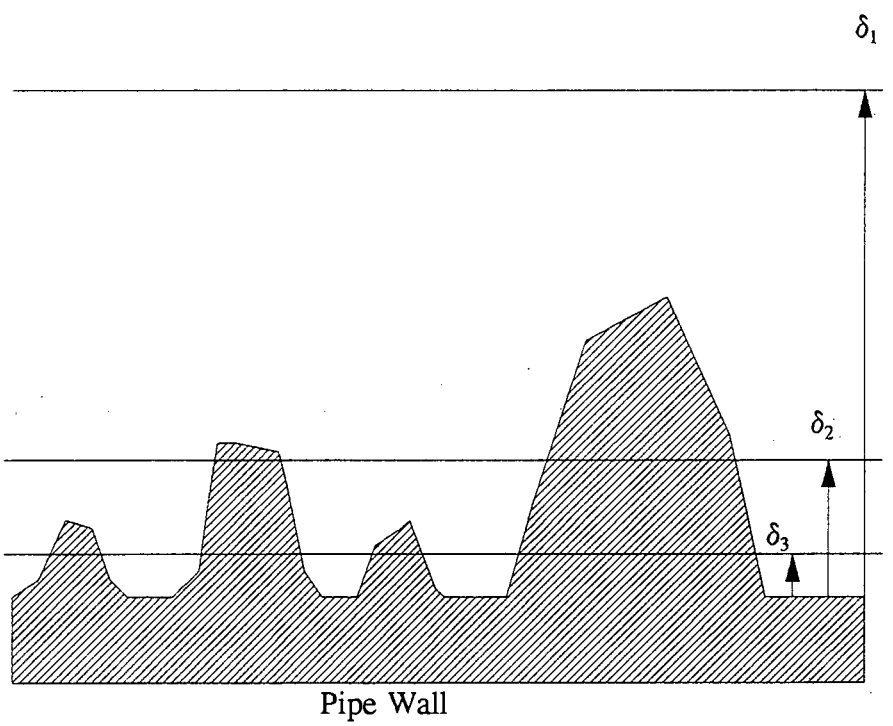

Figure 2.13 : Pipe surface roughness and laminar sub-layer thickness.

This progressive penetration of the laminar sub-layer by the surface roughness and the way they stimulate turbulence through the extra eddies they generate as they emerge from the laminar sub-layer, as the shear stress and flow rate are increased, is of fundamental

importance to the understanding of rough wall turbulent flow.

The above explanation is general and simplified. For example, the change from the laminar sub-layer to the turbulent core is not abrupt but is a smooth transition as shown by the thin broken line in the velocity profile in Figure 2.12 (this intermediate zone is referred to as the buffer zone), the surface roughnesses can affect the flow before becoming exposed (Massey, 1970) and the turbulent motion in the wake behind the bumps is complicated by mutual interference (Colebrook, 1939). However, it does express the main ideas which have influenced the development of turbulent flow theory. It is also in line with a practical, engineering approach (Wilson *et al*, 1992 and Govier & Aziz, 1972).

2.11.3 Analysis of Turbulent Flow of Newtonian Fluids in Smooth Pipes

In turbulent flow, momentum transfer between layers occurs due to eddy formation, quite different from laminar flow. This interchange of momentum sets up shear stresses, also known as Reynolds stresses. In order to obtain the velocity distribution and flow rate, the shear stress in the turbulent core must be related to the shear rate (Janna, 1983).

The turbulent flow of Newtonian fluids in smooth pipes is characterised by a logarithmic velocity distribution. This velocity distribution may be derived most simply by the method of Kilner (1971), using dimensional analysis as described below.

The shear stress in turbulent flow is assumed to depend on the density of the fluid (ρ), the velocity gradient (du/dy) and the curvature of the velocity distribution (d^2u/dy^2) ie:

$$\tau = \Phi \left(\rho, \left[\frac{du}{dy}\right], \left[\frac{d^2u}{dy^2}\right]\right), \qquad (2.35)$$

where y is the distance from the wall.

Dimensional analysis then yields:

$$\sqrt{\frac{\tau}{\rho}} = -\chi \left[\frac{du}{dy}\right]^2 \left[\frac{d^2u}{dy^2}\right]^{-1}, \qquad (2.36)$$

where

$\chi = 0{,}4 =$ von Karman constant.

Note that (d^2u/dy^2) is negative since du/dy decreases with increase in y.

It is now assumed that the shear stress τ is constant over the area of interest and equal to τ_0, the wall shear stress. Integration to obtain the velocity distribution yields

$$\frac{u}{V_*} = \frac{1}{\chi} \ln y + \text{const}, \qquad (2.37)$$

where $V_* = \sqrt{(\tau_0/\rho)}$.

Dimensional analysis provides no explanation of behaviour. It can only show how variables are related to produce a dimensionally homogeneous functional relationship. A theoretical approach which yields the same result has been developed by Prandtl (in Schlichting, 1960 and Ireland, 1971).

In an approach similar to the mean free path of a molecule approach in the kinetic theory of gases, Prandtl assumed that a particle of fluid would travel a distance $\mathcal{L}$ before its momentum is changed by its new surroundings, yielding the following relation for the shear stress

$$\tau = \rho \mathcal{L}^2 \left[\frac{du}{dy}\right]^2, \qquad (2.38)$$

where $\mathcal{L}$ is the Prandtl mixing length. It is then assumed that $\mathcal{L}$ will be proportional to y with χ as the proportionality constant. Then

$$V_* = \chi y \frac{du}{dy}. \qquad (2.39)$$

Integration will yield the same velocity distribution as before (Equation (2.37)).

This velocity distribution is strictly valid only in the region of the pipe wall and is at variance with the second boundary condition in Section 2.7.2 ($du/dr \neq 0$ at the pipe centre line). Also, the turbulent core is shielded from the wall by the laminar sub-layer. However, it agrees well with experimental data over the whole cross section of the pipe, except at the two boundaries. On the strength of this experimental evidence, this velocity distribution has been widely accepted even though the assumption regarding shear stress constancy is clearly in error.

The wall distance can be formulated in a non-dimensional Reynolds number form and after substitution of the appropriate boundary conditions the classical logarithmic universal velocity distribution results:

$$\frac{u}{V_*} = 2{,}5 \ln \left[\frac{\rho V_* y}{\mu} \right] + 5{,}5 \; . \tag{2.40}$$

This velocity distribution can be integrated over the cross sectional area of the pipe to yield the mean velocity. The presence of the laminar sub-layer is ignored for the purposes of the integration as it occupies a negligible portion of the cross sectional area (Kilner, 1971),

$$\frac{V}{V_*} = 2{,}5 \ln \left[\frac{\rho V_* R}{\mu} \right] + 1{,}75 \; . \tag{2.41}$$

It is customary to reformulate this equation in terms of the Reynolds number and the Fanning friction factor

$$\frac{1}{\sqrt{f}} = -4 \log \left[\frac{1{,}26}{Re \sqrt{f}} \right] \; . \tag{2.42}$$

This is known as Prandtl's universal law of friction for smooth pipes (Schlichting, 1960).

2.11.4 Analysis of Turbulent Flow of Newtonian Fluids in Rough Pipes

The logarithmic law for velocity distribution is valid in rough pipes except that the constant of integration must reflect the roughness size (Schlichting, 1960). Experiments show that the effect of pipe roughness is to decrease the velocity gradient at the pipe wall (*op cit*).

The velocity distribution for Newtonian turbulent flow in rough pipes is

$$\frac{u}{V_*} = A \ln \frac{y}{k} + B \ , \qquad (2.43)$$

where $A = 1/\chi$; $\chi = 0,4$ (von Karman's constant)

B = roughness function

k = roughness size.

B can be correlated using a roughness Reynolds number

$$Re_r = \frac{\rho V_* k}{\mu} \ . \qquad (2.44)$$

The correlation is shown in Figure 2.14 below.

The oblique asymptote in Figure 2.14 is the line

$$B = 2,5 \ln Re_r + 5,5 \ , \qquad (2.45)$$

which represents the equation for smooth wall turbulent flow (Equation (2.40)).

The horizontal asymptote is the line $B = 8,5$ which represents fully developed or rough wall turbulent flow.

The top curve is the locus of data for pipes with uniform roughness from the experiments with sand roughened pipes by Nikuradse (Schlichting, 1960).

The lower curve is the equation of Colebrook (1939) and White (Equation (2.48)) and

represents the locus of data for commercially available (randomly rough) pipes. This equation is widely used for the design of Newtonian pipelines.

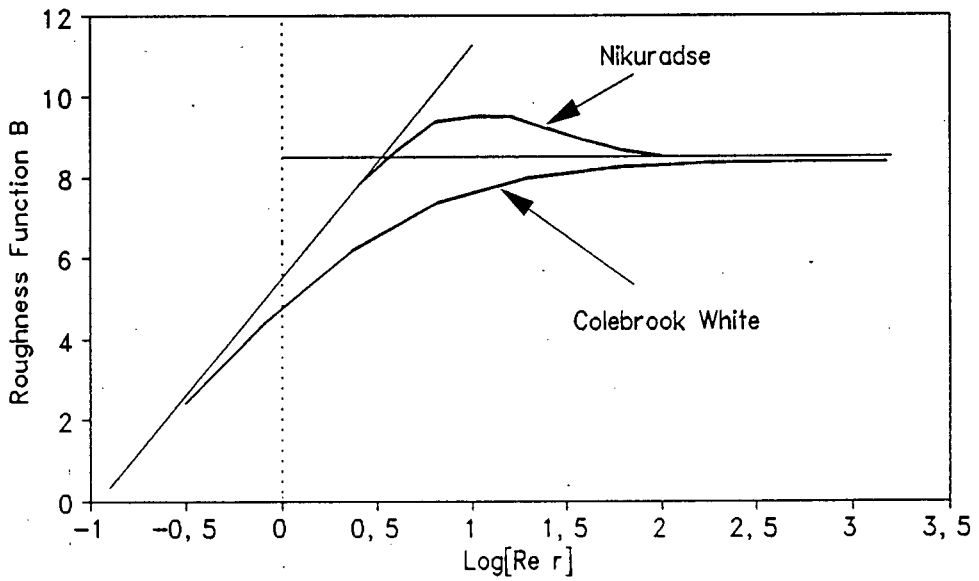

Figure 2.14 : Roughness function correlation for Newtonian fluids

For fully developed rough turbulent flow (B = 8,5) the velocity distribution can be integrated over the cross sectional area of the pipe to give the mean velocity

$$\frac{V}{V_*} = 2{,}5 \ln \left[\frac{R}{k} \right] + 4{,}75 \ . \qquad (2.46)$$

Thus the behaviour for the fully developed rough turbulent flow of Newtonian fluids in pipes is **totally independent of the viscous characteristics of the fluid.**

Relation (2.46) may be expressed in Reynolds number - friction factor format as

$$\frac{1}{\sqrt{f}} = -4 \log \left[\frac{k}{3{,}7\ D} \right] \ . \qquad (2.47)$$

2.11.5 Partially Rough Wall Turbulent Flow

The flow of Newtonian fluids in pipes is characterised by a gradual change from the smooth wall to the fully rough wall turbulent flow regions. The data of Nikuradse was determined for uniform sand roughened pipes and is the upper curve in Figure 2.14. However, commercially or randomly rough surfaces yield the line shown as the lower curve in Figure 2.14.

This transitional flow between the smooth and rough turbulent laws was investigated by Colebrook (1939). A judicious blend of the two asymptotes to fit the data was proposed by Colebrook and White (Kilner, 1971). This curve is accepted for most engineering design work.

The Colebrook White equation may be expressed in Reynolds number - friction factor format as

$$\frac{1}{\sqrt{f}} = -4 \log \left[\frac{k}{3,7\ D} + \frac{1,26}{Re\ \sqrt{f}} \right] . \qquad (2.48)$$

2.11.6 Moody Diagram

Figure 2.15 graphically depicts the behaviour of Newtonian flow in pipes. The diagram is termed a Moody diagram after Moody (1944).

The Moody diagram shows the independence of rough wall turbulent flow from Reynolds number, and hence viscosity, as the horizontal asymptote for each relative roughness.

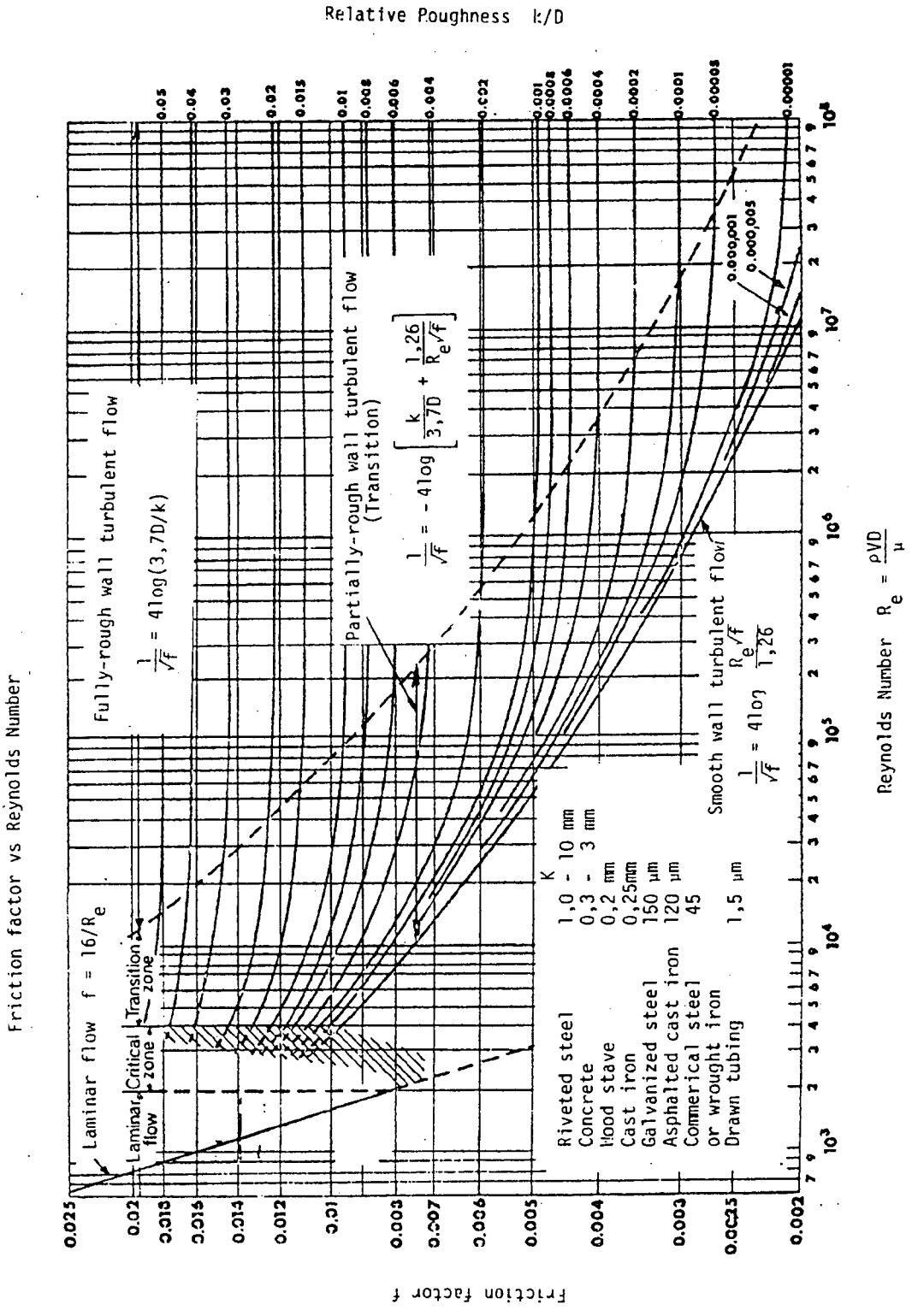

Figure 2.15 : Moody Diagram (taken from Lazarus, 1992).

2.12 NON-NEWTONIAN TURBULENT FLOW MODELS

Non-Newtonian turbulent flow models can be divided into three categories. Firstly there are the models which have a strong analytical approach, such as those of Torrance (1963) and Wilson & Thomas (1985). Secondly there are the models which are purely empirical, such as Bowen's (1961) approach. The third category lies between these two extremes, such as the models of Dodge & Metzner (1959) and Kemblowski & Kolodziejski (1973). These models are reviewed in this section.

2.12.1 The Torrance Model

Using the same mixing length model and method of derivation as for Newtonian turbulent flow, Torrance (1963) derived a model for non-Newtonian turbulent flow in pipes using the yield pseudoplastic rheological model (Equation (2.8)) as the starting point. The smooth wall turbulent velocity distribution is given by

$$u^+ = \frac{u}{V_*} = \frac{3,8}{n} + \frac{2,78}{n} \ln\left[1 - \frac{\tau_y}{\tau_0}\right] + \frac{2,78}{n} \ln\left[\frac{V_*^{2-n}\, \rho\, y^n}{K}\right] . \qquad (2.49)$$

An important departure is that the von Karman constant is taken to be **0,36n** and is therefore dependent on the viscous characteristics of the fluid. For this model the mean velocity for turbulent flow in smooth pipes is given by

$$\frac{V}{V_*} = \frac{3,8}{n} + \frac{2,78}{n} \ln\left[1 - \frac{\tau_y}{\tau_0}\right] + \frac{2,78}{n} \ln\left[\frac{V_*^{2-n}\, \rho\, R^n}{K}\right] - 4,17 . \qquad (2.50)$$

Similarly, Torrance derived a model for fully developed rough turbulent flow and the mean velocity is given by

$$\frac{V}{V_*} = \frac{2,5}{n} \ln \left[\frac{R}{k}\right] + 8,5 - \frac{3,75}{n} . \qquad (2.51)$$

Note that the von Karman constant is now assigned the value **0,4n**. The Torrance model for the fully developed rough turbulent flow of non-Newtonian fluids in pipes indicates that the behaviour is dependent on the viscous characteristics of the fluid.

Torrance makes no comment on partially rough wall turbulent flow.

The rheological parameters are treated separately, in separate terms in the expression. This leads to the problem, as mentioned before in Section 2.10.4, that the yield stress does not appear in the Reynolds number formulation.

2.12.2 The Wilson & Thomas Model

Wilson & Thomas (1985) (also Wilson, 1986 and Thomas & Wilson, 1987) produced an analysis of the turbulent flow of non-Newtonian fluids based on enhanced micro-scale viscosity effects. This model predicts a thickening of the laminar sub-layer by a factor called the area ratio A_r . This area ratio is defined as the ratio of the integrals of the non-Newtonian and assumed Newtonian rheograms (using the apparent or secant viscosity μ' as defined in Section 2.10.2) under identical shear conditions. The thickened laminar sub-layer results in an increase in the mean velocity over that for an equivalent Newtonian fluid.

For the yield pseudoplastic model, the area ratio is given by:

$$A_r = 2 \left[\frac{1 + \frac{\tau_y}{\tau_0} n}{1 + n}\right] . \qquad (2.52)$$

This relationship is shown graphically below in Figure 2.16.

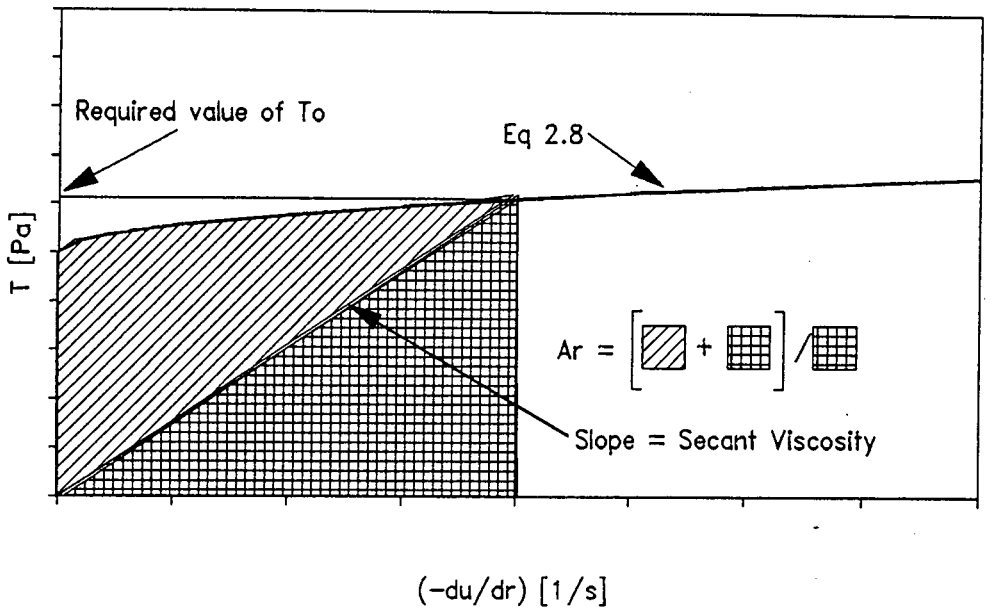

Figure 2.16 Illustration of the area ratio and secant viscosity - Wilson & Thomas model.

The laminar sub-layer thickness is therefore

$$\delta_{NN} = A_r \, \delta_N \, , \tag{2.53}$$

where δ_N and δ_{NN} are the equivalent Newtonian and non-Newtonian laminar sub-layer thicknesses respectively.

The velocity distribution is given by

$$u^+ = \frac{u}{V_*} = 2{,}5 \ln \left[\frac{\rho \, V_* \, y}{\mu'} \right] + 5{,}5 + 11{,}6 \, (A_r - 1) - 2{,}5 \ln(A_r) \, . \tag{2.54}$$

The mean velocity is given by

$$\frac{V}{V_*} = \frac{V_N}{V_*} + 11{,}6 \, (A_r - 1) - 2{,}5 \ln A_r - \Omega \, , \tag{2.55}$$

where V_N is the mean velocity for the equivalent Newtonian fluid based on a secant viscosity from the yield pseudoplastic rheogram. Ω is a term to account for the blunting of the velocity profile caused by the yield stress,

$$\Omega = -2{,}5 \ln \left[1 - \frac{\tau_y}{\tau_0} \right] - 2{,}5 \frac{\tau_y}{\tau_0} \left[1 + 0{,}5 \frac{\tau_y}{\tau_0} \right] . \qquad (2.56)$$

A method for scale up of turbulent data, based on the above model, has also been proposed (*op cit*).

Rough wall and partially rough wall turbulent flow can be accommodated in the model by using the appropriate roughness when determining V_N. However, this can only be approximate, since the interaction between the pipe roughness and the laminar sub-layer will clearly be different when the thickened laminar sub-layer is present.

2.12.3 The Dodge & Metzner Model

Dodge & Metzner (1959) developed a turbulent flow model based on the laminar model of Metzner & Reed (1955). The model was developed along the same lines as Newtonian turbulent flow, and the final relationship is of the same format as Newtonian smooth wall turbulent flow, and reverts to the Newtonian form under Newtonian conditions ($K' = \mu$ and $n' = 1$).

The relationship is

$$\frac{1}{\sqrt{f}} = \frac{4}{n'^{\,0{,}75}} \log \left[Re_{MR} \, f^{\frac{2-n'}{2}} \right] - \frac{0{,}4}{n'^{\,1{,}2}} . \qquad (2.57)$$

The turbulent flow head loss therefore depends on n', which is a rheological parameter, and the relationship between friction factor and Reynolds number is shown in Figure 2.17.

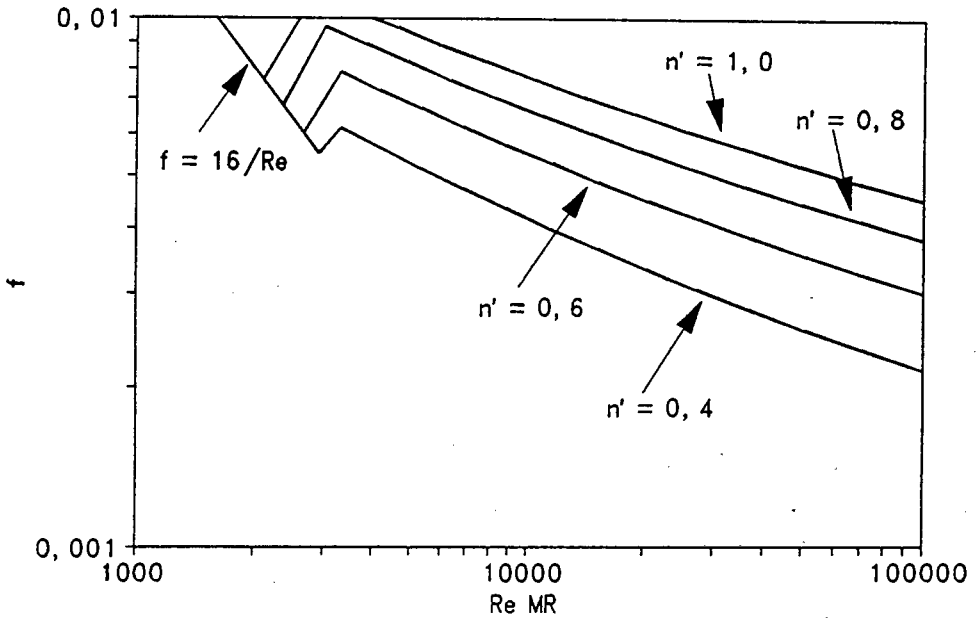

Figure 2.17 The Dodge & Metzner correlation shown on a friction factor-Reynolds number diagram

This diagram shows that this model will predict friction factors that decrease continuously with increasing Reynolds number.

2.12.4 The Kemblowski & Kolodziejski Model

Kemblowski & Kolodziejski (1973) found that the Dodge & Metzner model did not accurately describe the behaviour of kaolin slurries. They used an empirical approach to model this behaviour based on the pseudoplastic model (K′ and n′ constant) and a Blasius type equation

$$4f = \frac{0{,}3164}{Re_{MR}^{0{,}25}} \quad . \tag{2.58}$$

They further postulated that the data would lie on a virtually flat f-Re line between the Dodge & Metzner prediction and the above Blasius line, which they termed a "transition region".

This was modelled empirically as

$$4f = \frac{E}{Re_{MR}^{m}} \Phi^{1/Re_{MR}}, \qquad (2.59)$$

where E, m and Φ are rheological parameters which are unique functions of the apparent flow behaviour index n′. This relationship is shown graphically in Figure 2.18.

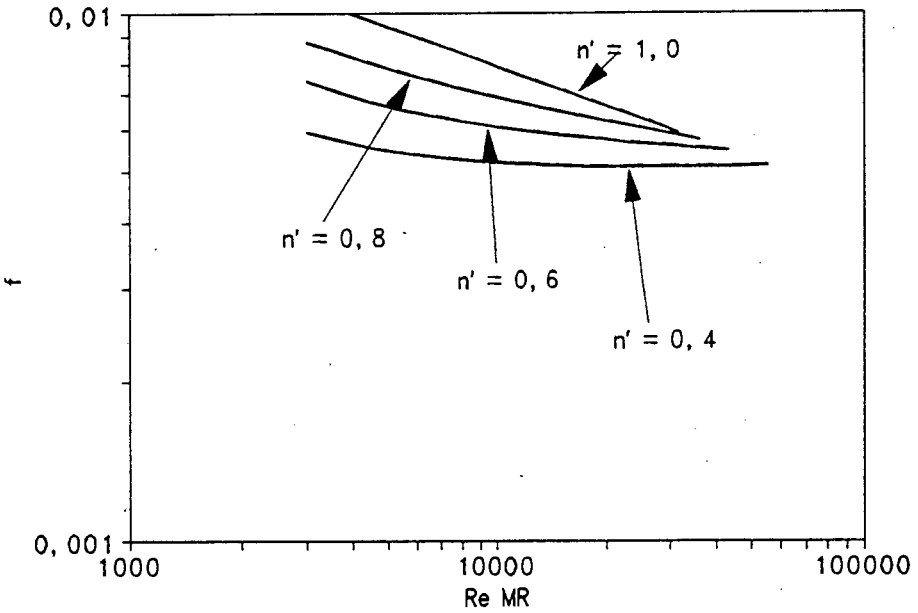

Figure 2.18 Friction factor-Reynolds number diagram for the Kemblowski & Kolodziejski model.

An important point which is brought to light by this work is the virtually constant value of the friction factor for these slurries at high Reynolds number, reminiscent of Newtonian fully rough wall turbulent flow. This is in sharp contrast to the predictions of the Dodge & Metzner model above.

2.12.5 The Bowen Correlation

Bowen (1961) noted that many of the proposed correlations were only able to correlate data in the limited range over which they had been tested. Outside this range, discrepancies were usually large. He further noted that there was a similarity between turbulent flow test data in different diameter pipes. In particular he noted that the

slopes of the turbulent branches of different diameters were very similar on a log-log pseudo shear diagram. He was further able to correlate the diameter effect by adapting the Blasius equation for Newtonian fluids

$$f = \frac{0,079}{Re^{0,25}} , \tag{2.60}$$

and produced the following correlation:

$$D^{1+b} \left[\frac{\Delta p}{L}\right] = k\, V^{2-b} . \tag{2.61}$$

The constants k and b can be evaluated from experimental data in turbulent flow using graphical techniques and Bowen presents worked examples. These constants can also be evaluated directly from experimental data using statistical techniques. Turbulent flow predictions can then be made using the above correlation.

Quader & Wilkinson (1980) have shown that the Metzner & Reed model can be regarded as a special form of the Bowen correlation.

Bowen also showed that his critical Reynolds number (similar to Re_{Newt} above) increased with increase in diameter.

The constant k contains the Newtonian Reynolds number and thus the viscosity μ to the power 0,25. Bowen states that the above correlation is applicable provided that the viscosity remains constant. This is clearly not true for the general non-Newtonian case where the "viscosity" is a variable quantity. However, Bowen's method does produce good correlation of non-Newtonian turbulent flow pipe data (Harris & Quader, 1971 and Quader & Wilkinson, 1980). This could be regarded as evidence that the viscous characteristics of a slurry are unimportant in turbulent flow.

This method provides accurate scale up to prototype diameter from turbulent flow

laboratory test data. However, it provides no explanation of the behaviour of the slurry in terms of the physical properties of the slurry.

2.13 ASPECTS OF NON-NEWTONIAN TURBULENT FLOW

There are several aspects of non-Newtonian turbulent flow which are not included in the previous discussions of models. However, they are important because they have an influence on the development of the new model. These aspects are discussed in this section.

2.13.1 Importance of rheology in turbulent flow

Cheng (1970) argues that the yield stress may be neglected in turbulent flow because the turbulent behaviour of a Bingham plastic fluid is independent of the yield stress. This could imply that the determination of a rheological parameter is not important for predicting turbulent flow behaviour.

However, the importance of the proper determination of the viscous characteristics of fluids in laminar flow for the prediction of their turbulent behaviour has been emphasised by Hanks & Ricks (1975). This is even more pertinent in the light of the known sensitivity of the yield pseudoplastic model (Al-Fariss & Pinder, 1987).

2.13.2 Partially Rough Wall Turbulent Flow

Partially rough wall turbulent flow in non-Newtonian flow can be approximated using an analogy to Newtonian analysis (Govier & Aziz, 1972). The friction factor or head loss is increased by multiplying by the ratio of the partially rough wall turbulent flow friction factor to the smooth wall friction factor from the Moody diagram (or the Colebrook White equation) at the same Reynolds number as the Torrance or Clapp Reynolds number. This will force the predicted slurry turbulent behaviour to follow the long transition region which is characteristic of Newtonian fluids (see Moody diagram, Figure 2.15).

2.13.3 Similarity between Newtonian and non-Newtonian turbulent flow

Many researchers report the similarity between the turbulent behaviour of Newtonian fluids and non-Newtonian slurries.

Caldwell & Babbitt (1941) studied the flow of muds, sludges and suspensions in circular pipes and concluded that head loss in turbulent flow can be predicted using Newtonian relationships provided that a viscosity similar to the secant viscosity described above was used.

Hedström (1952) performed a theoretical investigation of the Bingham model and used the experimental data of Wilhelm *et al* on cement rock suspensions. He recommends a design procedure for computing pressure drops which uses the usual smooth wall f-Re curve for Newtonian fluids.

Metzner & Reed (1955) studied sixteen different non-Newtonian materials and recommended that the "usual Newtonian" design procedures be used for the turbulent flow predictions of these materials.

Dodge & Metzner (1959) stated that earlier workers almost unanimously adopted the concept that the shear rates which occur under turbulent conditions are high enough to effect constancy of viscosity and thus standard Newtonian procedures could be used to predict non-Newtonian pressure drops. The only real difference in the approaches was as to how the constant viscosity was to be determined.

Tomita (1959) investigated clay, lime, starch, cement rock and sewage slurries and reports that the characteristics of non-Newtonian turbulent flows in pipelines are approximately equal to those of Newtonian flows.

Michiyoshi *et al* (1966) analysed an alumina slurry using the Bingham plastic model. They report that at high Reynolds numbers the friction factor approached that of a Newtonian fluid. They conclude that above these Reynolds numbers the slurry may

have characteristics similar to those of a Newtonian fluid.

Edwards & Smith (1980) used previously published velocity profiles and pressure drop measurements for carbopol and CMC solutions and thoria slurries and showed that if the velocity profiles are made dimensionless, using the apparent viscosity at the wall, then Newtonian and non-Newtonian velocity profiles are in good agreement. Consequently, they conclude that standard Newtonian correlations can be used to calculate pressure drops for turbulent non-Newtonian pipe flow.

Thomas & Wilson (1987) report that the data of non-Newtonian kaolin slurries at lower concentrations and high Reynolds number converge on Newtonian behaviour.

Sive (1988) suggests the use of the Colebrook White equation for determining friction factors when predicting energy gradients for kaolin slurries.

Park *et al* (1989) conclude that the transition region is much narrower than for Newtonian fluids. Their non-Newtonian slurry turbulent flow velocity profile agrees well with measurements of air (Newtonian fluid). This is perhaps the most convincing evidence to date on the similarity between Newtonian and non-Newtonian slurry turbulent flow, and is shown in Figure 2.19, Figure 2.19.

This diagram shows that the velocity distribution for air (a Newtonian fluid) is virtually identical to that of a non-Newtonian slurry which was modelled using the yield pseudoplastic rheological model (see also Section 2.13.3, 2.13.9 and Appendix A).

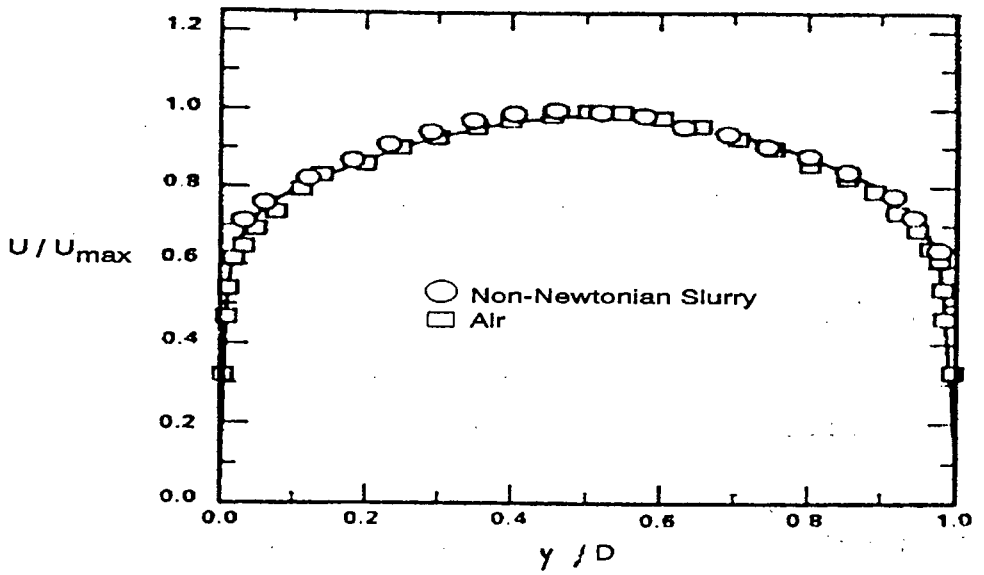

Figure 2.19 : Turbulent velocity distribution : Comparison between a non-Newtonian slurry and air (air at Re = 40 600). (From Park *et al*, 1989).

2.13.4 Von Karman constant

In Newtonian turbulent flow, the turbulent core conditions are independent of viscosity and the same can be expected of non-Newtonian fluids (Wilson *et al*, 1992) and the value of χ should remain 0,4. Wilson (1986) argues that, of the various mechanisms which can produce drag reduction in non-Newtonian slurry turbulent flow, the one most likely to be correct is the thickening of the laminar sub-layer and not a change in the value of the von Karman constant.

Abbas & Crowe (1986) report a lowering of the numerical value of χ as a function of concentration and particle size. However, this could be due to non-Newtonian behaviour as they used the viscosity of the Newtonian liquid phase of the slurry in their analysis.

A damping effect due to the presence of the yield stress can reduce the numerical value of χ (Xu *et al*, 1993), but this can only be expected at relatively high values of the yield stress.

2.13.5 Unsheared Core

In laminar flow, an unsheared core exists in the pipe due to the presence of the yield stress. Some researchers such as Wilson & Thomas (1985) and Hanks & Dadia (1982) maintain that this should also hold true in turbulent flow. However, the data of Park *et al* (1989) and Xu *et al* (1993) show no evidence of this.

2.13.6 Particle Size Effect

Maud & Whitmore (1958) and Mun (1988) report a particle size effect on energy gradients in turbulent flow. This would account for the incongruence of the turbulent behaviour of slurries which have similar viscous characteristics (Harris & Quader, 1971).

2.13.7 The Continuum Approximation

The continuum nature of these slurries is an approximation, and is a state to which the slurries tend asymptotically (Shook & Roco, 1991). Lumley (1978) has commented that this approximation is deemed to hold good so long as the scale of fineness required by the subsequent modelling is not surpassed by the particle size.

2.13.8 Turbulent Flow Predictions from Rheological Data

Harris & Quader (1971) report that fluids with similar viscous characteristics may be expected to behave differently under turbulent flow conditions. They conclude that the chances of accurate turbulent flow predictions from rheological data are therefore not good.

Their solution is to perform tests in turbulent flow and then to use the correlation of Bowen (1961) for turbulent flow predictions.

One possible conclusion is that the turbulent flow behaviour is affected by some other property of the slurry besides its rheology.

2.13.9 The work of Park *et al* (1989)

Park *et al* (1989) investigated the turbulent structure of a non-Newtonian slurry using laser doppler anemometry. A mixture of Stoddard solvent and mineral oil was used for the liquid phase and silica particles for the solid phase. The final mixture was a homogeneous non-Newtonian slurry which was characterised using the yield pseudoplastic rheological model. It is important to note that the behaviour of their slurry is in general terms identical to the behaviour of the slurries tested for this thesis.

Their findings are that the transition from laminar to fully developed turbulent flow is much narrower than for Newtonian fluids and the relative turbulence intensity for the tangential velocity profile was higher at the wall and lower at the pipe axis when compared to Newtonian flow. The longitudinal velocity profile agreed well with Newtonian flow.

2.13.10 The work of Xu *et al* (1993)

Xu *et al* (1993) tested kaolin clay slurries in a rotary viscometer and a pipe line test loop. The Bingham plastic model was used for the analysis, even though the rheogram showed distinct curvature. The turbulent flow model of Wilson & Thomas (1985) was unable to predict the turbulent flow energy gradients accurately (see Figure 1.1). However, the intersection method as proposed in Section 2.10.7 was a good indicator of the laminar/turbulent transition.

2.13.11 Fluid/Particle Interactions

The interactions between fluid and particles in suspensions are complex, especially in turbulent flow. However, a knowledge of this phenomenon is important for the development of any theoretical model for the flow predictions of slurries.

In the extreme case of the drag force on a single sphere, analytical description is difficult and fundamentally different in laminar and turbulent flow (Soo, 1967). The presence of a small yield stress can have a significant effect on this drag force (Valentik & Whitmore, 1965; Ansley & Smith, 1967 and Hanks & Sen, 1983). A practical problem which is evident from the experimental results (eg Hanks & Sen, 1983 and Dedegil, 1986) is that the data do not extend significantly into turbulent flow.

Maud & Whitmore (1958) argued that a liquid element would follow an oscillating passage down the tube in turbulent flow, whereas a solid particle would be prevented from following this path exactly by inertia forces, and would oscillate over a smaller amplitude. The mean mixing length of the suspension - which consists of both liquid and particles - will decrease when compared to liquid only. Another similar effect is that velocity components perpendicular to the pipe axis exist in turbulent flow which must lead to curved flow paths in the wall region. Once again, particles attempting to follow the liquid path will experience radial inertial forces and the particles will move towards the wall (*op cit*). Soo (1967) has stated that due to inertia, solid particles can be expected to dampen turbulence at lower concentrations and stimulate turbulence at higher concentrations.

A major problem in this area of the literature is the presence of apparent contradictions on important issues such as the effect of solid particles on turbulence and the velocity profile.

- Owen (1969) and Baw & Peskin (1971) report a decrease in turbulent energy spectra due to the presence of solid particles while Soo *et al* (1960) noticed no

such effect. More recent work by Park *et al* (1989) showed tangential turbulence intensities higher at the wall and lower at the pipe axis due to the presence of solids. For this thesis, this has been interpreted as meaning that the presence of the particles dampens turbulence in the core region, while stimulating turbulence in the wall region.

- There is evidence in the literature that the presence of solid particles, even at low concentrations, will flatten the velocity profile in the wall region (Soo, 1971). This flattening is contradicted by the fact that the solids concentration must approach zero at the pipe wall (Shook & Roco, 1991), resulting in a steepening of the velocity gradient.

Abbas & Crowe (1986) investigated the behaviour of a homogeneous slurry of silica particles in chloroform. The turbulent velocity profile was then measured using laser doppler anemometry. Their findings showed that the effect of the particles relative to the pure liquid phase was to reduce the turbulent boundary intercept value and increase the slope of the universal logarithmic velocity distribution. It is important to note that they did not acknowledge any rheological change due to the presence of the particles. The density and viscosity of the chloroform only was used in all calculations.

Much of the previous work done has been for gas and liquid suspensions of solids which are not homogeneous in the sense adopted for this thesis. The one exception is the work of Park *et al* (1989).

It can also be noted that there are no fewer than twelve physical aspects which can influence these interactions (Shook & Roco, 1991).

In spite of the above mentioned contradictions, it is clear that fluid/particle interactions are complex, non-linear and are different in laminar and turbulent conditions.

2.13.12 Particle Reynolds Number

Fluid/particle interaction in non-Newtonian slurries can be investigated using a particle Reynolds number (Govier & Aziz, 1972 and Shook & Roco, 1991). Furthermore, this Reynolds number must be formulated in terms of non-Newtonian rheology. An appropriate formulation for the slurries under consideration was developed by Dedegil (1986) for the Bingham plastic model. Working from the fundamental definition that the Reynolds number is proportional to the ratio of inertial to viscous force, and using the ratio V_s/d as a representative shear rate, the following formulation was obtained

$$Re_p = \frac{\rho V_s^2}{\tau_y + K\left[\frac{V_s}{d}\right]} . \qquad (2.62)$$

2.13.13 Experimental Work

Although there is experimental data on non-Newtonian slurry flow reported in the literature, there are several problems associated with the use of this data in developing or verifying theoretical models.

It is usually difficult to verify the rheological characterisation. Often, rotary type viscometers are used, and it is now known that it is preferable to use a tube viscometer (Lazarus & Slatter, 1986; Shook & Roco, 1991 and Wilson *et al*, 1992). Some researchers have consistently used restrictive rheological models such as the Bingham plastic (eg, Duckworth *et al*, 1986) or pseudoplastic models (eg, Kemblowski & Kolodziejski, 1973 and Chhabra & Richardson, 1985) and it is not possible to rework the viscometric data to verify the analyses.

There are often only one or two pipe diameters for the same slurry (eg, Metzner & Reed, 1955 and Thomas & Wilson, 1987).

Sometimes it is questionable whether exactly the same slurry was used for both the

viscometry and the pipeline tests (eg, Thomas & Wilson, 1987).

The correlation of viscometric data is also problematic. The subsequent interpolation of the data may lead to inaccuracies in the rheological parameters (Johnson, 1982)

Finally, very little data has been published with detailed particle size distributions.

2.14 CONCLUSIONS

The literature pertinent to the flow of non-Newtonian slurries in pipes has been reviewed, and the relevant theoretical models have been presented.

2.14.1 Laminar Flow

The laminar flow of non-Newtonian slurries can be modelled and predicted using the yield pseudoplastic rheological model. This model is not restrictive and allows for both a yield stress and rheogram curvature. Although the model is sensitive to small changes in the rheological parameters, laminar flow in different diameters can be used to verify results. The viscometry of non-Newtonian slurries is best performed using a tube viscometer. Rheological characterisation can be accurately performed using the Lazarus & Slatter (1988) method. The accuracy of the rheology of a slurry is probably more important for turbulent flow predictions than in laminar flow.

2.14.2 Laminar/Turbulent Transition

The laminar/turbulent transition of Newtonian fluids can be modelled using the Reynolds number. Several non-Newtonian Reynolds numbers applicable to non-Newtonian slurries exist as well as a stability criterion derived from fundamental theory. In the absence of any conclusive work as to which of these theoretical models is accurate, the practical approach using the intersection of the laminar and turbulent theoretical lines is recommended. Increasing values of the observed critical velocity above the expected or predicted values are reported in the literature. The stability

criterion is the only model which takes the presence of the unsheared plug at the pipe axis into account. It is possible that the presence of a yield stress may cause the critical velocity to become independent of the pipe diameter at larger pipe sizes - in sharp contrast to the Newtonian case.

2.14.3 Turbulent Flow

Smooth wall Newtonian turbulent flow can be modelled using the classical universal logarithmic velocity distribution. Rough wall Newtonian turbulent flow can be modelled using a logarithmic velocity distribution with a roughness function and a roughness Reynolds number to correlate the roughness function. Partially rough wall Newtonian turbulent flow can be modelled using the Colebrook-White relation which is a combination of the smooth and rough turbulent flow laws.

The theoretical analysis of non-Newtonian slurry turbulent flow has received much attention in the literature. The fundamental point of departure has either been a purely empirical turbulent correlation, such as the work of Bowen, or that turbulent flow predictions can be based on the laminar flow behaviour (rheology) of the slurry, such as the work of Torrance, and Wilson & Thomas. Recent experimental work has brought into question whether turbulent flow prediction is possible from viscous properties only. The striking similarity between Newtonian and non-Newtonian slurry turbulent flow is widely reported in the literature. Turbulent scale-up can be accurately performed from turbulent test data for non-Newtonian slurries. Non-Newtonian slurries can produce virtually constant friction factors at high Reynolds numbers. The continuum approximation may be compromised in the wall region and a particle size effect in turbulent slurry flow has been reported in the literature which supports this idea.

Fluid/particle interactions are complex and regime dependent and the literature contains contradictions on important aspects. Recent work by Park *et al* (1989) using a slurry similar to those tested in this thesis shows that particles are capable of stimulating turbulence in the wall region. A particle Reynolds number can be

formulated for non-Newtonian slurries and can be used to investigate fluid/particle interactions.

2.15 RESEARCH ASPECTS IDENTIFIED

Aspects requiring further research in this field are identified below.

2.15.1 Laminar Flow

Although laminar flow can be predicted using the theoretical laminar flow models, the accuracy of rheological characterisation could be of great importance for the prediction of turbulent flow behaviour. Verification of the rheological characterisation procedure is necessary.

2.15.2 Laminar/Turbulent Transition

There are many methods available for the prediction of the laminar/turbulent transition, which vary from analytical to empirical. However, there are no conclusive guidelines in the literature as to which methods are superior. The development of a simple, single, analytical criterion, such as exists for Newtonian fluids (Re=2100), is required.

2.15.3 Turbulent Flow

There are many methods available for the prediction of turbulent energy gradients, none of which are suitable for use as a design tool for non-Newtonian Slurries (Xu *et al*, 1993 and Appendix C). The development of a suitable, applicable analytical model is required.

2.15.4 Experimental Work

Although there is data reported in the literature, there are several problems involved in using this data for the development and verification of a new turbulent flow slurry flow analysis. An extensive experimental investigation covering wide ranges of diameter, velocity and slurry properties is necessary.

CHAPTER 3

CHAPTER 3

EXPERIMENTAL WORK

3.1 INTRODUCTION

The details of the apparatus and how it was used to gather data for the evaluation of the theoretical models is presented in this chapter.

Apparatus was built and test work performed specifically with the following objectives in mind

- to measure the rheology accurately
- to test over as wide a range of flow velocities and diameters as possible
- to do test work using different particle size distributions
- to accumulate a data base of test data for the evaluation of existing turbulent flow theory and the new model.

One of the most fundamental aspects of this thesis is that the turbulent pipe flow head loss can be predicted from the rheological data of the same fluid. As stated in Chapter 2, rheological data can only be obtained from tests under laminar flow conditions. It was therefore vital that experiments were performed so that reliable data over large ranges for both the laminar and turbulent regimes could be measured for the same non-Newtonian slurry.

Non-Newtonian mine tailings and kaolin clay slurries were tested in pipes of diameter ranging from 6mm to 200mm nominal bore with mean velocities ranging from 0,1m/s to 10m/s. An important aspect of the experiments is that the same slurry was used for each test set. A test set is a set of tests using different pipe diameters but the same slurry.

3.2 APPARATUS

Three different sets of apparatus were used to gather experimental data for this thesis. These were the Balanced Beam Tube Viscometer, the Mini Rig and the East Rig.

3.2.1 The Balanced Beam Tube Viscometer

The Balanced Beam Tube Viscometer (BBTV) developed by Hydrotransport Research at UCT is a device for measuring the flow characteristics of a slurry (Slatter, 1986). The BBTV is, in fact, a miniature pipeline (Slatter & Lazarus, 1988) and its use extends beyond viscometry.

This instrument consists of two pressure vessels which are located approximately 6m apart at either end of a steel beam. This beam is centrally supported on a knife edge and a load cell is located under the left hand vessel. The vessels can be connected by transparent tubes of different diameter.

The prime mover is compressed air which forces the slurry through a selected tube at a controlled rate. The average slurry velocity is obtained from the mass transfer rate. The pressure drop across a known length of the tube is measured using a differential pressure transducer.

All the test section entry lengths can be changed to detect for undeveloped flow or time dependency.

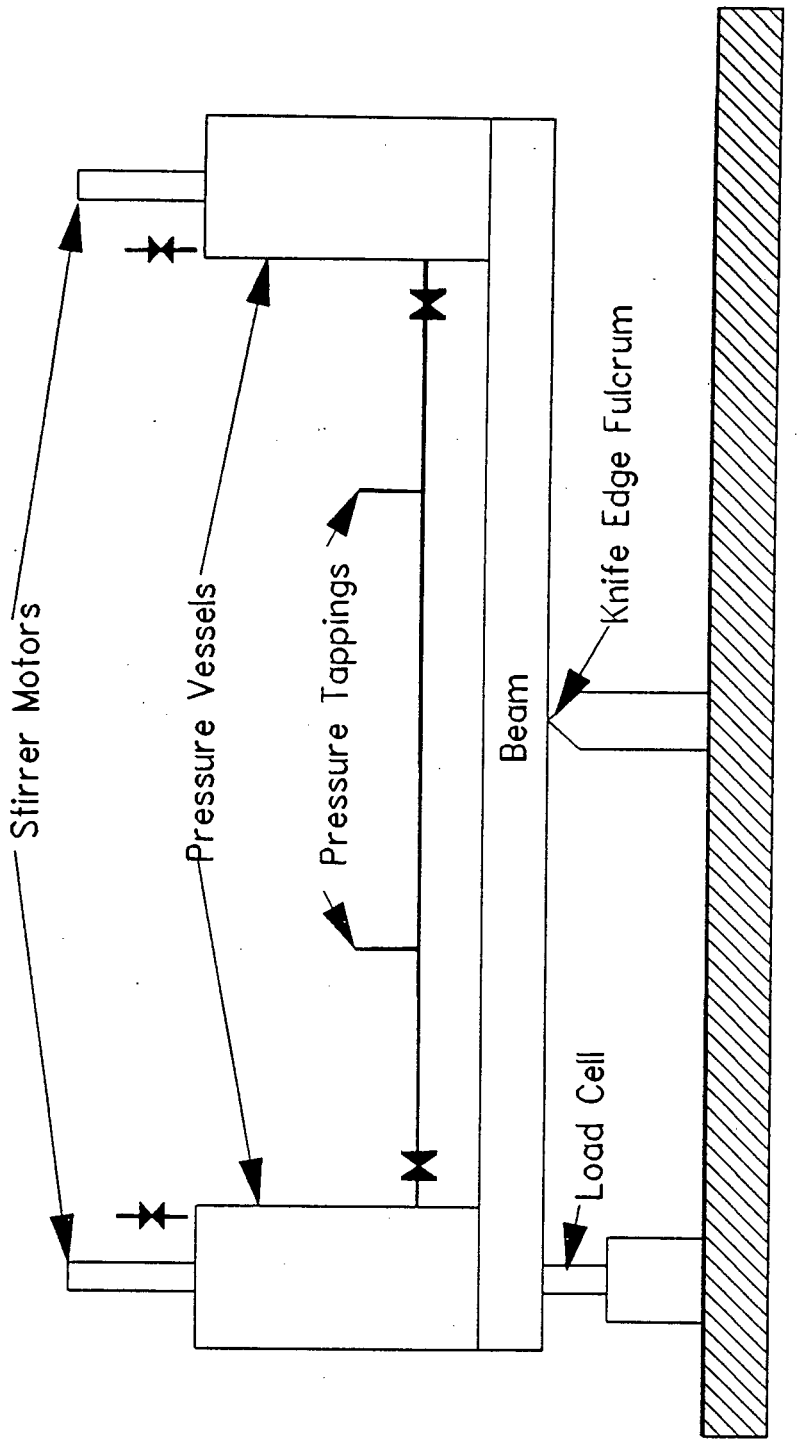

Figure 3.1 : Schematic Diagram of the Balanced Beam Tube Viscometer.

3.2.2 The Mini Rig

The mini rig at UCT is a pumped pipeline test loop using small diameter PVC pipes. This rig was built because the BBTV may have been giving results for critical velocity which were too high due to the absence of mechanical noise (Slatter & Lazarus, 1993).

This rig consists of a Warman 1,5x1 solids handling centrifugal pump, a 3m long test section with interchangeable clear PVC test sections of diameter 6mm, 15mm and 25mm nominal bore, and connecting pipes. The flow rate is measured with a 25mm nominal bore Altometer magnetic flux flowmeter. Slurry is pumped from the 150mm nominal bore pipe in the east rig, through the mini rig to the weigh tank. This ensures that the same slurry is tested in both the East and Mini Rigs. The pump has a variable speed hydraulic drive.

All the test section entry lengths can be changed to detect for undeveloped flow or time dependency.

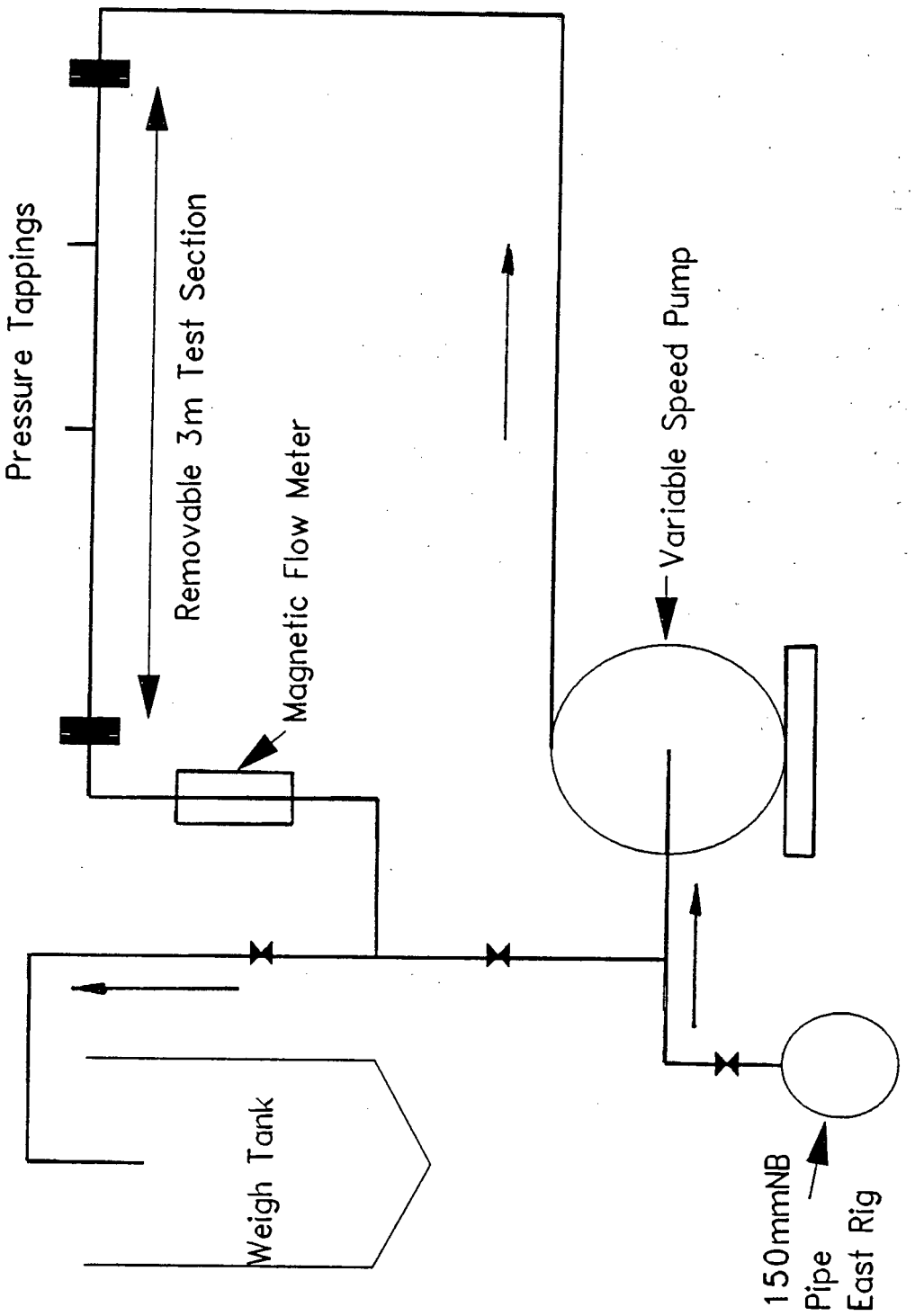

Figure 3.2 : Schematic Diagram of the Mini Rig

3.2.3 The East Rig

The east rig is a recirculating pumped pipeline test circuit with three test sections of diameter 80mm, 150mm and 200mm nominal bore.

Slurry is collected in the steel feed hopper which has a capacity of approximately $2m^3$. Slurry then passes directly from the hopper into the pump. The pump is a Mather and Platt 8x6 which is driven by a variable speed hydraulic drive.

After the pump, the line splits into the 80mm and 150mm lines. The two lines then have a vertical counterflow meter section followed by a horizontal section of approximately 17m. The magnetic flux flow meters are located in the vertical downcomer. Clear viewing and test sections are located in the return horizontal lines. The 150mm horizontal return line splits into the 150mm and 200mm lines, which join again after 12m. The 200mm line is steel, the others are PVC. The return lines are then fed back through an in-line heat exchanger and a pneumatic diverter valve into the hopper. The in-line heat exchanger maintains the slurry at a constant temperature. The diverter valve feeds the weigh tank which is used for flow rate determination. For the slurries tested, no external agitation was necessary to maintain solids suspension in the hopper.

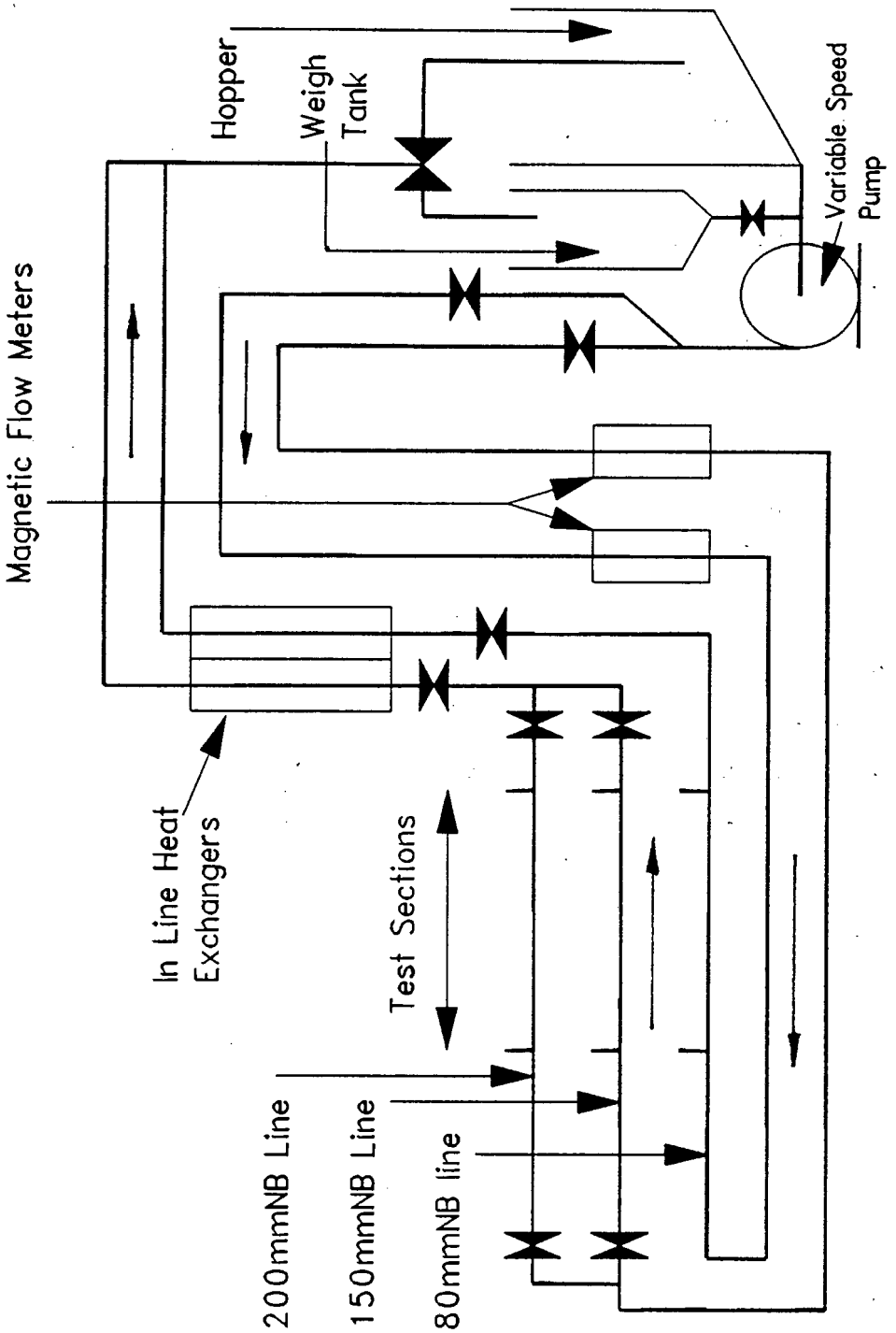

Figure 3.3 : Schematic Diagram of the East Rig

3.2.4 Pressure tappings

Differential pressure measurements are made from static pressure tappings located in the pipe walls of each of the horizontal test sections. The tappings have length to diameter ratios greater than four to ensure accurate readings (Hanks, 1981). The tappings are 3mm in diameter and great care was taken to remove any burrs from the inside edge of each tapping.

Each tapping is fed through a valve to an isolation pod which collects any solids that may enter the pressure tapping. Each pod has a valve for flushing away collected solids with clear water. Clear water lines then connect the pod to the manometer and differential pressure transducer (DPT).

The test sections are preceded by unobstructed straight pipe of at least 50 pipe diameters (Govier & Aziz, 1972 and Hanks, 1981). The only exception is the 200mm nominal bore pipe which, due to space constraints, has a straight entry length of 35 pipe diameters.

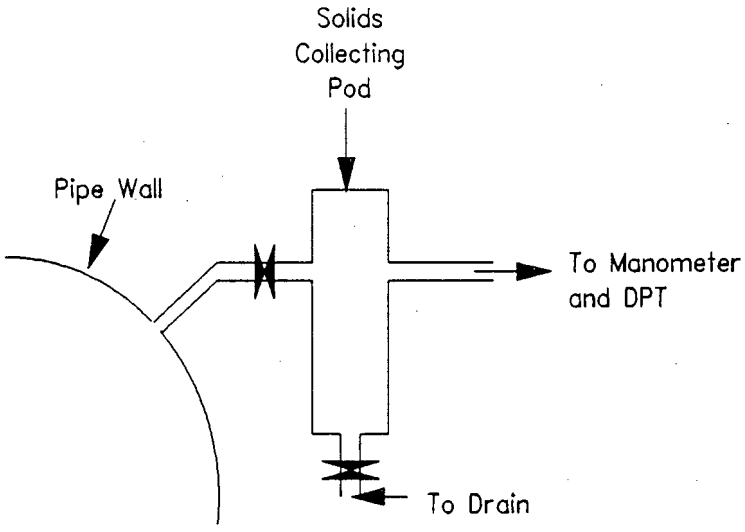

Figure 3.4 : Detail of a Pressure Tapping and Pod.

3.2.5 Weigh tank

Slurry from the East Rig can be fed into the weigh tank for a timed period using a pneumatically controlled diverter valve. The weigh tank has a capacity of 1,5m^3 and is placed on a 1750 kg mass scale. The Mini Rig is fed continuously into the weigh tank, which is drained back into the East Rig when necessary.

3.2.6 The manometer board (East and Mini Rigs)

The layout of the manometer and the connections to the differential pressure transducer (DPT), the pressure tappings and high pressure air and clear water are shown in Figure 3.5.

The following operations are performed from the manometer board:-

- Air and solids are flushed from all tubes and the DPT.
- A variable differential air over water head is set up in, and read off, the manometer tubes for calibration purposes.
- The air over water manometer tube head is maintained visible during testing to provide visual confirmation of head loss measurements.
- The DPT is connected to the tappings for data logging.

The high pressure water supply is passed through an air trap to ensure that water in the manometer lines is free of air.

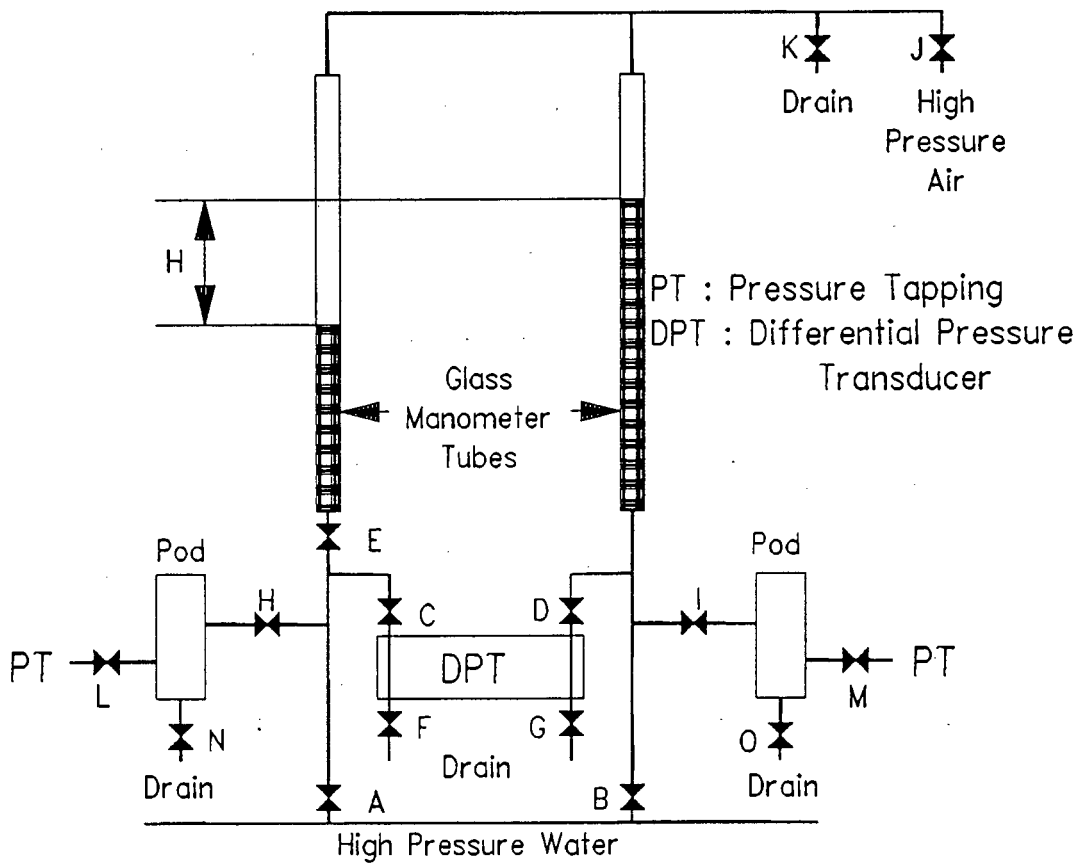

Figure 3.5 : Manometer fluid circuit for the east and Mini Rigs.

3.2.7 BBTV Manometer

The fluid circuit diagram of the BBTV DPT is shown in Figure 3.6. For slurry testing, the pods are connected to the pressure tappings. The circuit is used to flush air and solids from all lines and to set up a differential mercury/water head for calibration of the DPT. The high pressure water supply is passed through an air trap.

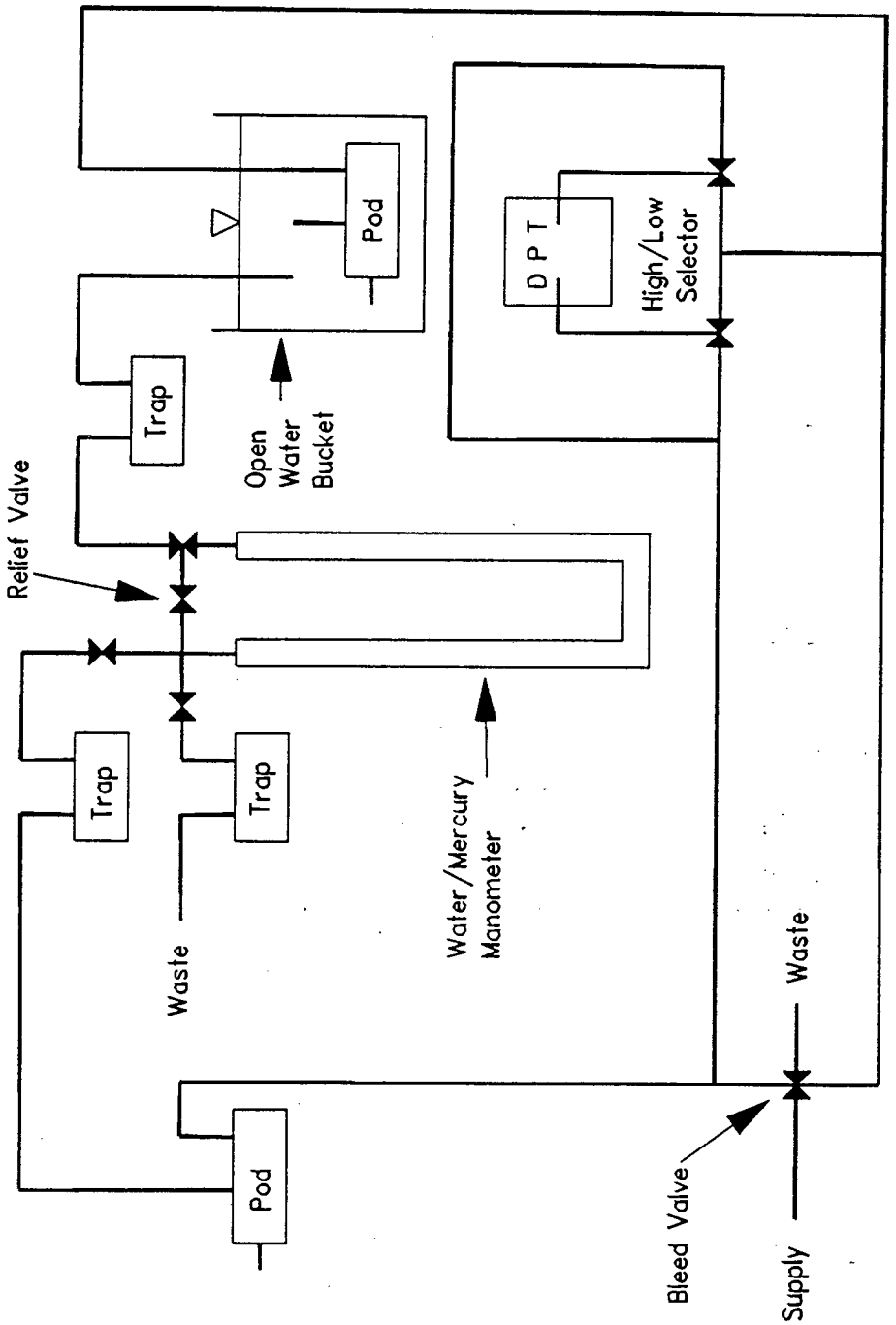

Figure 3.6 : Fluid circuit diagram for calibration of the DPT on the BBTV.

3.3 MEASURED VARIABLES AND CALIBRATION

The measurement of force, flow rate and differential pressure is done using transducers. The calibration procedure for the transducers is explained below. The transducers convert the desired quantity into a direct current electrical signal. The magnitude of this signal must be related accurately to the magnitude of the measured quantity in order to use the transducer. The purpose of the calibration procedure is to establish this functional relationship between transducer signal and measured quantity.

3.3.1 Linear Regression

The response of the transducers used for the experimental work was linear and calibration equations derived from least squares linear regression were used to process transducer readings.

The least squares regression line of a set of N physically observed measurements Y on the corresponding set of N transducer readings X is (Spiegel, 1972)

$$Y = mX + c \,, \tag{3.1}$$

where

$$m = \frac{N\,\Sigma XY - (\Sigma X)\,(\Sigma Y)}{N\,\Sigma(X^2) - (\Sigma X)^2} \,, \tag{3.2}$$

and

$$c = \frac{\Sigma Y\,\Sigma(X^2) - \Sigma X\,\Sigma(XY)}{N\,\Sigma(X^2) - (\Sigma X)^2} \,. \tag{3.3}$$

The correlation coefficient, r, provides an objective measure of how well the line represents the data (*op cit*);

$$r = \frac{N\,\Sigma XY - (\Sigma X)(\Sigma Y)}{\sqrt{\left[\,N\,\Sigma(X^2) - (\Sigma X)^2\,\right]\left[\,N\,\Sigma(Y^2) - (\Sigma Y)^2\,\right]}} \,. \tag{3.4}$$

A value of r=1 implies a perfect fit. Calibrations were accepted for r values in the range $0,99 < r < 1$.

In general the fit is not perfect and at each point there remains a small but finite difference or residual error E_{res} which is defined by

$$E_{res} = | Y_{obs} - (mX + c) | . \qquad (3.5)$$

The highest residual error from a calibration provides a measure of the absolute error involved in the use of the transducer under the test conditions.

3.3.2 Load Cell

The load cell on the BBTV is calibrated by applying an external force on the instrument using standard weights (Slatter, 1986). These weights are placed above the centroid of each vessel, on the stirrer motors. The weights are then moved progressively from the left hand side to the right hand side to simulate the movement of slurry from the one vessel to the other. The load cell output is logged at each loading condition together with the applied force values.

The calibration equation is then derived by performing a linear regression on the applied force values and the average of the transducer readings in each case.

3.3.3 Magnetic flow meters

The magnetic flow meters on the East and Mini Rigs produce a direct current signal which is linear with the flow rate through the meter. The transducer signal is digitised by a data logger. Due to the fact that the magnetic flux lines can never be perfectly parallel, the output can be influenced by the velocity profile (Heywood et al, 1993a). The approach has therefore been to calibrate the meters with the test slurry over the complete test range. This is the only method of ensuring accurate readings over the

laminar, turbulent and transition regimes (Mehta, 1993).

The following procedure was adopted for calibrating the magnetic flow meters.

1. The pump speed was set at the desired speed.
2. The weigh tank scale reading was noted (M_1).
3. The diverter valve was opened and the stopwatch and data logger started at the same time.
4. When sufficient slurry has been collected in the weigh tank, the diverter valve was closed and the stopwatch and data logger stopped at the same time.
5. The weigh tank scale reading was noted (M_2).

For the Mini Rig, which emptied continuously into the weigh tank, the time taken to collect a given mass of slurry was noted, together with the average transducer output.

The flow rate for each reading is therefore

$$Q = \frac{(M_2 - M_1)}{\rho\ t} . \qquad (3.6)$$

The calibration equation is then derived by performing a linear regression on the flow rate and the average of the transducer readings in each case.

Figure 3.7, a typical calibration, shows that there was no difference between the laminar and turbulent flow data when calibrated in this way.

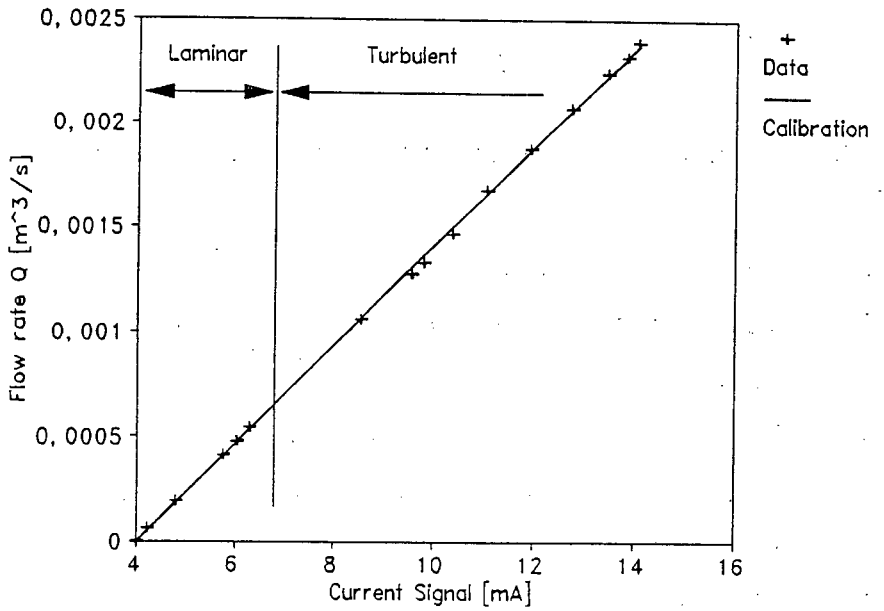

Figure 3.7 : Calibration of the Mini Rig Magnetic Flow Meter, showing both laminar and turbulent data. Kaolin slurry S_m=1,07.

3.3.4 Differential pressure transducer (BBTV)

The following procedure is used to calibrate the differential pressure transducer (DPT) on the BBTV.

1. Air and solids are flushed from all the lines.
2. A differential head is set up in the glass mercury/water manometer tubes using the control valves.
3. This head is physically measured and the DPT output is logged at the same time.
4. The differential head is then changed and the process repeated.

The pressure difference is given by

$$\Delta p = (S_{Hg} - S_w)\, \rho_w\, g\, H \,. \qquad (3.7)$$

The calibration equation is obtained by performing a linear regression on the pressure difference and transducer readings.

3.3.5 Differential pressure transducer (East and Mini Rigs)

The following procedure is used to calibrate the DPT on the East and Mini Rigs.

1. Air and solids are flushed from all the lines.
2. A differential head H is set up in the glass air over water manometer tubes.
3. This head H is physically measured and the DPT output is logged at the same time.

The calibration equation is obtained by performing a linear regression on the measured head and transducer readings.

3.4 OTHER MEASURED VARIABLES

3.4.1 Slurry Density

This investigation is concerned with non-Newtonian slurries and the density (and concentration) distribution is taken to be uniform. Slurry density (ρ) and relative density (S_m) are determined by performing the following steps.

1. A clean, dry one litre volumetric flask is weighed (M_1).
2. A slurry sample was taken in the volumetric flask from a tapping in the pipe wall on a vertical section above the pump. The volume of slurry taken is approximately 990ml
3. The flask plus slurry are weighed (M_2).
4. The flask is filled with water up to the graduated mark and weighed (M_3).
5. The flask is emptied, filled with clear water and weighed again (M_4).

The relative density S_m is defined as

$$S_m = \frac{\rho}{\rho_w} \quad , \tag{3.8}$$

which can be restated as

$$S_m = \frac{\text{mass of slurry sample}}{\text{mass of equal volume of water}} = \frac{M_2 - M_1}{(M_3 - M_2) - (M_4 - M_1)} \quad . \tag{3.9}$$

S_m is calculated using Equation (3.9) and ρ is calculated from

$$\rho = S_m \, \rho_w \quad . \tag{3.10}$$

3.4.2 Solids Relative Density

The relative density of the solids (S_s) is determined using test method 6B for fine grained soils from BS 1377 (1975).

3.4.3 Internal Pipe Diameter

The internal pipe diameter (D) is determined by measuring the mass of water (M_w) required to fill a known length of pipe (L). The diameter is then calculated from

$$D = \sqrt{\frac{4 \, M_w}{\pi \, \rho_w \, L}} \quad . \tag{3.11}$$

3.4.4 Slurry Temperature

The temperature of the slurry is measured by dipping a mercury thermometer into the slurry in the hopper. Essentially the slurry was maintained at a temperature of approximately 20°C. During the tests the temperature would rise by approximately 2°C. If the temperature rise was more than this, data at the extreme temperatures was compared. No temperature effects were found.

3.4.5 Particle Size Distributions

The particle size distributions were determined using a Malvern 2600/3600 Particle Sizer VF.6. The calibration of the instrument was confirmed using standard calibration particles. The instrument has three lenses and produces particle size distributions based on particle volume in the range $1{,}2\mu m < d < 564\mu m$.

It should be noted that the particle size distributions produced by the Malvern instrument do not necessarily agree with those obtained by other methods. Any comparison of particle size distributions should therefore be undertaken with due caution.

3.5 DERIVED VARIABLES

The following variables are derived from the measured variables.

3.5.1 Average Slurry Velocity

The average or mean slurry velocity (V) is defined as the volumetric flow rate (Q) divided by the cross sectional area (A) of the pipe and is calculated (also using (3.6)) from

$$V = \frac{Q}{A} = \frac{4\,Q}{\pi\,D^2} = \frac{4\,M}{\pi\,\rho\,t\,D^2}\,, \qquad (3.12)$$

where M is the mass of slurry of density ρ collected in the weigh tank in time t seconds.

3.5.2 Wall Shear Stress

The wall shear stress (τ_0) is determined from the water manometer head difference (H) over a known length of pipe (L), ie, the test section, as follows

$$\tau_0 = \frac{\rho_w \, g \, H \, D}{4 \, L} \, . \qquad (3.13)$$

3.5.3 Pipe Roughness

The hydraulic pipe roughness (k) is determined from tests using clear water in each pipe size. Mean velocity and wall shear stress are measured for velocities over the full test range and roughness is determined using the Colebrook White equation

$$\frac{1}{\sqrt{f}} = -4 \log \left[\frac{k}{3,7 \, D} + \frac{1,26}{Re \sqrt{f}} \right] \, . \qquad (3.14)$$

This procedure establishes the Colebrook White equation as the standard for pipe roughness.

3.6 EXPERIMENTAL ERRORS

Whenever scientific experimental work is done, it is important to quantify the magnitude of the errors associated with the measured data and computed results. These errors are presented below.

3.6.1 Differential Pressure Transducer (DPT)

The error in the measurement of head using the DPT was taken as the largest residual error from the calibrations, which was 1mm of water head.

3.6.2 Density and Relative Density Measurements

The errors in the individual measurements of density and relative density using a chemical balance were extremely small and were not taken as representative of the true errors involved in this measurement. Several relative density measurements were performed on each slurry, and the largest difference in these measurements was taken

as being more representative of the true error. The largest error in such measurements was found to be 0,4%.

3.6.3 Slurry Temperature

The error in the measurement of slurry temperature was 0,2°C.

3.6.4 Particle Size Distributions

In order to obtain a measure of the error in the particle size distributions as measured on the Malvern instrument, Coulter calibration latex spheres were tested in the Malvern instrument. The d_{50} size from the Malvern was compared to the number peak split from the calibration standard assay sheet value. The error was 6,7%.

3.7 COMBINED ERRORS

When a quantity involves more than one independent measurement, then the errors will combine in the following way. Errors are usually assumed to be randomly distributed following the Gaussian distribution and can be quantified using the procedure recommended by Brinkworth (1968). The highest expected error can be determined using a root mean square approach.

If a quantity X is a function of N other quantities ie:

$$X = \Phi (a, b, c, \ldots\ldots N) , \tag{3.15}$$

then the highest expected error ΔX can be calculated from

$$\left[\frac{\Delta X}{X}\right]^2 = \sum \left[\frac{\partial X}{\partial N}\right]^2 \left[\frac{N}{X}\right]^2 \left[\frac{\Delta N}{N}\right]^2 . \tag{3.16}$$

This error analysis has been used to quantify the following errors.

3.7.1 Pipe Diameter

Pipe diameter is calculated using Equation (3.11). The highest expected error is calculated from

$$\left[\frac{\Delta D}{D}\right]^2 = \left[\frac{1}{2}\sqrt{\frac{4}{\pi\,\rho_w\,M_w\,L}}\;\frac{M_w}{D}\;\frac{\Delta M_w}{M_w}\right]^2 + \left[-\frac{1}{2}\sqrt{\frac{4\,M_w}{\pi\,\rho_w\,L^3}}\;\frac{L}{D}\;\frac{\Delta L}{L}\right]^2 \qquad (3.17)$$

The highest expected errors for the East and Mini rig pipes are given in Table 3.I.

Table 3.I

Pipe Diameter D [mm]	Measurement Error ΔD/D [%]
5,623	0,078
13,21	0,022
21,60	0,050
78,99	0,017
140,5	0,017
207,0	0,017

3.7.2 Wall Shear Stress Errors

The wall shear stress τ_0 is calculated using Equation (3.13). The highest expected error is calculated from

$$\left(\frac{\Delta\tau_0}{\tau_0}\right)^2 = \left(\frac{\rho_w\, g\, H}{4\, L}\,\frac{D}{\tau_0}\,\frac{\Delta D}{D}\right)^2 + \left(\frac{D\,\rho_w\, g}{4\, L}\,\frac{H}{\tau_0}\,\frac{\Delta H}{H}\right)^2 + \left(-\frac{D\,\rho_w\, g\, H}{4\, L^2}\,\frac{L}{\tau_0}\,\frac{\Delta L}{L}\right)^2 \qquad (3.18)$$

The errors in diameter are given above for each pipe size, ΔH was taken as the largest residual from the calibration which was 1mm and ΔL was 1mm.

The highest expected errors are plotted on logarithmic axes below.

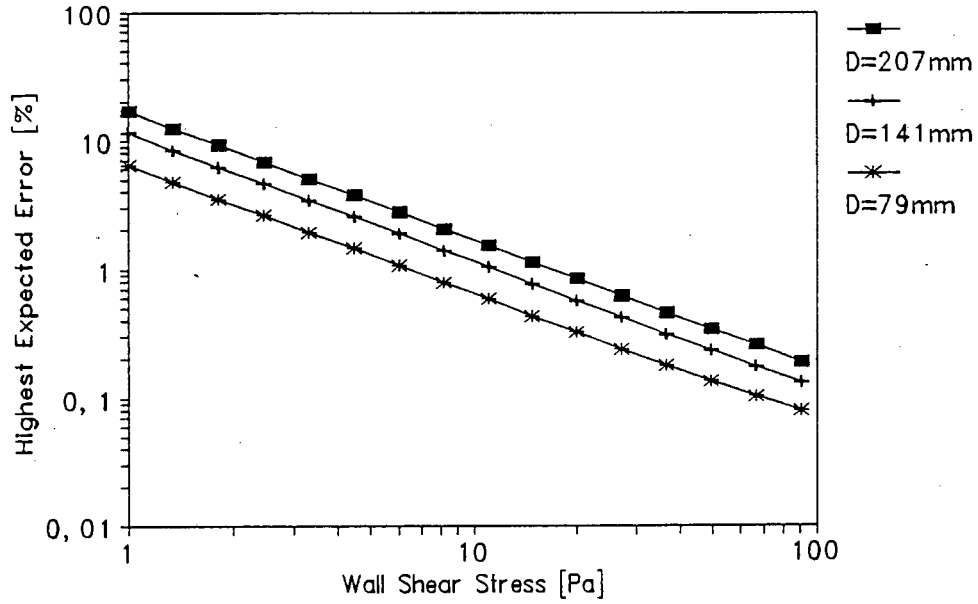

Figure 3.8 : Wall Shear Stress Errors - East Rig.

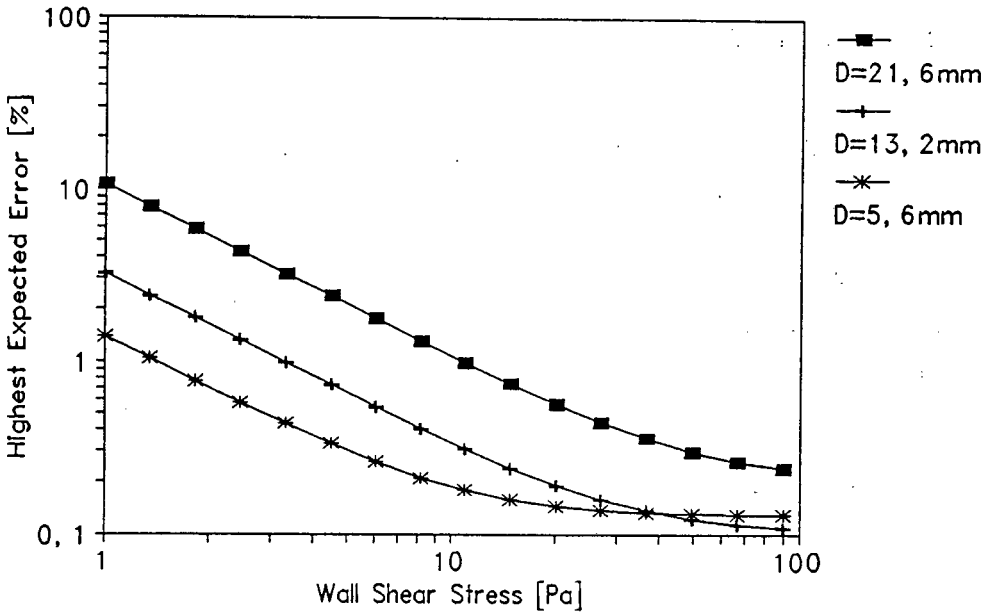

Figure 3.9 : Wall Shear Stress Errors - Mini Rig..

3.7.3 Pseudo-Shear Rate Errors

The pseudo-shear rate G=8V/D is calculated using

$$G = \frac{8\,V}{D} = \frac{32\,M}{\pi\,\rho\,t\,D^3}\,, \tag{3.19}$$

where M is the mass of slurry collected in the weigh tank in time t seconds.

The highest expected error is calculated from

$$\left[\frac{\Delta G}{G}\right]^2 = \left[\frac{32}{\pi\,\rho\,t\,D^3}\,\frac{M}{G}\,\frac{\Delta M}{M}\right]^2 + \left[-\frac{32\,M}{\pi\,\rho^2\,t\,D^3}\,\frac{\rho}{G}\,\frac{\Delta\rho}{\rho}\right]^2 + \left[-\frac{32\,M}{\pi\,\rho\,t^2\,D^3}\,\frac{t}{G}\,\frac{\Delta t}{t}\right]^2 + \left[-\frac{96\,M}{\pi\,\rho\,t\,D^4}\,\frac{D}{G}\,\frac{\Delta D}{D}\right]^2 \quad (3.20)$$

ΔM for the weigh tank scale was 250g, $\Delta\rho/\rho$ as given above was 0,4%, Δt was 0,1s and the errors in diameter are given in Table 3.I for each pipe size.

The highest expected errors are plotted below.

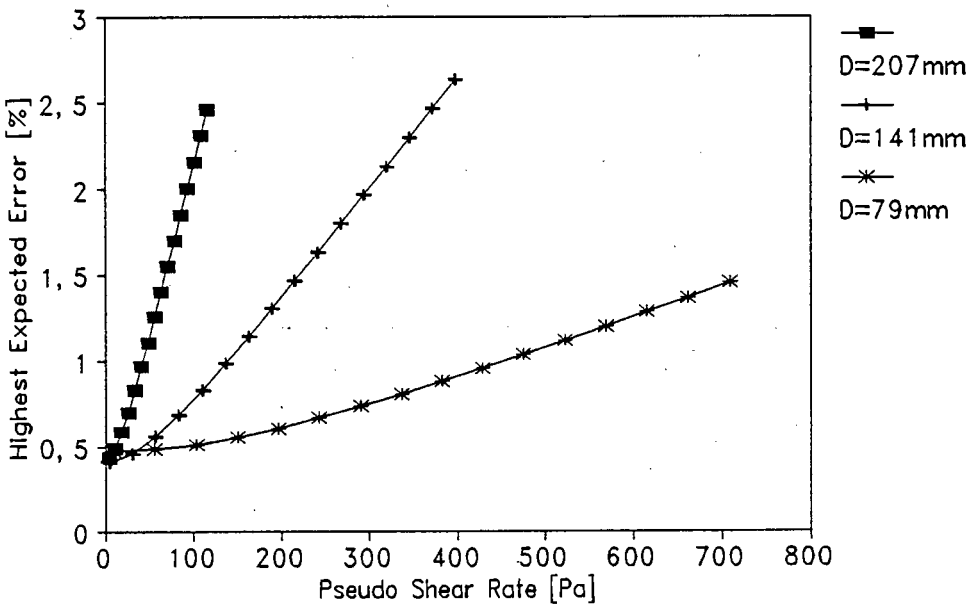

Figure 3.10 : Pseudo-Shear Rate Errors - East Rig.

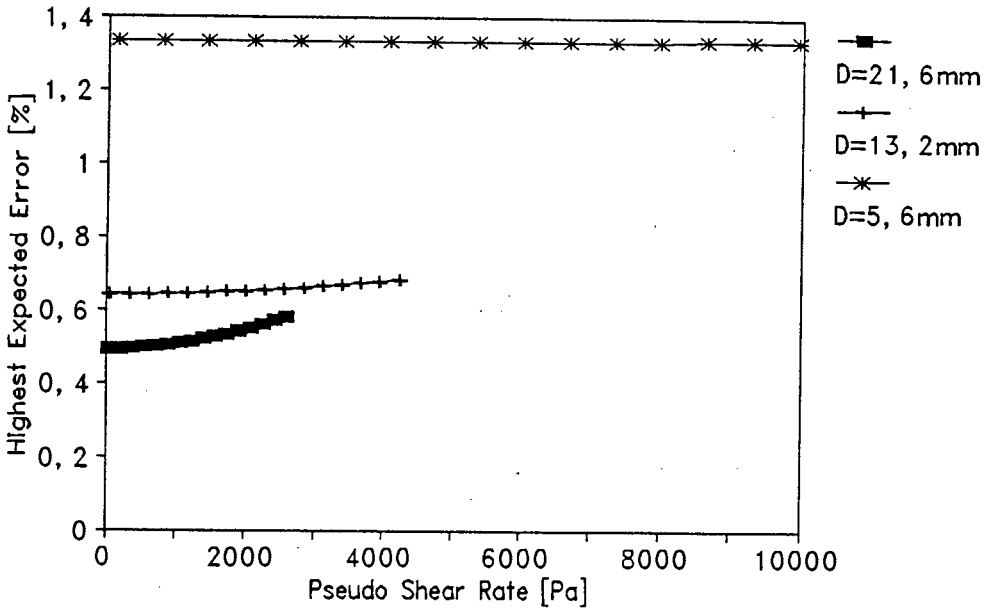

Figure 3.11 : Pseudo-Shear Rate Error - Mini Rig.

3.7.4 Pipe Roughness

The pipe roughness was determined using clear water pipeline tests over the full velocity range. The errors are summarised in Table 3.II.

Table 3.II

Diameter [mm]	Roughness [μm]	Error [μm]
5,623	1	1
13,214	3	1
21,60	4	1
79,00	9	1
140,5	13	2
207,0	112	6

3.7.5 BBTV Errors

The errors pertaining to the BBTV were given by Neill (1988). The highest expected errors are summarised in Table 3.III.

Table 3.III

Diameter [mm]	Diameter Error [%]	Velocity Error [%]	Shear Stress Error [%]
32,63	0,0026	1,46	0,803
28,38	0,0026	1,46	0,803
13,37	0,0034	1,47	0,803
4,20	0,0815	1,62	0,882

3.8 EXPERIMENTAL PROCEDURE

The experimental test procedures pertaining to each apparatus are presented in this section.

3.8.1 The Balanced Beam Tube Viscometer. (Slatter, 1986 and Neill, 1988)

The following procedure is followed to run a test on the BBTV.

1. The power is switched on and the vessels each half filled with slurry. The slurry is then pumped from vessel to vessel several times to ensure good mixing.

2. A sample of approximately one litre is taken for relative density and particle size distribution tests. The instruments are all calibrated.

3. The pods are connected to the tappings and the pressure measuring system (Figure 3.6) flushed of air and solids.

4. The vent valve on the full vessel side is closed and the vent valve opened on the empty vessel side. The high/low selectors for the DPT are set for the flow direction.

5. The air pressure regulator is set to the desired pressure and the full vessel pressurised. The tube valve is opened and the data logger started. The data logger will collect readings from the load cell and DPT at specified time intervals.

6. At the end of the run, the tube valve is slowly closed, avoiding shock waves (water hammer).

The data is then processed yielding a data point of $\{V; \Delta p\}$. The run is repeated until sufficient data points have been acquired.

3.8.2 The East Rig

The following procedure is followed to run a test on the East Rig.

1. Water or solids are loaded into the hopper until the required density is attained. All supplies are switched on. The slurry is pumped at the highest pump speed through all the pipes simultaneously to ensure thorough mixing.

2. A slurry relative density test is performed and the DPT is calibrated. The pods are connected to the selected pipe's pressure tappings.

3. The data logging programme is loaded and initialised.

4. The pump is set at the required speed and the data logging routine started. The magnetic flow meter and DPT outputs are logged for three to five minutes and checked for drift (Sive, 1988).

Timed weigh test samples are taken at intervals during the test for the calibration of the magnetic flow meter.

The run is repeated at different pump speeds until sufficient data has been collected. The data is then processed.

3.8.3 The Mini Rig

The following procedure is followed to run a test on the Mini Rig. The Mini Rig tests are normally done during or straight after the East Rig tests. The slurry is circulated at moderate speed in the East rig and slurry is then tapped from the 150mm nominal bore line into the Mini Rig on a continuous basis during the Mini Rig tests. This is done to ensure that exactly the same slurry is tested in all six pipe diameters.

1. The required test section is fixed into the Mini Rig and the pods are connected to the tube's pressure tappings.

2. The data logging programme is loaded and initialised.

3. The pump is set at the required speed and the data logging routine started. The magnetic flow meter and DPT outputs are logged for three to five minutes and checked for drift (Sive, 1988).

The Mini Rig empties continuously into the weigh tank and timed weigh test samples are taken at intervals during the test for the calibration of the magnetic flow meter.

The run is repeated at different pump speeds until sufficient data has been collected. The data is then processed.

A slurry relative density test is performed after the pipeline tests to ensure that the slurry density has remained constant.

3.9 MATERIAL

The following solids materials were used to make up the slurries for the tests.

3.9.1 Kaolin

Kaolin slurries were prepared from dry kaolin powder and pellets which were mixed with tap water to the required concentration and tested in the BBTV and the East and Mini Rigs. Although all the material was obtained from the same deposit, the particle size distributions differed slightly (detailed particle size distributions are given in Appendix A).

3.9.2 Uranium Tailings

Uranium mining tailings slimes slurries were obtained wet from the Rössing mine in Namibia. Various size fractions were obtained by mechanical sieving :

Slurry 1	$d < 100\ \mu m$
Slurry 2	$d < 250\ \mu m$

These slurries were then tested in the BBTV (Slatter, 1986).

3.9.3 Gold Slimes Tailings

Various size fractions were obtained by mechanical sieving :

Tailings 1	$d < 500\ \mu m$
Tailings 2	$d < 106\ \mu m$
Tailings 3	$d < 62\ \mu m$
Tailings 4	$d < 42\ \mu m$.

These slurries were then tested in the BBTV (Neill, 1988).

3.9.4 Tap Water

The tap water had a pH of 9, was slightly super saturated with respect to calcium carbonate (2 mg/l), total alkalinity was 35 mg/l as $CaCO_3$, total calcium was 35 mg/l as $CaCO_3$ and ionic strength was less than 0,001 (molar scale) (Loewenthal, 1994). Although the resulting mixtures were regarded as chemically stable, it should be noted that the rheology of these slurries can change with their ionic character. For this reason, tests on a given slurry were carried out on the same day. The time available for any chemically related rheology changes was therefore kept to a minimum.

3.10 RESULTS AND DISCUSSION

The results are presented in Appendix A. Each pipe test is presented using three tables and a pseudo-shear diagram.

The first table gives the test code, apparatus and material description, and operator details.

The second table gives the slurry properties : solids relative density (S_s), slurry relative density (S_m), volumetric concentration (C_v), yield stress (τ_y), fluid consistency index (K), flow behaviour index (n) and the representative particle size.

The third table gives the analysis results for Chapters 4 and 6. The turbulent flow data is compared with the theoretical predictions for each model.

The pseudo-shear diagram shows each data point graphically. In addition the theoretical model lines are shown on the data, providing a visual appraisal of the performance of each model.

3.10.1 Pipeline Tests

The test data from the BBTV and the pipeline rigs can be grouped into test sets. A test set is defined as the group of tests that were performed on the same slurry, but using a different pipe diameter for each test. A test set can be plotted as wall shear stress [DΔp/4L] vs pseudo-shear rate [8V/D], called a pseudo-shear diagram. A typical pseudo-shear diagram is shown in Figure 3.12.

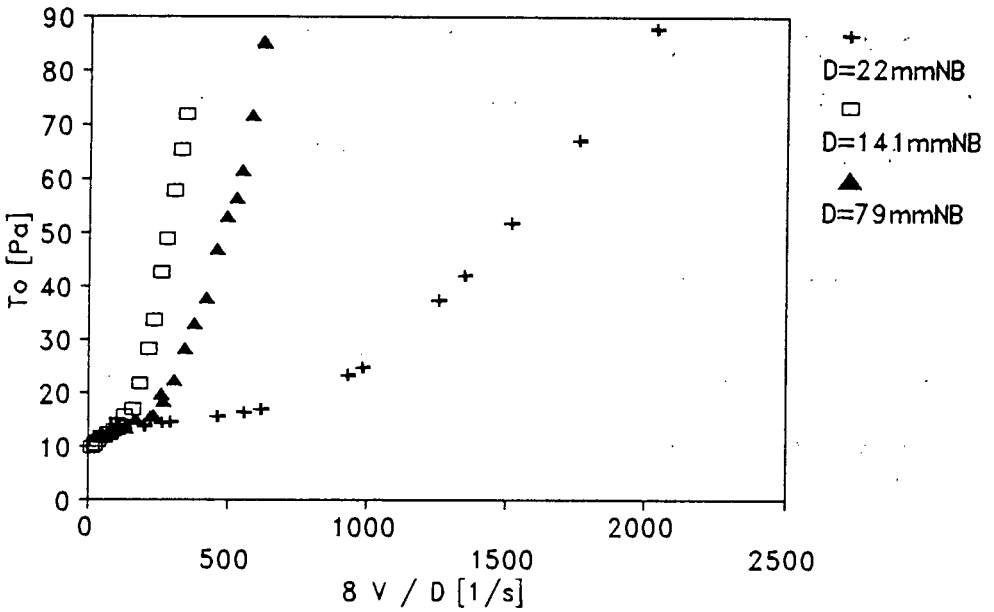

Figure 3.12 : Typical Results ; Kaolin slurry ; $S_m = 1,13$; Test set 09.

This diagram shows graphically the change in behaviour between the laminar and turbulent regimes. The locus of the viscous data in the laminar region is coincident for the different tube diameters and the rheological constants (τ_y, K and n) can be determined from the data in the laminar region of the smaller diameter pipes (rheological characterisation).

The change in behaviour from laminar to turbulent flow is visible by observation of the slurry particles in the transparent tubes during testing. The differential pressure transducer output also shows significantly more variation in the transition region during a test. This evidence supports the notion that true turbulence is indeed occurring. The critical point at which turbulence begins for each tube size can be

clearly seen on the pseudo-shear diagram and the critical velocity is thus determined as the intersection of the laminar and turbulent data loci.

3.10.2 The Influence of Diameter

As can be seen in Figure 3.12, pipe diameter has no influence on wall shear stress at a given pseudo-shear rate in the laminar regime. This shows that the slurry properties were time independent over the time duration of the tests (one day). Some of the tests in the larger pipe sizes show a slight deviation from the theoretical laminar flow line. This is probably due to the velocity profile effect (Heywood et al, 1993a) together with the fact that the transducers were reading at the bottom of their range and the cumulative wall shear stress experimental error increases as the shear stress decreases (Section 3.7.2), and not time dependency.

The laminar/turbulent critical point occurs at lower pseudo-shear rates for larger diameter pipes than for smaller diameter pipes. The locus of turbulent data diverges from the laminar line at this point in each case. This is very much in keeping with typical data from the literature (eg Bowen, 1961).

3.10.3 The influence of concentration

The influence of concentration on laminar flow is to increase the wall shear stress, because the viscous forces increase with an increase in concentration. In turbulent flow, however, an increase in concentration produces no significant increase in the wall shear stress.

Figure 3.13 shows these two points clearly. There is a marked increase in the laminar flow wall shear stress with increase in concentration, while the turbulent flow behaviour remains virtually unaffected by concentration and the resulting significant change in rheology. This data confirms the findings of Bowen (1961) and Harris & Quader (1971).

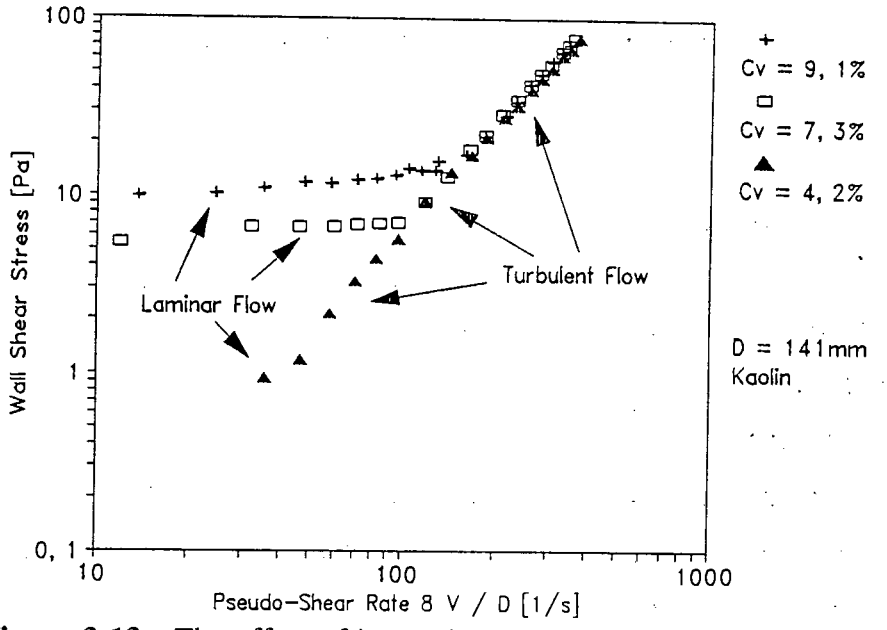

Figure 3.13 : The effect of increasing the concentration of a kaolin slurry.

3.10.4 Settling and Homogeneity

A broad band of impurities could be seen on the pipe invert during most of the tests. In order to ensure that there was no concentration distribution across the vertical section of the pipes, relative density tests were performed on samples taken from the pressure tappings, near the top of the pipe and compared with values obtained from samples taken from the vertical (well mixed) section above the pump. No difference was detected. There was no visible settling at the top of the pipes or in the hopper during tests. It was therefore assumed that all the slurries tested could be analysed as homogeneous suspensions.

3.10.5 Particle Size Distributions

The particle size distributions are given in Appendix A. The solid particles of these slurries are known to congregate into flocs, which must be broken down so that true particle size and not the floc size is measured. This is normally achieved by the dilution which is necessary during particle size measurement in the Malvern instrument. In order to check that deflocculation had indeed occurred, the same

samples were retested after addition of a surfactant (calgon) and also after extended ultrasound agitation. No significant changes were observed. It was therefore assumed that true particle size was measured (Knight, 1993).

3.11 CONCLUSIONS

Apparatus for the reliable collection of pipeline test data for non-Newtonian slurries over wide ranges of pipe diameter and velocity in both the laminar and turbulent regimes was constructed and commissioned using clear water tests. The three facilities used for this thesis were the Balanced Beam Tube Viscometer (BBTV), the East Rig and the Mini Rig. This apparatus has been fully described and its use has enabled testing of the same slurry over wide ranges of both laminar and turbulent flow.

Calibration and test procedures have been developed for the apparatus so that valid and accurate pipeline data can be collected and the relevant slurry properties can be measured.

The experimental errors pertaining to the apparatus and measurement techniques have been analysed and quantified and are within acceptable limits.

The solids materials used for the slurry preparation were kaolin clay, and uranium and gold mining tailings slimes. Different size ranges were obtained by mechanical sieving. A varied range of slurry properties was therefore obtained.

These slurries were then tested in the apparatus and a data base of non-Newtonian slurry pipeline test data over wide ranges of both the laminar and turbulent regimes was compiled. The test results are presented in Appendix A. Details of the apparatus test conditions and slurry properties are presented for each test, together with a graphical presentation of wall shear stress (τ_0) against pseudo-shear rate (8V/D) for the test data. These graphs show the laminar and turbulent regimes for each test, and the critical point at which the laminar flow changes to turbulent flow can be established from these graphs.

The locus of turbulent data leaves the laminar line (locus of laminar data) at lower velocities

with increase in diameter. An increase in concentration produces a significant increase in the laminar wall shear stress, but no significant change in the turbulent flow behaviour.

This data base was then used to evaluate models for the prediction of the behaviour of non-Newtonian slurries in pipes. This has been done in Chapter 4.

CHAPTER 4

CHAPTER 4

ANALYSIS OF RESULTS USING MODELS FROM THE LITERATURE

4.1 INTRODUCTION

The purpose of this chapter is to analyse the pipeline test data using the theoretical models presented in Chapter 2. Since these models all require the rheological parameters, the first step in the analysis of the data is to rheologically characterise the data from the laminar flow regions for each slurry.

The rheological characterisations are then used to analyse the test data base using the various laminar/turbulent and turbulent flow models.

4.2 RHEOLOGICAL CHARACTERISATION

The rheological characterisation procedure consists of using the data points in laminar flow from the small diameter tubes from the test data (co-ordinates of $\{\tau_0 ; 8V/D\}$) to extract the rheological constants τ_y, K and n as outlined in Chapter 2.

4.2.1 Sensitivity

The procedure optimises the values of the constants according to the least squares error function. The actual values of the rheological constants K and n are sensitive to the optimisation procedure as shown in Figure 4.1 below.

In practice, optimum values for K and n are determined for an arbitrarily selected τ_y value. This τ_y value is then adjusted until the error function E has been minimized. This procedure results in a least squares curve fit of Equation (2.13) to the laminar flow data.

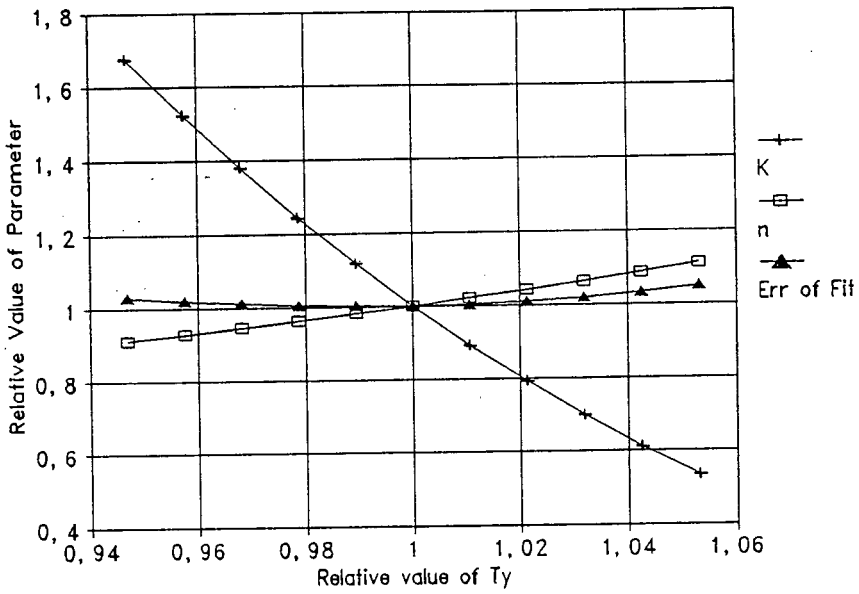

Figure 4.1 : Sensitivity of the Rheological Characterisation Procedure

Figure 4.1 shows the values of the constants and the error function, relative to the optimum values, for a typical slurry, as the value of τ_y is changed to minimise the error function and thus obtain the optimum values for τ_y, K and n.

This figure shows that a change of 2% in the τ_y value produces a change of more than 20% in the K value and 5% in the n value. This sensitivity of the rheological parameters τ_y, K and n during the model fitting process is in keeping with the findings of Al-Fariss & Pinder (1987).

It is important to note that other rheological models such as the power law and Bingham plastic models are not actively rejected in this process. For example, if the slurry is a Bingham plastic, then the n value of unity will be obtained. Similarly, if the slurry is a power law fluid, then the τ_y value of zero will be obtained.

The above procedure optimises the values of all three rheological constants (τ_y, K and n) for a best fit over the full laminar range available. The value of τ_y is not necessarily the true value at which solid/fluid behaviour changes. The BBTV is capable of measuring very low shear rates, and was used to try and determine the true value of τ_y experimentally (eg test KBBM18). As can be seen, the slurry continued

to shear at minute shear rates (less than 10 reciprocal seconds), showing no clear limiting value. Since the behaviour of the slurry at these very low shear rates is of little practical importance in slurry pipelining problems, this approach was abandoned and the best fit approach for the evaluation of τ_y was retained. Data points with a wall shear stress less than the assumed value for τ_y were therefore neglected. Although this procedure may result in some small error in τ_y, it will be considerably less than the error obtained by previous researchers using the Bingham plastic model (eg Valentik & Whitmore, 1967 and Xu *et al*, 1993).

4.2.2 Forced Fits

It is possible to force the procedure to fit either a pseudoplastic or a Bingham plastic. The data of Xu *et al* (1993) has been used to illustrate the forced fits. The laminar flow data from the 17% kaolin slurry (*op cit*) was fitted to Equation (2.13) in three different ways. The first fit was done without restriction and resulted in a yield pseudoplastic rheology. The second fit was forced to a pseudoplastic rheology by setting τ_y to zero and then obtaining the optimum values for K and n. The third fit was obtained by setting n to unity and then obtaining the optimum values for τ_y and K, forcing a Bingham plastic fit. The results of the forced fit are shown in the Table 4.I.

Table 4.I : Rheological Characterisation using Forced Fits

Model	τ_y [Pa]	K [Pa s^n]	n	E
Yield Pseudoplastic	7,040	0,2671	0,5880	0,66
Pseudoplastic	-	5,037	0,1723	0,86
Bingham Plastic	8,192	0,02779	1,000	0,76

The value of the error function E shows that the yield pseudoplastic model provides the best fit and is the most appropriate rheological model.

Figure 4.2 to Figure 4.4 show all the data from the 17% kaolin test (*op cit*) together with the theoretical laminar and Wilson & Thomas turbulent predictions.

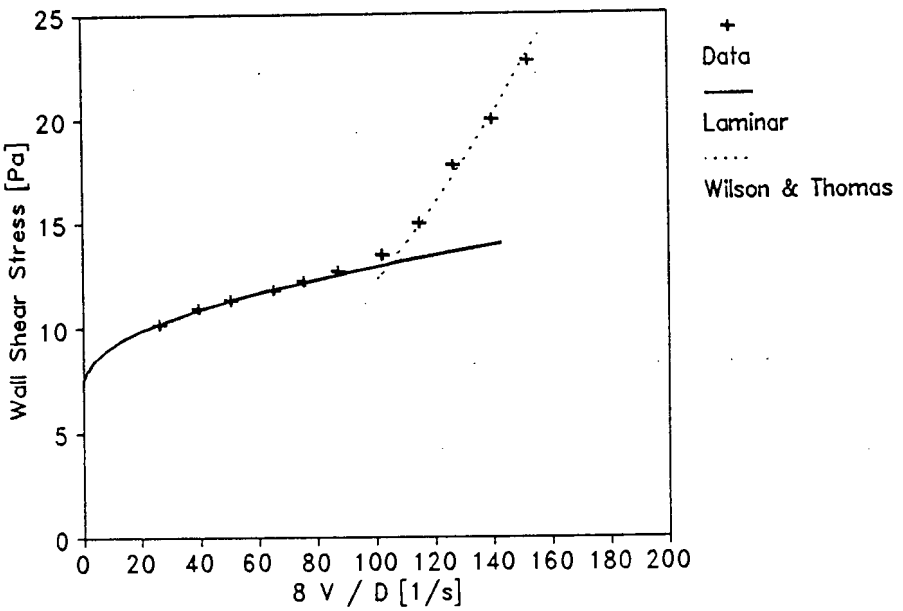

Figure 4.2 : Yield pseudoplastic fit (natural).

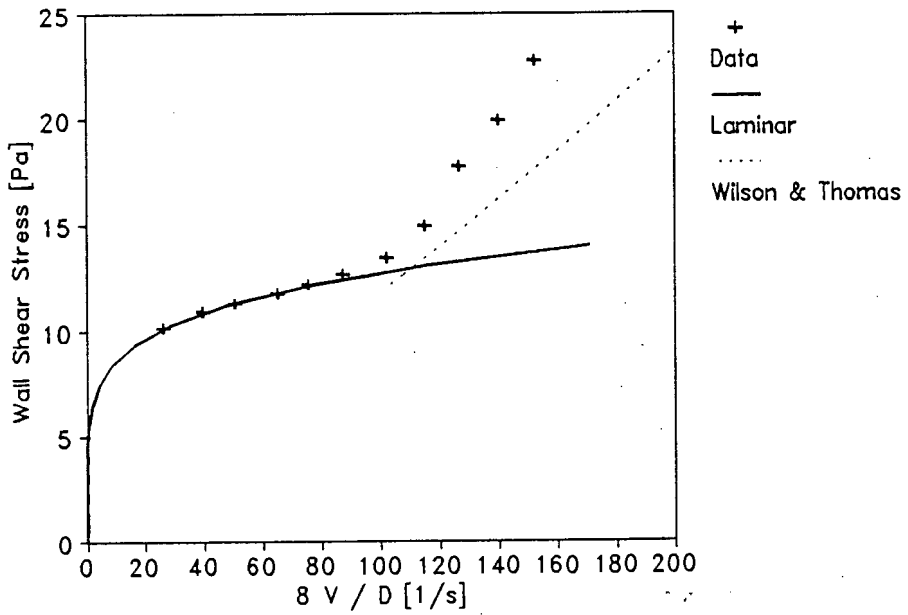

Figure 4.3 : Pseudoplastic forced fit.

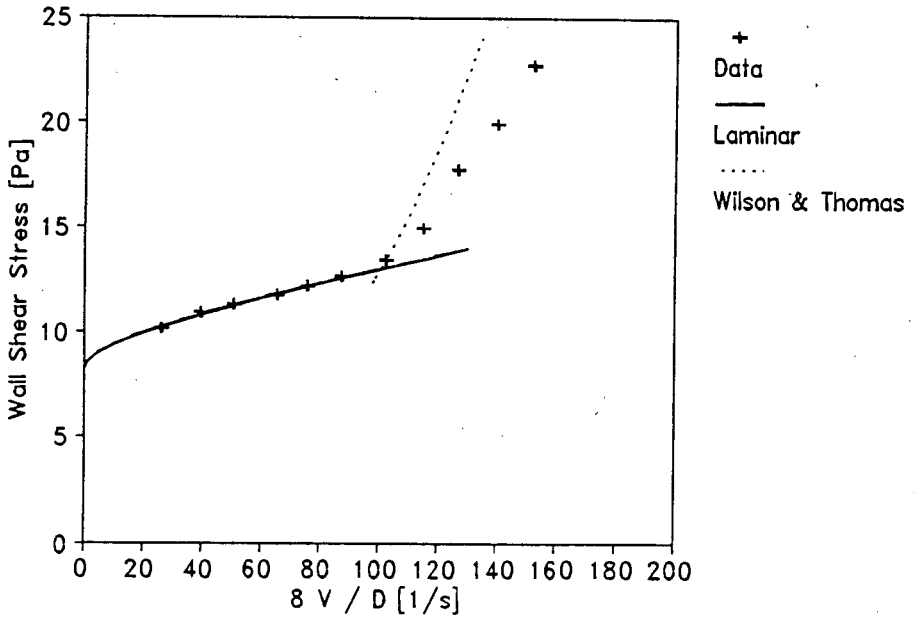

Figure 4.4 : Bingham plastic forced fit.

These results show that while the fit may seem acceptable over the laminar range considered, the extrapolation of the rheology into the turbulent flow regime will produce over prediction in the case of the Bingham plastic model and under prediction in the case of the pseudoplastic model.

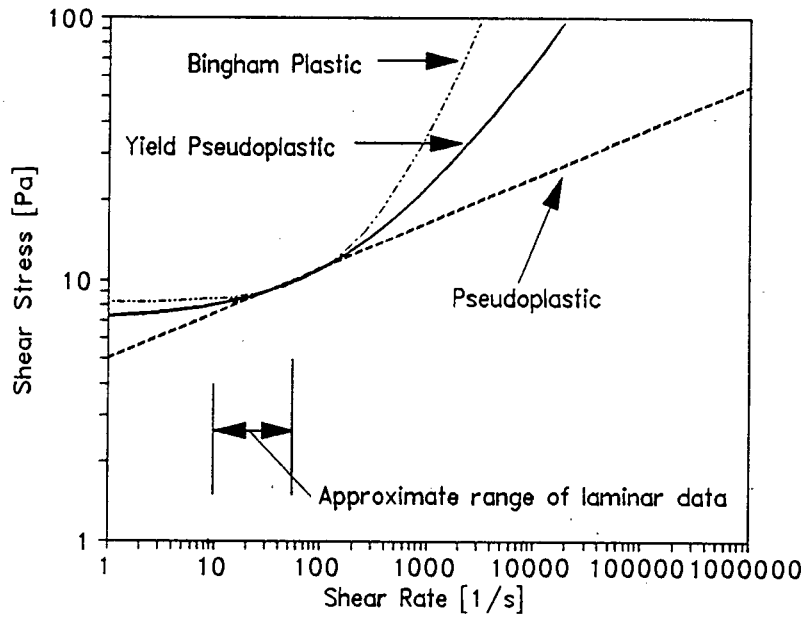

Figure 4.5 : Rheogram of forced fits - extrapolation to high shear rates.

Figure 4.5 shows the forced fit rheologies extrapolated to high shear rates so that shear stresses in the turbulent regime are covered. Quite clearly, order of magnitude differences in shear rate will occur in the laminar sub-layer in turbulent flow, dependent on which rheological model is used.

In the case of the yield pseudoplastic fit, both the laminar and Wilson & Thomas turbulent predictions show excellent agreement with the experimental data points.

The results of forcing in this way depends on what range of values is considered (Thomas & Wilson, 1987). Data over larger ranges of shear stress will show larger values of the error function, E, for inappropriate rheological models.

It should be noted that the solids relative density for kaolin of 2,4449 has been used for all calculations of the Xu *et al* data.

4.3 LAMINAR/TURBULENT TRANSITION

The laminar/turbulent transition data are presented in Appendix A together with the processed results for each model.

4.3.1 Results of Analysis Using Models from the Literature

The critical velocity and rheology for each test in the data base was used to determine the Reynolds numbers, stability criterion and intersection velocity in each case. A summary of these results is given in Table 4.II. The results have been reduced to average, standard deviation and range of the results in each case.

Table 4.II : Laminar/turbulent transition results

	Re_{Newt}	Re_{MR}	Re_{nn}	Z_{max}
Avg	5715	3268	10057	1336
Std Dev	2912	981	8535	526
Std Dev %	51	30	85	39
Min	2169	1516	2382	529
Max	12610	6451	40183	2685
Range	10441	4935	37801	2156
Range %	183	151	376	161

Intersection Method	Avg % Err	Std Dev	Max % Err
	16	12	43

The intersection velocity of the intersection method has been compared on a percentage error basis with the actual critical velocity.

4.3.2 Graphical Comparison of Models with Data

Graphical comparisons of the models from the literature with the three sets of data that cover the widest range of pipe diameter are presented in Figure 4.6 to Figure 4.8 .

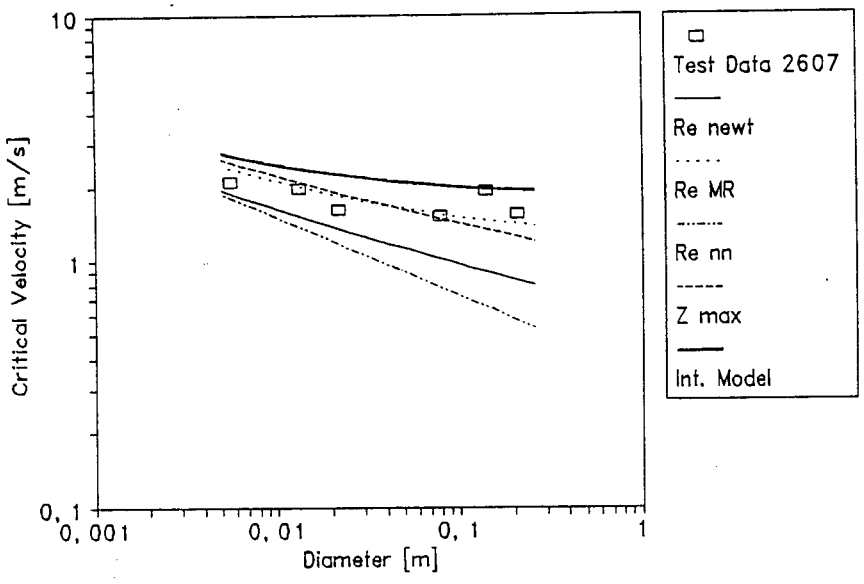

Figure 4.6 : Critical velocity vs pipe diameter - Data set 2607.

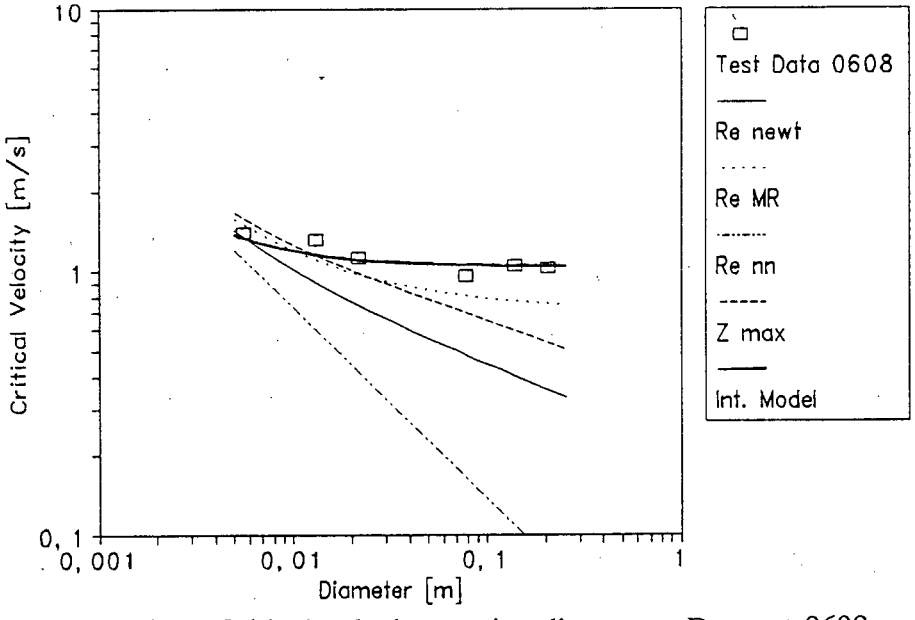

Figure 4.7 : Critical velocity vs pipe diameter - Data set 0608.

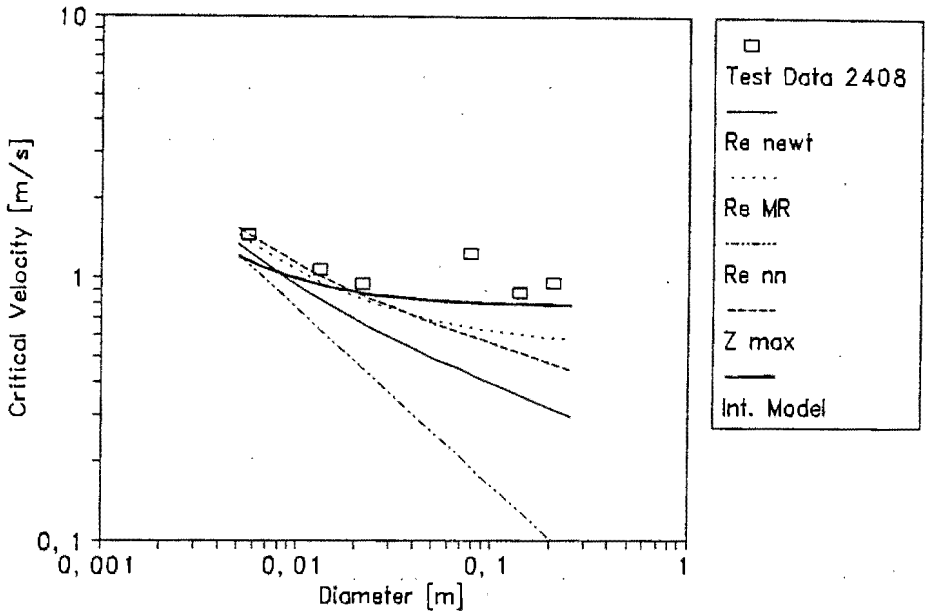

Figure 4.8 : Critical velocity vs pipe diameter - Data set 2408.

4.3.3 Discussion of Results

One of the objectives of this thesis is to provide a single laminar/turbulent transition criterion, similar to the Newtonian criterion (Re=2100). For the models to be successful, they should obtain values close enough to some fixed constant value so that the laminar/turbulent transition can be predicted with some degree of confidence.

The results in Table 4.II show that, of the Reynolds number formulations, the model of Metzner & Reed (1955) is the best, followed by the stability criterion and the Newtonian approximation. The Torrance Reynolds number (Torrance, 1963) does not predict the transition, probably due to the fact that the full rheology is not included (yield stress is excluded).

The graphical presentations in Figure 4.6 to Figure 4.8 confirm these observations and show that the data approaches a horizontal asymptote with increasing diameter. This effect was predicted by the Bingham plastic Reynolds number and is most likely due to the presence of a yield stress. The intersection method, and the Metzner Reed Reynolds number to a lesser extent, is able to predict this trend. It can also be seen that the intersection method becomes less accurate as the diameter decreases, while

all the other models become more accurate. The reason for this is that as the diameter decreases, the critical velocity increases, increasing the wall shear stress at the transition. This means that the velocity profile at the transition becomes closer to parabolic (Newtonian) as the pipe diameter decreases. The Reynolds numbers converge because they all revert to the Newtonian model under Newtonian conditions. The intersection method does not revert to the Newtonian model under Newtonian conditions and diverges from the data and the other models as the pipe diameter decreases.

An increasing trend is shown when the stability criterion, Z_{max}, at the experimental critical velocity for each test in the data base is plotted against the Hedström number, He, as shown in Figure 4.9 . This is clearly in opposition to the assumption that this value remains constant. This trend can also be found in the literature (eg Sajet, 1989, Bowen, 1961 and Hanks, 1963).

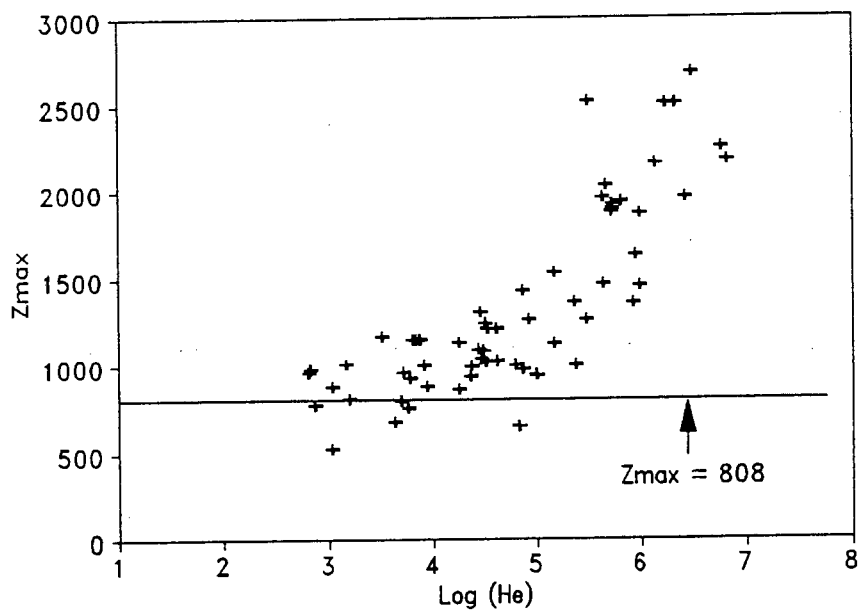

Figure 4.9 : Stability Criterion vs Hedström number.

The intersection method gives the overall best performance for the data base, but does not explain the behaviour of the slurry.

4.3.4 Sensitivity

The sensitivity of the Reynolds Numbers, the stability criterion and intersection method can be gauged by using the values given in Table 4.I (the values from the forced fits). The results of this analysis are shown in Table 4.III.

Table 4.III : Sensitivity of the Laminar/Turbulent Transition Models using the Forced Fit Data

	Re_{Newt}	Re_{MR}	Re_{nn}	Z_{max}	Intersection velocity [m/s]
Yield Pseudoplastic	5612	2929	9489	1214	2,10
Pseudoplastic	6514	2960	3391	1173	2,22
Bingham Plastic	5072	2904	13767	1256	2,02

These results show that, with the exception of the Torrance Reynolds number, Re_{nn}, the transition models are stable with respect to the rheological characterisation procedure, and are not sensitive to small changes in the rheological parameters. The probable reason for the sensitivity of Re_{nn} is the exclusion of the yield stress from the formulation.

4.4 TURBULENT FLOW

Full results of the pipeline tests are given in Appendix A. The analytical models of Torrance (1963 and Wilson & Thomas (1985) gave the most accurate predictions for the data base, and are used for the turbulent flow analyses.

Typical results are shown in Figure 4.10 .

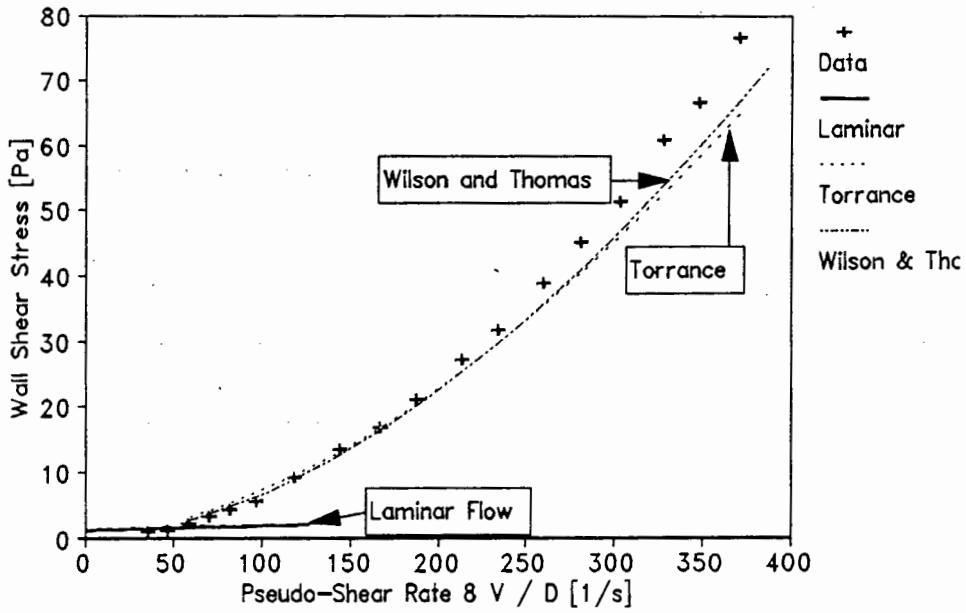

Figure 4.10 : Typical Results showing divergence of the models
Test KERM2408

The turbulent flow predictions of both Wilson & Thomas and Torrance are similar and give good results in the early turbulent region. This is probably due to the accurate measurement of rheology. However, their models diverge from the data at higher flow rates. This is in agreement with the reported trends of other researchers (Mun, 1988 and Xu *et al*, 1993).

4.4.1 Turbulent Model Performance

The accuracy of the turbulent flow model predictions can be gauged by the respective lines shown on the pseudo-shear diagrams for each pipe test in Appendix A. A more objective measure is provided by the average percentage error and the log standard error for the turbulent data in each test. The log standard error, LSE, was found to be useful for such comparisons by Lazarus & Neilson (1978) and is defined as

$$LSE = \frac{\sqrt{\sum \left[\log (\tau_{0\,obs}) - \log (\tau_{0\,calc}) \right]^2}}{N - 1} . \qquad (4.1)$$

Each pipe test sheet in Appendix A contains a table giving the turbulent model performance for the turbulent data of that test. Table 4.IV shows the overall turbulent

model performance for all turbulent data points in the data base.

Table 4.IV Turbulent Model Evaluation - Whole Data Base.

	Torrance	Wilson & Thomas
Average % Error	17,18	15,07
Log Standard Error	0,0050	0,0038

The results in Table 4.IV show that the Torrance model gives an average error of 17% and an LSE of 0,005, while the Wilson & Thomas model is more accurate with an average error of 15% and an LSE of 0,0038. The reason for the relatively good performance of these models compared to the errors reported in Chapter 1 is probably due to accurate rheological characterisation. However, divergence of the models from the data loci at higher shear stresses indicates that these models do not adequately describe the turbulent behaviour of the slurries.

4.4.2 Laminar Sub-layer Thickness

The laminar sub-layer thicknesses predicted by the Newtonian approximation and the model of Wilson & Thomas (1985) are shown in Figure 4.11 , for typical slurry values [density=1200kg/m^3; τ_y=5,0921Pa; K=0,3008Pa s^n; n=0,4832].

Figure 4.11 shows that the thickness of the laminar sub-layer is of the same order of magnitude as the larger particles in the slurries (50-100μm) over the range of wall shear stress tested in the data base. Since the larger particles will be larger than the thickness of the laminar sub-layer at the higher wall shear stress values, the particles must therefore have an obstructing effect on the laminar sub-layer, thus influencing the turbulent behaviour.

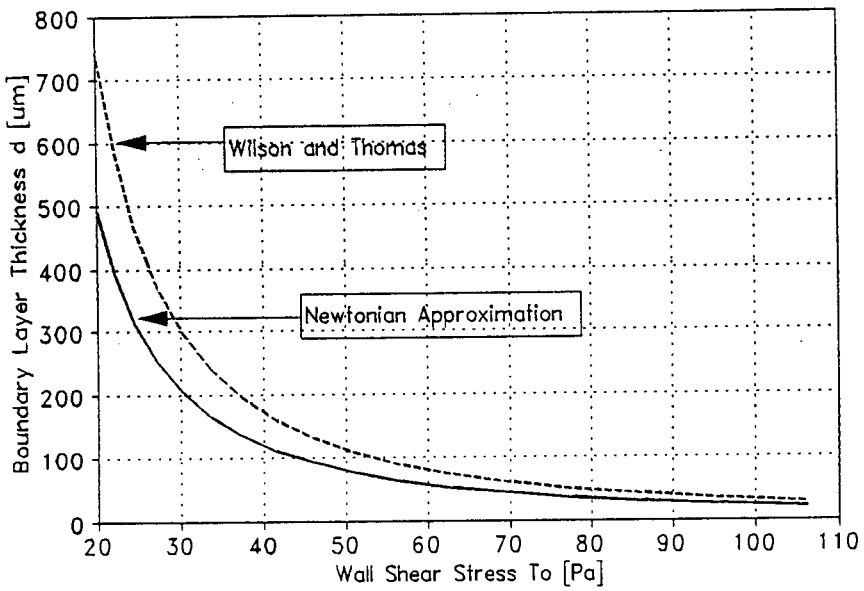

Figure 4.11 : Boundary layer thickness.

4.4.3 Velocity Profiles

The velocity profiles for the two models are shown below

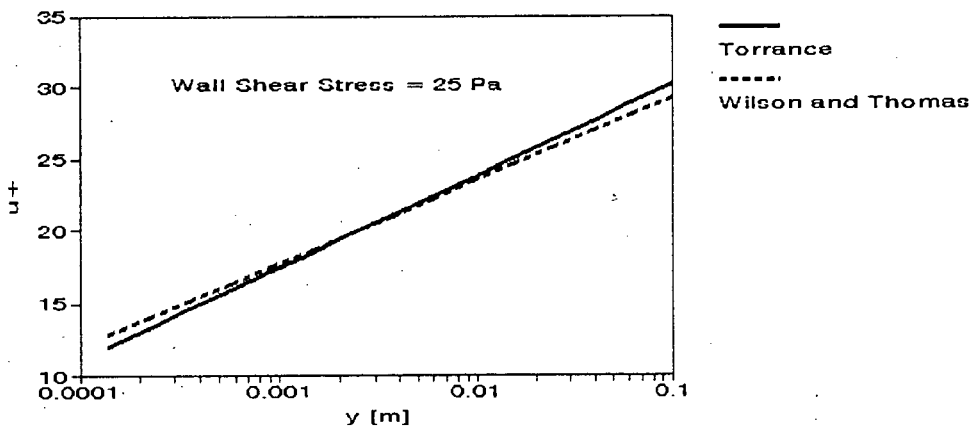

Figure 4.12 : Velocity Profiles for Turbulent Flow.

The difference in slopes can be seen due to the inclusion of the rheology in the von Karman constant by Torrance.

4.4.4 Torrance Rough Wall Model

By analogy with Newtonian turbulent flow, a rough wall model should produce higher shear stresses than the corresponding smooth wall model, due to the extra turbulence generated by the roughness as it penetrates the laminar sub-layer.

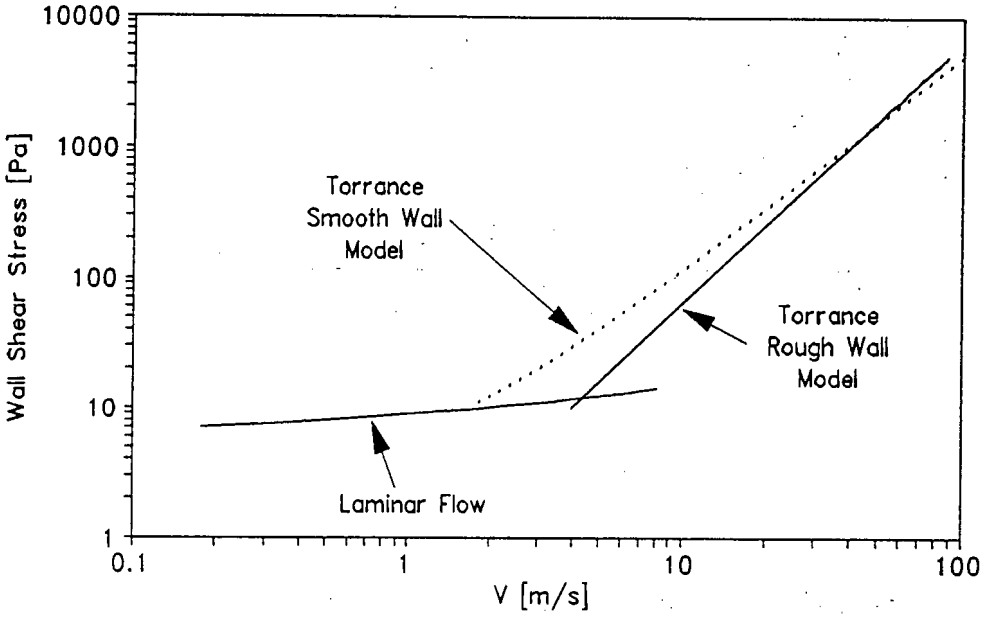

Figure 4.13 : Graphical comparison of the Torrance smooth and rough wall models.

Figure 4.13 shows that the Torrance rough wall model only achieves realistic results at unrealistically high velocities. Furthermore, this model is dependent on the rheology of the slurry (flow behaviour index n). [Values used : density=1200kg/m^3; diameter=100mm; τ_y=5,0921Pa; K=0,3008Pa s^n; n=0,4832]

Figure 4.14 shows that this dependence is significant. Since turbulence is an inertial rather than a viscous phenomenon (Wilson *et al*, 1992) this significant dependence on rheology should not be accepted.

This model has been rejected for these reasons.

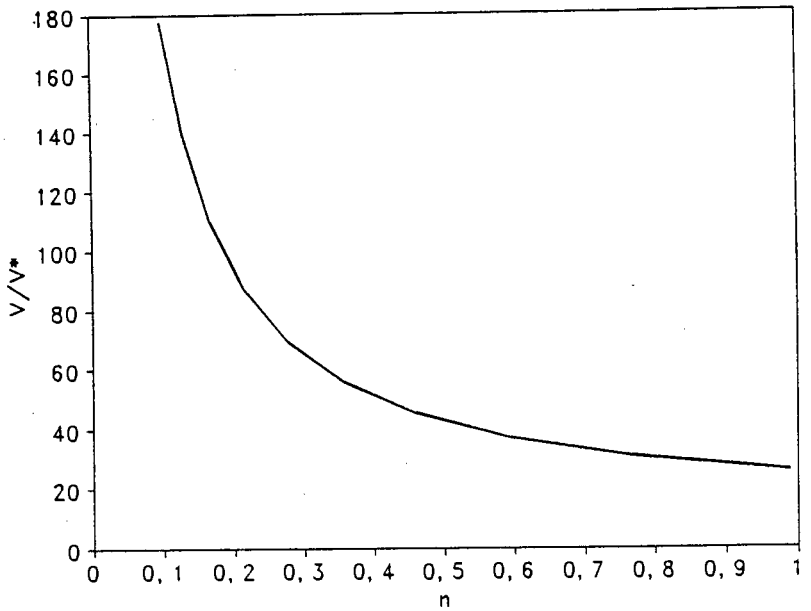

Figure 4.14 : Graphical presentation of Torrance rough wall equation (Equation 2.51).

4.4.5 Sensitivity of the Newtonian Model

The sensitivity of the Newtonian model to a change in viscosity is shown in Figure 4.15 .

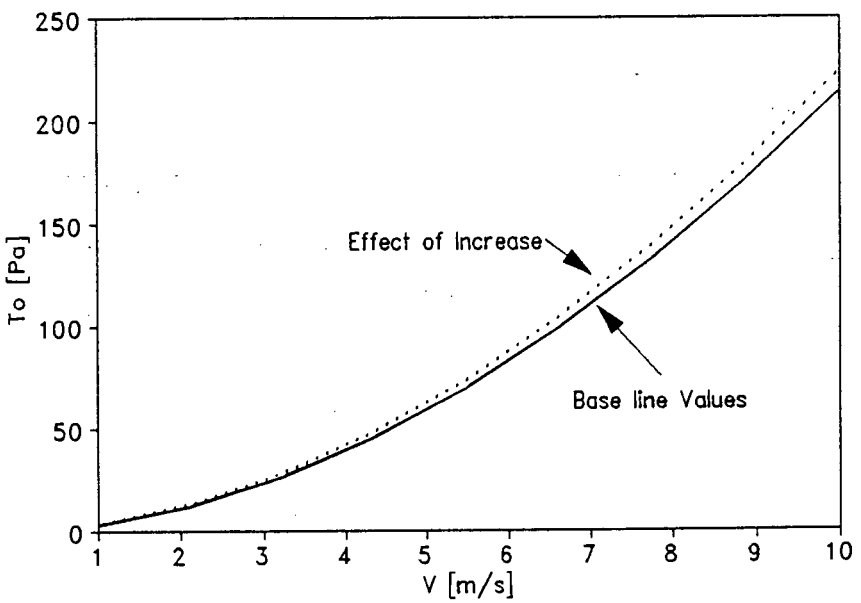

Figure 4.15 : Sensitivity of the Newtonian model ; 40% increase in viscosity.

An average increase of 6,0% in the wall shear stress for a 40% increase in viscosity was obtained.

[Base line values: density-1000kg/m^3; diameter-21,6mm; viscosity=0,001Pa s and pipe roughness=5μm]

4.4.6 Sensitivity of the Torrance Model

The sensitivity of the Torrance model to an increase in the rheological parameters is shown in Figures 4.16 to 4.18. The model is the most sensitive to a change in the n value. This value was therefore changed by only 10% while the other parameters were changed by 40% as with the Newtonian viscosity above.

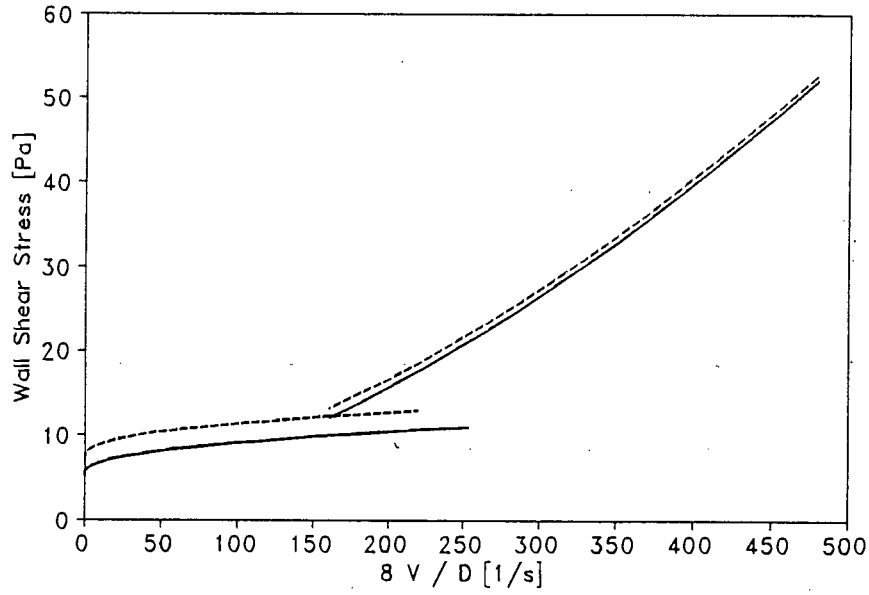

Figure 4.16 : Sensitivity Torrance : 40% increase in τ_y.

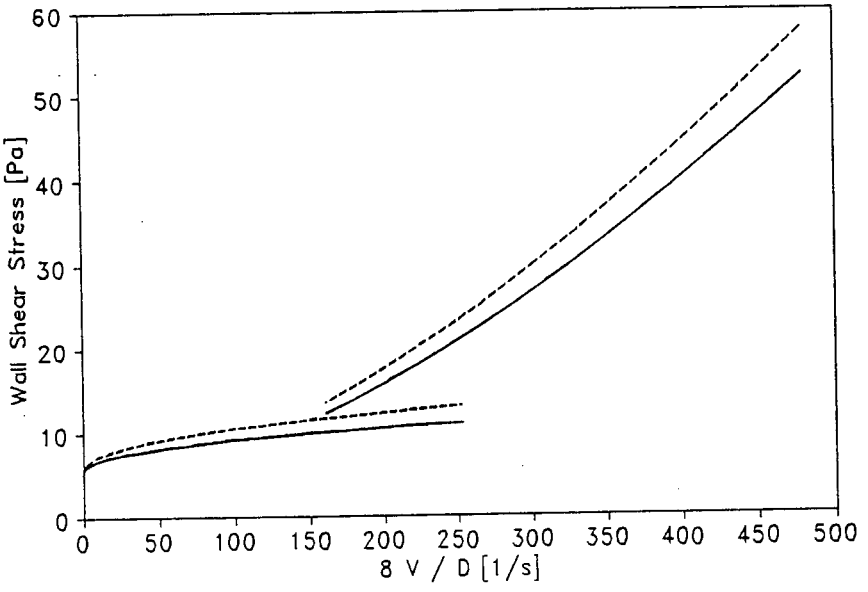

Figure 4.17 : Sensitivity : Torrance : 40% increase in K.

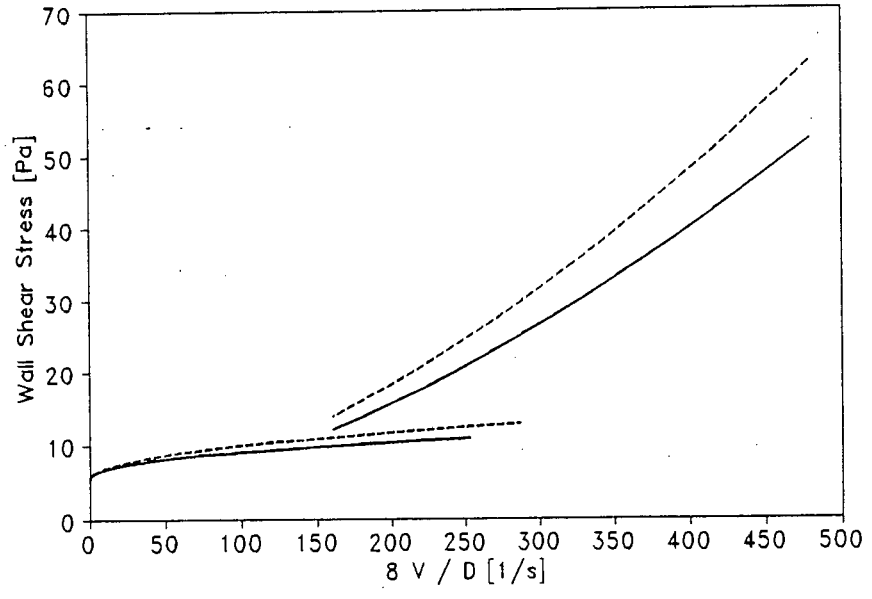

Figure 4.18 : Sensitivity : Torrance : 10% increase in n.

4.4.7 Sensitivity of the Wilson & Thomas Model

The sensitivity of the Wilson & Thomas model to an increase in the rheological parameters is shown in figures 4.19 to 4.21.

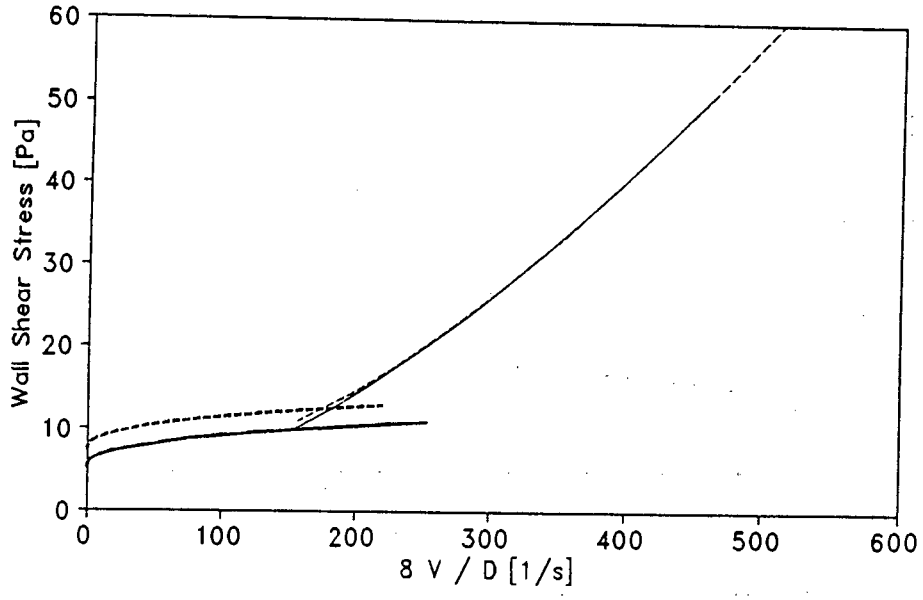

Figure 4.19 : Sensitivity : Wilson & Thomas : 40 % increase in τ_y.

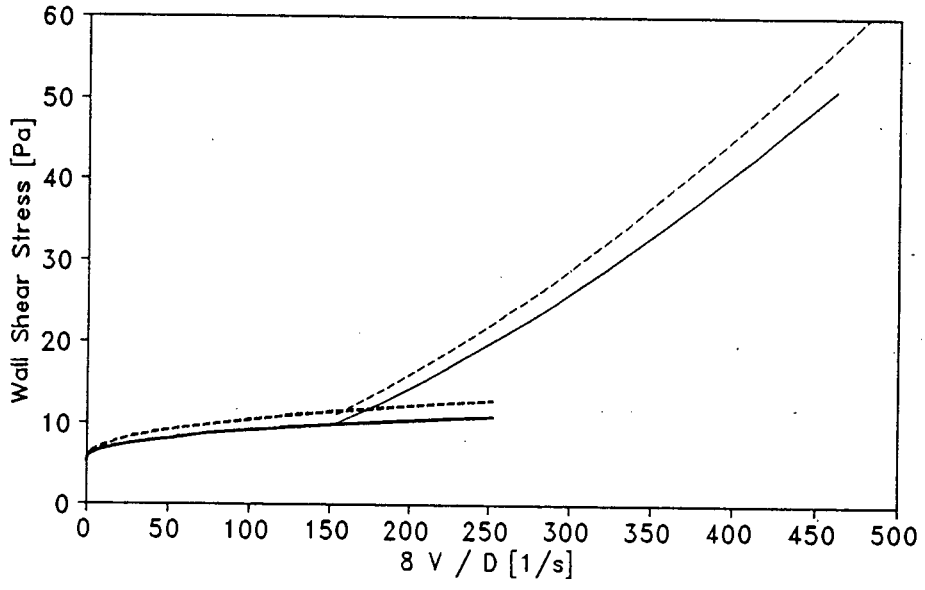

Figure 4.20 : Sensitivity : Wilson & Thomas : 40% increase in K.

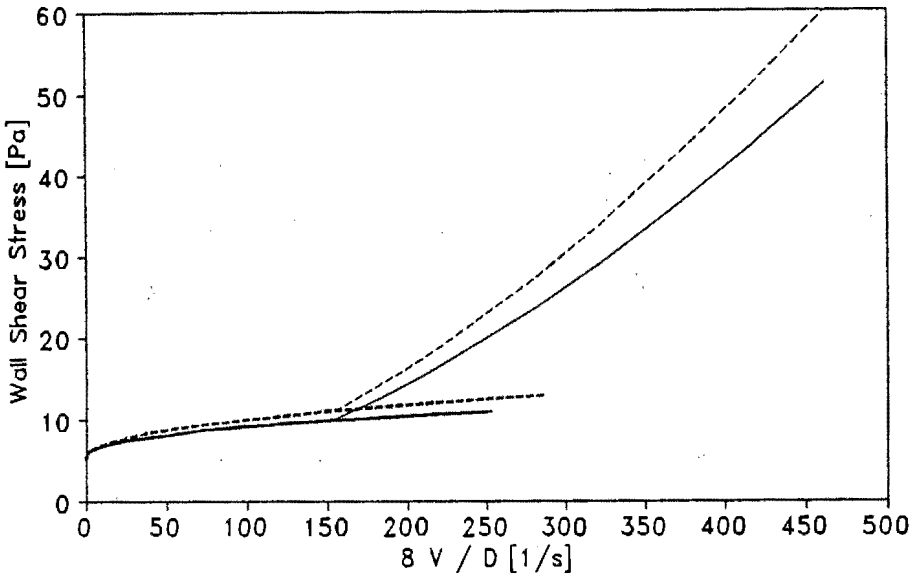

Figure 4.21 : Sensitivity : Wilson & Thomas : 10% increase in n.

[Base line values: density=1200kg/m^3; diameter=100mm; τ_y=5,0921Pa; K=0,3008Pa s^n; n=0,4832]

The sensitivity of the Wilson & Thomas model can also be seen qualitatively in Figures 4.2 to 4.4.

The sensitivity of the models can be summarised as an average percentage increase for each response variable, as shown in Table 4.V.

Table 4.V : Summary of Sensitivities.

Variable	Increase in variable [%]	Average increase in Laminar Flow [%]	Average inc Torrance Model [%]	Average inc Wilson & Thomas Model [%]
τ_y	40	22,4	3,6	0,8
K	40	9,5	11,3	10,9
n	10	5,9	18,7	15,8

4.4.8 Discussion of the sensitivity of the models

The sensitivity calculation results apply only to the base values given. However, these are typical values and the results are meaningful within the range of slurries tested for this thesis. The Newtonian model is relatively insensitive to changes in viscosity. The relative sensitivity is $\Delta\tau_0/\Delta\mu = 15\%$.

The relative sensitivities of the non-Newtonian laminar and turbulent flow models are tabulated in Table 4.VI.

Table 4.VI : Relative Sensitivities.

Parameter	Laminar	Torrance	Wilson & Thomas
$\Delta\tau_0/\Delta\tau_y$	56%	9%	2%
$\Delta\tau_0/\Delta K$	24%	28%	27%
$\Delta\tau_0/\Delta n$	59%	187%	158%

The laminar model is relatively insensitive and is the least sensitive to changes in K. The turbulent flow models are insensitive to changes in τ_y but very sensitive to changes in n. As shown above in the rheological characterisation procedure, changes in τ_y and K will produce large changes in n. It can therefore be concluded that the models are sensitive to any change in rheology. The turbulent flow models are more sensitive to changes in rheology than the laminar flow model.

A possible reason for the marked sensitivity of the turbulent flow models to changes in rheology is that they are formulated for smooth wall turbulence. This means that they rely on the laminar sub-layer to provide the boundary velocity condition at the interface between the laminar sub-layer and the turbulent core. This could account for the undue influence of rheology.

4.5 CONCLUSIONS

4.5.1 Rheological Characterisation

The rheological characterisation procedure used is of a general nature in that it can accommodate the yield pseudoplastic, pseudoplastic and Bingham plastic models. Further, it is based on the widely accepted least squares method. It has produced accurate rheologies for this work and its use is recommended.

The yield pseudoplastic model is sensitive to small changes in the material and the selection of values for the rheological parameters. Assumption of a rheological model that is restrictive (eg pseudoplastic or Bingham plastic) results in flow prediction errors which are far more pronounced in turbulent flow than in laminar flow for the Torrance and Wilson & Thomas models. The reason for this is that the extrapolation of the rheology to the range of shear stresses necessary in turbulent flow can produce order of magnitude differences in the shear rates for the different models.

4.5.2 Laminar/Turbulent Transition

The models from the literature have been analysed and evaluated using the test data base.

The Torrance Reynolds number is unable to predict the transition. This could be regarded as evidence that the full rheology must be used and that the yield stress cannot be neglected.

There is an increasing trend in the value of the stability criterion with increasing Hedström number. This is clearly at variance with the concept that it should remain constant.

The Reynolds number of Metzner & Reed shows the best predictive ability of the Reynolds number formulations, probably because it uses the full rheology. However,

the average value of 3200 is well above the anticipated value of 2100.

The data shows that, because of the presence of a yield stress, the critical velocity becomes independent of pipe diameter at large diameters. Only the intersection method and the Metzner Reed Reynolds number are able to predict this effect.

The intersection method produces the overall best results. However, it cannot explain behaviour, it does not revert to the Newtonian case under Newtonian conditions and it becomes less accurate at small pipe diameters.

4.5.3 Turbulent Flow

The turbulent flow predictions of the Torrance and Wilson & Thomas models are similar and are good at lower shear stresses but deteriorate as the shear stress increases. The shape of the graphs of the models is different from that of the test data. The turbulent flow model predictions have been compared with the turbulent data in the data base using average percentage error and log standard error. The models from the literature do not adequately describe the behaviour of the slurries as determined from the test data base.

The thickness of the laminar sub-layer is less than the diameter of the larger particles at high values of shear stress. The size of the particles should be considered in the analysis of non-Newtonian turbulent flow.

The slope of the velocity distributions of the Torrance and Wilson & Thomas model are different due to the inclusion of n in the Torrance formulation of the von Karman constant term.

The Torrance rough wall model does not produce realistic results, is rheology dependent and has been rejected.

The non-Newtonian models are much more sensitive to changes in rheology than the

Newtonian model.

The rheological properties alone are insufficient for accurate prediction of energy gradients in turbulent flow and other physical properties of the slurry such as the particle size distribution need to be considered.

CHAPTER 5

CHAPTER 5

NEW ANALYSIS

5.1 INTRODUCTION

In this chapter the new analysis proposed by this thesis is presented. This work is believed to be new and it makes a contribution to theoretical knowledge in this field.

The principle objectives in the development of the new analysis are:-

- to try and retain the rheological parameters together and not treat them separately
- to use the fact that an unsheared plug exists at the axis of the pipe at the transition to turbulent flow
- to accommodate the break down of continuum admissibility in the region of the pipe wall where the particles must have an effect because of their physical size.

The new approach is an attempt to explain the behaviour of non-Newtonian slurries and to base the mathematical modelling on these quantitative descriptions.

There are two main components to this new analysis; the identification of the laminar/turbulent transition and the modelling of turbulent flow.

5.2 LAMINAR/TURBULENT TRANSITION

Three approaches to the formulation of a non-Newtonian Reynolds number have been made. The first approach extends the Newtonian analogy to the yield pseudoplastic model. The second approach works from the fundamental force assumption regarding inertial and viscous forces. The third approach considers the unsheared plug at the pipe axis. (The first two approaches have been published (Slatter & Lazarus, 1993).)

5.2.1 First approach

The approach of Metzner & Reed (1955) is widely used (eg. Heywood *et al*, 1993a). However, as stated earlier, there is great difficulty involved in the application of this model to non-power law fluids because the slope n′ is not constant and must be evaluated at each point. The first approach was therefore to simplify the Metzner & Reed approach so that K′ and n′ do not have to be evaluated. A Reynolds number Re_1 is defined as

$$Re_1 = \frac{16}{f_{lam}} . \qquad (5.1)$$

The laminar Fanning friction factor, f_{lam}, is evaluated using the equations in Chapter 2. Note that the values for Re_{MR} and Re_1 are the same, but the procedure is greatly simplified.

This approach can also be seen as the extension of the Bingham plastic Reynolds number to the yield pseudoplastic model.

5.2.2 Second approach

The second approach is to derive a Reynolds Number from the fundamental assumption

$$Re \; \alpha \; \frac{\text{INERTIAL FORCE}}{\text{VISCOUS FORCE}} , \qquad (5.2)$$

where (Massey, 1970)

$$\text{INERTIAL FORCE} \; \alpha \; \rho \, D^2 \, V^2 . \qquad (5.3)$$

It is necessary to establish a representative viscous force across the pipe. The characteristic length is D and the representative area, as above, is D^2 and this must

be multiplied by a representative viscous shear stress τ_{visc} ie

$$\text{VISCOUS FORCE } \alpha \ D^2 \ \tau_{visc} \ . \tag{5.4}$$

Viscous stress is related to shear rate by the constitutive rheological relation, in this case, the yield pseudoplastic model. The problem therefore resolves to finding a representative shear rate over the pipe cross section. Dimensionally, any characteristic velocity divided by a characteristic length can be used as a representative shear rate. Dedegil (1986) has simply used V/D in his formulation for a particle Reynolds number. However, it has been shown that the pseudo shear rate, flow characteristic or bulk shear rate 8V/D is an important parameter in non-Newtonian laminar flow and can be related to true shear rate by the Rabinowitsch-Mooney relation. Heywood *et al* (1993b) used the flow characteristic as a representative shear rate to model successfully the laminar flow of fly ash slurries. This parameter has also been used by Metzner & Reed and Torrance in their formulations. The flow characteristic (8V/D) is used as the representative shear rate and the representative viscous stress is given by

$$\tau_{visc} = \tau_y + K \left[\frac{8V}{D} \right]^n \ , \tag{5.5}$$

and the representative viscous force is given by

$$\text{VISCOUS FORCE } \alpha \ D^2 \left[\tau_y + K \left[\frac{8V}{D} \right]^n \right] \ . \tag{5.6}$$

Therefore : .

$$Re_2 \ \alpha \ \frac{\rho \ V^2}{\tau_y + K \left[\frac{8V}{D} \right]^n} \ . \tag{5.7}$$

A value of 8 is chosen as the proportionality constant so that Re_2 reduces to the standard form $Re=\rho VD/\mu$ under Newtonian conditions ($\tau_y = 0$, $K = \mu$ and $n = 1$).

The final form is

$$Re_2 = \frac{8 \rho V^2}{\tau_y + K \left[\frac{8V}{D}\right]^n} . \qquad (5.8)$$

This can be compared to the Clapp Reynolds number used by Torrance (1963), which does not include the yield stress in the formulation of the viscous force.

It should be noted that this same formulation for Re_2 can be derived by considering the Newtonian approximation (Section 2.10.2) and substituting the bulk shear rate in place of the true shear rate.

5.2.3 Third Approach

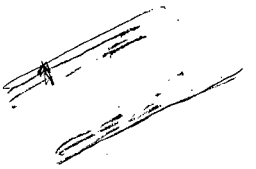

It is well known that solid boundaries inhibit turbulence because velocity components perpendicular to the surface cannot exist in the region of the surface. This is the reason for the existence of the laminar sub-layer adjacent to a solid surface.

Implicit in the definition of yield stress is the fact that when the shear stresses are less than the yield stress, such as the conditions which exist in the unsheared core, the material will behave as a solid. The preceding models (Re_1 and Re_2) ignore the fact that an unsheared solid plug exists, concentric with the pipe axis, due to the presence of the yield stress, under laminar flow conditions.

At the critical point where laminar flow breaks down into turbulent flow, laminar flow conditions do exist still, although this is the upper limit at which such conditions exist (Hanks & Ricks, 1974). At this point a coaxial solid plug exists at the pipe centre. Furthermore, this plug can be regarded as a solid boundary, and must therefore affect the stability of the laminar flow in the annulus.

Furthermore, the flow of only the sheared fluid in the annulus is considered. The geometry of the pipe and plug are shown in Figure 5.1.

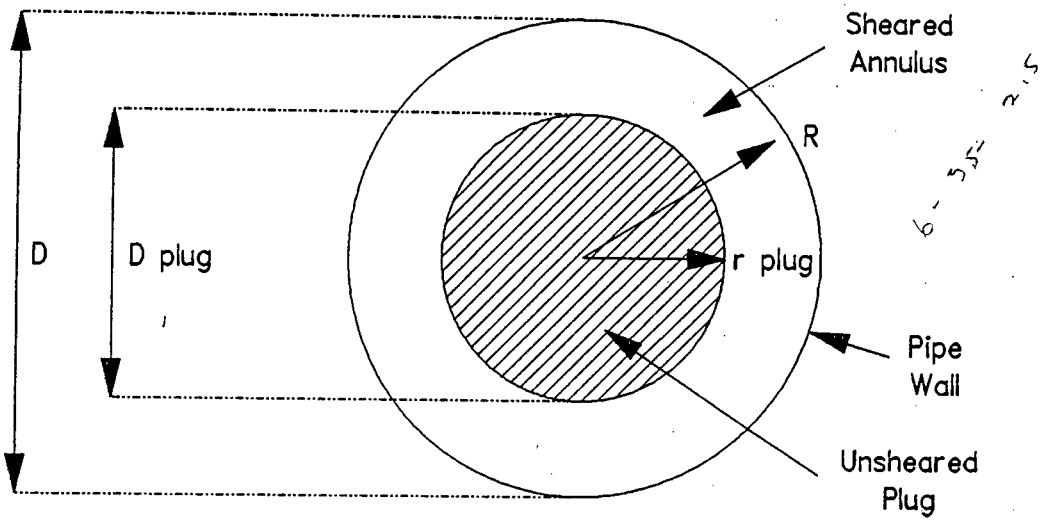

Figure 5.1 : Unsheared Plug Geometry

The radius of the plug is

$$r_{plug} = \frac{\tau_y}{\tau_0} R \ , \qquad (5.9)$$

and the area of the annulus is

$$A_{ann} = \pi \ (R^2 - r_{plug}^2) \ . \qquad (5.10)$$

The sheared diameter, D_{shear}, is now taken as the characteristic dimension, because this represents the zone in which shearing of the fluid actually takes place, and it is defined as

$$D_{shear} = D - D_{plug} \ , \qquad (5.11)$$

where $D_{plug} = 2\ r_{plug}$.

Since the unsheared core is treated as a solid body in the centre of the pipe, the flow which the core represents must be subtracted as it is no longer being treated as part of the fluid flow. The corrected mean velocity in the annulus V_{ann} is then obtained as follows,

$$V_{ann} = \frac{Q_{ann}}{A_{ann}} \quad (5.12)$$

Using the same fundamental assumption as for Re_2, the final form of the formulation is

$$Re_3 = \frac{8 \rho V_{ann}^2}{\tau_y + K \left(\frac{8 V_{ann}}{D_{shear}} \right)^n} \quad (5.13)$$

An important coincidence arises with the choice of the sheared diameter as the characteristic length for Re_3. This same length can also be interpreted as the hydraulic mean diameter or effective diameter (Holland, 1973) which is derived by consideration of the wetted perimeter for flow through a concentric annular conduit. These two cases are fundamentally different. However, if one considers the whole diameter to be the zone in which fluid shear actually takes place in Newtonian pipe flow, then the sheared diameter would be the logical choice for the plug flow case.

5.2.4 Dimensional Analysis

The absence of any dimensional analysis in the above arguments deserves comment, since dimensional analysis has traditionally played a major role in Reynolds number formulation. Dimensional analysis is based upon the premise that the functional relationship between the problem variables is multiplicative and exponential. A thorough treatment for the yield pseudoplastic model is given in Appendix B. This method is unable to resolve the additive nature of the fundamental rheological relationship (Equation (2.8)) of the yield pseudoplastic model. This is perhaps the reason why the yield stress has not been taken into account in other Reynolds number formulations. The new formulations clearly resolve this problem. Note that a single criterion cannot result from this approach.

5.3 NEW ANALYSIS OF NON-NEWTONIAN SLURRY TURBULENT FLOW IN PIPES

5.3.1 Velocity distribution

It is well established in the literature that there is a strong similarity between the turbulent behaviour of Newtonian fluids and non-Newtonian slurries, despite their significantly different behaviour in the laminar flow regime (Caldwell & Babbitt, 1941; Hedström, 1952; Metzner & Reed, 1955; Dodge & Metzner, 1959; Tomita, 1959; Michiyoshi *et al*, 1959; Edwards & Smith, 1980; Thomas & Wilson, 1987; and Sive, 1988), as discussed in Section 2.14.

Other researchers have shown that the velocity distribution in the turbulent core of turbulent non-Newtonian slurry pipe flow is similar to that of Newtonian fluids (Govier & Aziz, 1972). The logarithmic nature of these velocity distributions has been demonstrated experimentally (Abbas & Crowe, 1986, Park *et al*, 1989 and Xu *et al*, 1993) and can be accepted for the purpose of theoretical analysis.

5.3.2 The effect of solid particles

Because non-Newtonian slurries are widely regarded as homogeneous and their behaviour can apparently be described by continuum models, it is customary to ignore the fact that solid particles are present. However, the presence of solid particles as an inherent component of the fluid becomes important when one considers the following:

(i) One of the cornerstones of classical turbulent analysis is the existence of a laminar sub-layer. The non-Newtonian turbulent theory of Wilson & Thomas (1985) predicts a thickened laminar sub-layer over and above that for an equivalent Newtonian fluid. However, the size of the solid particles which must be present in the laminar sub-layer are of a similar order of magnitude to the thickness of the laminar sub-layer. One possible conclusion is that the boundary layer is affected in some way by the presence of the solid particles.

(ii) The velocity gradients in the region of the pipe wall are known to be steep (Janna, 1983). Calculations to determine the change in velocity which can be expected over the diameter of a particle under average test conditions show that it is of the order of 1m/s in the region of the pipe wall. Obviously, such rapid changes in velocity will be impeded because the solid particles will resist shear. The velocity gradients in the region of the pipe wall are therefore so steep that the presence of solid particles must have a diminishing effect on these velocity gradients.

(iii) Clearly, the continuum approximation (Lumley, 1978) must break down in the region of the pipe wall when the size of the solid particles becomes large compared with the scale of the modelling. The effect of the particles must be accounted for.

(iv) If the continuum approximation is untenable in the wall region, the implication is that the particles and the slurry pseudofluid will have to be considered as separate phases at the crucial interface between the laminar sub-layer and the turbulent core. Particles of various sizes will be subjected to drag forces in an environment which is neither wholly laminar or turbulent, but somewhere in between. In the face of this extremely complex situation, it is logical to model the behaviour in terms of a dimensionless group which encompasses both the particle and fluid characteristics. A particle Reynolds number is one such dimensionless group.

The particles must therefore physically obstruct the theoretical steep velocity gradients in the region of the wall resulting in a decrease in the velocity gradient at the pipe wall. As mentioned above, the effect of pipe roughness is known to cause a decrease in the velocity gradient at the pipe wall. However, in this case the particles, although they are indeed sand particles, they are not fixed or uniform, as in Nikuradse's experiments (in Schlichting, 1960), but they will have an effect similar to a surface roughness. It can therefore be postulated that the results will lie somewhere between the two data curves of Nikuradse and Colebrook & White (Colebrook, 1939), as

shown in Figure 2.14 in Chapter 2.

5.3.3 Partially Rough Wall Turbulent Flow

The partially rough wall turbulent flow region has been postulated to be relatively broad by researchers such as Dodge & Metzner (1959) and Wilson & Thomas (1985). However, the above remarks on particle roughness, as well as the experiments by Park *et al* (1989) indicate that the transition region is much narrower for non-Newtonian slurries than for Newtonian fluids.

5.3.4 Fully Developed Rough Wall Turbulent Flow

In the derivation of the relationships in turbulent flow, it is standard practice to assume that the viscous stresses are negligible when compared with the turbulent stresses in the turbulent core region (Janna, 1983). Because of the striking similarity between the turbulent behaviour of Newtonian fluids and non-Newtonian slurries, it would appear unlikely that the behaviour of the slurry in fully developed rough turbulent flow should depend on the viscous characteristics of the slurry. Wilson *et al* (1992) have stated that turbulence is a process dominated by inertial forces. Indeed an absolute asymptote, independent of the viscous characteristics of the slurry, such as exists for Newtonian fluids, would be a useful engineering tool, in view of the highly sensitive nature of the yield pseudoplastic model.

5.3.5 Plug flow

The shear stress distribution in a pipe is linear, being zero at the centre line and reaching the maximum value τ_0 at the pipe wall. For the laminar flow of fluids with a yield stress, where $\tau < \tau_y$ the fluid cannot shear and plug flow occurs. Previous researchers (eg Hanks & Dadia, 1982 and Wilson & Thomas, 1985) have assumed that the same phenomenon will occur in turbulent flow.

However, the velocity profiles of Park *et al* (1989) and Xu *et al* (1993) show no such effect and indicate rather that the flow is turbulent over the entire core region. Plug flow has therefore not been admitted on the strength of this experimental evidence.

5.3.6 Reversion to the Newtonian Model

One of the problems that has arisen with previous models is that they apply only to the specific materials tested, or upon the test results used to generate correlation coefficients. These models then relate only to those specific circumstances and cannot be universally applied. One of the obvious ways of solving this problem is to ensure that the model reverts to the Newtonian model when the rheological parameters are relaxed to Newtonian conditions ($\tau_y = 0$, $K = \mu$ and $n=1$). Note that this condition cannot guarantee universality - rather, it implies the opposite; any analysis which does not revert to the Newtonian form can never be universally applicable.

5.3.7 New analysis

The analysis of non-Newtonian turbulent flow has therefore proceeded from the following initial assumptions based on the previous arguments:-

- The velocity distribution is logarithmic and similar to the classical Newtonian turbulent velocity distribution over the entire core region.
- There is a roughness effect caused by the solid particles in the slurry.
- Fully developed rough wall turbulent flow does exist and the partially rough wall turbulent region is much narrower than for Newtonian fluids.
- Fully developed turbulent flow is independent of the viscous characteristics of the slurry.

- Plug flow does not occur.

Furthermore, the new model should revert to the Newtonian model.

The basic velocity distribution for Newtonian turbulent flow in rough pipes is taken to be valid based on the above assumptions, ie:

$$\frac{u}{V_*} = A \ln \frac{y}{d_x} + B \,, \qquad (5.14)$$

where A is a constant and B is a roughness function.

It now remains to determine values for A and B.

5.3.8 The von Karman constant

The value of the coefficient A has usually been taken as the inverse of the von Karman universal constant. Now, turbulence is an inertial rather than a viscous process (Wilson *et al*, 1992) and so viscous forces are taken to be negligible in the turbulent region (Janna, 1983). Experimental evidence shows that the velocity distributions in Newtonian and non-Newtonian turbulent flow are similar. For these reasons the value of A has been chosen as the inverse of the von Karman universal constant, $1/\chi = 2{,}5$.

5.3.9 Formulation of the roughness Reynolds number

In order to correlate the roughness function B, it is necessary to formulate the roughness Reynolds number in terms of the yield pseudoplastic model.

A problem with previous models has been the inadequate formulation of this important parameter, eg a formulation excluding the yield stress (Torrance, 1963 and Hanks & Dadia, 1982). The new work on non-Newtonian Reynolds numbers (Re_2 in Section 5.2.2) proves particularly valuable at this point.

By analogy with the Newtonian approach, the roughness Reynolds number for a yield pseudoplastic slurry can be formulated using the same basic form as Re_2 as follows

$$Re_r = \frac{8 \rho V_*^2}{\tau_y + K \left[\frac{8 V_*}{d_x}\right]^n} . \qquad (5.15)$$

Higher turbulence intensities in the wall region reported by Park *et al* (1989) provide strong experimental evidence in support of a particle roughness effect in the wall region.

An alternative derivation of the roughness Reynolds number can also be considered, by envisioning the interaction between a particle and the slurry. Unfortunately, as stated in Section 2.13.10, much of the literature deals with low concentration settling slurries which are investigated under turbulent conditions where the concentration distribution becomes uniform. The slurry condition is then accepted as homogeneous. However, this thesis deals with homogeneous slurries which are, for practical purposes, non-settling. A particle Reynolds number would imply some measurable velocity differential to exist between the particle and the fluid. Under normal circumstances, the particle and the fluid are essentially inseparable in the case of the homogeneous slurries in this thesis, and it is not physically possible to create velocity differentials, and thus impose drag forces on the particles. However, in the wall region the continuum approximation must be compromised and it is important to consider the effect that the pseudofluid slurry will have on discrete particles. A particle Reynolds number can be formulated using the method of Dedegil (1986) and incorporating the fundamental Reynolds number definitions used in this thesis, as follows:

$$Re_p = \frac{8 \rho V_s^2}{\tau_y + K \left[\frac{8 V_s}{d}\right]^n} . \qquad (5.16)$$

where d_p is the particle diameter and V_s is the velocity differential between the particle

and the surrounding fluid.

As stated above, the velocity differential can only materialize once the continuum approximation breaks down in the wall region. Since this is a region of steep velocity gradient and indeterminate regime (neither fully laminar nor fully turbulent), an exact value of the velocity differential cannot be determined. In the face of this complex situation, the shear velocity could be used as a dimensionally representative velocity parameter.

From this formulation, Equation (5.16), it can be seen that by introducing the shear velocity as a dimensionally representative velocity parameter in the wall region, and the representative particle size d_x, the roughness Reynolds number (Equation (5.15)) will result. This important dimensionless group, and the rationale behind its formulation, can be seen as part of the new analysis.

In this case, as outlined above, the size of the solid particles must play a role and the roughness size d_x must be chosen accordingly. Since slurries typically contain a continuous range of particle sizes, a representative particle size must be found.

The effect of roughness on turbulence can be thought of as an aggravation at the wall which stimulates turbulence. Clearly then the larger particles will have a more dominant effect on turbulence than the smaller particles. Also, the larger particles will shield the smaller ones, reducing their effectiveness in stimulating turbulence (Colebrook, 1939).

For the slurries tested, the d_{85} size was found to be a good representation of the turbulent roughness size effect of the solid particles in the slurry, ie $d_x = d_{85}$. This decision is supported by the sensitivity analysis in Section 5.3.11. It is important to note that the Malvern instrument was used for particle size measurements - other methods may produce significantly different results (Knight, 1993).

The mean velocity can be obtained by integrating over the cross section of the pipe

yielding

$$\frac{V}{V_*} = \frac{1}{\chi} \ln \left[\frac{R}{d_{85}} \right] + B - 3{,}75 \quad . \tag{5.17}$$

Experimental data is now needed to correlate the roughness function B against the roughness Reynolds number.

5.3.10 Correlation of the Roughness Function

The roughness function B was correlated against the roughness Reynolds number in the same way as for Newtonian turbulent flow.

The correlation of data for the new model is shown in Figure 5.2, with the curves and asymptotes for the Nikuradse and Colebrook White loci. All turbulent data from the data base has been used in this Figure (some 500 data points).

The data lie above the Colebrook White curve.

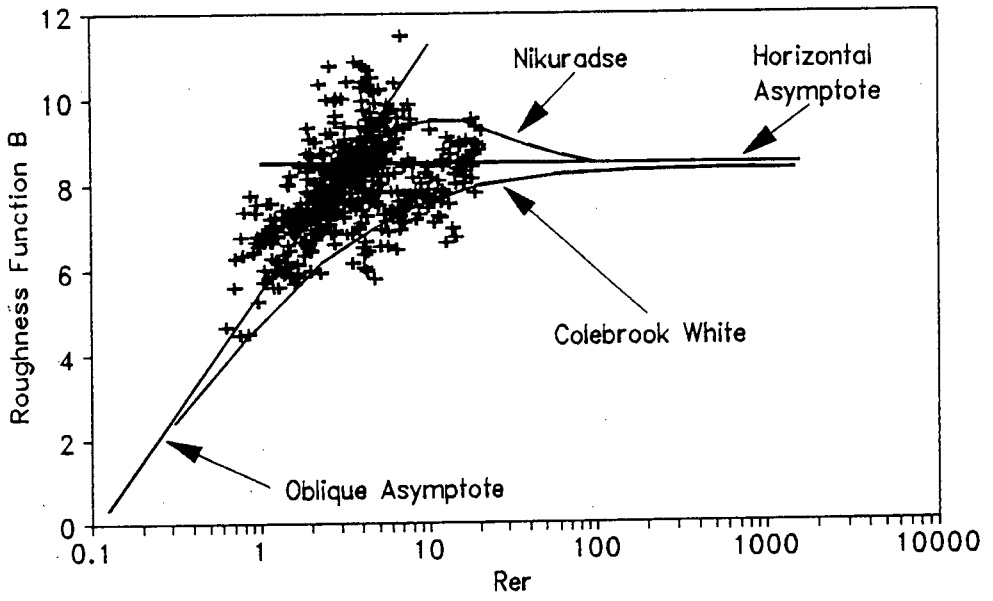

Figure 5.2 : Roughness function correlation for non-Newtonian Slurries

Since the particles in the slurry are neither fixed nor uniform in size, as they were for Nikuradse's experiments, the roughness effect of the solid particles is not expected to be as great as in Nikuradse's experiments. This is reflected in Figure 5.2.

The figure also shows that the data lies close to the two asymptotes which describe the limits of behaviour of Newtonian turbulent flow. On the strength of these two points, the correlation chosen for this analysis is therefore the two asymptotes ie:

(i) Smooth Wall Turbulent Flow

If $Re_r \leq 3,32$ then $B = 2,5 \ln Re_r + 5,5$. This is analogous with smooth wall turbulent flow.

$$\therefore \frac{V}{V_*} = 2,5 \ln \left[\frac{R}{d_{85}}\right] + 2,5 \ln Re_r + 1,75 \ . \qquad (5.18)$$

(ii) Fully Developed Rough Wall Turbulent Flow

If $Re_r > 3,32$ then $B = 8,5$. This is analogous with fully developed or rough wall turbulent flow and will yield a constant value for the Fanning friction factor f.

$$\frac{V}{V_*} = 2,5 \ln \left[\frac{R}{d_{85}}\right] + 4,75 \ , \qquad (5.19)$$

which reduces to

$$\frac{1}{\sqrt{f}} = 4,07 \log \left[\frac{3,34\ D}{d_{85}}\right] \ . \qquad (5.20)$$

The average percentage error when calculating the roughness function, B, using this correlation is 9,2% with a standard deviation of 7,8%, and a log standard error of 0,0024.

This correlation produces a transition from the smooth to the rough flow condition which is abrupt.

The correlation further shows that the assumptions regarding the turbulent behaviour of non-Newtonian slurries are valid for the slurries tested.

5.3.11 Sensitivity Analysis of the Representative Particle Size

The above analysis relies on the assumption that the d_{85} size is the best representative particle size. In order to justify this assumption, a sensitivity analysis of the effect of various representative particle sizes would have on the accuracy of the analysis has been carried out.

A wall shear stress prediction error function can be defined as:

$$E_\tau = \frac{\sum_{i=1}^{N} \frac{100^* \left| \tau_{0\ obs\ i} - \tau_{0\ calc\ i} \right|}{\tau_{0\ obs\ i}}}{N} . \qquad (5.21)$$

This error function gives an average percentage error. The error function for the new model and the standard deviation of this error is shown in Table 5.I and Figure 5.3 for all tests in the data base (excluding the 200mm diameter pipe results - see Section 6.3.7).

Table 5.I and Figure 5.3 show that the d_{85} size provides the minimum error, and shows the sensitivity of the new model to a change in representative particle size. The asymmetry of Figure 5.3 is due to the shape of the particle size distributions which are much steeper for $d < d_{85}$ than for $d > d_{85}$.

Table 5.I : Wall shear stress error sensitivity to representative particle size

d_x Percentile	E_r [%]	Standard Deviation
d_{50}	12,88	9,88
d_{55}	12,24	9,54
d_{60}	11,59	9,19
d_{65}	10,91	8,89
d_{70}	10,18	8,63
d_{75}	9,42	8,49
d_{80}	8,75	8,46
d_{85}	8,58	8,99
d_{90}	9,79	10,35
d_{95}	13,57	12,95
d_{100}	42,67	26,98

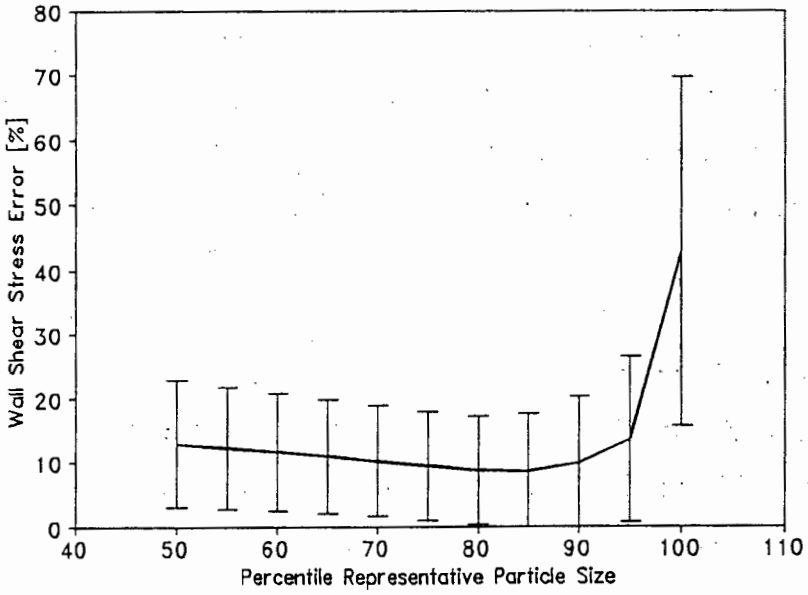

Figure 5.3 : Wall shear stress error sensitivity to representative particle size

5.4 CONCLUSION

The new analysis for the flow of non-Newtonian slurries in pipes has been presented in two main sections viz. the laminar/turbulent transition and turbulent flow.

5.4.1 Laminar/Turbulent Transition

The laminar/turbulent transition has been modelled using widely accepted fundamental definitions and including the full rheology.

The first Reynolds number formulation Re_1 has been modelled using the assumption that the laminar friction factor is related to the Reynolds number by $Re=16/f$. This model extends the approach of the Bingham Plastic Reynolds number to the yield pseudoplastic rheological model. The second Reynolds number formulation Re_2 has been modelled using the definition that the Reynolds number is proportional to the ratio of the inertial and viscous forces. The third Reynolds number formulation Re_3 has been modelled using the assumption that the unsheared plug present due to the yield stress acts as a solid at the pipe axis and inhibits turbulence.

All three Reynolds numbers revert to the Newtonian form under Newtonian conditions.

5.4.2 Turbulent Flow

Turbulent flow has been modelled along the lines of classical Newtonian turbulent theory.

The velocity distribution is assumed to be logarithmic and the standard von Karman constant value of 0,4 has been used.

It has been argued that the solid particles present in the slurry must play an important role in the reduction of the velocity gradient in the wall region due to their physical

size. The continuum approximation, which can be applied to laminar flow and which is usually applied to turbulent flow, must be compromised in the wall region and a particle roughness effect must be admitted. The roughness function can be modelled using a new formulation of the roughness Reynolds number which includes a representative particle size. This representative particle size can be taken as the d_{85} size for the slurries tested.

The transition from smooth to rough turbulent flow is abrupt.

The classical Newtonian turbulent flow asymptotes can be used to correlate the roughness function. The new model will revert to these asymptotes under Newtonian conditions.

CHAPTER 6

CHAPTER 6

EVALUATION AND DISCUSSION OF THE NEW ANALYSIS

6.1 INTRODUCTION

In this Chapter, the test data from the data base (Appendix A) is analysed using the new models. The results of these analyses and the models themselves are evaluated and discussed. There are two main sections - the laminar/turbulent transition and turbulent flow.

6.2 LAMINAR/TURBULENT TRANSITION

6.2.1 Results

The critical data from Appendix A is used to compute values of the new Reynolds number formulations. These are presented in Table 6.I, reduced to arithmetic mean and standard deviation and range.

Table 6.I : Laminar/turbulent transition results

	Re_1	Re_2	Re_3
Avg	3268	3742	2643
Std	981	1178	658
Std%	30	31	25
Min	1516	1740	1310
Max	6451	7577	4606
Range	4935	5837	3296
Range %	151	156	125
V_c at $Re_3 = 2100$	Avg % Err	Std Dev	Max % Err
	13	9	35

As stated earlier, for the proposed formulations to be successful, they should obtain values close enough to some fixed constant value so that the laminar/turbulent transition can be predicted with some degree of confidence.

Comparing these results, Table 6.I, with Table 4.II, Re_1 obtains the same value as Re_{MR} as explained in Chapter 5, but is computationally simpler. Re_2 obtains a marginally higher standard deviation (%) than Re_1 and is much better than the stability criterion. Re_3 yields the overall best performance, based on its lower variance. The average value for Re_3 is 2643 which is higher than the Newtonian value of 2100. Since the discrepancy is not large, and because the value 2100 is within one standard deviation from the average value, the criterion Re_3=2100 has been chosen for the lower bound of the transition. Using this criterion for Re_3 and calculating the resulting critical velocity for each test, the average percentage error, standard deviation and maximum percentage error (bottom of Table 6.I) are all better than the intersection method.

It should be emphasised that the decision to use the number 2100 as the transition criterion is arbitrary and was chosen for convenience to align with the Newtonian case in the limit. Furthermore, the superiority of Re_3 is based on its lower variance, not on its closeness to the Newtonian value of 2100.

6.2.2 Effect of Velocity

The new Reynolds numbers are not linear functions of velocity as is the case with Newtonian fluids. The relationship is shown in Figure 6.1. Furthermore, since the new turbulent flow model postulates that the plug disappears at the onset of turbulence, Re_3=Re_2 once the critical velocity has been exceeded. This discontinuity in Re_3 is shown in Figure 6.1.

This is probably the first Reynolds number to have a discontinuity. The discontinuity is not a matter for concern since it is based on the actual behaviour of the slurry in the pipe. The behaviour at the transition changes fundamentally, the plug/pipe geometry changes and the discontinuity in Re_3 reflects these changes.

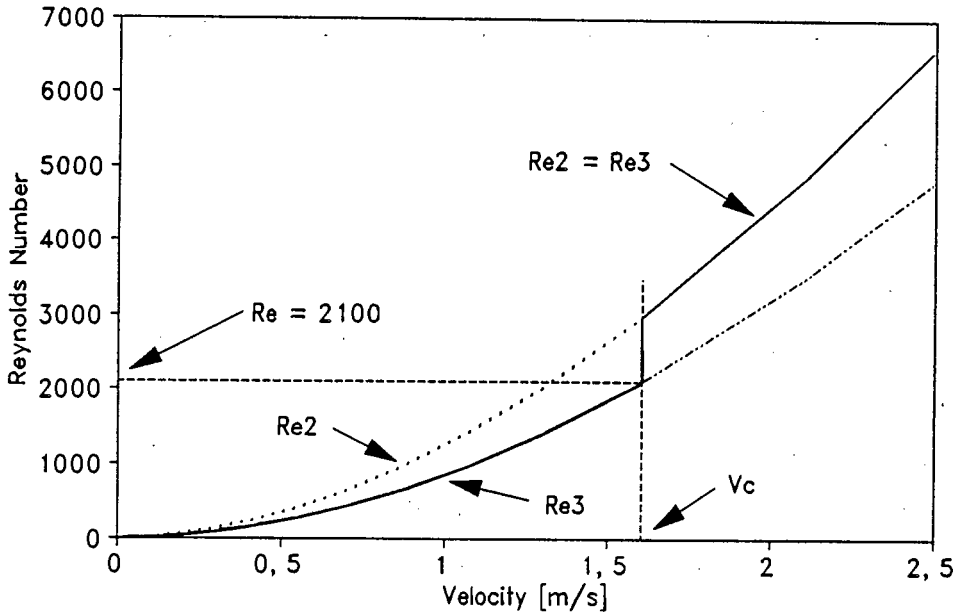

Figure 6.1 : New Reynolds numbers (Re_2 and Re_3) plotted against velocity.

6.2.3 Effect of Diameter

For Newtonian fluids the relationship between critical velocity and diameter (other factors remaining constant) is hyperbolic, and the product V_cD is constant. The behaviour of non-Newtonian slurries is known to be much flatter due to the presence of a yield stress (Section 2.10.5) and this relationship is shown in Figure 6.2 using Re_3.

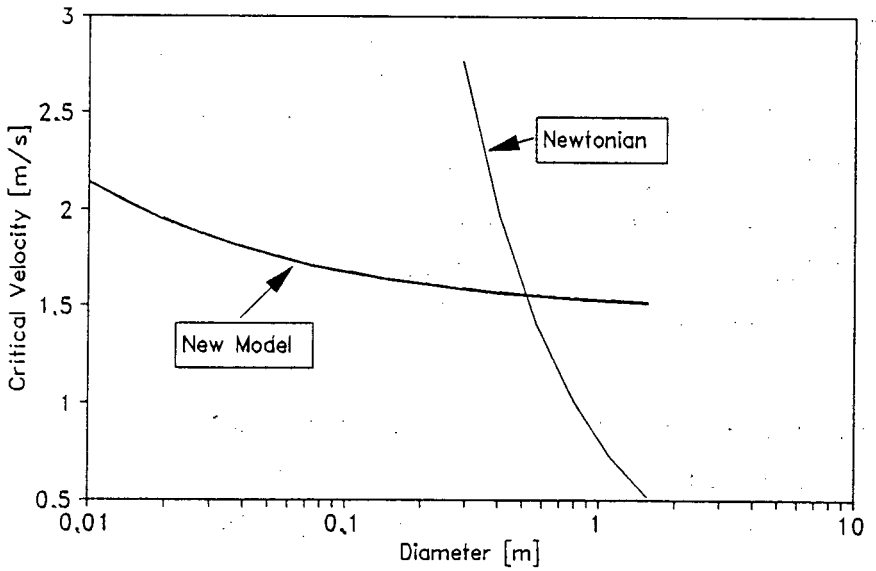

Figure 6.2 : Critical velocity vs Diameter

Graphical comparisons of the new models with the three data sets which cover the widest pipe diameter range are shown in Figure 6.3 to Figure 6.5.

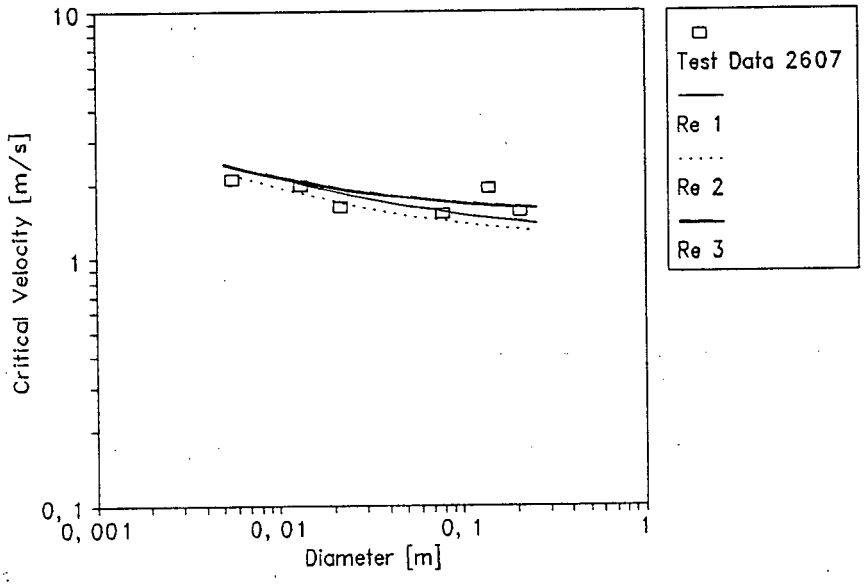

Figure 6.3 : Critical velocity vs pipe diameter - Data set 2607

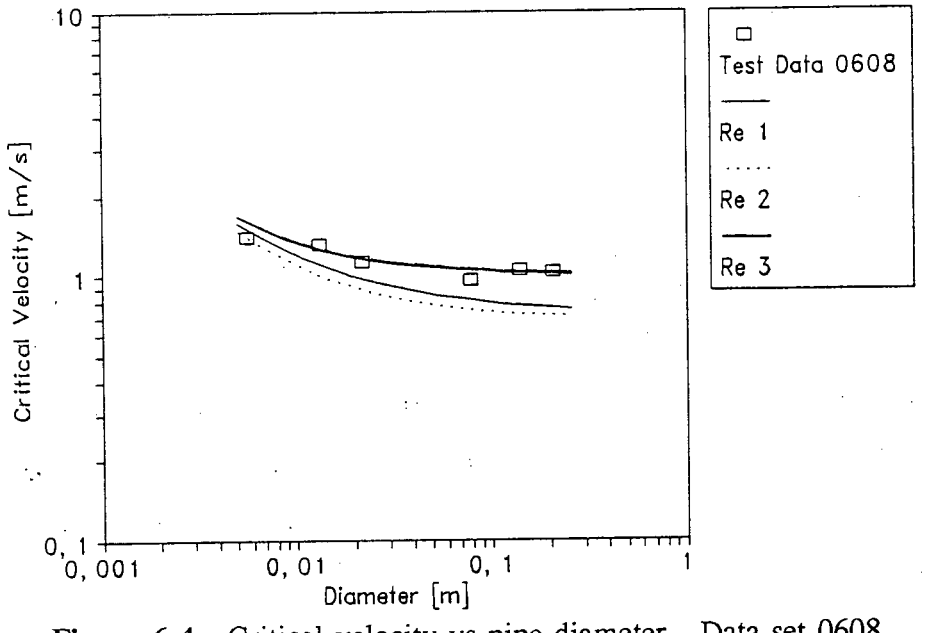

Figure 6.4 : Critical velocity vs pipe diameter - Data set 0608

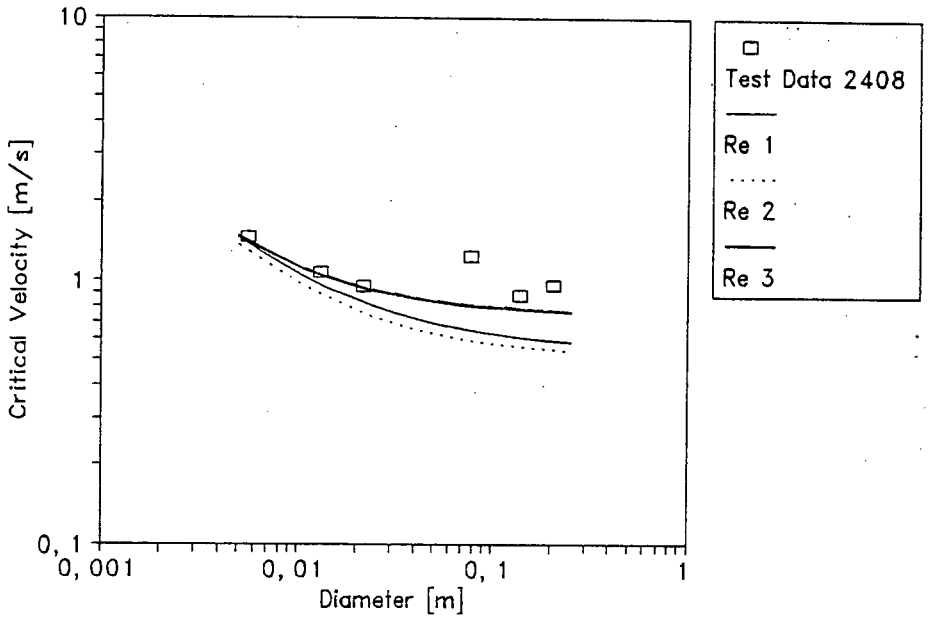

Figure 6.5 : Critical velocity vs pipe diameter - Data set 2408

These diagrams can be compared directly with the diagrams of the models from the literature (Section 4.3.2). The yield stress effect, which the Bingham plastic Reynolds number brought to light, can clearly be seen in all of the new models. Re_3 provides the most accurate modelling of the actual behaviour, followed by Re_1, which is marginally better than Re_2.

6.2.4 Hedström Number Trend

As stated before, there is an increasing trend of the stability criterion, Z_{max}, with increase in Hedström number. This value has previously been assumed to be constant for all fluids at the Newtonian value of $Z_{max}=808$. The new model Re_3 can be used to determine the critical velocity (for typical rheology) and then the stability criterion can be plotted against the Hedström number for the transition data in the data base.

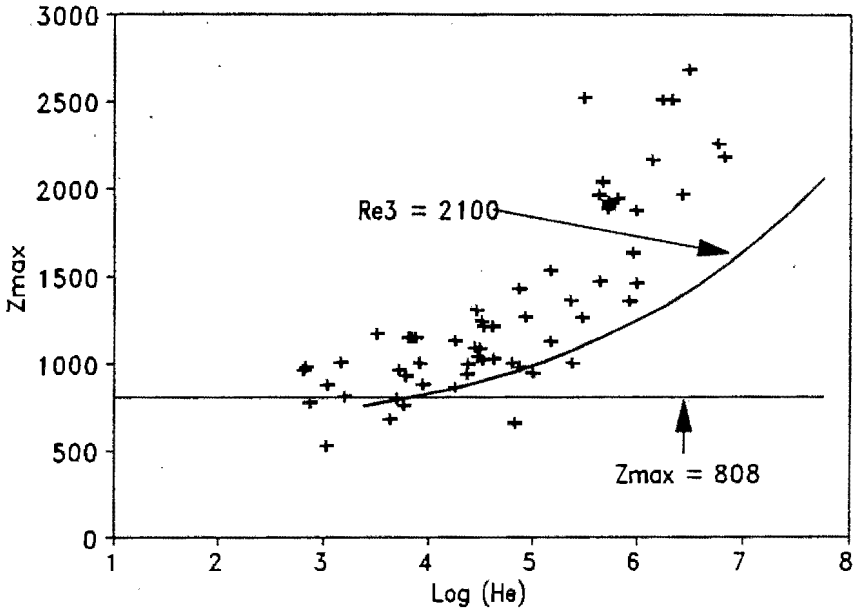

Figure 6.6 : Z_{max} vs Hedström number

Figure 6.6 shows that the Re_3 formulation is able to models the behaviour of the stability criterion, which is clearly not constant.

[Unless otherwise stated, the following values are used for graphs in this chapter: density=1200kg/m^3; diam=100mm; τ_y=5,0921Pa; K=0,3008Pa s^n; n=0,4832; d_x=32μm]

6.2.5 Sensitivity

As in Section 4.3.3, the sensitivity of the new models can be gauged by using the three rheologies given in the section on forced fits. These results are tabulated below.

Table 6.II : Sensitivity of the New Laminar/Turbulent Transition Models using the Forced Fit Data.

	Re_1	Re_2	Re_3
Yield Pseudoplastic	2929	3421	2253
Pseudoplastic	2960	3391	3391
Bingham Plastic	2904	3446	1738

These results show that Re_1 is the least sensitive and Re_3 is the most sensitive to changes in the rheology. This sensitivity is exaggerated here as the different sets of rheologies were purposely chosen as extreme cases. Note that Re_2 and Re_3 obtain the same value for the pseudoplastic model as there is no yield stress and consequently, no plug.

6.2.6 Roughness Reynolds Number

An important fact which comes to light is that Re_2 is at least as good as previous Reynolds numbers and stability criteria in predicting the onset of turbulence. This justifies the extrapolated use of Re_2 in the form of the roughness Reynolds number formulation used in the turbulent flow model.

6.2.7 Reversion to the Newtonian Model

The new Reynolds numbers revert to the Newtonian form under Newtonian conditions.

6.2.8 Use of the new Reynolds Numbers

The use of the new Reynolds numbers can be considered in three sections - laminar, transitional and turbulent flow.

(i) Laminar Flow

In conventional Newtonian flow, the Reynolds number can be used to correlate data against friction factor. This will produce a correlation on the line $f=16/Re$. Similarly, the new Reynolds numbers can be used to correlate slurry flow data in laminar flow. In order to accommodate the annular flow concepts associated with plug flow, an annular friction factor is defined as

$$f_{ann} = \frac{2\,\tau_0}{\rho\, V_{ann}^2} \qquad (6.1)$$

Using Equation (2.13) these correlations are plotted using the new Reynolds numbers in Figure 6.7 and Figure 6.8.

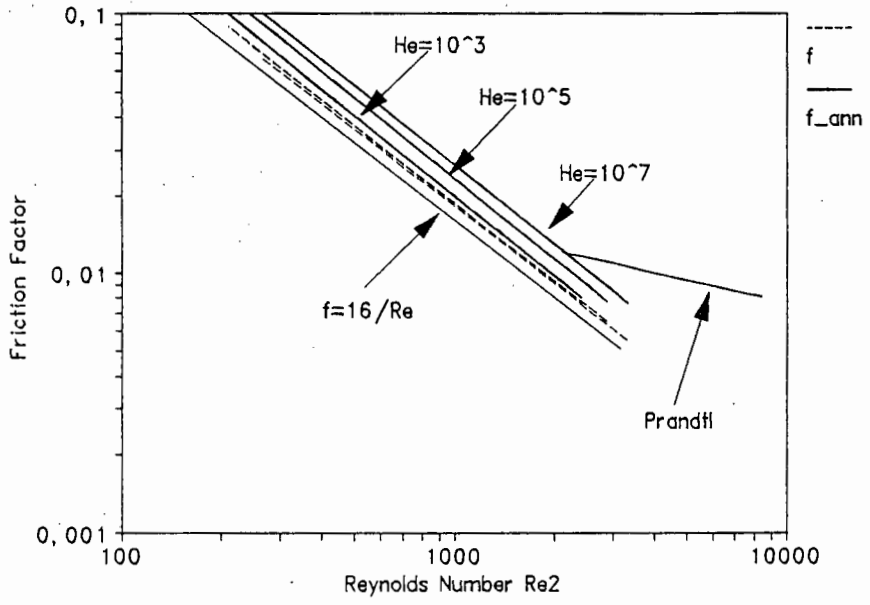

Figure 6.7 : Laminar flow correlation using Re_2

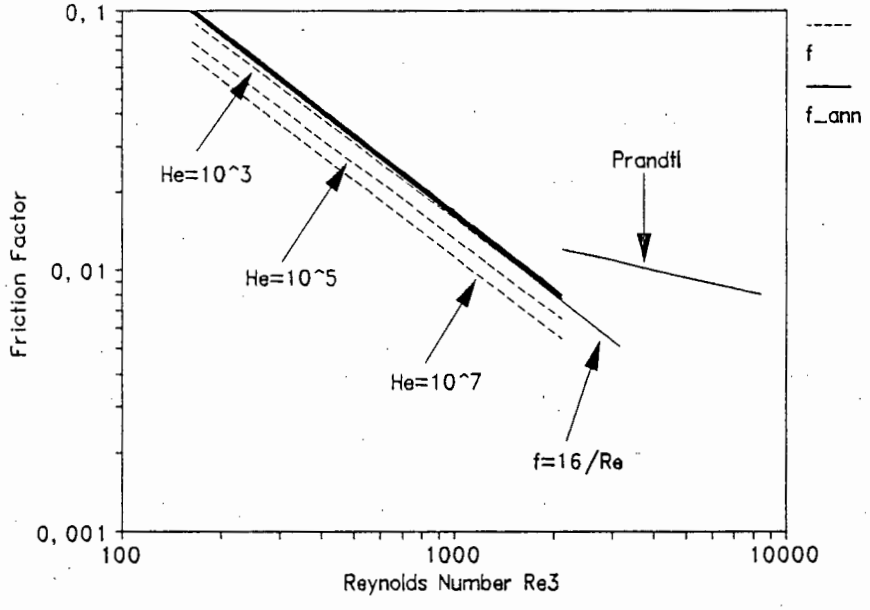

Figure 6.8 : Laminar flow correlation using Re_3

Figure 6.7 shows that Re_2 will provide an approximate correlation using the standard friction factor, with a slight Hedström number effect. Using the annular friction factor produces a more pronounced Hedström number effect.

Figure 6.8 shows that Re_3 will correlate laminar flow data in the conventional

way provided that the annular friction factor is used. Using the standard friction factor produces a pronounced Hedström number effect. Both friction factors have been plotted for the same range of Hedström number.

(ii) Transitional Flow

The new formulation Re_3 can be used for the determination of the critical velocity, V_c. In this respect, Re_3 performs a similar service to the conventional Reynolds number in Newtonian flow and is superior to Re_2.

(iii) Turbulent Flow

Once the critical velocity has been exceeded, the flow becomes turbulent, the plug is assumed to be broken down by the turbulent eddies, and Re_2 and Re_3 become identical. By extrapolation of the extended use of the Reynolds number in conventional turbulent flow, Re_3 can be used to correlate the friction factor, as is done in Figure 6.18 to Figure 6.20.

While the above points emphasize the similarity between the use of the new formulations and the use of the conventional Reynolds number, there is an important difference which should be stressed. The conventional Reynolds number can be used to establish dynamic similarity between two flows past geometrically similar surfaces provided that they are affected only by viscous, pressure and inertia forces (Massey, 1970). A prerequisite is that the characteristic length used is significant in determining the pattern of flow. As stated in Section 4.3.3, the velocity profile for two different diameter pipes conveying the same non-Newtonian slurry at the critical velocity will be geometrically different. Even if the sheared diameter is used, as in Re_3, geometric and consequently dynamic similarity will only be approximate.

Generally, Re_3 can be regarded as being superior to Re_2 in laminar and transitional flow, and identical in turbulent flow. Re_2 can be regarded as the generic predecessor to Re_3, and the roughness and particle Reynolds numbers.

6.3 TURBULENT FLOW

The results of a typical test are shown in Figure 6.9 with the predictions of the theoretical models.

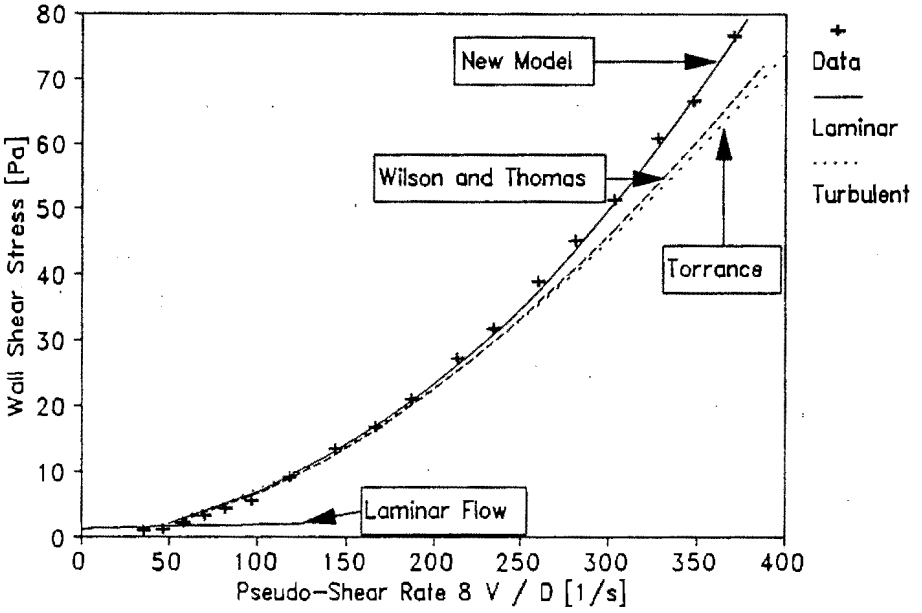

Figure 6.9 : Typical test results showing turbulent flow predictions.
Test KERM2408.

The full results are shown in Appendix A. Each data set has been analysed with the log standard error and average percentage error for each set of data. These tables and figures show that the new model provides a better prediction than the other models, particularly in the fully developed turbulent flow region.

The turbulent model evaluations for the entire data base are presented in Table 6.III.

Table 6.III Turbulent Model Evaluation - Whole Data Base.

	Torrance	Wilson & Thomas	New Model
Average % Error	17,18	15,07	10,04
Log Standard Error	0,0050	0,0038	0,0024

Table 6.III shows that the new model provides more accurate predictions than previous models for all the slurries tested.

6.3.1 Sensitivity of the New Model

The sensitivity of the new model with respect to the rheological characterisation procedure is shown using the rheologies from the forced fits and the 17% kaolin slurry test results from Xu *et al* (1993).

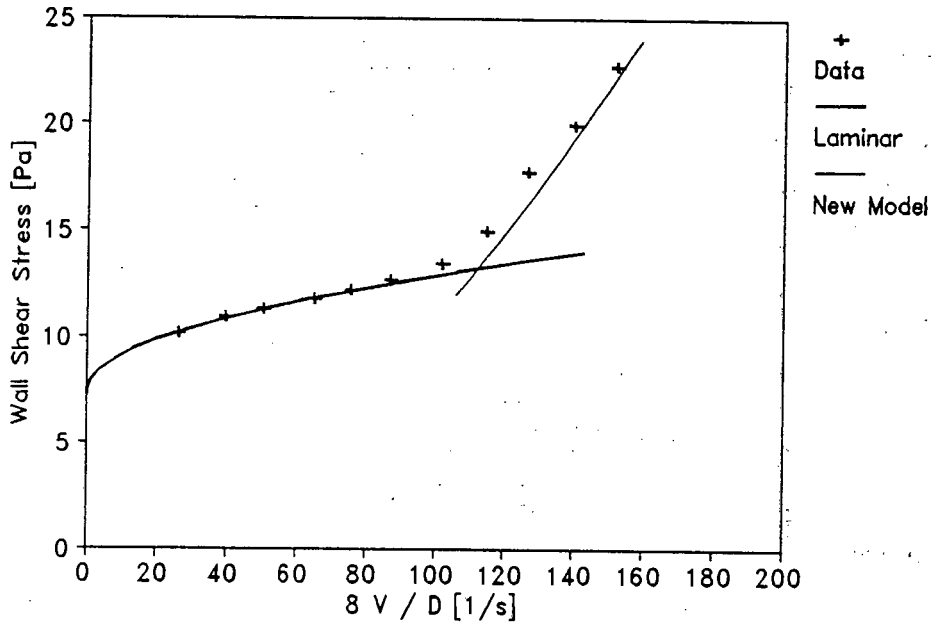

Figure 6.10 : Turbulent flow predictions for the new model using the forced fit **yield pseudoplastic** rheology. Data from Xu *et al*, 1993, Kaolin - 17%.

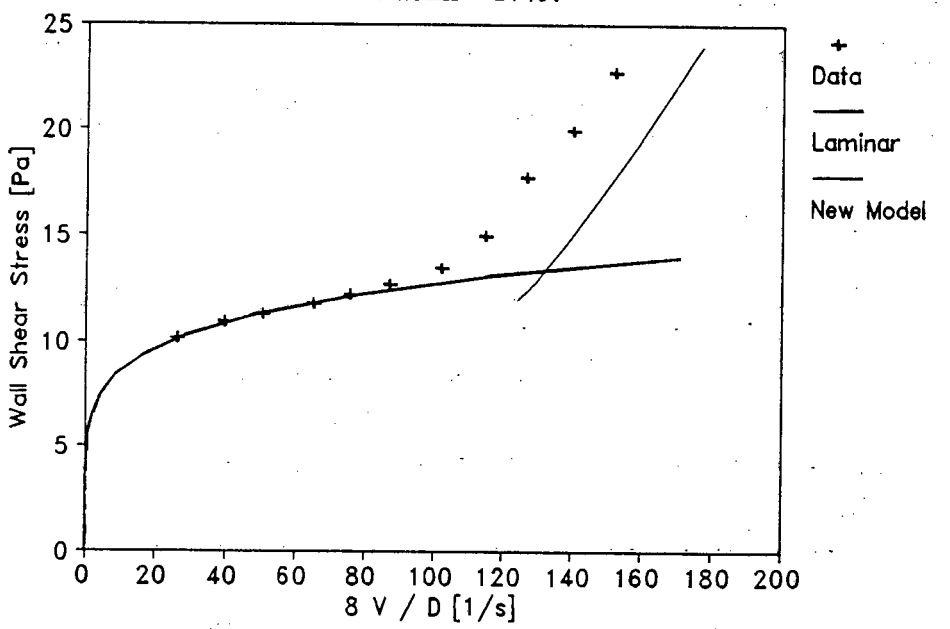

Figure 6.11 : Turbulent flow predictions for the new model using the forced fit **pseudoplastic** rheology. Data from Xu *et al*, 1993, Kaolin - 17%.

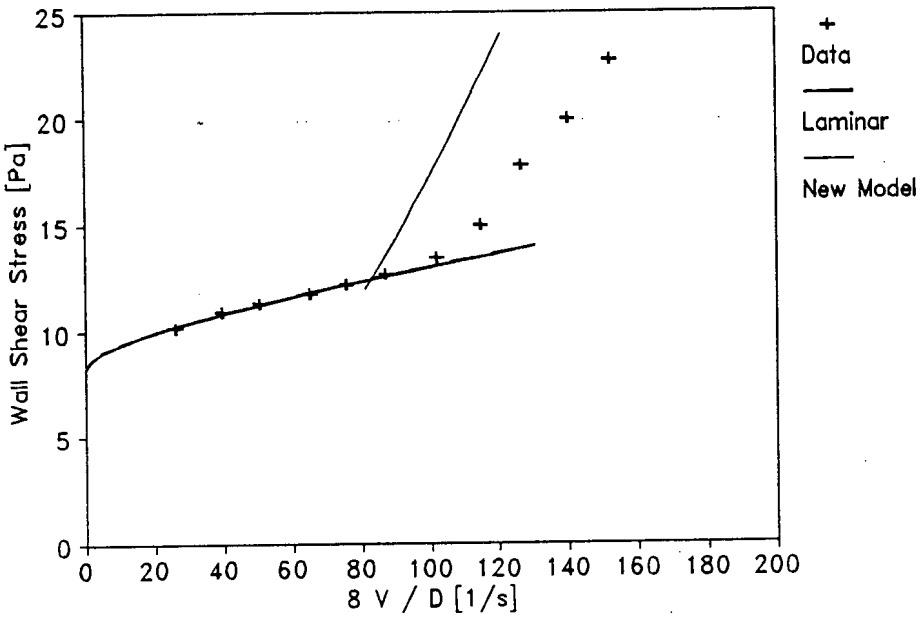

Figure 6.12 : Turbulent flow predictions for the new model using the forced fit **Bingham plastic** rheology. Data from Xu *et al*, 1993, Kaolin - 17%.

Figure 6.10 to Figure 6.12 show that the new model is sensitive to the choice of rheological model in the smooth wall region and will yield inaccurate results if an inappropriate rheological model is chosen. However, the new model is not as sensitive as the Wilson & Thomas model under these same conditions (see Chapter 4).

The sensitivity of the new model with respect to changes in variable are plotted in Figure 6.13 to Figure 6.16 below.

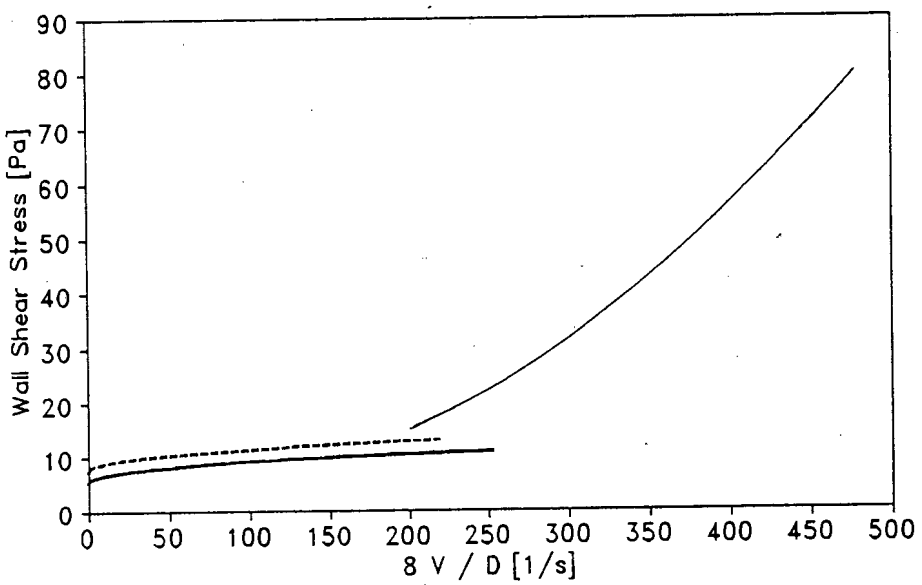

Figure 6.13 : Sensitivity : New Model : 40% increase in τ_y

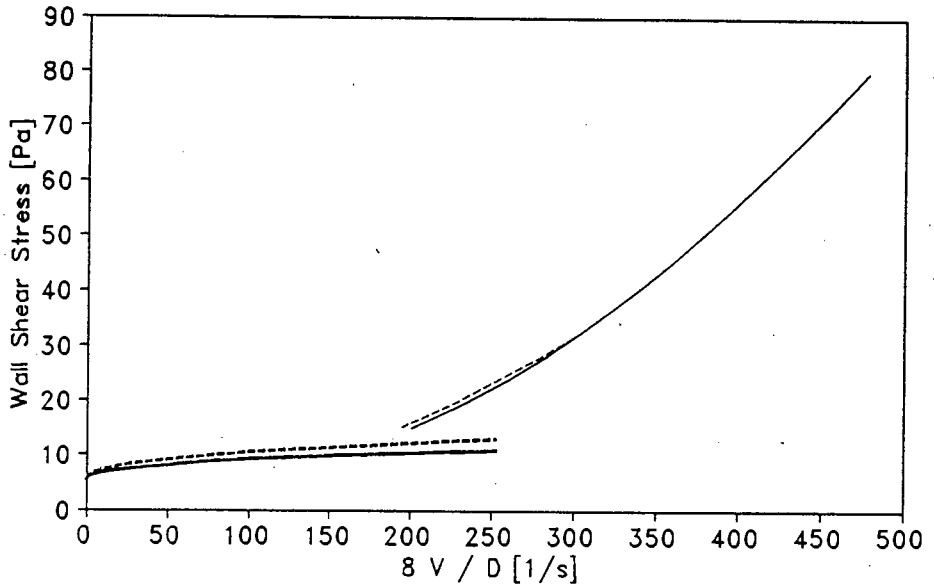

Figure 6.14 : Sensitivity : New Model : 40% increase in K

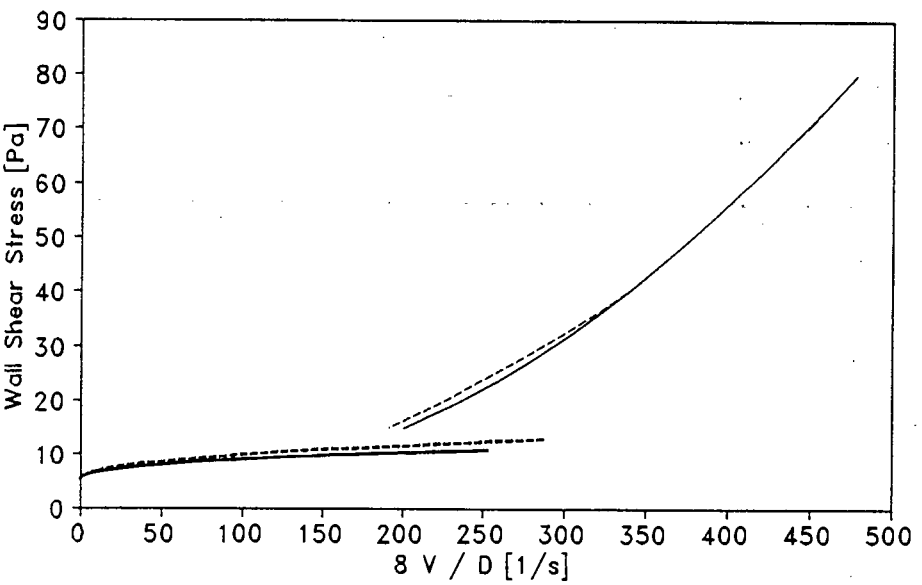

Figure 6.15 : Sensitivity : New Model : 10% increase in n

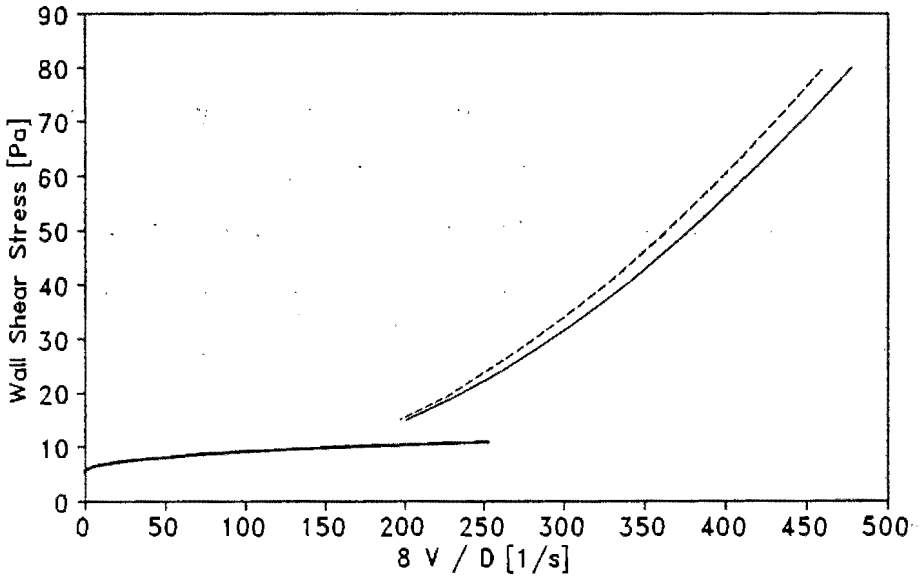

Figure 6.16 : Sensitivity : New Model : 40% increase in d_{85}

The average increases in the wall shear stress in each case are summarised in Table 6.IV below.

Table 6.IV : Sensitivity of the New Model

Variable	Increase in variable [%]	Average increase in Turbulent Flow τ_0 New Model [%]
τ_y	40	0,1
K	40	1,1
n	10	2,2
d_x	40	7,3

The new model is much less sensitive to changes in variable than the other models, in the rough turbulent region.

6.3.2 Laminar Sub-layer Thickness

The thickness of the laminar sub-layer can be determined as the intersection of the velocity distributions in the laminar sub-layer and the turbulent core (Wilson *et al*, 1992). This thickness is plotted against wall shear stress in Figure 6.17.

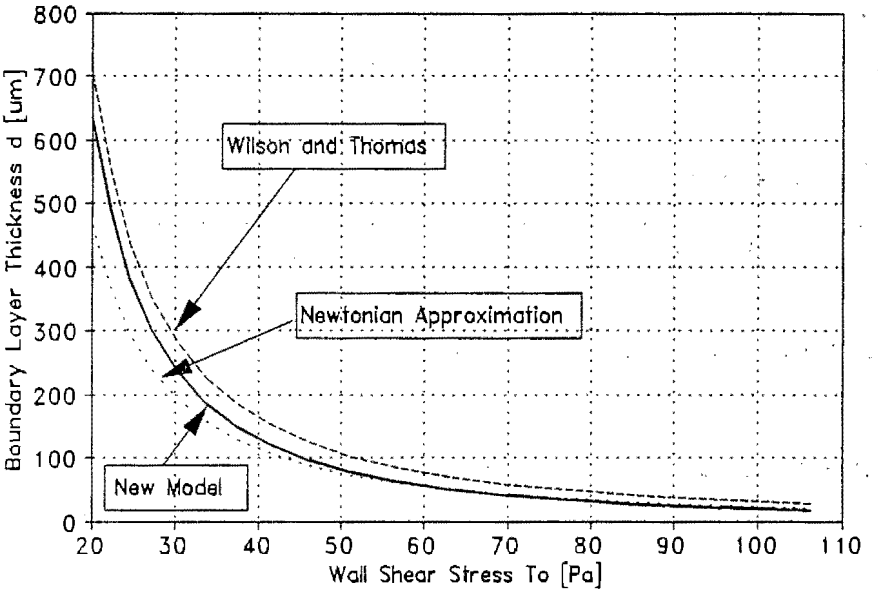

Figure 6.17 : Laminar Sublayer Thickness

This figure shows that the laminar sub-layer thickness predicted by the new model lies between the thicknesses predicted by the Newtonian approximation model and the model of Wilson & Thomas. The new model is closer to the predictions of Wilson & Thomas at low shear stresses and closer to the Newtonian approximation at higher shear stresses.

6.3.3 Smooth wall turbulent flow

The correlation of the roughness function B shows that smooth wall turbulent flow occurs if the roughness Reynolds number is less than 3,32. By analogy with Newtonian flow, smooth wall turbulent flow is characterised by an intact laminar sub-layer. In this region, the solid particles do not generate extra turbulence due to form drag.

Smooth wall turbulent flow is further characterised by a continuously decreasing friction factor. Unfortunately, due to the additive nature of both the constitutive rheological equation and the Reynolds number formulation, the equations do not resolve into a compact Re-f form. Also due to the additive nature of the fundamental relationships is the fact that the roughness size (representative particle size) does not vanish from the smooth wall equation as in the Newtonian case. However, the effect is small and has not affected the accuracy of the model for the slurries tested.

In this region, the new model predictions are similar to those of Torrance and Wilson & Thomas. As concluded earlier, these models perform well in this early turbulent region. The actual accuracy depends more on the accuracy of the rheological characterisation than the choice of model.

6.3.4 Fully developed or rough wall turbulent flow

Fully developed or rough wall turbulent flow is characterised by a constant friction factor and total obstruction of the laminar sub-layer by the particles.

This constitutes a useful engineering tool, because in this region, the energy gradients depend only on the relative size of the particles (D/d_{85}), and provides an asymptote for the designer to work to in the absence of accurate rheological data.

The correlation of Bowen (1961) exploits this similarity of the fully developed turbulent flow region and it is used in his scale up law.

6.3.5 Partially rough wall turbulent flow

One of the characteristics of the new turbulent flow model is the abrupt change from smooth wall turbulent flow to fully developed or rough wall turbulent flow. However, as far as can be ascertained by observation of the test data graphs, this is the way in which the slurry behaves. An example of this is given in Figure 6.18. The abrupt change and therefore the absence of any significant transition region, is a true

reflection of the real behaviour of these slurries. This is in sharp contrast to the Newtonian case, where the transition region spans several orders of magnitude of Reynolds number (see Moody diagram - Chapter 2.) This abrupt change can also be seen in the results of Bowen (1961).

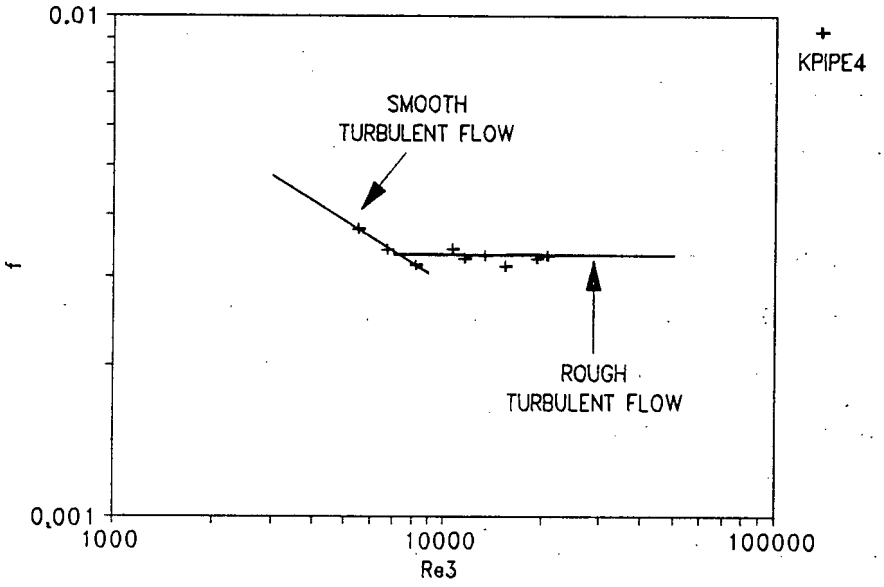

Figure 6.18 : Data from test KPIPE4 showing abrupt change from smooth to rough wall turbulence.

6.3.6 Friction Factor/Reynolds Number Diagrams

The new model can be plotted on a friction factor/Reynolds number diagram [Base values : density=1130kg/m^3; diameter=100mm; τ_y=10Pa; K=0,03Pa s^n; n=0,8; d_x=50μm]

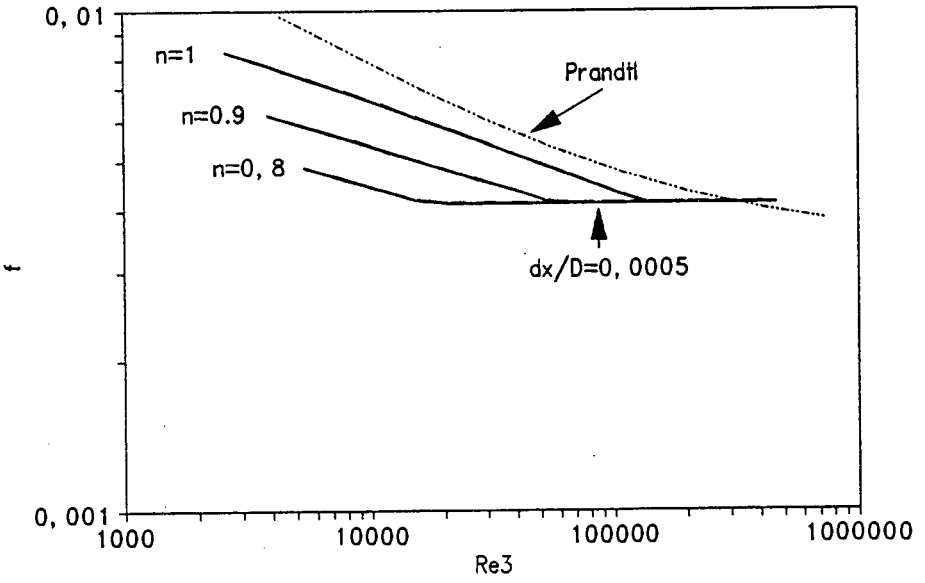

Figure 6.19 : Friction Factor vs Re_3 for the New Model

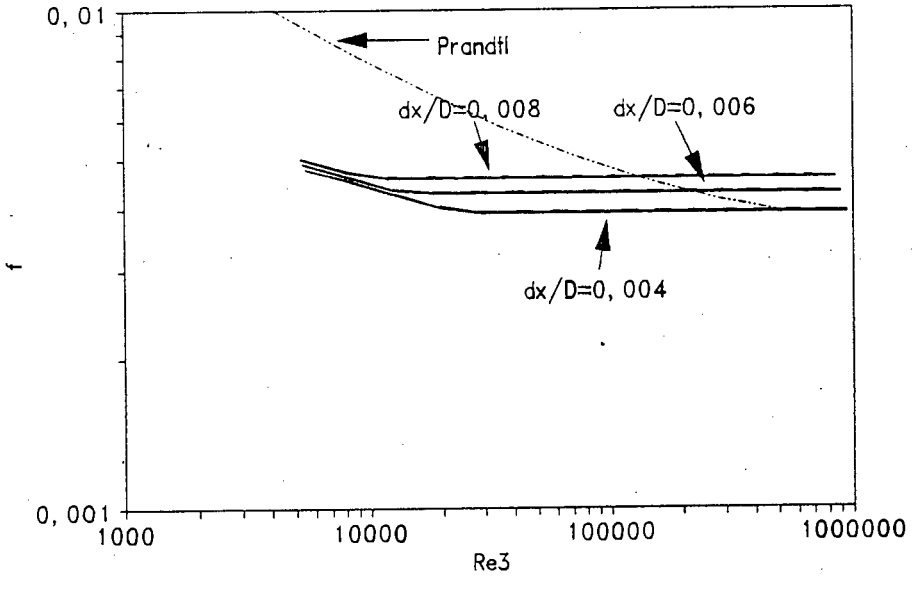

Figure 6.20 : Friction factor vs Re_3; New Model

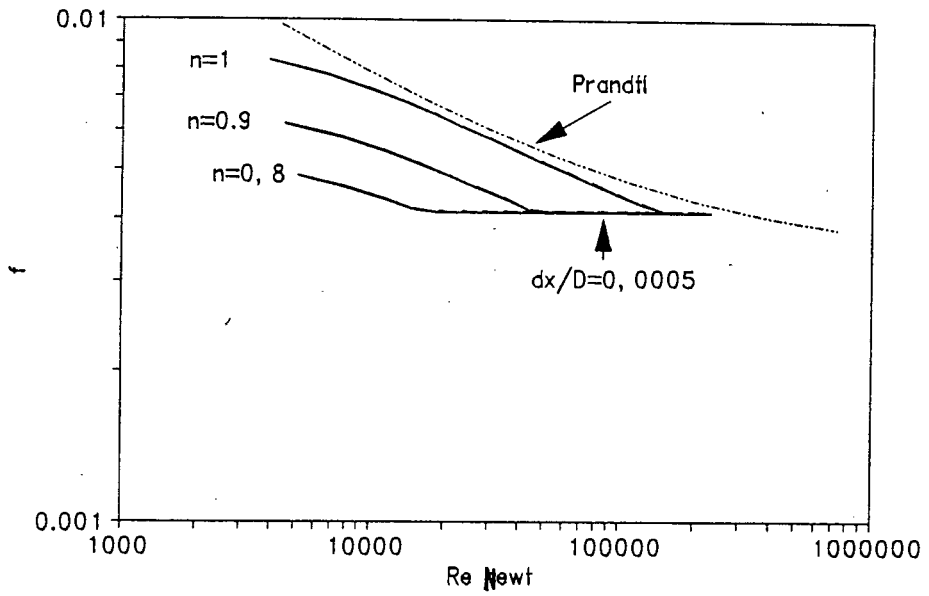

Figure 6.21 : Friction factor vs Re_{Newt}; New model

Figure 6.19 emphasises the importance of the slurry rheology in the smooth wall turbulent region. The friction factor is constant in the rough wall turbulent region.

Figure 6.20 shows the effect of different particle sizes for the same rheology. This is analogous to the relative roughness effect shown on the Moody diagram.

Figure 6.21 shows the convex nature of the smooth wall turbulent region when Re_{Newt} is used. A similar curved relationship is shown by Thomas & Wilson (1987) for this range of n values.

6.3.7 Pipe Roughness

An interesting dilemma arises in the new turbulent flow model when the pipe roughness approaches or exceeds the representative particle roughness size. The 200mm nominal bore steel pipe had a hydraulic roughness of 112μm and the tests of Park *et al* (1989) were in a steel pipe for which a reasonable hydraulic roughness is estimated at 45μm. These values exceeded the representative particle roughness sizes. In these two cases the matter was resolved by using the larger value of either the representative particle size or the pipe hydraulic roughness when calculating the

roughness-Reynolds number.

6.3.8 Analysis of the Particle Roughness Effect

The effect of relative particle size on wall velocity gradient for the new model is shown in Figure 6.22.

This Figure shows the turbulent velocity profile for the new model plotted for different representative particle sizes (d_x) for a constant average pipe velocity of 3m/s.

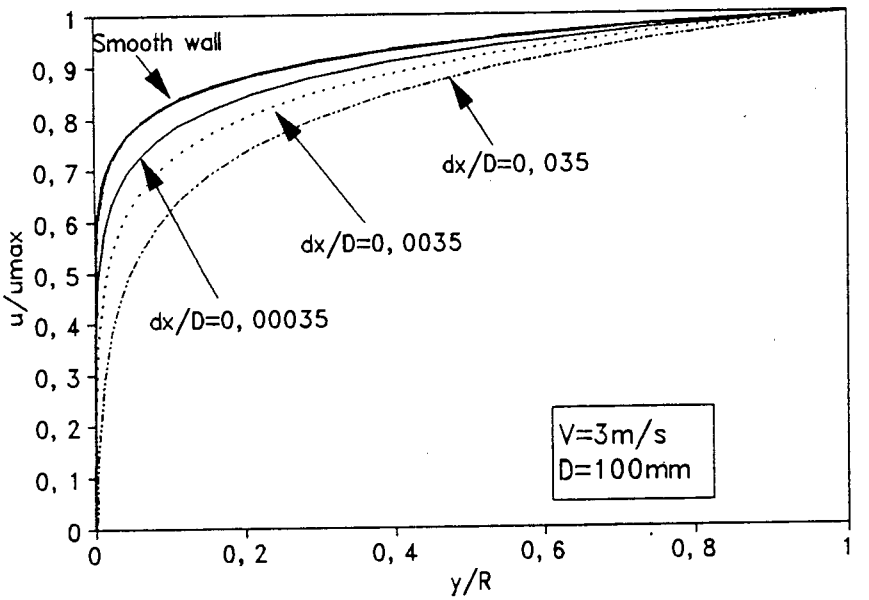

Figure 6.22 : The effect of relative particle size on wall velocity gradient

Figure 6.22 shows that the effect of relative particle size in the new model is to reduce the velocity gradient in the wall region, in a similar way to conventional pipe roughness.

The new model does not take into account any other fluid/particle interaction which may occur.

6.4 CONCLUSIONS - LAMINAR/TURBULENT TRANSITION MODEL

The new formulations of Reynolds number are reliable predictors of the laminar/turbulent transition for the slurries tested. The average value at the transition, obtained in this investigation $Re_3 \approx 2600$, may be higher than the true lower bound. For Newtonian fluids this value is taken as 2100. The lower bound of 2100 is retained to agree with, and ensure reversion to, the Newtonian model. The use of Re_3 is recommended for design purposes.

The new Reynolds number Re_3 displays a discontinuity at the transition which is in keeping with the fundamental change in behaviour of the slurry at this point.

It has been found that the stability criteria of Ryan & Johnson (1959) and Hanks (1981) is not a constant value, but increases with Hedström number. The new Reynolds number, Re_3, is able to model this increase.

The new models revert to the Newtonian model under Newtonian conditions.

6.5 CONCLUSIONS - TURBULENT FLOW MODEL

6.5.1 Rheological Characterisation

The correct procedure for obtaining the rheology of the slurries is critical in the smooth wall turbulent region and assumptions regarding rheological model should be kept as general as possible. The method employed here (Lazarus & Slatter, 1988) has yielded consistently accurate rheological characterisations. Accurate rheology is particularly important for turbulent flow predictions in the smooth wall turbulent region.

6.5.2 The effect of solid particles

The presence of solid particles present in a non-Newtonian slurry affects both quantitatively and qualitatively the turbulent pipe flow behaviour of the slurry.

6.5.3 Particle Roughness Effect

The turbulent pipe flow behaviour of these slurries can be understood qualitatively in terms of a particle roughness effect.

6.5.4 Velocity Distribution

The velocity distribution is logarithmic and similar to the classical Newtonian turbulent velocity distribution. Plug flow does not occur in the turbulent core region.

The velocity distribution is shown in Figure 6.23 below.

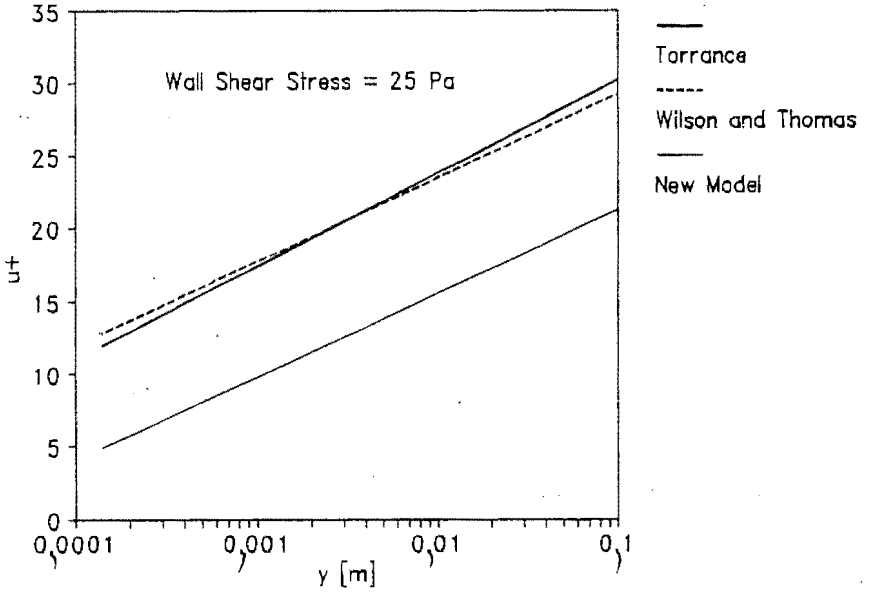

Figure 6.23 : Turbulent Velocity Distributions

6.5.5 Energy Gradient Prediction

Energy gradients for non-Newtonian turbulent slurry flow can be predicted using the rheology of the slurry and the particle size distribution. The predictive capability of the new model is more accurate than previous models for the test data base.

For design purposes, the model can be used to accurately predict energy gradients for the turbulent flow of non-Newtonian slurries. This model is mathematically simple and easy to apply. This will facilitate more efficient design of pipe systems conveying non-Newtonian slurries.

6.5.6 Fully Developed Rough Turbulent Flow

The fully developed rough turbulent flow behaviour for non-Newtonian slurries in pipes is independent of the viscous characteristics of the slurry. This constitutes a useful engineering tool which can be used as an asymptote by designers.

When the pipe roughness exceeds the representative particle size, then the pipe roughness size should be used to model the flow.

The new model confirms the findings and method of Bowen, and provides a rationale for his correlation.

The particle roughness effect reduces the velocity gradient in the wall region, similar to the effect of conventional pipe roughness. Outside of the wall region, the continuum approximation as been accepted and no particle/fluid interactions have been considered.

6.5.7 Sensitivity

The new model is relatively insensitive to changes in the rheology.

6.5.8 Reversion to the Newtonian Model

The new model reverts to the Newtonian model asymptotes under Newtonian conditions.

6.6 FINAL CONCLUSIONS

Despite the fact that the new theoretical analysis is based on qualitative interpretations of physical behaviour, it remains, to some significant extent, an empirical description.

In the absence of any exact theoretical analysis, it is important, from an engineering perspective, to develop models which satisfactorily interpret experimental data and which provide a competent basis for design. The assumptions, approximations and simplifications present in the new analysis will doubtless prove controversial, but this is to be seen as healthy debate which, it is hoped, will further both the science and practice which comprises engineering technology.

The ultimate test of the new analysis is whether it is an improvement on existing analyses and models. The evidence presented in this chapter shows that the new analysis does provide a significant improvement and can be used as a basis for practical design.

CHAPTER 7

CHAPTER 7
SUMMARY, SIGNIFICANT CONTRIBUTIONS AND RECOMMENDATIONS

7.1 INTRODUCTION

This thesis describes a research project which has culminated in a new model for turbulent flow of non-Newtonian slurries in pipes. The model is based on widely accepted fundamentals and is the first cohesive study to include both the rheology of the slurry and the particle size distribution of the solids.

This work seeks to make a direct contribution to the understanding of the laminar/turbulent transition and turbulent flow behaviour of non-Newtonian slurry flow in pipes, in both a qualitative and quantitative sense. Previous research has failed to find an adequate explanation for, and a mathematical model of, transitional and turbulent flow of non-Newtonian slurries in pipes.

7.2 SUMMARY

Vast tonnages of solids in suspension as non-Newtonian slurries are transported each year in pipelines in many different industries. The problem of accurate design for these slurries has remained unresolved and the transitional and turbulent behaviour is not well understood, despite much research in this area. Often, the design of these pipelines is based on full scale pipe tests - an expensive procedure. The main aim of this thesis is to develop a theoretical analysis which reliably predicts pipeline energy requirements for non-Newtonian slurries in the turbulent flow regime.

The laminar flow of non-Newtonian slurries is well understood and a general method for reliably determining the rheology of a slurry from small diameter pipeline tests has been verified. The literature contains several models for the prediction of the laminar/turbulent transition. The non-Newtonian Reynolds numbers of the Newtonian approximation, Metzner & Reed and Torrance, as well as the stability criterion models of Ryan & Johnson and Hanks,

and the practical intersection method are investigated. The Newtonian turbulent flow model, and the non-Newtonian models of Torrance, Wilson & Thomas, Dodge & Metzner and Kemblowski & Kolodziejski, and the correlation of Bowen are reviewed. Other pertinent points from the literature are the striking similarity between Newtonian and non-Newtonian turbulent flow, the value of the von Karman constant for non-Newtonian turbulence, the presence of the unsheared plug at the pipe axis due to the yield stress, the particle size effect and the continuum approximation. Recent experimental work has highlighted the problem of accurate turbulent behaviour prediction.

Three test facilities were built for the establishment of a data base of non-Newtonian slurry tests - the Balanced Beam Tube Viscometer and two pumped pipe recirculating rigs known as the East Rig and the Mini Rig. Reliable test techniques were developed for these facilities and test data covering wide ranges of diameter (5mm to 200mm nominal bore), mean pipe velocity (0,1m/s to 10m/s), slurry relative density (1,02 to 1,65), volumetric concentration (2% to 37%), solids relative density (2,4 to 2,8) and particle size range (d_{85} = 24 to 120μm) has been collected. The experimental errors pertaining to the apparatus were analysed, quantified and are within acceptable limits. This data base is used for the analysis and evaluation of the models from the literature.

The rheological characterisation procedure is found to be general and accurate. The Torrance Reynolds number is unable to predict the onset of turbulence, implying that the complete rheology must be considered. The Metzner & Reed Reynolds number produces the best results of the Reynolds number formulations and the intersection method is the overall best at predicting the laminar/turbulent transition. An increasing trend in the value of the stability criterion with increasing Hedström number is evident. The turbulent flow predictions of the Torrance and Wilson & Thomas models are similar and produce good results in the early turbulent region. However, the shape of the graphs of the models is different from the test data loci and the accuracy of the models decreases as the shear stress increases. Predicted thicknesses of the laminar sub-layer are less than the size of the larger particles indicating that the continuum approximation is being compromised in the wall region. The models are shown to be sensitive to changes in rheology. It is concluded that the models from the literature do not accurately describe the behaviour of the slurries tested and that the particle size as well

as the rheology of the slurry is necessary to describe the behaviour.

A new analysis is introduced in two main parts. The laminar/turbulent transition for pipe flow is modelled using a Reynolds number proportional to the inertial-to-viscous force ratio and considering the unsheared plug at the pipe axis. Turbulent flow is modelled using the classical universal logarithmic velocity distribution and a new formulation of the roughness Reynolds number which incorporates a representative particle size. The Newtonian turbulent flow asymptotes are used to correlate the roughness function.

The new analysis is evaluated using the data base. The new pipe Reynolds number Re_3 is found to be a reliable predictor of the laminar/turbulent transition and the increase in the value of the stability criterion can be predicted using Re_3. The new Reynolds number reverts to the Newtonian form under Newtonian conditions. Turbulent flow predictions using the new turbulent model are accurate and better that previous models, particularly in the rough wall region. The turbulent pipe flow behaviour of non-Newtonian slurries can be understood in terms of a particle roughness effect. The new model is computationally simple and will facilitate more efficient design. Fully developed rough turbulent flow is independent of the slurry rheology and this constitutes a useful engineering design tool. The new model reverts to the Newtonian asymptotes under Newtonian conditions.

The new model represents an improvement over previous models and is recommended for the design of non-Newtonian slurry pipelines.

7.3 SIGNIFICANT CONTRIBUTIONS

A new analysis of non-Newtonian slurries in pipelines has been developed. The recommended design procedure which has resulted from this thesis is presented in Appendix D.

The contributions for the flow analysis of these slurries can be divided into four sections - laminar flow, the laminar/turbulent transition, turbulent flow and experimental work.

7.3.1 Laminar Flow

(i) The correct rheological model and the accurate application of this model are of paramount importance for accurate smooth wall turbulent flow predictions.

(ii) The yield pseudoplastic rheological model and the rheological characterisation approach of Lazarus & Slatter (1988) have been shown to yield consistently accurate rheologies for the slurries tested.

7.3.2 Laminar/Turbulent Transition

(i) The stability criteria of Ryan & Johnson and Hanks are not constant and can be modelled with the new Reynolds number (Re_3).

(ii) A new non-Newtonian Reynolds number formulation has been developed which uses the complete rheology and the unsheared core geometry.

(iii) The laminar/turbulent transition can be reliably predicted using the new Reynolds number (Re_3).

An important feature of the new Reynolds number formulations is that they revert to the Newtonian form for Newtonian rheology ($\tau_y=0$, $K=\mu$ and $n=1$).

7.3.3 Turbulent Flow

(i) Previous models (Torrance and Wilson & Thomas) are smooth wall models and cannot take a particle size effect into account.

(ii) The turbulent behaviour of the slurries tested can be interpreted in terms of a particle roughness effect which has been described both qualitatively and quantitatively.

(iii) A roughness Reynolds number has been formulated in terms of the complete rheology and the representative particle size of the solids. This number has been used successfully to correlate the roughness function with test data for the new turbulent flow model.

(iv) The transition from smooth to rough turbulent flow is abrupt and is successfully described by the new turbulent flow model.

(v) Fully developed (rough) turbulent flow is an inertial process and is independent of the rheology.

(vi) The new rough turbulent flow model is not sensitive to changes in rheology.

(vii) The rough turbulent flow friction factor is constant and related to the representative particle size for fully developed non-Newtonian turbulent flow.

(viii) The new analysis can be used to describe the behaviour of non-Newtonian slurries both qualitatively and quantitatively.

The new turbulent flow model has been validated using the experimental data. Consequently, the following assumptions used in the analysis are considered to be valid:

(i) The continuum approximation breaks down in the wall region because the effect of the particles must be considered.

(ii) The solid particles present in the slurry are capable of obstructing the laminar sub-layer and the steep velocity gradients in the wall region.

(iii) Plug flow does not occur in non-Newtonian turbulent flow.

(iv) The non-Newtonian turbulent velocity distribution is similar to the classical

Newtonian logarithmic universal velocity distribution over the entire core region.

(v) The von Karmen universal constant value of $\chi = 0,4$ is unaffected by the slurry rheology and can be used in non-Newtonian turbulent flow.

7.3.4 Experimental Work

The theoretical investigation is supported by a unique and extensive experimental investigation covering wide ranges of slurry properties and flow conditions.

7.4 FUTURE RESEARCH RECOMMENDATIONS

It has been shown that both the pipe surface and the solid particles produce a roughness effect in turbulent flow. The interaction of these two phenomena should be investigated further. This could be done by testing the same slurry in progressively rougher pipes.

The shape of the particle size distribution was similar (well graded) for all the slurries tested in this work. The effect of different shaped particle size distributions (eg, bimodal) and in particular, its effect on the representative particle size to be used for the roughness Reynolds number, should be investigated.

The highest roughness Reynolds number achieved in this work was approximately 16. This was a limitation of both the highest shear stress measurable in the apparatus under test conditions and the representative particle roughness size. An investigation to test the validity of the new model at higher roughness Reynolds numbers, using higher shear rates and larger particles, should be done.

In mixed regime flow (Wilson *et al*, 1993, Lazarus & Cooke, 1993, Maciejewski *et al*, 1993), the slurry can be divided into three portions; the bed load, the suspended load and the vehicle (non-Newtonian slurry). The new model should be incorporated into a mixed regime model to predict the vehicle energy requirements under these conditions.

7.5 CONCLUSION

The major findings of this thesis and the contribution that this work seeks to make to existing knowledge in this subject have been presented and the following final conclusions can be made.

- The laminar flow of the non-Newtonian slurries tested for this thesis can be modelled successfully using the yield pseudoplastic rheological model, provided that accurate rheological characterisation is performed.

- Existing models for the prediction of transitional and turbulent flow have been investigated, analysed, and their shortcomings have been illustrated. New analytical models for transitional and turbulent flow have been developed.

- The laminar/turbulent transition for non-Newtonian slurry pipe flow can be modelled using the complete rheology and the geometry of the unsheared plug. A new Reynolds number has been developed which is able to predict the laminar/turbulent transition with greater accuracy than before.

- A particle roughness effect has been discovered and it has been shown that accurate analysis of non-Newtonian slurry turbulent flow must utilise both the rheology of the slurry and the representative particle size of the solids. A new roughness Reynolds number has been formulated which leads to the new method of analysing non-Newtonian turbulent flow.

- These findings are supported by a unique experimental investigation over wide ranges of pipe diameter, flow regime and slurry properties.

- The final recommended design procedure is presented in Appendix D. This new method should lead to more efficient design of slurry pipe systems.

REFERENCES

REFERENCES

ABBAS M A and CROWE C T (1986), The effect of particle size and concentration on the flow properties of a homogeneous slurry. In *International symposium on slurry flows,* M C Roco and W Wiedenroth, eds. New York: ASME Vol FED-38 109-112.

ANSLEY R W and SMITH T N (1967), Motion of a spherical particle in a Bingham plastic, *AIChE Journal*, Vol 13 No 6.

AL-FARISS T and PINDER K L (1987), Flow through porous media of a shear-thinning liquid with a yield stress, *Can. J. Chem. Eng.*, 65, 391-405.

BARR G (1931), *A Monograph of Viscometry*, Oxford University Press.

BAW P S and PESKIN R L (1971), Some aspects of gas-solid suspension turbulence, *J. Basic Engng*, 93D.

BOWEN R LeB (1961), Designing turbulent flow systems, *Chem. Eng.* 68 143-150

BRINKWORTH B J (1968), *An introduction to experimentation,* English University Press, London.

BS 1377 (1975), *Methods of test for soils for civil engineering purposes*, British Standards Institution, London.

CALDWELL D H and BABBITT H E (1941), The flow of muds, sludges and suspensions in circular pipes, *Trans. Am. Inst. Chem. Eng.*, 37, 237-266.

CHENG D C-H (1970), A design procedure for pipeline flow of non-Newtonian dispersed systems, *1st Int. Conf. on the hydraulic transport of solids in pipes,* Hydrotransport 1 Paper J5.

CHHABRA R P and RICHARDSON J F (1985), Hydraulic transport of coarse particles in viscous Newtonian and non-Newtonian media in a horizontal pipe, *Chem. Eng. Res. Des.*63 390-397.

CLAPP R M (1961), Turbulent heat transfer in pseudoplastic non-Newtonian fluids, *International developments in heat transfer,* ASME Part III, Section A, 652.

COLEBROOK C F (1939), Turbulent flow in pipes, with particular reference to the transition region between the smooth and rough pipe laws, *J. Instn. Civil Engrs.,* No. 4, Paper 5204.

DEDEGIL M Y (1986), Drag coefficient and settling velocity of particles in non-Newtonian suspensions. In *International symposium on slurry flows,* M C Roco and W Wiedenroth, eds. New York: ASME Vol FED-38 9-15.

DODGE D W and METZNER A B (1959), Turbulent flow of non-Newtonian systems, *AIChE Journal*, Vol. 5, No. 2, 189-204.

DUCKWORTH R A, PULLUM L, LOCKYEAR C F, and ADDIE G R (1986), The pipeline transport of coarse materials in a non-Newtonian carrier fluid, *10th Int. Conf. on the hydraulic transport of solids in pipes,* Hydrotransport 10 Paper C2.

EDWARDS M F and SMITH R (1980), The turbulent flow of non-Newtonian fluids in the absence of anomalous wall effects, *Journal of non-Newtonian fluid mechanics,* 7, 77-90.

FADDICK, R R (1986), Slurry flume design, *10th Int. Conf. on the hydraulic transport of solids in pipes,* Hydrotransport 10 Paper E1.

GOVIER G W and AZIZ K (1972), The Flow of Complex Mixtures in Pipes, *van Nostrand Reinhold Co.*

HANKS R W (1963), The laminar/turbulent transition for fluids with a yield stress, *AIChE Journal*, Vol 9 No 3.

HANKS R W (1978), Low Reynolds number turbulent pipeline flow of pseudohomogeneous slurries, *5th Int. Conf. on the hydraulic transport of solids in pipes,* Hydrotransport 5 Paper C2.

HANKS R W (1979), The axial laminar flow of yield-pseudoplastic fluids in a concentric annulus, *Ind Eng Chem Process Des Dev,* 18, 3.

HANKS R W (1981), Course notes. Hydraulic design for flow of complex fluids., *1981 Richard W Hanks Associates, Inc. Orem, Utah.* USA.

HANKS R W and DADIA B H (1971), Theoretical analysis of the turbulent flow of non-Newtonian slurries in pipes, *AIChE Journal,* Vol 17 No 3, 554-557.

HANKS R W and RICKS B L (1974), Laminar-transition in flow of pseudoplastic fluids with yield stress, *J. Hydronautics*, Vol. 8, No. 4.

HANKS R W and RICKS B L (1975), Transitional and turbulent pipeflow of pseudoplastic fluids, *J. Hydronautics*, Vol. 9, No. 1.

HANKS R W and SEN S (1983), The influence of yield stresses and fluid rheology on particle drag coefficients, *8th International Technical Conference of the Slurry Transport Association (held in San Francisco),* Washington DC.

HARRIS J and QUADER A K M A (1971), Design procedures for pipelines transporting non-Newtonian fluids and solid liquid systems, *Brit. Chem. Engrg.*, Vol 16 No 4/5.

HEDSTRÖM B O A (1952), Flow of plastics materials in pipes, *Industrial and engineering chemistry,* v.44 No.3.

HERSCHEL W H and BULKLEY R (1926), Measurement of consistency as applied to rubber-benzene solutions, *Proc ASTM,* 26 Part 2 621-633.

HEYWOOD N I, MEHTA K B and POPLAR D (1993a), Evaluation of seven commercially available electromagnetic flowmeters with Newtonian and non-Newtonian china clay slurry in pipeflow, *12th Int. Conf. on slurry handling and pipeline transport,* Hydrotransport 12, BHR Group, p353.

HEYWOOD N I, MEHTA K B, POPLAR D and MOORE C D (1993b), Assessment of flow properties of pulverised fuel ash slurries at high concentration, *12th Int. Conf. on slurry handling and pipeline transport,* Hydrotransport 12, BHR Group, Supplement to the proceedings.

HOLLAND F A (1973), *Fluid flow for chemical engineers,* Edward Arnold, London.

IRELAND, J W (1971), *Mechanics of fluids*, Butterworths.

JACOBS B E A (1993), Laminar/turbulent flow through an annulus with sudden constrictions; as found in the Gannet project flowline bundles, *12th Int. Conf. on slurry handling and pipeline transport,* Hydrotransport 12, BHR Group, Supplement to the proceedings.

JANNA, W S (1983), *Introduction to fluid mechanics*, Brooks/Cole Engineering Division.

JOHNSON M (1982), Non-Newtonian fluid system design - some problems and their solutions, *8th Int. Conf. on the hydraulic transport of solids in pipes,* Hydrotransport 8 Paper F3.

KEMBLOWSKI Z and KOLODZIEJSKI J (1973), Flow resistances of non-Newtonian fluids in transitional and turbulent flow, *Int. Chem. Eng.* 13 265-279.

KILNER F A (1971). Notes on velocity distribution and friction factor equations for circular pipes. Course notes, University of Cape Town.

KNIGHT, J (1993), Private communication, Physics Dept, University of Cape Town.

LAZARUS J H (1992). The hydraulic transport of solids in pipes. Course notes, University of Cape Town.

LAZARUS J H and COOKE R (1993), Generalised mechanistic model for heterogeneous flow in a non-Newtonian vehicle, *12th Int. Conf. on slurry handling and pipeline transport,* Hydrotransport 12, BHR Group, p671.

LAZARUS J H and NEILSON I D (1978), A generalised correlation for friction head losses of settling mixtures in horizontal smooth pipelines, *5th Int. Conf. on the hydraulic transport of solids in pipes,* Hydrotransport 5, Paper B1.

LAZARUS J H and SLATTER P T (1988), A method for the rheological characterisation of tube viscometer data, *Journal of pipelines,* v.7.

LAZARUS J H and SLATTER P T (1986), Comparative rheological characterisation using a balanced beam tube viscometer and rotary viscometer, *10th Int. Conf. on the hydraulic transport of solids in pipes,* Hydrotransport 10, Paper J2.

LOEWENTHAL R E (1994), Private Communication, University of Cape Town.

LUMLEY J L (1978), In *Topics in applied physics; Volume 12; Turbulence,* Ed P Bradshaw 2nd edition, Springer-Verlag, New York.

MACIEJEWSKI W, OXENFORD J and SHOOK C A (1993), Transport of coarse rock with sand and clay slurries, *12th Int. Conf. on slurry handling and pipeline transport,* Hydrotransport 12, BHR Group, p705.

MASSEY B S (1970), *Mechanics of fluids,* Second edition, van Nostrand Reinhold Co.

MAUD A D and WHITMORE R L (1958), The turbulent flow of suspensions in tubes, *Trans. I. Chem Eng.,* 36 296-310.

MEHTA, K B (1993), Private communication, Warren Spring Labs, UK.

METZNER A B and REED J C (1955), Flow of non-Newtonian fluids - correlation of the laminar, transition and turbulent flow regions, *AIChE Journal*, v.1 n.4.

MICHIYOSHI I, MATSUMOTO R, MIZUNO K and NAKAI M (1966), Flow of slurry through a circular tube. Friction factor for tubes. Part II., *Int Chem Eng*, 6,2.

MOODY L F (1944), Friction factors for pipe flow, *Trans ASME November, 1944.*

MUN R (1988), Turbulent pipe flow of yield stress fluids, M Eng Sci Thesis, University of Melbourne.

NEILL R I G (1988), The rheology and flow behaviour of high concentration mineral slurries, Msc Dissertation, University of Cape Town.

OWEN P R (1969), Pneumatic transport, *J. Fluid Mech.*, 39.

PARK J T, MANNHEIMER R J, GRIMLEY T A, MORROW T B (1989), Pipe flow measurements of a transparent non-Newtonian slurry, *Journal of fluids engineering*, Vol. 111, 331-336.

PATERSON A J C (1991), The hydraulic transportation of high concentration stabilized flow full plant mineral tailings. Ph. D. thesis, University of Cape Town.

QUADER A K M A and WILKINSON W L (1980), Correlation of turbulent flow rate-pressure drop data for non-Newtonian solutions and slurries in pipes, *Int. J. Multiphase Flow*, 6, 553-561.

RABINOWITSCH B (1929), Über die viskosität und elastizität van solen, *Z. phisikal. Chem.*, 145,1.

RYAN N W and JOHNSON M M (1959), Transition from laminar to turbulent flow in pipes, *AIChE Journal,* 5 433-435.

SCHLICHTING H (1960), Chapter XX in *Boundary layer theory*, 4th edition, M^{c}Graw-Hill, New York.

SHOOK C A and ROCO M C (1991), *Slurry flow: principles and practice*, Butterworth-Heinemann.

SIVE A W (1988), An analytical and experimental investigation of the hydraulic transport of high concentration mixed regime slurries, PhD thesis, University of Cape Town.

SKELLAND A H P (1967), *Non-Newtonian flow and heat transfer,* John Wiley and Sons Inc, New York.

SLATTER P T (1986), The rheological characterisation of non-Newtonian slurries using a novel balanced beam tube viscometer, Msc Dissertation, University of Cape Town.

SLATTER P T and LAZARUS J H (1988), The application of viscometry to the hydraulic transport of backfill material, *Conf. Backfill in South African mines. (SAIMM).*

SLATTER P T and LAZARUS J H (1993), Critical flow in slurry pipelines, *12th Int. Conf. on slurry handling and pipeline transport,* Hydrotransport 12, BHR Group, p639.

SOO S L (1967), *Fluid dynamics of multiphase systems*, Blaisdell Publishing Company, Massachusetts.

SOO S L, IHRIG H K, and EL KOUGH A F (1960), Experimental determination of two phase turbulent motion, *J. Basic Engng*, 82D.

SOO S L and TUNG S K (1971), Pipe flow of suspensions in turbulent fluid. Electrostatic and gravity effects. *Appl. Scient. Res.*, 24.

SPIEGEL M R (1972), *Theory and problems of statistics in SI units*, McGraw-Hill New York.

TENNEKES H and LUMLEY J L (1972), *A first course in turbulence*, The MIT Press, Cambridge, Massachusetts.

TOMITA Y (1959), A study on non-Newtonian flow in pipes, *Bull JSME*, Vol 2 No 5.

THOMAS A D (1979), The role of laminar/turbulent transition in determining the critical deposit velocity and the operating pressure gradient for long distance slurry pipelines, *6th Int. Conf. on the hydraulic transport of solids in pipes*, Hydrotransport 6 Paper A2.

THOMAS A D and WILSON K C (1987), New analysis of non-Newtonian flow- yield-power-law fluids, *Can J Chem Eng*, 65 335-338.

TORRANCE B M°K (1963), Friction factors for turbulent non-Newtonian flow in circular pipes, *S. A. Mechanical Engineer*, v.13.

VALENTIK L and WHITMORE R L (1965), The termonal velocity of spheres in Bingham plastics, *British Journal of Applied Physics*, Vol 16 1197-1203.

WILSON K C (1986), Modelling the effects of non-Newtonian and time-dependent slurry behaviour, *10th Int. Conf. on the hydraulic transport of solids in pipes*, Hydrotransport 10 Paper J1.

WILSON K C, ADDIE G R and CLIFT R (1992), *Slurry transport using centrifugal pumps*, Elsevier Science Publishers Ltd, Essex, England.

WILSON K C and THOMAS A D (1985), A new analysis of the turbulent flow of non-Newtonian fluids. *Can. J. Chem. Eng.*, 63, 539-546.

WILSON K C, PUGH F J, ADDIE G R, VISINTAINER R J and CLIFT R (1993), Slurries with non-Newtonian carrier fluids: up, down and sideways, *12th Int. Conf. on slurry handling and pipeline transport,* Hydrotransport 12, BHR Group, p657.

XU J, GILLIES R, SMALL M and SHOOK C A (1993), Laminar and turbulent flow of kaolin slurries, *12th Int. Conf. on slurry handling and pipeline transport,* Hydrotransport 12, BHR Group, p595.

APPENDICES

APPENDIX A

A.1 TEST DATA SUMMARY

This section summarises the data from each test.

The first four letters of the test code indicate the following:

Example KERM2408

K This describes the material ie kaolin.

ER This describes the apparatus ie East Rig.

M This indicates the pipe size, Small, Medium or Large.

2408 Test identifier.

This summary shows the range of concentration, diameter, critical velocity, rheology and solids relative density covered by the test data base.

Test Data Summary									
No	Test	Slurry	Cv[%	D[mm	Vc[m/s	Ty[Pa]	K[Pa.s^n	n	Ss
1	KMRL09	Kaolin	9,1	21,6	2,19	7,51	0,8580	0,3324	2,4449
2	KERM09	Kaolin	9,1	140,5	2,61	7,51	0,8580	0,3324	2,4449
3	KERS09	Kaolin	9,1	79,0	2,27	7,51	0,8580	0,3324	2,4449
4	KERL0608	Kaolin	4,9	207,0	1,04	1,88	0,0102	0,8428	2,4449
5	KERM0608	Kaolin	4,9	140,5	1,05	1,88	0,0102	0,8428	2,4449
6	KERS0608	Kaolin	4,9	79,0	0,97	1,88	0,0102	0,8428	2,4449
7	KMRL0608	Kaolin	4,9	21,6	1,13	1,88	0,0102	0,8428	2,4449
8	KMRM0608	Kaolin	4,9	13,2	1,32	1,88	0,0102	0,8428	2,4449
9	KMRS0608	Kaolin	4,9	5,6	1,40	1,88	0,0102	0,8428	2,4449
10	KERL2408	Kaolin	4,2	207,0	0,96	1,04	0,0136	0,8031	2,4449
11	KERM2408	Kaolin	4,2	140,5	0,88	1,04	0,0136	0,8031	2,4449
12	KERS2408	Kaolin	4,2	79,0	1,23	1,04	0,0136	0,8031	2,4449
13	KMRL2408	Kaolin	4,2	21,6	0,95	1,04	0,0136	0,8031	2,4449
14	KMRM2408	Kaolin	4,2	13,2	1,07	1,04	0,0136	0,8031	2,4449
15	KMRS2408	Kaolin	4,2	5,6	1,46	1,04	0,0136	0,8031	2,4449
16	KERL2607	Kaolin	7,3	207,0	1,55	4,18	0,0351	0,7190	2,4449
17	KERM2607	Kaolin	7,3	140,5	1,93	4,18	0,0351	0,7190	2,4449
18	KERS2607	Kaolin	7,3	79,1	1,52	4,18	0,0351	0,7190	2,4449
19	KMRL2607	Kaolin	7,3	21,6	1,62	4,18	0,0351	0,7190	2,4449
20	KMRM2607	Kaolin	7,3	13,2	1,98	4,18	0,0351	0,7190	2,4449
21	KMRS2607	Kaolin	7,3	5,6	2,11	4,18	0,0351	0,7190	2,4449
22	KBBM002	Kaolin	2,1	13,4	0,56	0,40	0,0544	0,5148	2,4449
23	KBBL002	Kaolin	2,1	31,6	0,50	0,60	0,0180	0,6630	2,4449
24	KBBM004	Kaolin	4,0	13,4	1,30	1,40	0,0610	0,5930	2,4449
25	KBBL004	Kaolin	4,0	31,6	1,10	1,40	0,0610	0,5930	2,4449
26	KBBM006	Kaolin	5,9	13,4	1,50	3,00	0,2010	0,4740	2,4449
27	KBBL006	Kaolin	5,9	31,6	1,70	3,00	0,2010	0,4740	2,4449
28	KBBM08	Kaolin	7,8	13,4	2,20	6,00	0,0267	0,8207	2,4449
29	KBBL08	Kaolin	7,8	31,6	1,80	6,00	0,0267	0,8207	2,4449
30	KBBM12	Kaolin	12,1	13,4	4,40	23,00	0,5000	0,5000	2,4449
31	KBBL12	Kaolin	12,1	31,6	4,00	23,00	0,5000	0,5000	2,4449

Test Data Summary									
No	Test	Slurry	Cv[%	D[mm	Vc[m/s	Ty[Pa]	K[Pa.s ^ n	n	Ss
32	KBBL15	Kaolin	14,9	31,6	6,20	44,00	1,1700	0,4900	2,4449
33	KBBM18	Kaolin	17,7	13,4	7,00	80,00	2,2900	0,4300	2,4449
34	KBBL18	Kaolin	17,7	31,6	6,00	80,00	2,2900	0,4300	2,4449
35	UBBM01	Slurry 1	22,5	13,4	5,40	17,00	0,1800	0,7400	2,7500
36	UBBL01	Slurry 1	22,5	31,6	3,90	17,00	0,1800	0,7400	2,7500
37	UBBM02	Slurry 2	28,6	13,4	4,60	10,00	0,1200	0,8100	2,7500
38	UBBL02	Slurry 2	28,6	31,6	3,10	10,00	0,1200	0,8100	2,7500
39	BBBL-500	Tailings	37,4	31,6	2,33	6,00	0,0942	0,8309	2,7435
40	BBBM-500	Tailings	37,4	13,4	3,42	6,00	0,0942	0,8309	2,7435
41	FBBL-100	Tailings	31,5	28,4	2,08	5,00	0,0269	0,8955	2,7468
42	FBBM-100	Tailings	31,5	13,4	2,62	5,00	0,0269	0,8955	2,7468
43	FBBS-100	Tailings	31,5	4,2	4,59	5,00	0,0269	0,8955	2,7468
44	FBBL-62	Tailings	29,3	28,4	3,02	12,00	0,0418	0,8902	2,7566
45	FBBM-62	Tailings	29,3	13,4	3,95	12,00	0,0418	0,8902	2,7566
46	FBBS-62	Tailings	29,3	4,2	5,65	12,00	0,0418	0,8902	2,7566
47	FBBL-42	Tailings	28,3	28,4	2,33	8,00	0,0371	0,8791	2,7733
48	FBBM-42	Tailings	28,3	13,4	3,29	8,00	0,0371	0,8791	2,7733
49	FBBS-42	Tailings	28,3	4,2	5,68	8,00	0,0371	0,8791	2,7733
50	KERM1501	Kaolin	3,4	140,5	0,88	1,07	0,0452	0,5890	2,4449
51	KERM1502	Kaolin	2,1	140,5	0,79	0,61	0,0149	0,6840	2,4449
52	KERM1503	Kaolin	4,3	140,5	1,24	1,60	0,0841	0,5447	2,4449
53	KERM1504	Kaolin	5,9	140,5	1,77	3,05	0,1943	0,4998	2,4449
54	KERM1505	Kaolin	7,8	140,5	2,38	6,11	0,3511	0,4809	2,4449
55	KERM1506	Kaolin	4,8	140,5	1,38	1,96	0,1133	0,5273	2,4449
56	KPIPE1	Kaolin	5,5	80,0	1,31	2,63	0,1639	0,5074	2,4400
57	KPIPE2	Kaolin	5,6	80,0	1,60	2,71	0,1690	0,5058	2,4400
58	KPIPE3	Kaolin	5,2	139,0	1,57	2,32	0,1410	0,5151	2,4400
59	KPIPE4	Kaolin	8,1	139,0	2,50	6,61	0,3703	0,4804	2,4400
60	PARK1	SILICA	3,4	50,6	2,84	9,30	0,0894	0,7254	1,3640
61	XU_17	Kaolin	17,0	158,0	1,99	7,00	0,2671	0,5880	2,4449

A.2 LAMINAR/TURBULENT TRANSITION RESULTS

The detailed results from the laminar/turbulent transition models are presented and summarised in this section.

Laminar/Turbulent Transition Model Results						
No	Test	Slurry	Re Newt	Re MR	Re nn	Z max
1	KMRL09	Kaolin	5331	2436	5460	1019
2	KERM09	Kaolin	11874	4482	13633	2158
3	KERS09	Kaolin	7983	3181	8888	1470
4	KERL0608	Kaolin	10624	3785	40183	2254
5	KERM0608	Kaolin	9004	3691	29476	1962
6	KERS0608	Kaolin	6000	2888	16513	1358
7	KMRL0608	Kaolin	3824	2674	6649	1000
8	KMRM0608	Kaolin	3548	2769	5238	996
9	KMRS0608	Kaolin	2200	1898	2729	676
10	KERL2408	Kaolin	11377	5163	31471	2510
11	KERM2408	Kaolin	8278	4111	20797	1870
12	KERS2408	Kaolin	10261	6451	19606	2522
13	KMRL2408	Kaolin	3425	2604	5048	937
14	KMRM2408	Kaolin	3029	2482	3958	880
15	KMRS2408	Kaolin	2560	2275	2878	810
16	KERL2607	Kaolin	10612	3814	31911	2177
17	KERM2607	Kaolin	12610	5441	32028	2685
18	KERS2607	Kaolin	6683	3162	15521	1456
19	KMRL2607	Kaolin	4011	2590	6650	979
20	KMRM2607	Kaolin	4200	3031	6039	1091
21	KMRS2607	Kaolin	2860	2284	3545	802
22	KBBM002	Kaolin	2169	1516	2382	529
23	KBBL002	Kaolin	2792	1684	4622	651
24	KBBM004	Kaolin	3779	2739	4528	960
25	KBBL004	Kaolin	4361	2830	5964	1036
26	KBBM006	Kaolin	3367	2096	3870	760
27	KBBL006	Kaolin	5704	3292	7046	1242
28	KBBM08	Kaolin	3088	2412	4449	865
29	KBBL08	Kaolin	3781	2446	7117	945
30	KBBM12	Kaolin	5504	3216	7091	1214
31	KBBL12	Kaolin	6508	3322	9453	1362

Laminar/Turbulent Transition Model Results						
No	Test	Slurry	Re Newt	Re MR	Re nn	Z max
32	KBBL15	Kaolin	6602	3690	5460	1425
33	KBBM18	Kaolin	4936	2608	13633	1024
34	KBBL18	Kaolin	5066	2342	8888	1005
35	UBBM01	Slurry 1	3943	3328	40183	1168
36	UBBL01	Slurry 1	4187	3187	29476	1133
37	UBBM02	Slurry 2	3140	2826	16513	1010
38	UBBL02	Slurry 2	3398	2830	6649	1003
39	BBBL-500	Tailings	3048	2607	5238	926
40	BBBM-500	Tailings	2672	2444	2729	879
41	FBBL-100	Tailings	4494	3620	31471	1305
42	FBBM-100	Tailings	3583	3199	20797	1151
43	FBBS-100	Tailings	2742	2614	19606	964
44	FBBL-62	Tailings	4258	3346	5048	1212
45	FBBM-62	Tailings	3626	3202	3958	1149
46	FBBS-62	Tailings	2240	2118	2878	778
47	FBBL-42	Tailings	3830	2988	31911	1082
48	FBBM-42	Tailings	3632	3206	32028	1149
49	FBBS-42	Tailings	2825	2674	15521	981
50	KERM1501	Kaolin	7758	3670	6650	1629
51	KERM1502	Kaolin	11634	5465	6039	2506
52	KERM1503	Kaolin	9255	4548	3545	1939
53	KERM1504	Kaolin	9445	4701	7653	1960
54	KERM1505	Kaolin	9224	4414	10024	1879
55	KERM1506	Kaolin	9083	4498	14842	1897
56	KPIPE1	Kaolin	5319	2795	7653	1127
57	KPIPE2	Kaolin	7154	3861	10024	1530
58	KPIPE3	Kaolin	9739	4874	14842	2034
59	KPIPE4	Kaolin	9435	4515	13838	1922
60	PARK1	Silica	5174	3325	8703	1262
61	XU_17	Kaolin	5833	3064	9806	1265

Average	5715	3268	10057	1336
Standard Deviation	2912	981	8535	526
Standard Deviation %	51	30	85	39
Minimum	2169	1516	2382	529
Maximum	12610	6451	40183	2685
Range	10441	4935	37801	2156
Range %	183	151	376	161

Laminar/Turbulent Transition Model Results					
No	Test	Slurry	Re 1	Re 2	Re 3
1	KMRL09	Kaolin	2436	2809	2290
2	KERM09	Kaolin	4482	5126	3904
3	KERS09	Kaolin	3181	3648	2826
4	KERL0608	Kaolin	3785	4354	2146
5	KERM0608	Kaolin	3691	4294	2165
6	KERS0608	Kaolin	2888	3394	1780
7	KMRL0608	Kaolin	2674	3115	1985
8	KMRM0608	Kaolin	2769	3156	2244
9	KMRS0608	Kaolin	1898	2091	1711
10	KERL2408	Kaolin	5163	6041	3199
11	KERM2408	Kaolin	4111	4831	2629
12	KERS2408	Kaolin	6451	7577	4606
13	KMRL2408	Kaolin	2604	2983	2129
14	KMRM2408	Kaolin	2482	2784	2182
15	KMRS2408	Kaolin	2275	2469	2202
16	KERL2607	Kaolin	3814	4384	2335
17	KERM2607	Kaolin	5441	6334	3507
18	KERS2607	Kaolin	3162	3699	2104
19	KMRL2607	Kaolin	2590	3026	2006
20	KMRM2607	Kaolin	3031	3495	2544
21	KMRS2607	Kaolin	2284	2575	2102
22	KBBM002	Kaolin	1516	1740	1499
23	KBBL002	Kaolin	1684	1969	1310
24	KBBM004	Kaolin	2739	3138	2584
25	KBBL004	Kaolin	2830	3286	2455
26	KBBM006	Kaolin	2096	2427	1988
27	KBBL006	Kaolin	3292	3824	2978
28	KBBM08	Kaolin	2412	2747	1993
29	KBBL08	Kaolin	2446	2870	1753
30	KBBM12	Kaolin	3216	3739	2854
31	KBBL12	Kaolin	3322	3864	2740

Laminar/Turbulent Transition Model Results					
No	Test	Slurry	Re 1	Re 2	Re 3
32	KBBL15	Kaolin	3690	4292	3224
33	KBBM18	Kaolin	2608	3027	2353
34	KBBL18	Kaolin	2342	2711	1981
35	UBBM01	Slurry 1	3328	3687	3190
36	UBBL01	Slurry 1	3187	3640	2749
37	UBBM02	Slurry 2	2826	3047	2766
38	UBBL02	Slurry 2	2830	3158	2518
39	BBBL-500	Tailings	2607	2882	2350
40	BBBM-500	Tailings	2444	2613	2403
41	FBBL-100	Tailings	3620	4099	2902
42	FBBM-100	Tailings	3199	3471	2886
43	FBBS-100	Tailings	2614	2722	2599
44	FBBL-62	Tailings	3346	3815	2631
45	FBBM-62	Tailings	3202	3494	2861
46	FBBS-62	Tailings	2118	2219	2088
47	FBBL-42	Tailings	2988	3411	2353
48	FBBM-42	Tailings	3206	3498	2888
49	FBBS-42	Tailings	2674	2799	2662
50	KERM1501	Kaolin	3670	4276	2701
51	KERM1502	Kaolin	5465	6385	3721
52	KERM1503	Kaolin	4548	5296	3535
53	KERM1504	Kaolin	4701	5467	3833
54	KERM1505	Kaolin	4414	5124	3601
55	KERM1506	Kaolin	4498	5236	3565
56	KPIPE1	Kaolin	2795	3253	2322
57	KPIPE2	Kaolin	3861	4494	3257
58	KPIPE3	Kaolin	4874	5672	3926
59	KPIPE4	Kaolin	4515	5242	3685
60	PARK1	Silica	3325	3886	2554
61	XU_17	Kaolin	3064	3579	2364

Average	3268	3742	2643
Standard Deviation	981	1178	658
Standard Deviation %	30	31	25
Minimum	1516	1740	1310
Maximum	6451	7577	4606
Range	4935	5837	3296
Range %	151	156	125

Critical Velocity Predictions							
No	Test	Slurry	Vc exp	Vint	%error	Vc(Re3=2100)	%error
			[m/s]	[m/s]		[m/s]	
1	KMRL09	Kaolin	2,19	2,76	26	2,09	5
2	KERM09	Kaolin	2,61	2,51	4	1,89	28
3	KERS09	Kaolin	2,27	2,57	13	1,94	14
4	KERL0608	Kaolin	1,04	1,06	2	1,02	1
5	KERM0608	Kaolin	1,05	1,06	1	1,03	2
6	KERS0608	Kaolin	0,97	1,07	10	1,06	9
7	KMRL0608	Kaolin	1,13	1,12	1	1,17	3
8	KMRM0608	Kaolin	1,32	1,17	11	1,27	4
9	KMRS0608	Kaolin	1,40	1,36	3	1,61	15
10	KERL2408	Kaolin	0,96	0,80	16	0,77	20
11	KERM2408	Kaolin	0,88	0,80	8	0,78	11
12	KERS2408	Kaolin	1,23	0,81	34	0,81	35
13	KMRL2408	Kaolin	0,95	0,89	6	0,94	1
14	KMRM2408	Kaolin	1,07	0,95	11	1,05	2
15	KMRS2408	Kaolin	1,46	1,17	20	1,41	3
16	KERL2607	Kaolin	1,55	1,93	25	1,47	5
17	KERM2607	Kaolin	1,93	1,60	17	1,48	23
18	KERS2607	Kaolin	1,52	1,61	6	1,51	0
19	KMRL2607	Kaolin	1,62	1,70	5	1,66	3
20	KMRM2607	Kaolin	1,98	1,78	10	1,77	11
21	KMRS2607	Kaolin	2,11	2,01	5	2,11	0
22	KBBM002	Kaolin	0,56	0,76	36	0,68	22
23	KBBL002	Kaolin	0,50	0,69	37	0,65	30
24	KBBM004	Kaolin	1,30	1,22	6	1,15	12
25	KBBL004	Kaolin	1,10	1,10	0	1,01	8
26	KBBM006	Kaolin	1,50	1,81	21	1,55	3
27	KBBL006	Kaolin	1,70	1,67	2	1,40	17
28	KBBM08	Kaolin	2,20	2,10	4	2,27	3
29	KBBL08	Kaolin	1,80	1,95	8	1,99	10
30	KBBM12	Kaolin	4,40	4,34	1	3,72	16
31	KBBL12	Kaolin	4,00	4,10	2	3,47	13

Critical Velocity Predictions							
No	Test	Slurry	Vc exp	Vint	%error	Vc(Re3=2100)	%error
			[m/s]	[m/s]		[m/s]	
32	KBBL15	Kaolin	6,20	5,79	7	4,91	21
33	KBBM18	Kaolin	7,00	8,07	15	6,58	6
34	KBBL18	Kaolin	6,00	7,64	27	6,19	3
35	UBBM01	Slurry 1	5,40	3,77	30	4,10	24
36	UBBL01	Slurry 1	3,90	3,25	17	3,32	15
37	UBBM02	Slurry 2	4,60	3,09	33	3,76	18
38	UBBL02	Slurry 2	3,10	2,49	20	2,76	11
39	BBBL-500	Tailings	2,33	1,88	19	2,16	7
40	BBBM-500	Tailings	3,42	2,43	29	3,09	10
41	FBBL-100	Tailings	2,08	1,54	26	1,71	18
42	FBBM-100	Tailings	2,62	1,73	34	2,10	20
43	FBBS-100	Tailings	4,59	2,64	42	3,84	16
44	FBBL-62	Tailings	3,02	2,40	20	2,64	13
45	FBBM-62	Tailings	3,95	2,68	32	3,20	19
46	FBBS-62	Tailings	5,65	3,98	30	5,68	0
47	FBBL-42	Tailings	2,33	1,99	15	2,18	7
48	FBBM-42	Tailings	3,29	2,22	32	2,65	20
49	FBBS-42	Tailings	5,68	3,32	42	4,68	18
50	KERM1501	Kaolin	0,88	0,87	1	0,77	12
51	KERM1502	Kaolin	0,79	0,64	19	0,59	26
52	KERM1503	Kaolin	1,24	1,09	12	0,94	24
53	KERM1504	Kaolin	1,77	1,53	14	1,29	27
54	KERM1505	Kaolin	2,38	2,14	10	1,79	25
55	KERM1506	Kaolin	1,38	1,21	12	1,04	24
56	KPIPE1	Kaolin	1,31	1,46	11	1,24	5
57	KPIPE2	Kaolin	1,60	1,48	7	1,26	21
58	KPIPE3	Kaolin	1,57	1,33	16	1,13	28
59	KPIPE4	Kaolin	2,50	2,23	11	1,86	26
60	PARK1	Silica	2,84	2,91	3	2,84	0
61	XU_17	Kaolin	1,99	2,10	5	1,87	6

	V int	Vc
Average Percentage Error	15,5	13,1
Standard Deviation	11,6	9,2
Maximum Percentage Error	42,5	34,5

A.3 SUMMARY OF TURBULENT MODEL PERFORMANCE RESULTS

The average % error and log standard error for the turbulent data from each test are presented and summarised in this section.

Average Percentage Error						
No	Test	Slurry	Points	Torrance	W & T	Model
1	KMRL09	Kaolin	7	12,82	12,09	4,26
2	KERM09	Kaolin	9	11,62	6,71	6,78
3	KERS09	Kaolin	8	10,76	9,65	5,77
4	KERL0608	Kaolin	8	13,04	13,78	6,81
5	KERM0608	Kaolin	9	5,80	3,20	3,25
6	KERS0608	Kaolin	14	12,43	12,17	10,38
7	KMRL0608	Kaolin	18	5,20	6,77	8,55
8	KMRM060	Kaolin	13	9,81	9,80	6,12
9	KMRS0608	Kaolin	13	23,89	10,54	15,75
10	KERL2408	Kaolin	16	14,48	13,06	9,94
11	KERM2408	Kaolin	16	13,33	7,45	5,42
12	KERS2408	Kaolin	9	8,61	7,16	5,12
13	KMRL2408	Kaolin	11	5,90	3,23	5,95
14	KMRM240	Kaolin	10	9,66	11,97	9,31
15	KMRS2408	Kaolin	8	20,78	14,45	20,18
16	KERL2607	Kaolin	10	11,50	11,71	15,66
17	KERM2607	Kaolin	12	12,13	13,27	5,06
18	KERS2607	Kaolin	11	9,37	10,17	9,38
19	KMRL2607	Kaolin	16	9,61	11,80	2,86
20	KMRM260	Kaolin	11	11,85	17,42	4,08
21	KMRS2607	Kaolin	7	25,56	13,43	20,03
22	KBBM002	Kaolin	5	3,78	24,66	17,40
23	KBBL002	Kaolin	2	16,00	17,76	19,34
24	KBBM004	Kaolin	28	32,93	34,30	12,92
25	KBBL004	Kaolin	23	37,77	36,71	6,73
26	KBBM006	Kaolin	7	18,50	26,92	17,97
27	KBBL006	Kaolin	19	44,18	41,20	4,21
28	KBBM08	Kaolin	17	10,42	7,18	6,68
29	KBBL08	Kaolin	15	17,11	7,06	11,70
30	KBBM12	Kaolin	8	10,99	27,18	25,21
31	KBBL12	Kaolin	12	12,32	9,47	7,84

Average Percentage Error						
No	Test	Slurry	Points	Torrance	W & T	Model
32	KBBL15	Kaolin	8	12,45	7,84	7,52
33	KBBM18	Kaolin	9	11,08	17,57	26,69
34	KBBL18	Kaolin	5	5,11	13,63	9,33
35	UBBM01	Slurry 1	10	37,38	27,13	32,51
36	UBBL01	Slurry 1	8	5,83	11,04	6,93
37	UBBM02	Slurry 2	7	54,24	37,03	50,35
38	UBBL02	Slurry 2	17	13,30	8,93	9,80
39	BBBL-500	Tailings	20	8,69	9,51	6,36
40	BBBM-500	Tailings	14	5,83	7,42	4,23
41	FBBL-100	Tailings	14	7,93	5,62	3,92
42	FBBM-100	Tailings	14	9,60	3,52	6,04
43	FBBS-100	Tailings	8	19,99	7,78	24,27
44	FBBL-62	Tailings	11	26,08	8,70	14,93
45	FBBM-62	Tailings	13	22,69	9,09	12,80
46	FBBS-62	Tailings	4	74,39	51,35	57,21
47	FBBL-42	Tailings	15	7,92	4,98	3,75
48	FBBM-42	Tailings	13	10,10	8,03	7,34
49	FBBS-42	Tailings	10	47,03	29,07	33,46
50	KERM1501	Kaolin	11	13,30	17,64	5,34
51	KERM1502	Kaolin	11	13,33	20,35	5,67
52	KERM1503	Kaolin	10	13,33	20,42	9,22
53	KERM1504	Kaolin	7	13,33	14,11	7,40
54	KERM1505	Kaolin	5	13,33	6,24	2,92
55	KERM1506	Kaolin	7	13,33	20,14	6,77
56	KPIPE1	Kaolin	9	29,44	28,69	6,89
57	KPIPE2	Kaolin	8	25,39	23,18	3,22
58	KPIPE3	Kaolin	13	23,12	19,59	3,79
59	KPIPE4	Kaolin	11	15,64	11,07	3,24
60	PARK1	Silica	6	13,45	10,93	5,29
61	XU_17	Kaolin	4	17,56	2,05	5,44

Average Percentage Error	Torrance	W & T	Model
Whole Data Base	17,18	15,07	10,04

Average LSE						
No	Test	Slurry	Points	Torrance	W & T	Model
1	KMRL09	Kaolin	7	0,0252	0,0269	0,0084
2	KERL09	Kaolin	9	0,0233	0,0117	0,0129
3	KERS09	Kaolin	8	0,0151	0,0158	0,0082
4	KERL0608	Kaolin	8	0,0240	0,0298	0,0145
5	KERM0608	Kaolin	9	0,0111	0,0066	0,0063
6	KERS0608	Kaolin	14	0,0213	0,0226	0,0209
7	KMRL0608	Kaolin	18	0,0072	0,0079	0,0115
8	KMRM060	Kaolin	13	0,0161	0,0138	0,0103
9	KMRS0608	Kaolin	13	0,0319	0,0157	0,0223
10	KERL2408	Kaolin	16	0,0260	0,0242	0,0172
11	KERM2408	Kaolin	16	0,0184	0,0097	0,0092
12	KERS2408	Kaolin	9	0,0193	0,0147	0,0139
13	KMRL2408	Kaolin	11	0,0135	0,0064	0,0109
14	KMRM240	Kaolin	10	0,0169	0,0192	0,0166
15	KMRS2408	Kaolin	8	0,0457	0,0344	0,0408
16	KERL2607	Kaolin	10	0,0195	0,0238	0,0258
17	KERM2607	Kaolin	12	0,0195	0,0208	0,0075
18	KERS2607	Kaolin	11	0,0174	0,0181	0,0181
19	KMRL2607	Kaolin	16	0,0128	0,0151	0,0038
20	KMRM260	Kaolin	11	0,0205	0,0280	0,0071
21	KMRS2607	Kaolin	7	0,0480	0,0397	0,0385
22	KBBM002	Kaolin	5	0,0104	0,0700	0,0484
23	KBBL002	Kaolin	2	0,1021	0,1290	0,1321
24	KBBM004	Kaolin	28	0,0388	0,0398	0,0141
25	KBBL004	Kaolin	23	0,0474	0,0451	0,0091
26	KBBM006	Kaolin	7	0,0418	0,0572	0,0363
27	KBBL006	Kaolin	19	0,0622	0,0569	0,0056
28	KBBM08	Kaolin	17	0,0157	0,0150	0,0137
29	KBBL08	Kaolin	15	0,0231	0,0145	0,0173
30	KBBM12	Kaolin	8	0,0180	0,0542	0,0504
31	KBBL12	Kaolin	12	0,0179	0,0145	0,0124

Average LSE						
No	Test	Slurry	Points	Torrance	W & T	Model
32	KBBL15	Kaolin	8	0,0229	0,0180	0,0149
33	KBBM18	Kaolin	9	0,0171	0,0277	0,0415
34	KBBL18	Kaolin	5	0,0179	0,0456	0,0441
35	UBBM01	Slurry 1	10	0,0544	0,0419	0,0491
36	UBBL01	Slurry 1	8	0,0175	0,0239	0,0146
37	UBBM02	Slurry 2	7	0,0867	0,0638	0,0828
38	UBBL02	Slurry 2	17	0,0279	0,0182	0,0201
39	BBBL-500	Tailings	20	0,0138	0,0107	0,0098
40	BBBM-500	Tailings	14	0,0207	0,0274	0,0137
41	FBBL-100	Tailings	14	0,0136	0,0079	0,0076
42	FBBM-100	Tailings	14	0,1360	0,0059	0,0093
43	FBBS-100	Tailings	8	0,0342	0,0166	0,0387
44	FBBL-62	Tailings	11	0,0348	0,0131	0,0211
45	FBBM-62	Tailings	13	0,0298	0,0147	0,0190
46	FBBS-62	Tailings	4	0,1625	0,1225	0,1331
47	FBBL-42	Tailings	15	0,0113	0,0071	0,0056
48	FBBM-42	Tailings	13	0,0168	0,0116	0,0113
49	FBBS-42	Tailings	10	0,0611	0,0425	0,0471
50	KERM1501	Kaolin	11	0,0371	0,0338	0,0091
51	KERM1502	Kaolin	11	0,0348	0,0351	0,0102
52	KERM1503	Kaolin	10	0,0428	0,0402	0,0200
53	KERM1504	Kaolin	7	0,0387	0,0345	0,0167
54	KERM1505	Kaolin	5	0,0250	0,0233	0,0075
55	KERM1506	Kaolin	7	0,0525	0,0499	0,0150
56	KPIPE1	Kaolin	9	0,0630	0,0600	0,0186
57	KPIPE2	Kaolin	8	0,0596	0,0543	0,0069
58	KPIPE3	Kaolin	13	0,0387	0,0337	0,0071
59	KPIPE4	Kaolin	11	0,0279	0,0235	0,0061
60	PARK1	Kaolin	6	0,0327	0,0266	0,0138
61	XU_17	Kaolin	4	0,0473	0,0078	0,0185

New

Log Standard Error	Torrance	W & T	Model
Whole Data Base	0,0050	0,0038	0,0024

A.4 DETAILED PIPE TEST RESULTS I

The detailed pipe test results are presented in this section.

Each test sheet contains the test apparatus, material, slurry properties, turbulent model performance and the test data plotted on a pseudo-shear diagram.

Kaolin : 2704

Particle Size Distribution

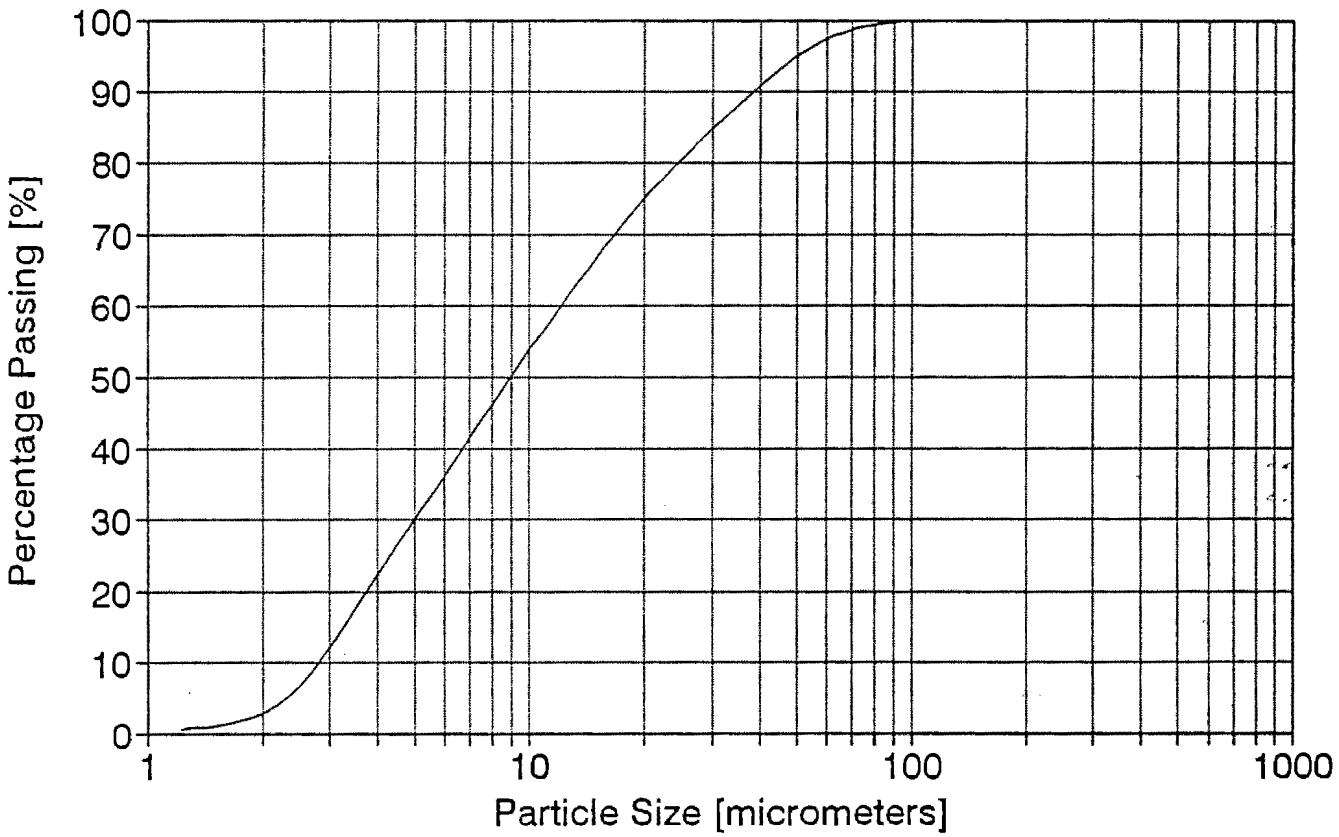

DATA FROM TEST	KMRL09
APPARATUS	
Facility	Mini Rig
Diameter	22 mm
Material	Kaolin
Operator	PTS
Supervisor	PTS

SLURRY PROPERTIES	
Solids Relative Density	2,4449
Slurry Relative Density	1,1315
Volumetric Concentration	9,1 %
Yield Stress	10,7 Pa
Fluid Consistency Index	0,0162 Pa s^n
Flow Behaviour Index	0,838
Representative Particle size	32 um

TURBULENT MODEL PERFORMANCE		
Model	Avg Err%	Avg LSE
Torrance	12,82	0,0252
Wilson and Thomas	12,09	0,0269
New Model	4,26	0,0084

Pseudo-Shear Diagram:KMRL09

Sm = 1,1315 : Diam = 22mm

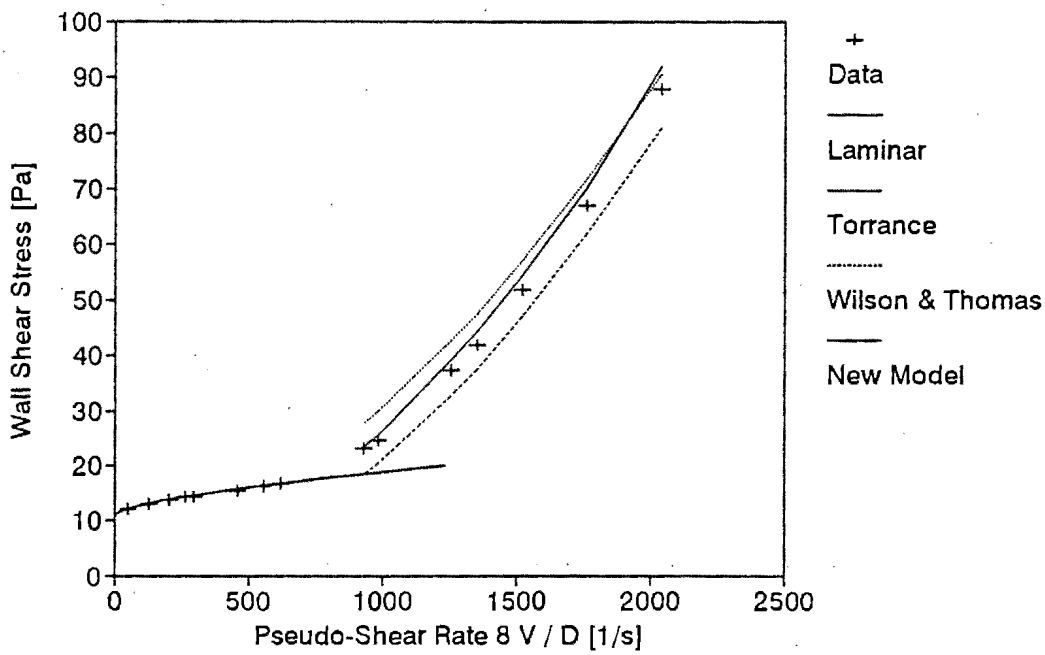

DATA FROM TEST	KERL09
APPARATUS	
Facility	East Rig
Diameter	141 mm
Material	Kaolin
Operator	PTS
Supervisor	PTS

SLURRY PROPERTIES	
Solids Relative Density	2,4449
Slurry Relative Density	1,1315
Volumetric Concentration	9,1 %
Yield Stress	10,7 Pa
Fluid Consistency Index	0,0162 Pa s ^ n
Flow Behaviour Index	0,838
Representative Particle size	32 um

TURBULENT MODEL PERFORMANCE		
Model	Avg Err%	Avg LSE
Torrance	11,62	0,0233
Wilson and Thomas	6,71	0,0117
New Model	6,78	0,0129

Pseudo-Shear Diagram:KERL09

Sm = 1,1315 : Diam = 141mm

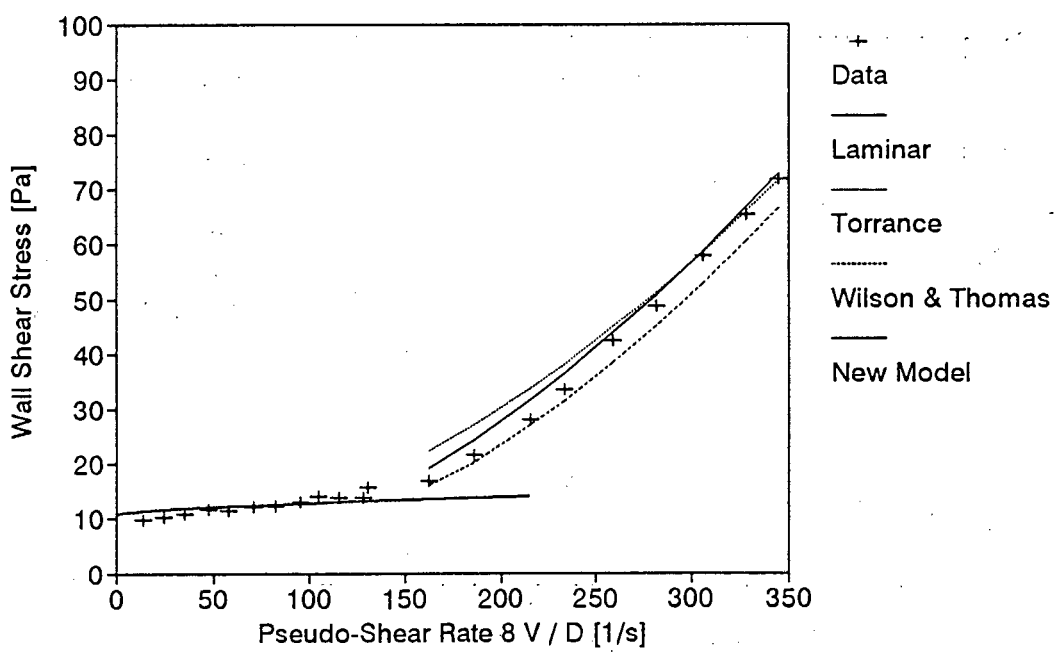

DATA FROM TEST	KERS09
APPARATUS	
Facility	East Rig
Diameter	79 mm
Material	Kaolin
Operator	PTS
Supervisor	PTS

SLURRY PROPERTIES	
Solids Relative Density	2,4449
Slurry Relative Density	1,1315
Volumetric Concentration	9,1 %
Yield Stress	10,7 Pa
Fluid Consistency Index	0,0162 Pa s ^ n
Flow Behaviour Index	0,838
Representative Particle size	32 um

TURBULENT MODEL PERFORMANCE		
Model	Avg Err%	Avg LSE
Torrance	10,76	0,0151
Wilson and Thomas	9,65	0,0158
New Model	5,77	0,0082

Pseudo-Shear Diagram:KERS09

Sm = 1,1315 : Diam = 79mm

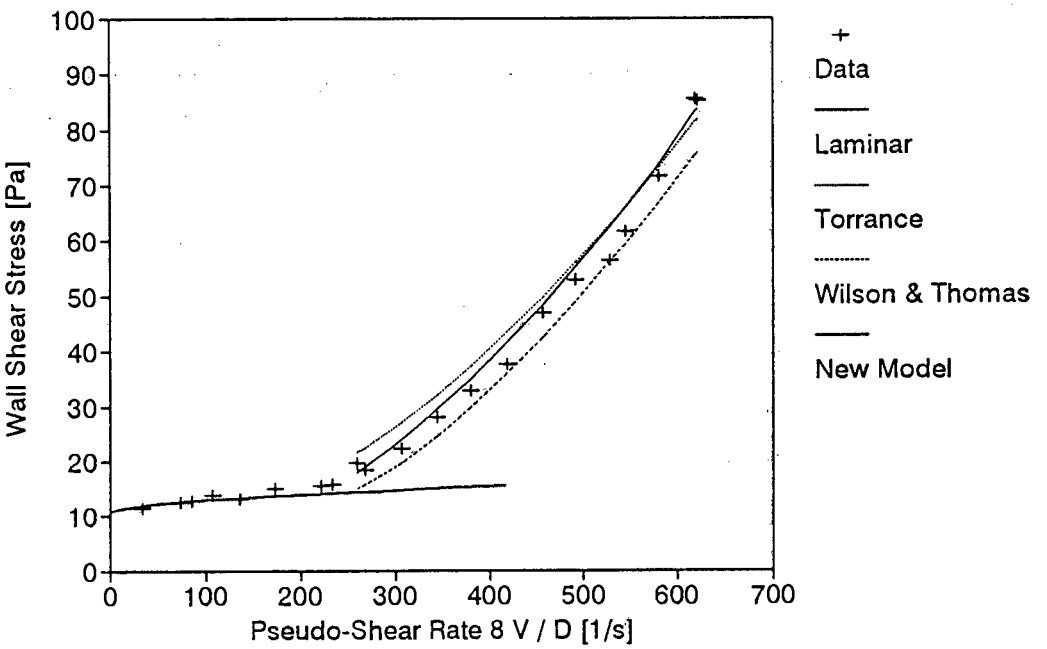

Kaolin : 2607

Particle Size Distribution

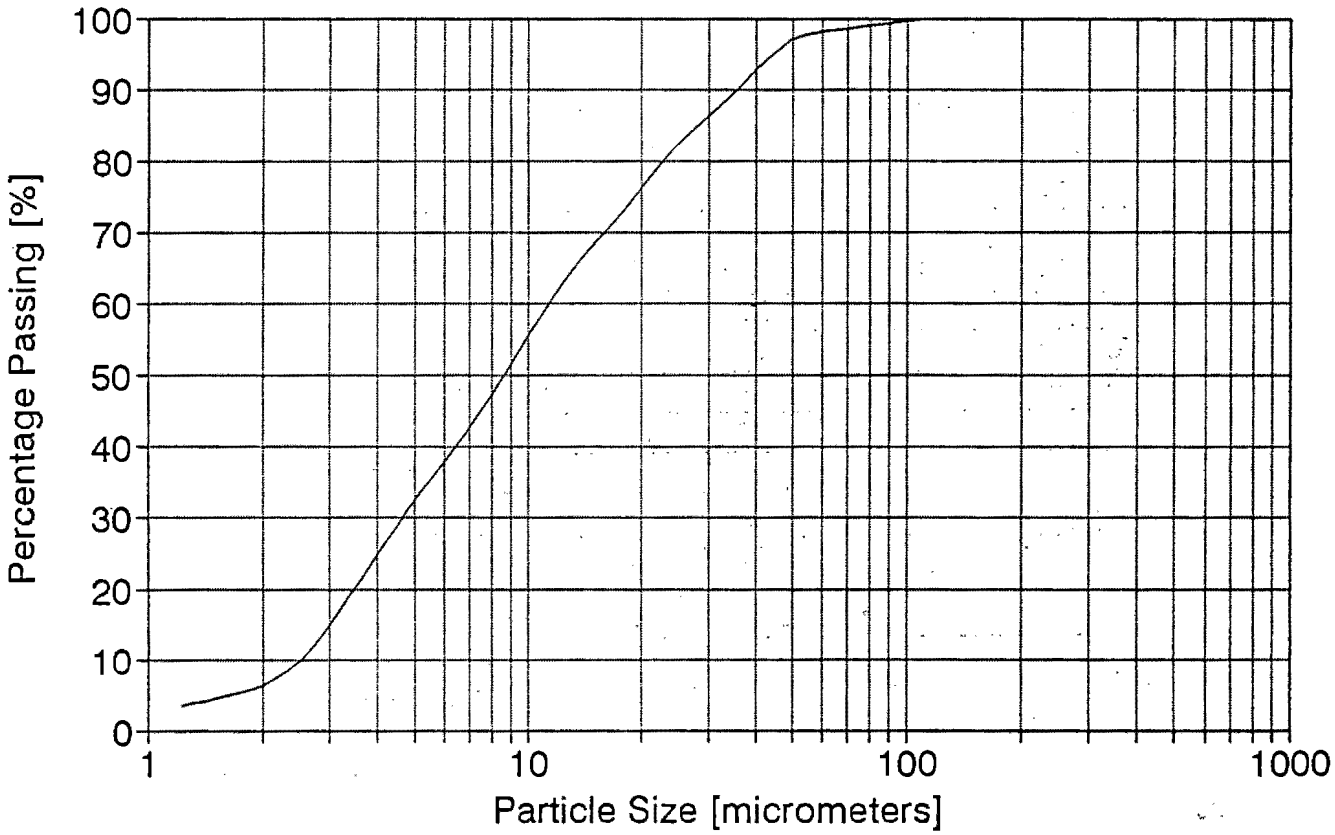

DATA FROM TEST	KERL0608
APPARATUS	
Facility	East Rig
Diameter	207 mm
Material	Kaolin
Operator	PTS
Supervisor	PTS

SLURRY PROPERTIES	
Solids Relative Density	2,4449
Slurry Relative Density	1,0713
Volumetric Concentration	4,9 %
Yield Stress	1,880 Pa
Fluid Consistency Index	0,0102 Pa s ^ n
Flow Behaviour Index	0,8428
Representative Particle size	112 um*

* Pipe Roughness

TURBULENT MODEL PERFORMANCE		
Model	Avg Err%	Avg LSE
Torrance	13,04	0,0240
Wilson and Thomas	13,78	0,0298
New Model	6,81	0,0145

Pseudo-Shear Diagram: KERL0608

Sm = 1,0713 : Diam = 207 mm

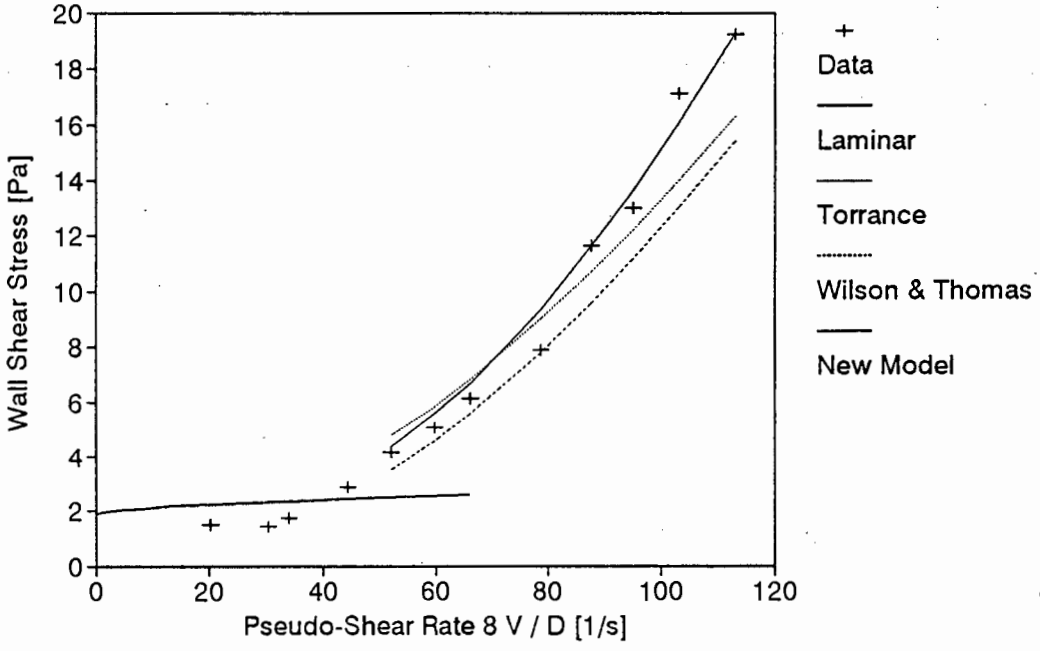

DATA FROM TEST	KERM0608
APPARATUS	
Facility	East Rig
Diameter	141 mm
Material	Kaolin
Operator	PTS
Supervisor	PTS

SLURRY PROPERTIES	
Solids Relative Density	2,4449
Slurry Relative Density	1,0713
Volumetric Concentration	4,9 %
Yield Stress	1,880 Pa
Fluid Consistency Index	0,0102 Pa s ^ n
Flow Behaviour Index	0,8428
Representative Particle size	28 um

TURBULENT MODEL PERFORMANCE		
Model	Avg Err%	Avg LSE
Torrance	5,80	0,0111
Wilson and Thomas	3,20	0,0066
New Model	3,25	0,0063

Pseudo-Shear Diagram: KERM0608

Sm = 1,0713 : Diam = 141 mm

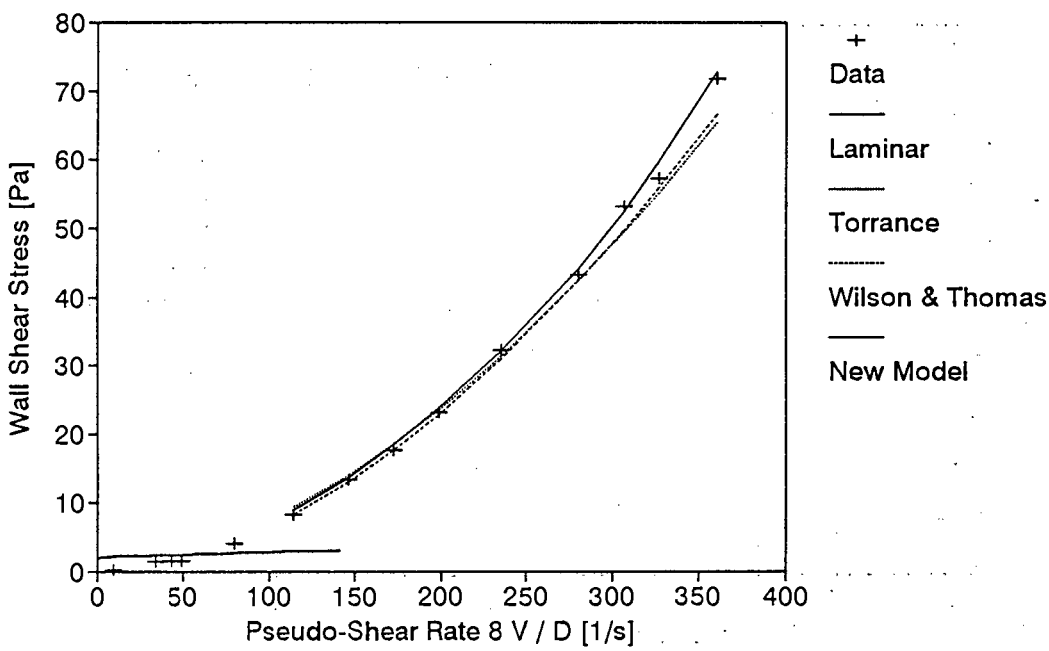

DATA FROM TEST	KERS0608
APPARATUS	
Facility	East Rig
Diameter	79 mm
Material	Kaolin
Operator	PTS
Supervisor	PTS

SLURRY PROPERTIES	
Solids Relative Density	2,4449
Slurry Relative Density	1,0713
Volumetric Concentration	4,9%
Yield Stress	1,880 Pa
Fluid Consistency Index	0,0102 Pa s ^ n
Flow Behaviour Index	0,8428
Representative Particle size	28 um

TURBULENT MODEL PERFORMANCE		
Model	Avg Err%	Avg LSE
Torrance	12,43	0,0213
Wilson and Thomas	12,17	0,0226
New Model	10,38	0,0209

Pseudo-Shear Diagram: KERS0608

Sm = 1,0713 : Diam = 79 mm

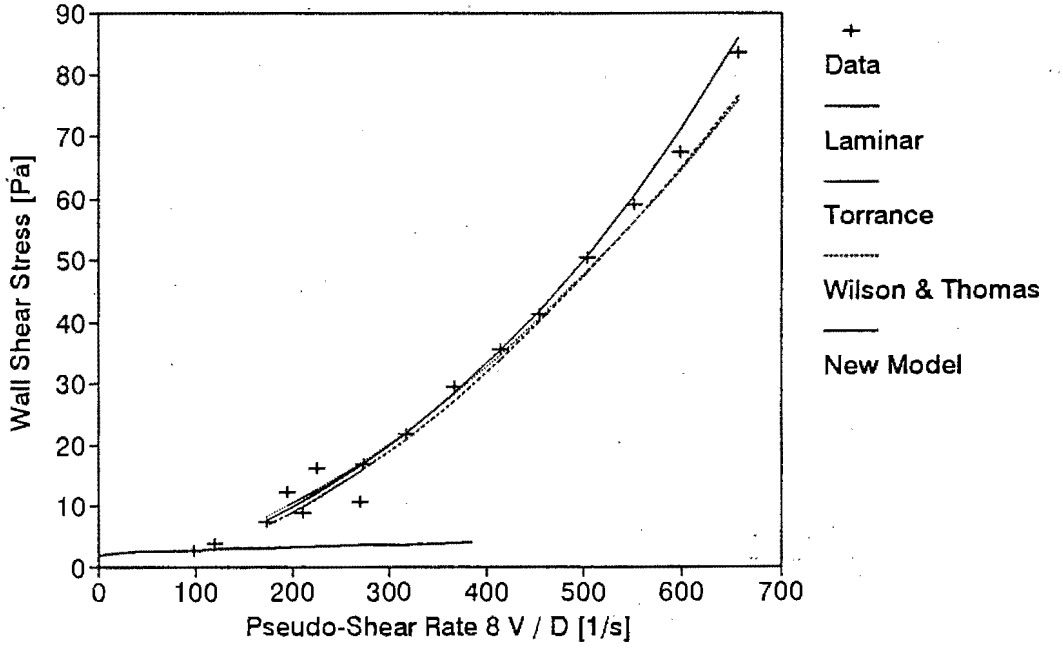

DATA FROM TEST	KMRL0608
APPARATUS	
Facility	Mini Rig
Diameter	21,6 mm
Material	Kaolin
Operator	PTS
Supervisor	PTS

SLURRY PROPERTIES	
Solids Relative Density	2,4449
Slurry Relative Density	1,0713
Volumetric Concentration	4,9 %
Yield Stress	1,880 Pa
Fluid Consistency Index	0,0102 Pa s ^ n
Flow Behaviour Index	0,8428
Representative Particle size	28 um

TURBULENT MODEL PERFORMANCE		
Model	Avg Err%	Avg LSE
Torrance	5,20	0,0072
Wilson and Thomas	6,77	0,0079
New Model	8,55	0,0115

Pseudo-Shear Diagram: KMRL0608

Sm = 1,0713 : Diam = 21,6 mm

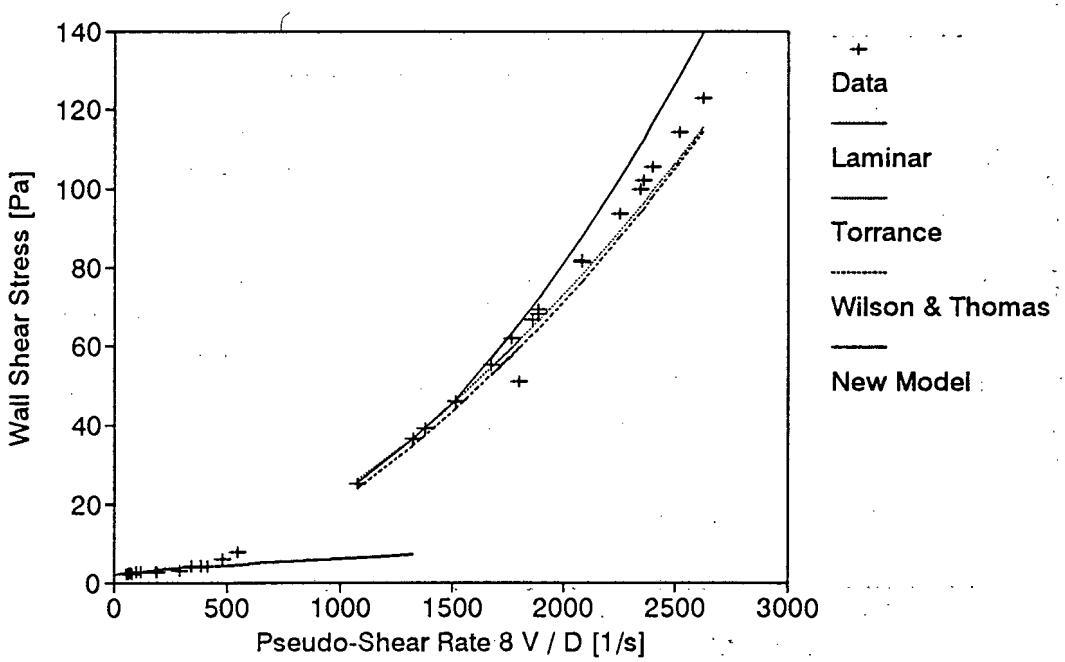

DATA FROM TEST	KMRM0608
APPARATUS	
Facility	Mini Rig
Diameter	13,2 mm
Material	Kaolin
Operator	PTS
Supervisor	PTS

SLURRY PROPERTIES	
Solids Relative Density	2,4449
Slurry Relative Density	1,0713
Volumetric Concentration	4,9 %
Yield Stress	1,880 Pa
Fluid Consistency Index	0,0102 Pa s ^ n
Flow Behaviour Index	0,8428
Representative Particle size	28 um

TURBULENT MODEL PERFORMANCE		
Model	Avg Err%	Avg LSE
Torrance	9,81	0,0161
Wilson and Thomas	9,80	0,0138
New Model	6,12	0,0103

Pseudo-Shear Diagram: KMRM0608

Sm = 1,0713 : Diam 13,2 mm

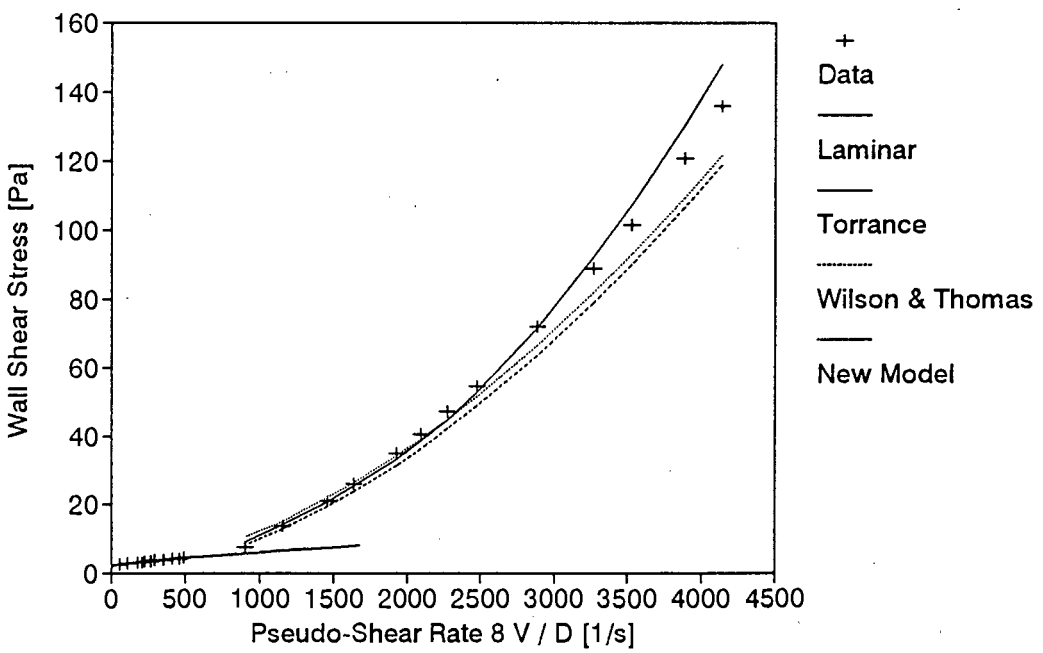

DATA FROM TEST	KMRS0608
APPARATUS	
Facility	East Rig
Diameter	5,623 mm
Material	Kaolin
Operator	PTS
Supervisor	PTS

SLURRY PROPERTIES	
Solids Relative Density	2,4449
Slurry Relative Density	1,0713
Volumetric Concentration	4,9 %
Yield Stress	1,880 Pa
Fluid Consistency Index	0,0102 Pa s ^ n
Flow Behaviour Index	0,8428
Representative Particle size	28 um

TURBULENT MODEL PERFORMANCE		
Model	Avg Err%	Avg LSE
Torrance	23,89	0,0319
Wilson and Thomas	10,54	0,0157
New Model	15,75	0,0223

Pseudo-Shear Diagram: KMRS0608

Sm = 1,0713 : Diam = 5,623 mm

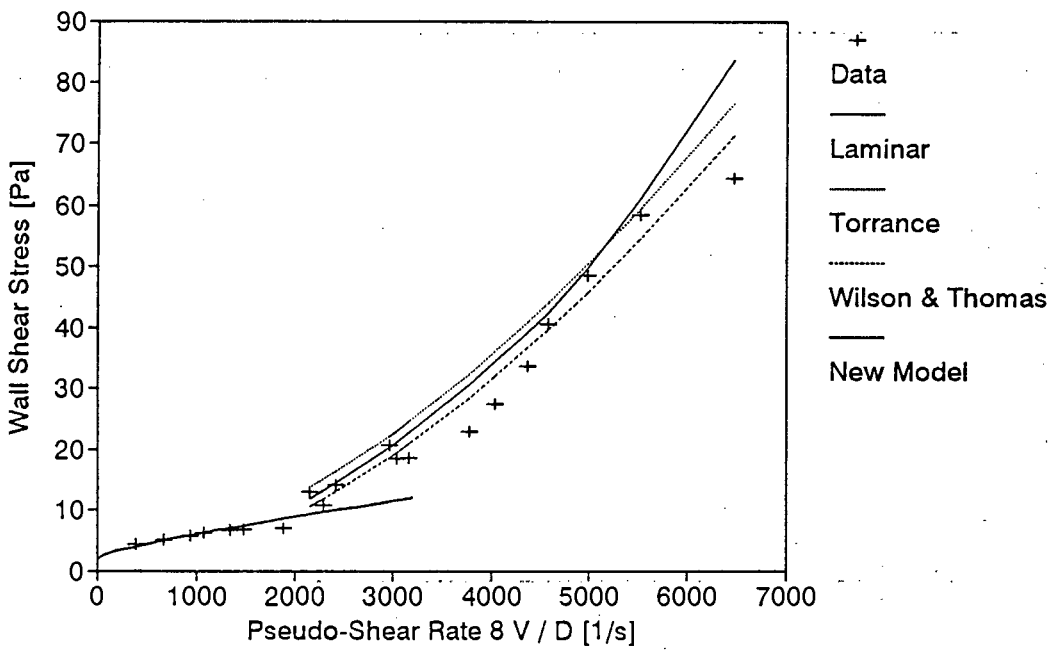

DATA FROM TEST	KERL2408
APPARATUS	
Facility	East Rig
Diameter	207 mm
Material	Kaolin
Operator	PTS
Supervisor	PTS

SLURRY PROPERTIES	
Solids Relative Density	2,4449
Slurry Relative Density	1,0613
Volumetric Concentration	4,2 %
Yield Stress	1,040 Pa
Fluid Consistency Index	0,0136 Pa s ^ n
Flow Behaviour Index	0,8031
Representative Particle size	112 um*

* Pipe Roughness

TURBULENT MODEL PERFORMANCE		
Model	Avg Err%	Avg LSE
Torrance	14,48	0,0260
Wilson and Thomas	13,06	0,0242
New Model	9,94	0,0172

Pseudo-Shear Diagram: KERL2408

Sm = 1,0613 : Diam = 207 mm

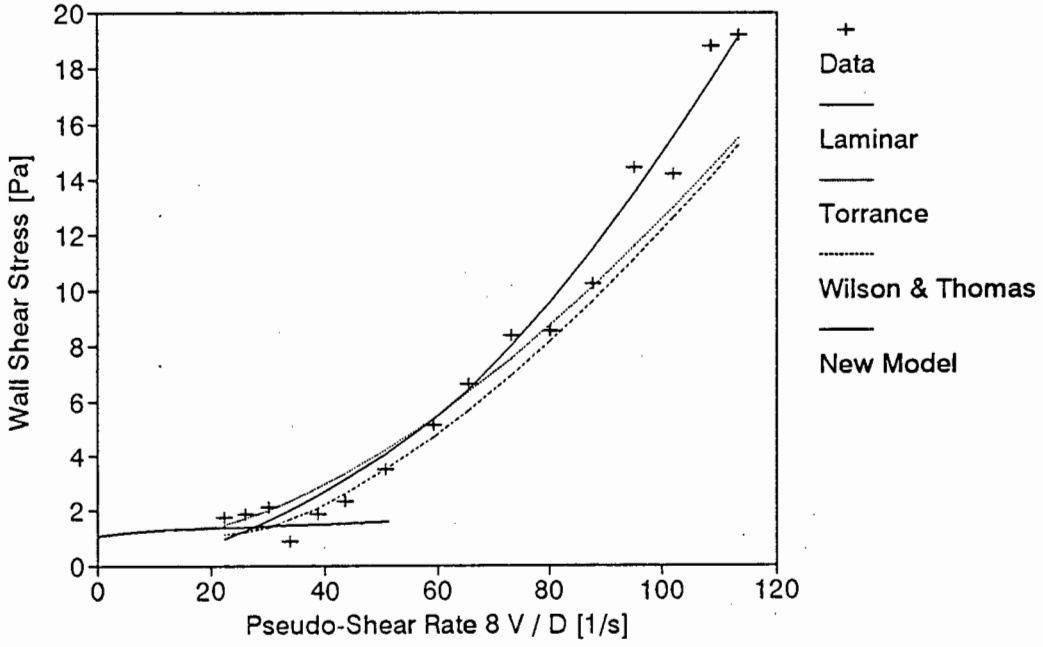

DATA FROM TEST	KERM2408
APPARATUS	
Facility	East Rig
Diameter	141 mm
Material	Kaolin
Operator	PTS
Supervisor	PTS

SLURRY PROPERTIES	
Solids Relative Density	2,4449
Slurry Relative Density	1,0613
Volumetric Concentration	4,2 %
Yield Stress	1,040 Pa
Fluid Consistency Index	0,0136 Pa s ^ n
Flow Behaviour Index	0,8031
Representative Particle size	28 um

TURBULENT MODEL PERFORMANCE		
Model	Avg %	Avg LSE
Torrance	13,33	0,0184
Wilson and Thomas	7,45	0,0097
New Model	5,42	0,0092

Pseudo-Shear Diagram: KERM2408

Sm = 1,0613 : Diam = 141 mm

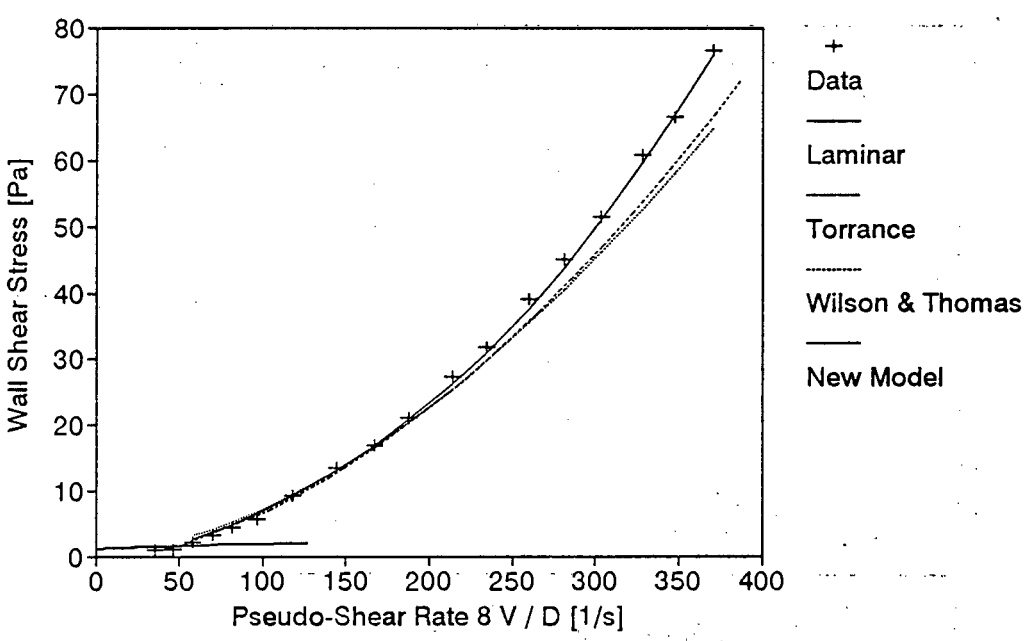

DATA FROM TEST	KERS2408
APPARATUS	
Facility	East Rig
Diameter	79 mm
Material	Kaolin
Operator	PTS
Supervisor	PTS

SLURRY PROPERTIES	
Solids Relative Density	2,4449
Slurry Relative Density	1,0613
Volumetric Concentration	4,2 %
Yield Stress	1,040 Pa
Fluid Consistency Index	0,0136 Pa s ^ n
Flow Behaviour Index	0,8031
Representative Particle size	28 um

TURBULENT MODEL PERFORMANCE		
Model	Avg Err%	Avg LSE
Torrance	8,61	0,0193
Wilson and Thomas	7,16	0,0147
New Model	5,12	0,0139

Pseudo-Shear Diagram: KERS2408

Sm = 1,0613 : Diam = 79 mm

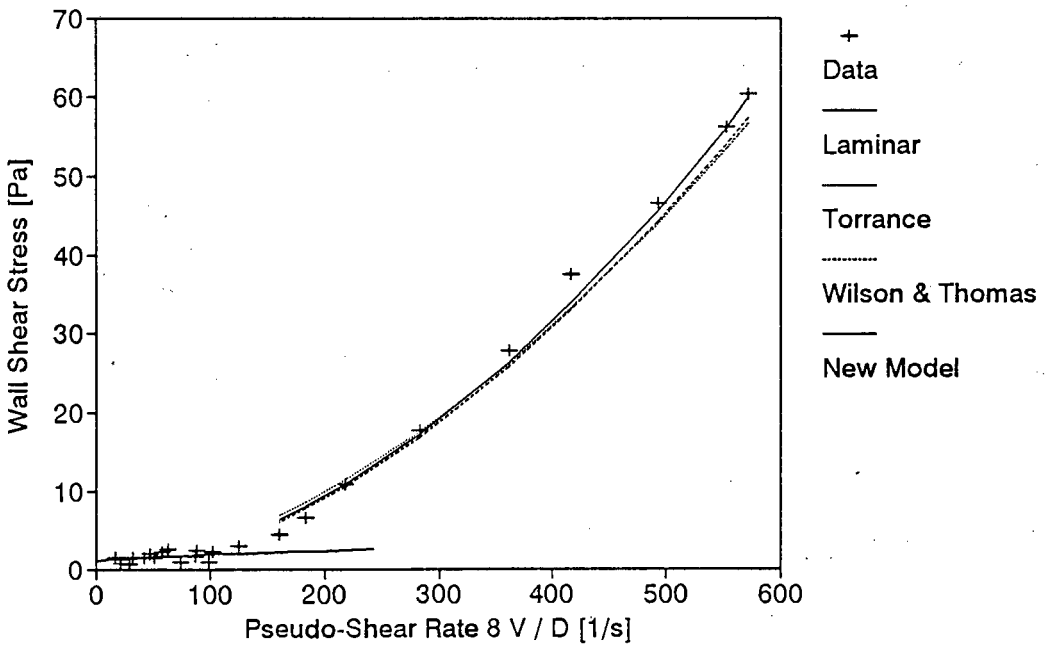

DATA FROM TEST	KMRL2408
APPARATUS	
Facility	Mini Rig
Diameter	21,6 mm
Material	Kaolin
Operator	PTS
Supervisor	PTS

SLURRY PROPERTIES	
Solids Relative Density	2,4449
Slurry Relative Density	1,0613
Volumetric Concentration	4,2 %
Yield Stress	1,040 Pa
Fluid Consistency Index	0,0136 Pa s ^ n
Flow Behaviour Index	0,8031
Representative Particle size	28 um

TURBULENT MODEL PERFORMANCE		
Model	Avg Err%	Avg LSE
Torrance	5,90	0,0135
Wilson and Thomas	3,23	0,0064
New Model	5,95	0,0109

Pseudo-Shear Diagram: KMRL2408

Sm = 1,0613 : Diam = 21,6 mm

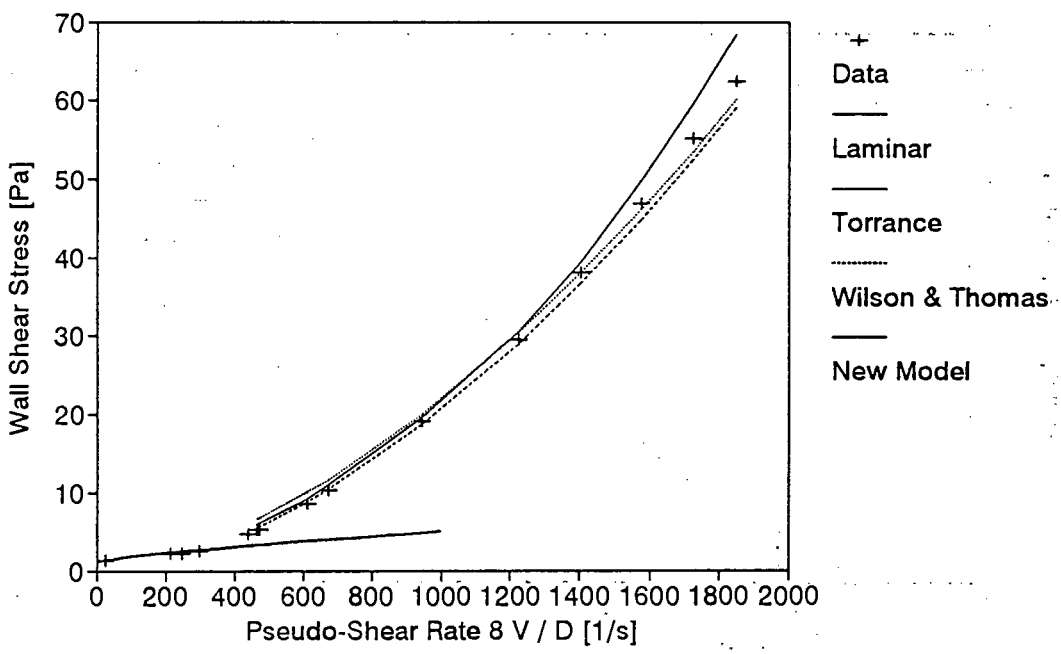

DATA FROM TEST	KMRM2408
APPARATUS	
Facility	Mini Rig
Diameter	13,2 mm
Material	Kaolin
Operator	PTS
Supervisor	PTS

SLURRY PROPERTIES	
Solids Relative Density	2,4449
Slurry Relative Density	1,0613
Volumetric Concentration	4,2 %
Yield Stress	1,040 Pa
Fluid Consistency Index	0,0136 Pa s ^ n
Flow Behaviour Index	0,8031
Representative Particle size	28 um

TURBULENT MODEL PERFORMANCE		
Model	Avg Err%	Avg LSE
Torrance	9,66	0,0169
Wilson and Thomas	11,97	0,0192
New Model	9,31	0,0166

Pseudo-Shear Diagram: KMRM2408

Sm = 1,0613 : Diam = 13,2 mm

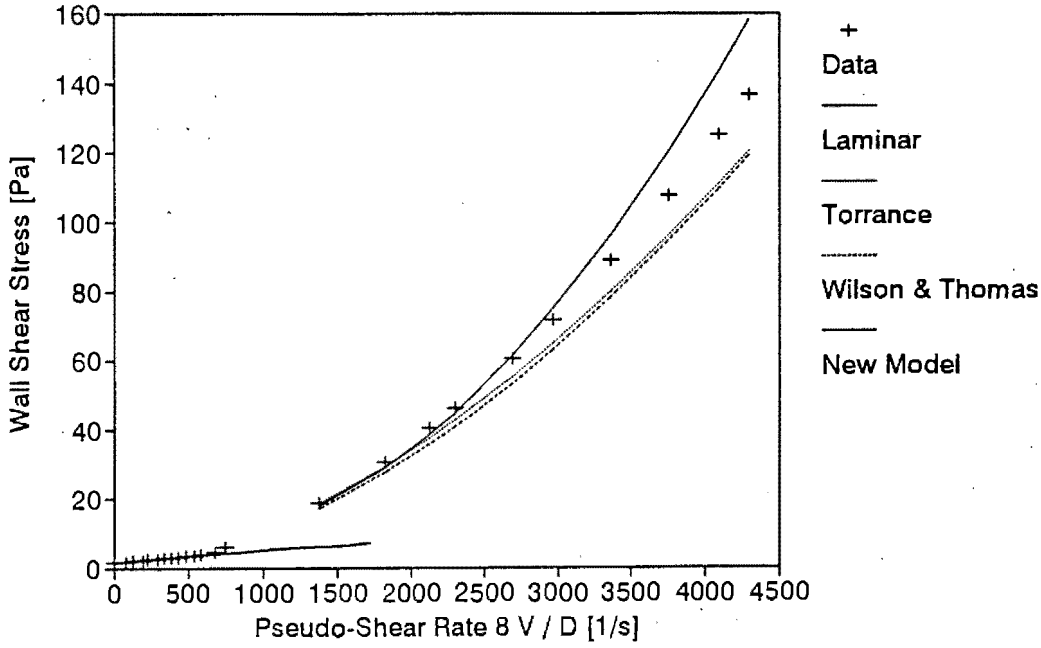

DATA FROM TEST	KMRS2408
APPARATUS	
Facility	Mini Rig
Diameter	5,623 mm
Material	Kaolin
Operator	PTS
Supervisor	PTS

SLURRY PROPERTIES	
Solids Relative Density	2,4449
Slurry Relative Density	1,0613
Volumetric Concentration	4,2 %
Yield Stress	1,040 Pa
Fluid Consistency Index	0,0136 Pa s ^ n
Flow Behaviour Index	0,8031
Representative Particle size	28 um

TURBULENT MODEL PERFORMANCE		
Model	Avg Err%	Avg LSE
Torrance	20,78	0,0457
Wilson and Thomas	14,45	0,0344
New Model	20,18	0,0408

Pseudo-Shear Diagram: KMRS2408

Sm = 1,0613 : Diam = 5,623 mm

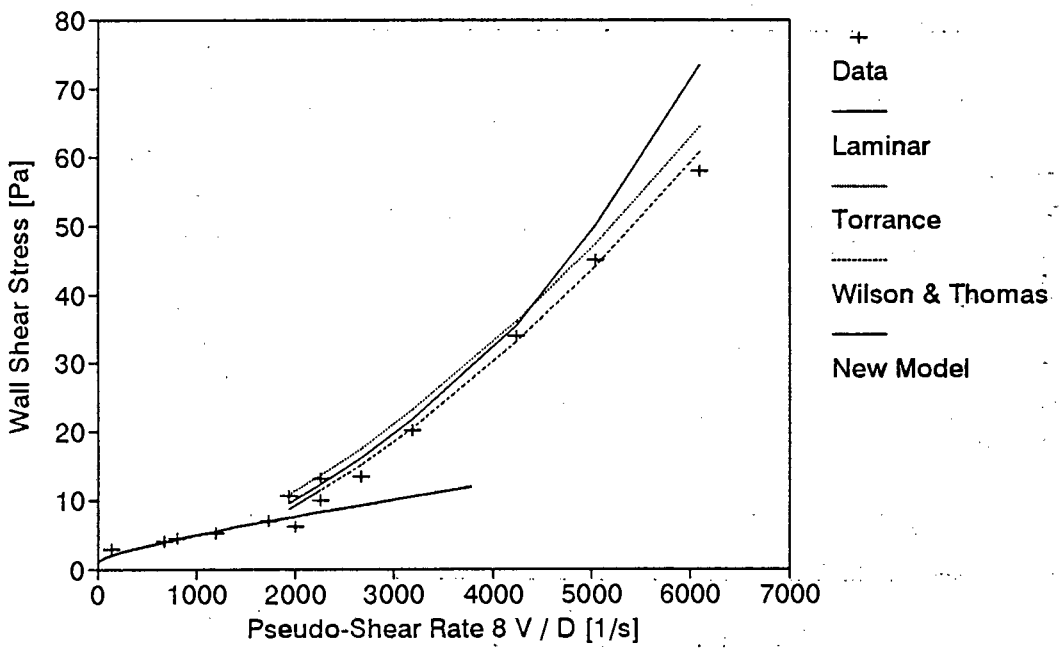

DATA FROM TEST	KERL2607
APPARATUS	
Facility	East Rig
Diameter	207 mm
Material	Kaolin
Operator	PTS
Supervisor	PTS

SLURRY PROPERTIES	
Solids Relative Density	2,4449
Slurry Relative Density	1,1053
Volumetric Concentration	7,3 %
Yield Stress	4,180 Pa
Fluid Consistency Index	0,0351 Pa s^n
Flow Behaviour Index	0,7190
Representative Particle size	112 um*

* Pipe Roughness

TURBULENT MODEL PERFORMANCE		
Model	Avg Err%	Avg LSE
Torrance	11,50	0,0195
Wilson and Thomas	11,71	0,0238
New Model	15,66	0,0258

Pseudo-Shear Diagram: KERL2607

Sm = 1,1053 : Diam = 207 mm

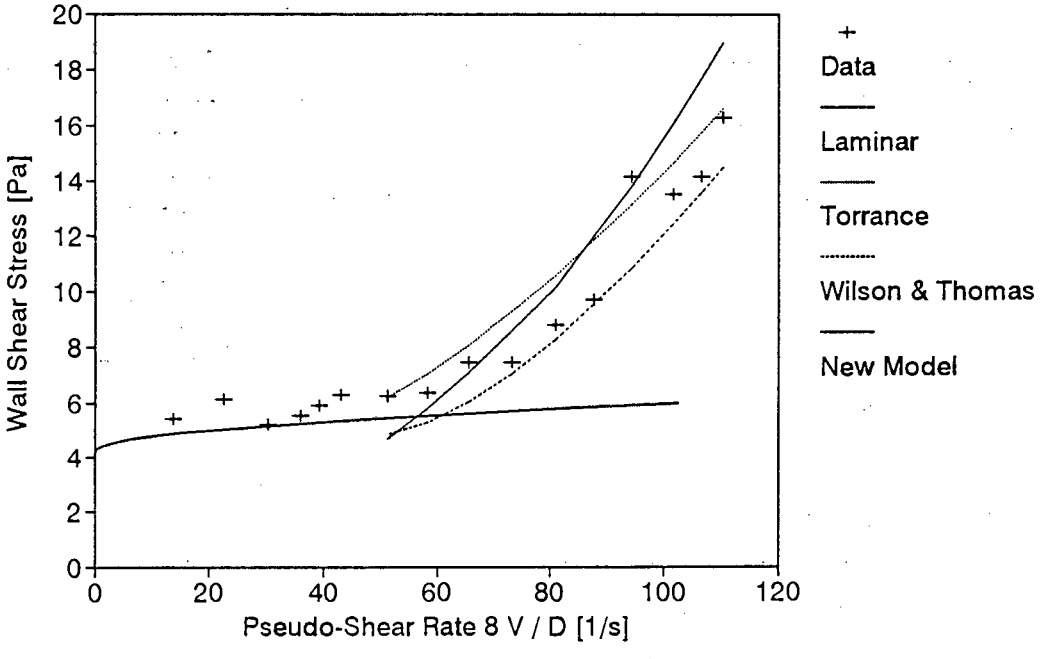

DATA FROM TEST	KERM2607
APPARATUS	
Facility	East Rig
Diameter	141 mm
Material	Kaolin
Operator	PTS
Supervisor	PTS

SLURRY PROPERTIES	
Solids Relative Density	2,4449
Slurry Relative Density	1,1053
Volumetric Concentration	7,3 %
Yield Stress	4,180 Pa
Fluid Consistency Index	0,0351 Pa s ^ n
Flow Behaviour Index	0,7190
Representative Particle size	28 um

TURBULENT MODEL PERFORMANCE		
Model	Avg Err%	Avg LSE
Torrance	12,13	0,0195
Wilson and Thomas	13,27	0,0208
New Model	5,06	0,0075

Pseudo-Shear Diagram: KERM2607

Sm = 1,1053 : Diam = 141 mm

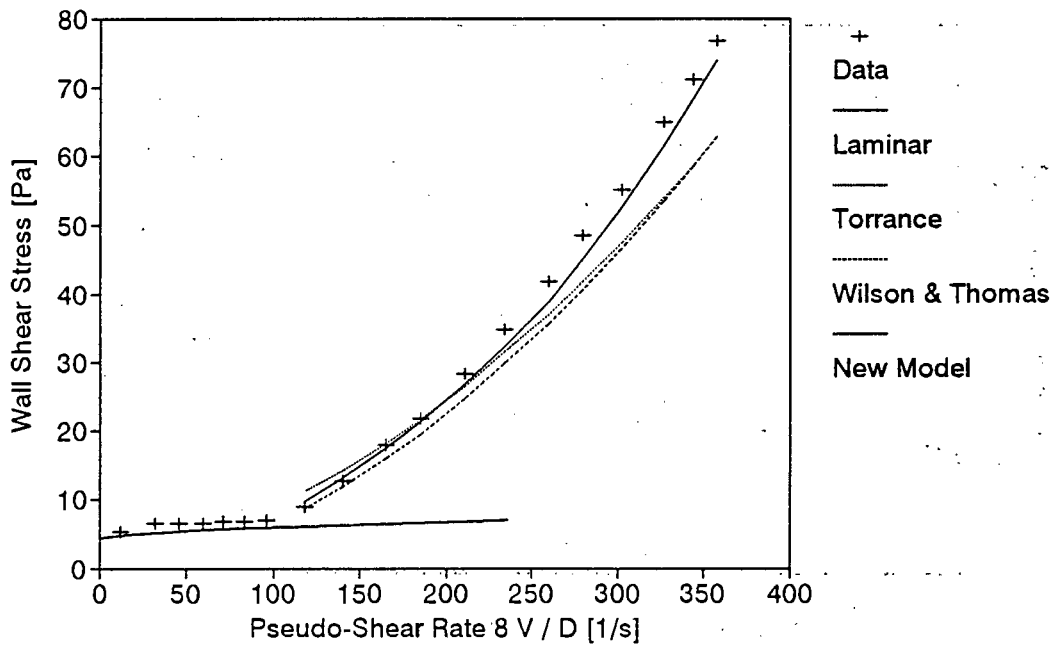

DATA FROM TEST	KERS2607
APPARATUS	
Facility	East Rig
Diameter	79 mm
Material	Kaolin
Operator	PTS
Supervisor	PTS

SLURRY PROPERTIES	
Solids Relative Density	2,4449
Slurry Relative Density	1,1053
Volumetric Concentration	7,3 %
Yield Stress	4,180 Pa
Fluid Consistency Index	0,0351 Pa s ^ n
Flow Behaviour Index	0,7190
Representative Particle size	28 um

TURBULENT MODEL PERFORMANCE		
Model	Avg Err%	Avg LSE
Torrance	9,37	0,0174
Wilson and Thomas	10,17	0,0181
New Model	9,38	0,0181

Pseudo-Shear Diagram: KERS2607

Sm = 1,1053 : Diam = 79 mm

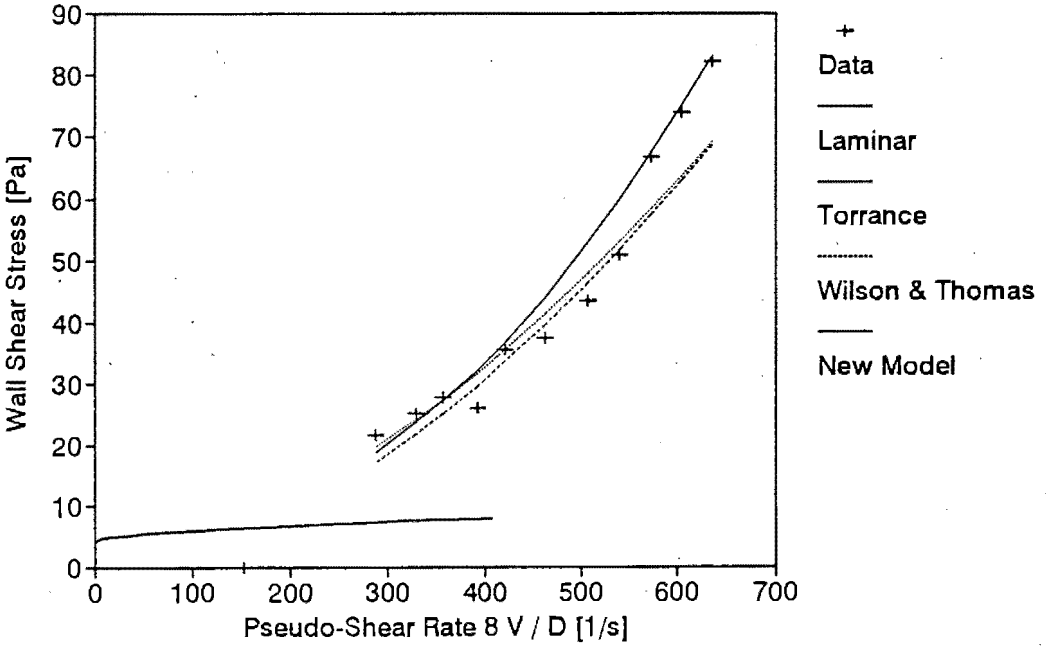

DATA FROM TEST	KMRL2607
APPARATUS	
Facility	Mini Rig
Diameter	21,6 mm
Material	Kaolin
Operator	PTS
Supervisor	PTS

SLURRY PROPERTIES	
Solids Relative Density	2,4449
Slurry Relative Density	1,1053
Volumetric Concentration	7,3 %
Yield Stress	4,180 Pa
Fluid Consistency Index	0,0351 Pa s ^ n
Flow Behaviour Index	0,7190
Representative Particle size	28 um

TURBULENT MODEL PERFORMANCE		
Model	Avg Err%	Avg LSE
Torrance	9,61	0,0128
Wilson and Thomas	11,80	0,0151
New Model	2,86	0,0038

Pseudo-Shear Diagram: KMRL2607

Sm = 1,1053 : Diam = 21,6 mm

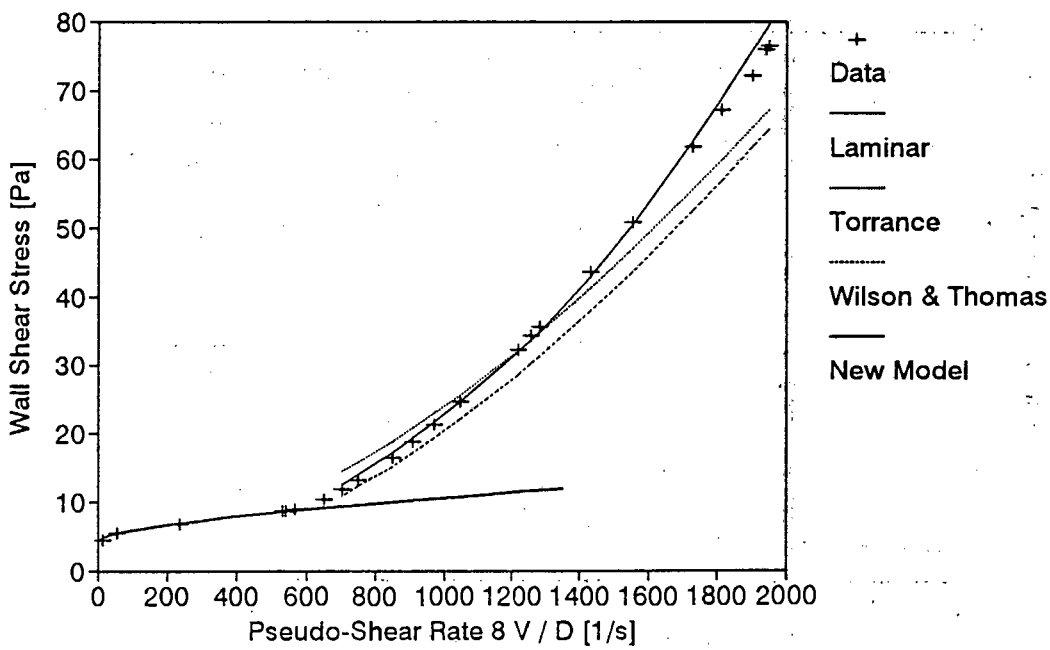

DATA FROM TEST	KMRM2607
APPARATUS	
Facility	Mini Rig
Diameter	13,2 mm
Material	Kaolin
Operator	PTS
Supervisor	PTS

SLURRY PROPERTIES	
Solids Relative Density	2,4449
Slurry Relative Density	1,1053
Volumetric Concentration	7,3 %
Yield Stress	4,180 Pa
Fluid Consistency Index	0,0351 Pa s ^ n
Flow Behaviour Index	0,7190
Representative Particle size	28 um

TURBULENT MODEL PERFORMANCE		
Model	Avg Err%	Avg LSE
Torrance	11,85	0,0205
Wilson and Thomas	17,42	0,0280
New Model	4,08	0,0071

Pseudo-Shear Diagram: KMRM2607

Sm = 1,1053 : Diam = 13,2 mm

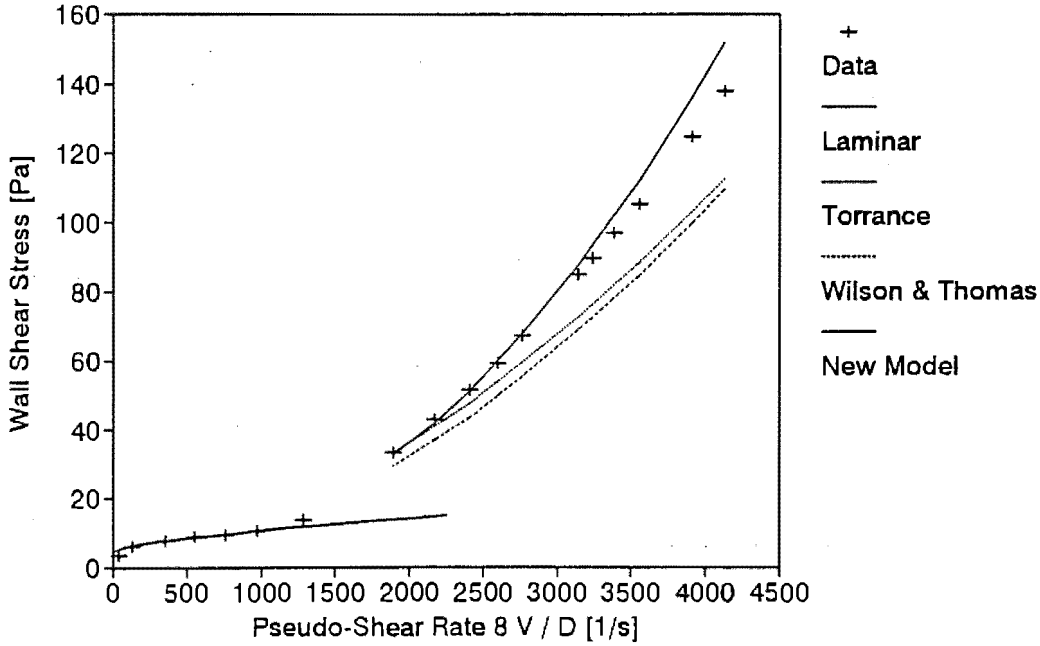

DATA FROM TEST	KMRS2607
APPARATUS	
Facility	Mini Rig
Diameter	5,623 mm
Material	Kaolin
Operator	PTS
Supervisor	PTS

SLURRY PROPERTIES	
Solids Relative Density	2,4449
Slurry Relative Density	1,1053
Volumetric Concentration	7,3 %
Yield Stress	4,180 Pa
Fluid Consistency Index	0,0351 Pa s ^ n
Flow Behaviour Index	0,7190
Representative Particle size	28 um

TURBULENT MODEL PERFORMANCE		
Model	Avg Err%	Avg LSE
Torrance	25,56	0,0480
Wilson and Thomas	13,43	0,0397
New Model	20,03	0,0385

Pseudo-Shear Diagram: KMRS2607

Sm = 1,1053 : Diam = 5,623 mm

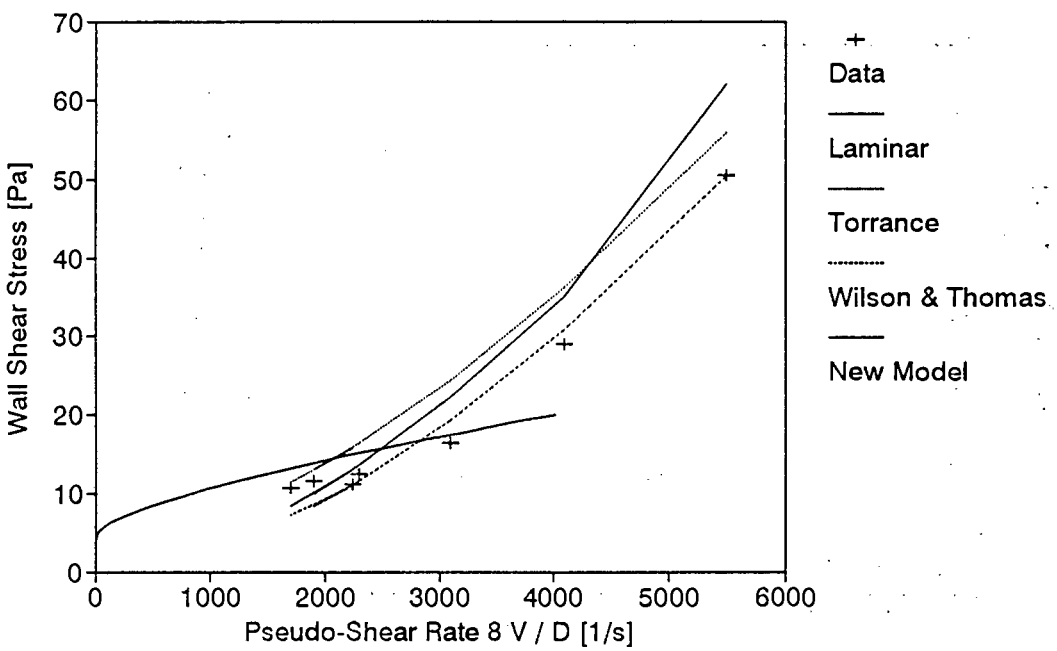

A.5 BBTV TEST RESULTS

The detailed Balanced Beam Tube Viscometer test results are presented in this section.

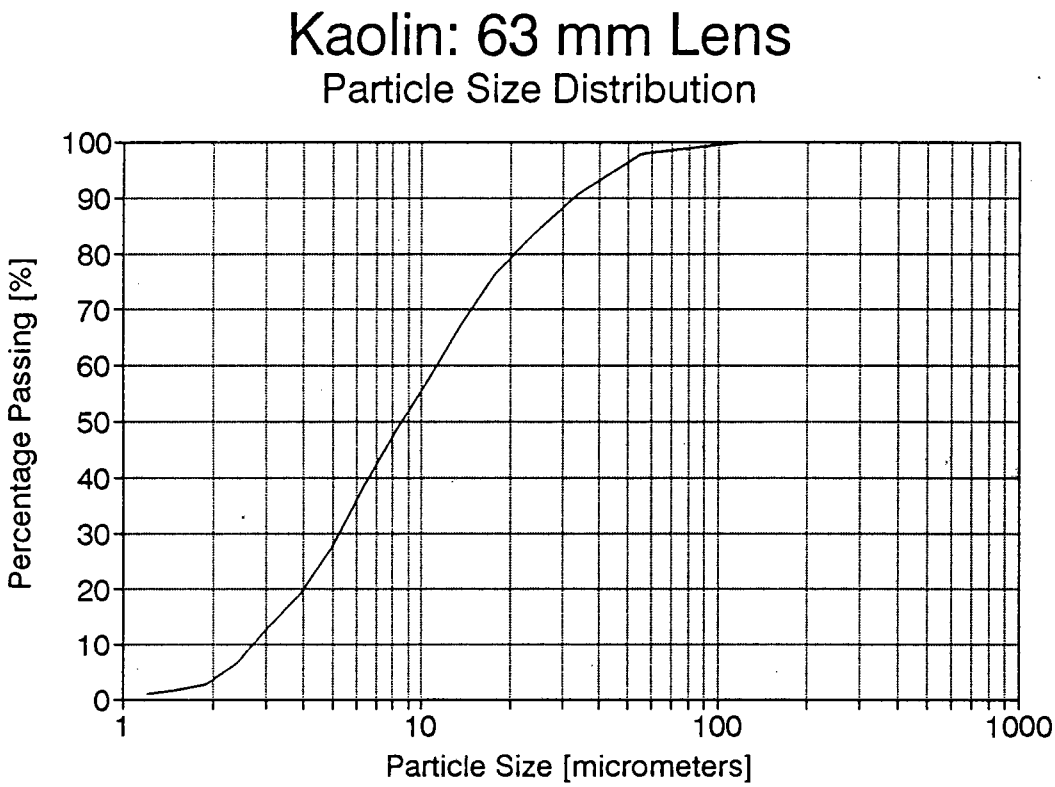
Kaolin: 63 mm Lens
Particle Size Distribution
Percentage Passing [%]
100
90
80
70
60
50
40
30
20
10
0
1
10
100
1000
Particle Size [micrometers]

DATA FROM TEST	KBBM002
APPARATUS	
Facility	BBTV
Diameter	13 mm
Material	Kaolin
Operator	PTS
Supervisor	PTS

SLURRY PROPERTIES	
Solids Relative Density	2,4449
Slurry Relative Density	1,0296
Volumetric Concentration	2,0 %
Yield Stress	0,6 Pa
Fluid Consistency Index	0,0180 Pa s ^ n
Flow Behaviour Index	0,663
Representative Particle size	26 um

TURBULENT MODEL PERFORMANCE		
Model	Avg Err%	Avg LSE
Torrance	3,78	0,0104
Wilson and Thomas	24,66	0,0700
New Model	17,40	0,0484

Pseudo-Shear Diagram:KBBM002

Sm = 1,0296 : Diam = 13mm

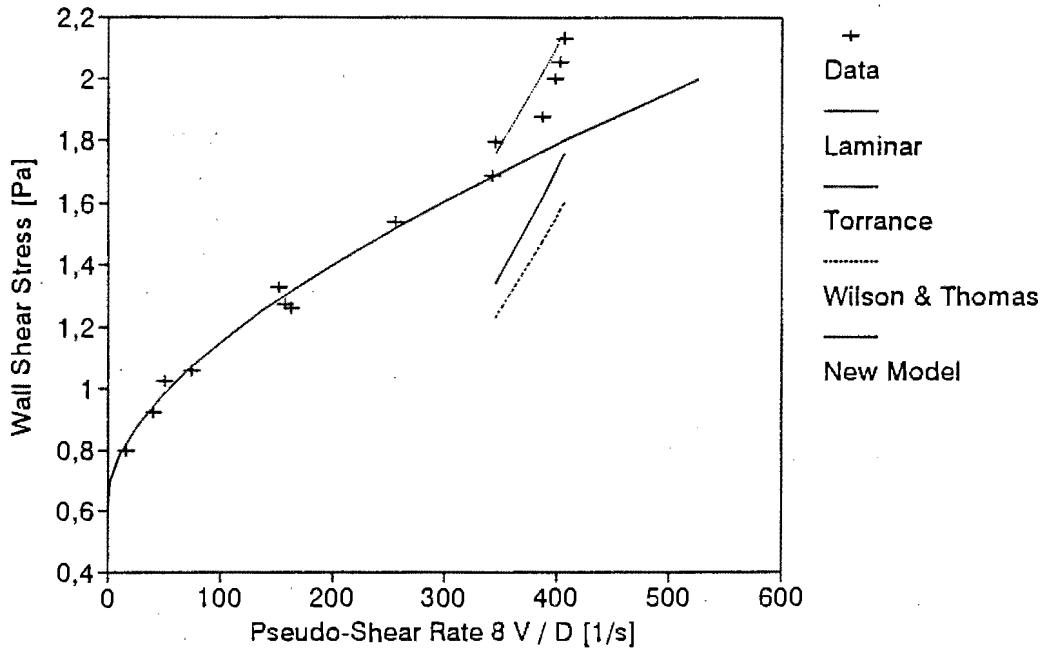

DATA FROM TEST	KBBL002
APPARATUS	
Facility	BBTV
Diameter	32 mm
Material	Kaolin
Operator	PTS
Supervisor	PTS

SLURRY PROPERTIES	
Solids Relative Density	2,4449
Slurry Relative Density	1,0296
Volumetric Concentration	2,0 %
Yield Stress	0,6 Pa
Fluid Consistency Index	0,0180 Pa s ^ n
Flow Behaviour Index	0,663
Representative Particle size	26 um

TURBULENT MODEL PERFORMANCE		
Model	Avg Err%	Avg LSE
Torrance	16,00	0,1021
Wilson and Thomas	17,76	0,1290
New Model	19,34	0,1321

Pseudo-Shear Diagram:KBBL002

Sm = 1,0296 : Diam = 32mm

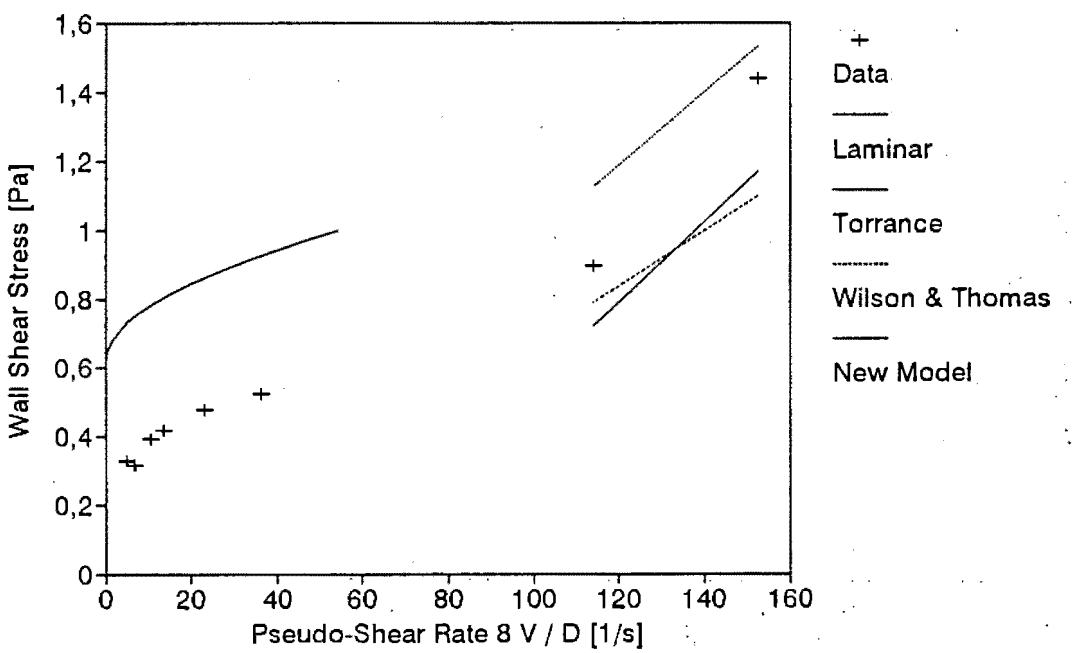

DATA FROM TEST	KBBM004
APPARATUS	
Facility	BBTV
Diameter	13 mm
Material	Kaolin
Operator	PTS
Supervisor	PTS

SLURRY PROPERTIES	
Solids Relative Density	2,4449
Slurry Relative Density	1,0582
Volumetric Concentration	4,0 %
Yield Stress	1,4 Pa
Fluid Consistency Index	0,0610 Pa s ^ n
Flow Behaviour Index	0,593
Representative Particle size	26 um

TURBULENT MODEL PERFORMANCE		
Model	Avg Err%	Avg LSE
Torrance	32,93	0,0388
Wilson and Thomas	34,30	0,0398
New Model	12,92	0,0141

Pseudo-Shear Diagram:KBBM004

Sm = 1,0582 : Diam = 13mm

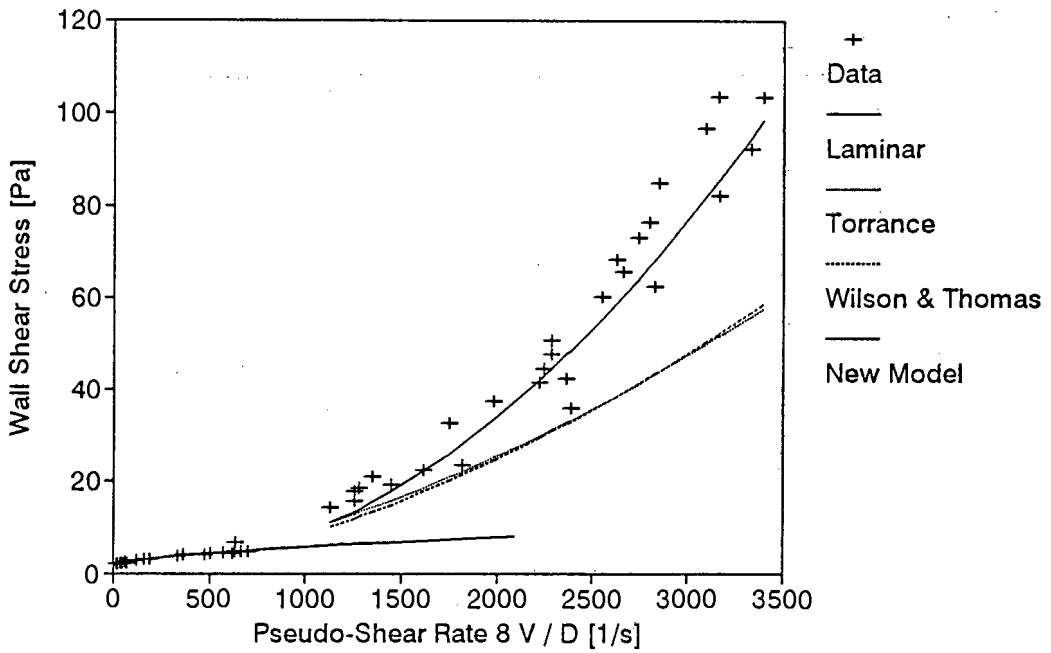

DATA FROM TEST	KBBL004
APPARATUS	
Facility	BBTV
Diameter	32 mm
Material	Kaolin
Operator	PTS
Supervisor	PTS

SLURRY PROPERTIES	
Solids Relative Density	2,4449
Slurry Relative Density	1,0582
Volumetric Concentration	4,0 %
Yield Stress	1,4 Pa
Fluid Consistency Index	0,0610 Pa s ^ n
Flow Behaviour Index	0,593
Representative Particle size	26 um

TURBULENT MODEL PERFORMANCE		
Model	Avg Err%	Avg LSE
Torrance	37,77	0,0474
Wilson and Thomas	36,71	0,0451
New Model	6,73	0,0091

Pseudo-Shear Diagram:KBBL004

Sm = 1,0582 : Diam = 32mm

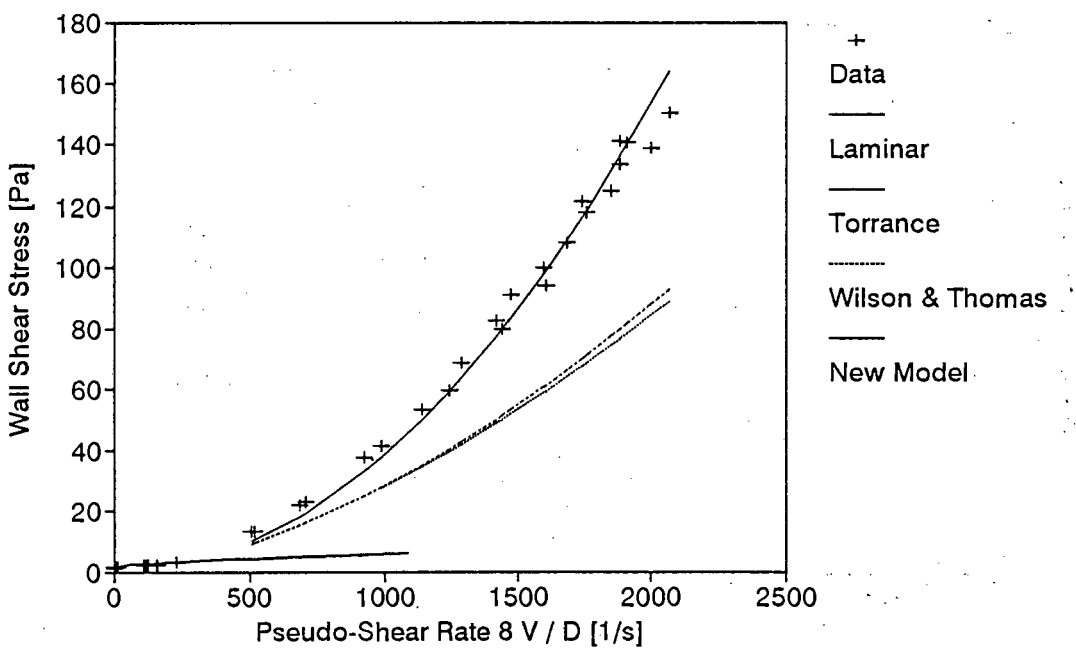

DATA FROM TEST	KBBM006
APPARATUS	
Facility	BBTV
Diameter	13 mm
Material	Kaolin
Operator	PTS
Supervisor	PTS

SLURRY PROPERTIES	
Solids Relative Density	2,4449
Slurry Relative Density	1,0850
Volumetric Concentration	5,9 %
Yield Stress	3,0 Pa
Fluid Consistency Index	0,2010 Pa s ^ n
Flow Behaviour Index	0,474
Representative Particle size	26 um

TURBULENT MODEL PERFORMANCE		
Model	Avg Err%	Avg LSE
Torrance	18,50	0,0418
Wilson and Thomas	26,92	0,0572
New Model	17,97	0,0363

Pseudo-Shear Diagram:KBBM006

Sm = 1,0850 : Diam = 13mm

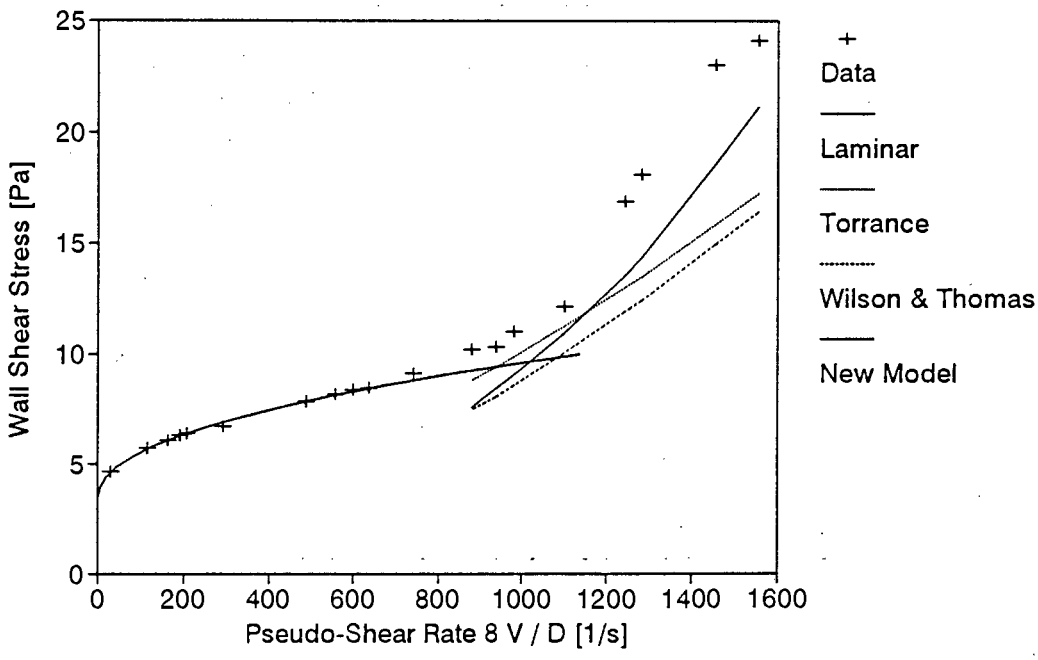

DATA FROM TEST	KBBL006
APPARATUS	
Facility	BBTV
Diameter	32 mm
Material	Kaolin
Operator	PTS
Supervisor	PTS

SLURRY PROPERTIES	
Solids Relative Density	2,4449
Slurry Relative Density	1,0850
Volumetric Concentration	5,9 %
Yield Stress	3,0 Pa
Fluid Consistency Index	0,2010 Pa s ^ n
Flow Behaviour Index	0,474
Representative Particle size	26 um

TURBULENT MODEL PERFORMANCE		
Model	Avg Err%	Avg LSE
Torrance	44,18	0,0622
Wilson and Thomas	41,20	0,0569
New Model	4,21	0,0056

Pseudo-Shear Diagram:KBBL006

Sm = 1,0850 : Diam = 32mm

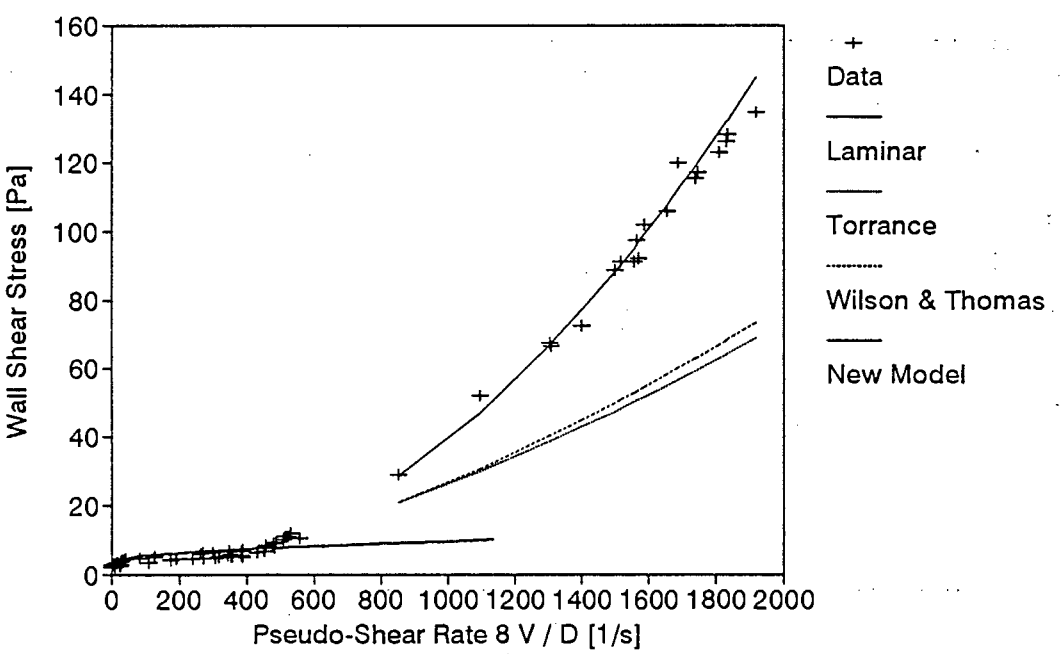

DATA FROM TEST	KBBM08
APPARATUS	
Facility	BBTV
Diameter	13 mm
Material	Kaolin
Operator	PTS
Supervisor	PTS

SLURRY PROPERTIES	
Solids Relative Density	2,4449
Slurry Relative Density	1,1132
Volumetric Concentration	7,8 %
Yield Stress	6,0 Pa
Fluid Consistency Index	0,0270 Pa s ^ n
Flow Behaviour Index	0,820
Representative Particle size	26 um

TURBULENT MODEL PERFORMANCE		
Model	Avg Err%	Avg LSE
Torrance	10,42	0,0157
Wilson and Thomas	7,18	0,0150
New Model	6,68	0,0137

Pseudo-Shear Diagram:KBBM08

Sm = 1,1132 : Diam = 13mm

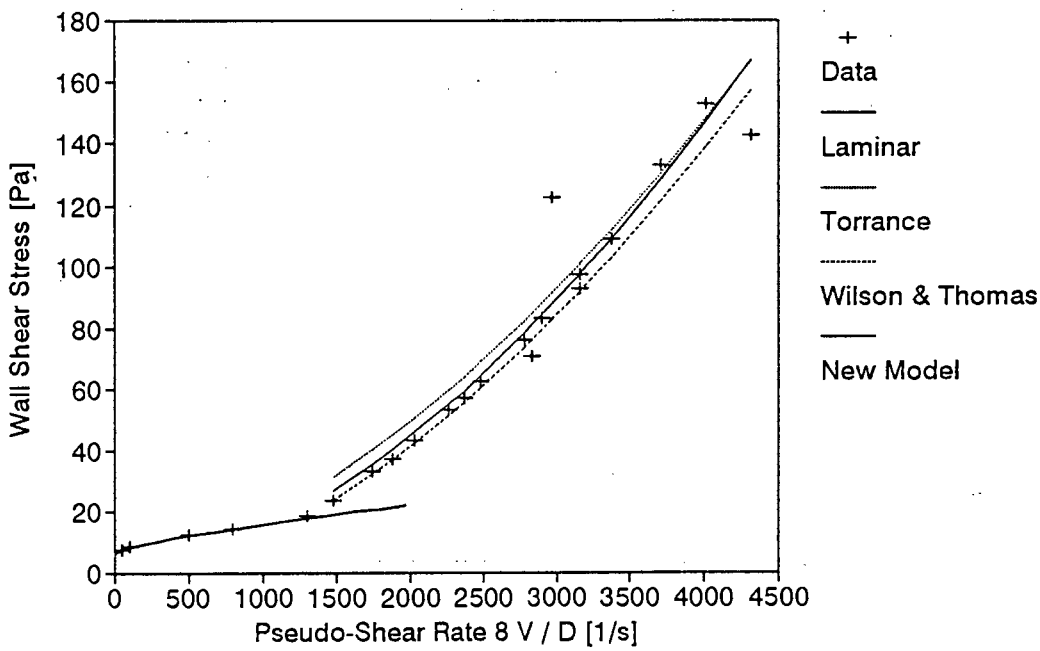

DATA FROM TEST	KBBL08
APPARATUS	
Facility	BBTV
Diameter	32 mm
Material	Kaolin
Operator	PTS
Supervisor	PTS

SLURRY PROPERTIES	
Solids Relative Density	2,4449
Slurry Relative Density	1,1132
Volumetric Concentration	7,8 %
Yield Stress	6,0 Pa
Fluid Consistency Index	0,0270 Pa s ^ n
Flow Behaviour Index	0,820
Representative Particle size	26 um

TURBULENT MODEL PERFORMANCE		
Model	Avg Err%	Avg LSE
Torrance	17,11	0,0231
Wilson and Thomas	7,06	0,0145
New Model	11,70	0,0173

Pseudo-Shear Diagram:KBBL08

Sm = 1,1132 : Diam = 32mm

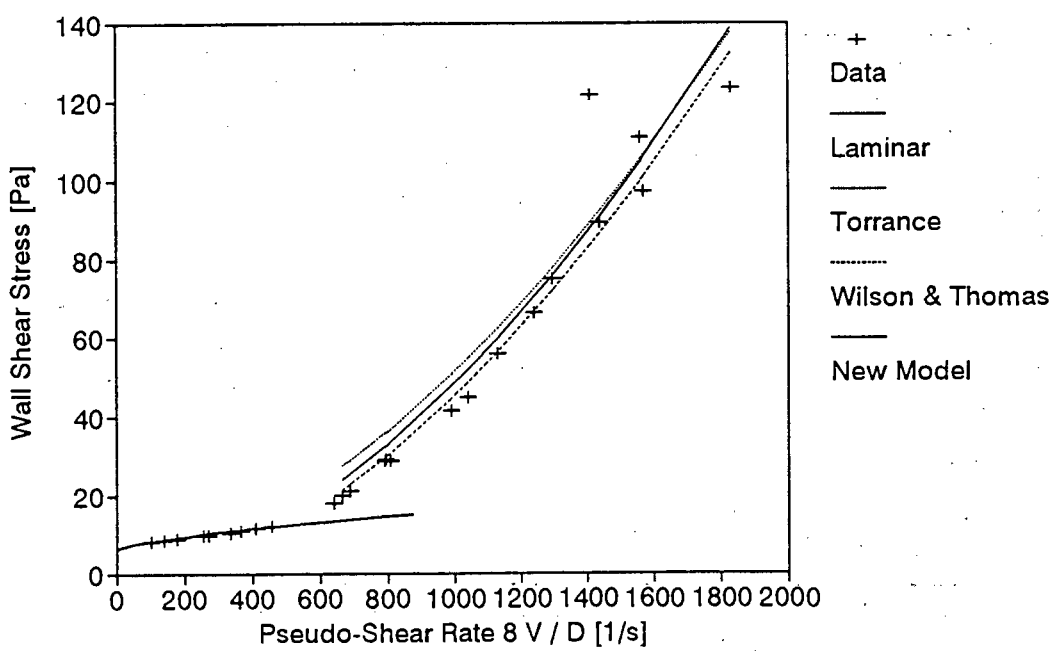

DATA FROM TEST	KBBM12
APPARATUS	
Facility	BBTV
Diameter	13 mm
Material	Kaolin
Operator	PTS
Supervisor	PTS

SLURRY PROPERTIES	
Solids Relative Density	2,4449
Slurry Relative Density	1,1745
Volumetric Concentration	12,1 %
Yield Stress	23,0 Pa
Fluid Consistency Index	0,5000 Pa s ^ n
Flow Behaviour Index	0,50
Representative Particle size	26 um

TURBULENT MODEL PERFORMANCE		
Model	Avg Err%	Avg LSE
Torrance	10,99	0,0180
Wilson and Thomas	27,18	0,0542
New Model	25,21	0,0504

Pseudo-Shear Diagram:KBBM12

Sm = 1,1745 : Diam = 13mm

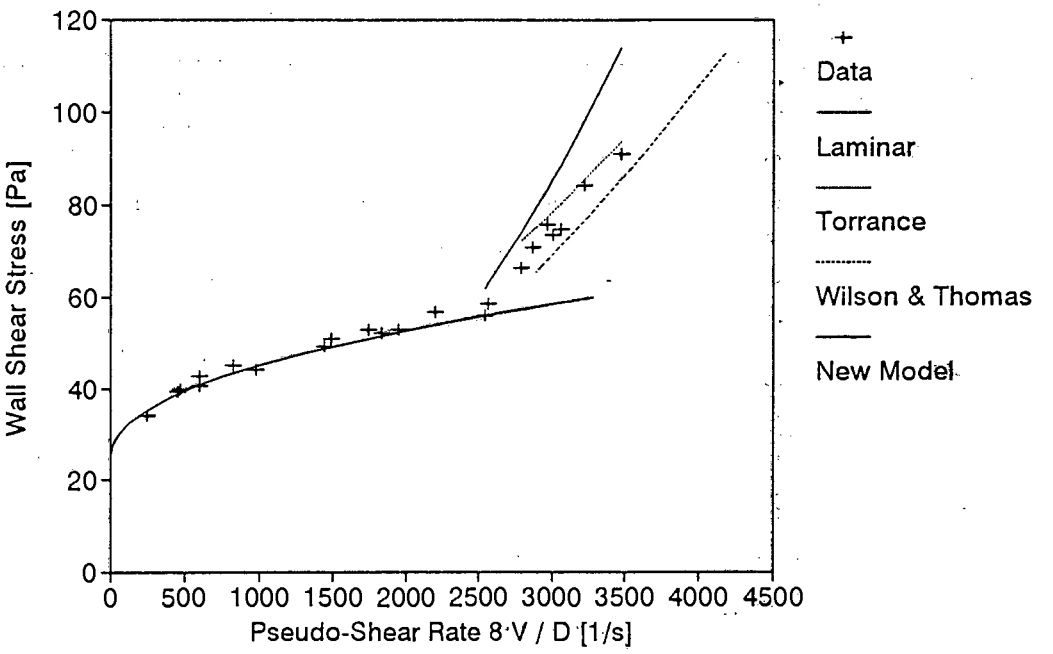

DATA FROM TEST	KBBL12
APPARATUS	
Facility	BBTV
Diameter	32 mm
Material	Kaolin
Operator	PTS
Supervisor	PTS

SLURRY PROPERTIES	
Solids Relative Density	2,4449
Slurry Relative Density	1,1745
Volumetric Concentration	12,1 %
Yield Stress	23,0 Pa
Fluid Consistency Index	0,5000 Pa s ^ n
Flow Behaviour Index	0,50
Representative Particle size	26 um

TURBULENT MODEL PERFORMANCE		
Model	Avg Err%	Avg LSE
Torrance	12,32	0,0179
Wilson and Thomas	9,47	0,0145
New Model	7,84	0,0124

Pseudo-Shear Diagram:KBBL12

Sm = 1,1745 : Diam = 32mm

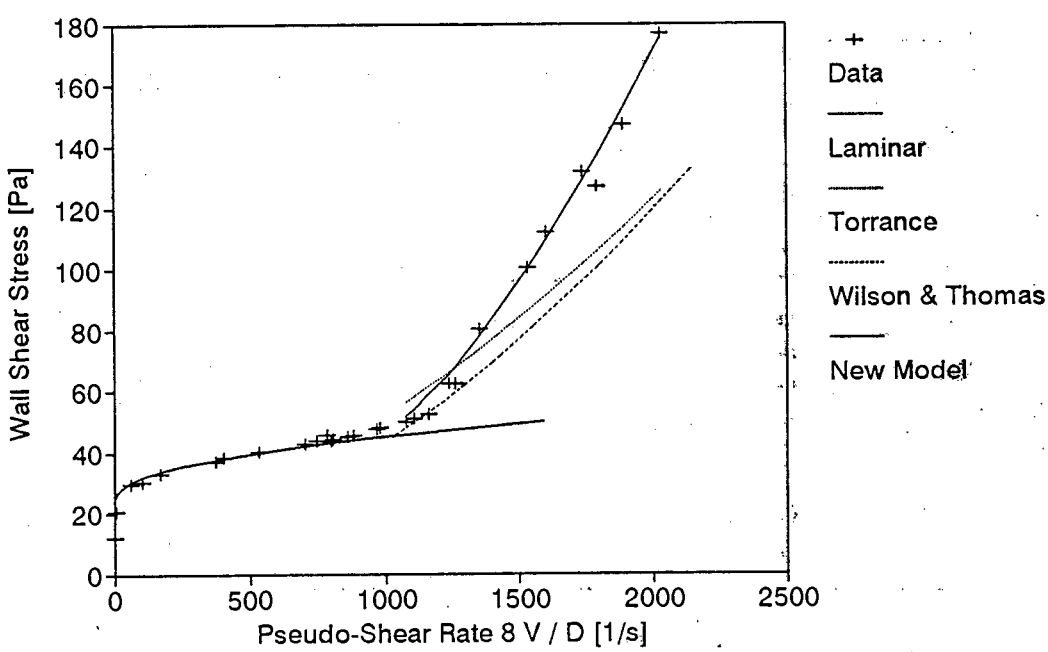

DATA FROM TEST	KBBL15
APPARATUS	
Facility	BBTV
Diameter	32 mm
Material	Kaolin
Operator	PTS
Supervisor	PTS

SLURRY PROPERTIES	
Solids Relative Density	2,4449
Slurry Relative Density	1,2150
Volumetric Concentration	14,9 %
Yield Stress	44,0 Pa
Fluid Consistency Index	1,1700 Pa s ^ n
Flow Behaviour Index	0,490
Representative Particle size	26 um

TURBULENT MODEL PERFORMANCE		
Model	Avg Err%	Avg LSE
Torrance	12,45	0,0229
Wilson and Thomas	7,84	0,0180
New Model	7,52	0,0149

Pseudo-Shear Diagram:KBBL15

Sm = 1,2150 : Diam = 32mm

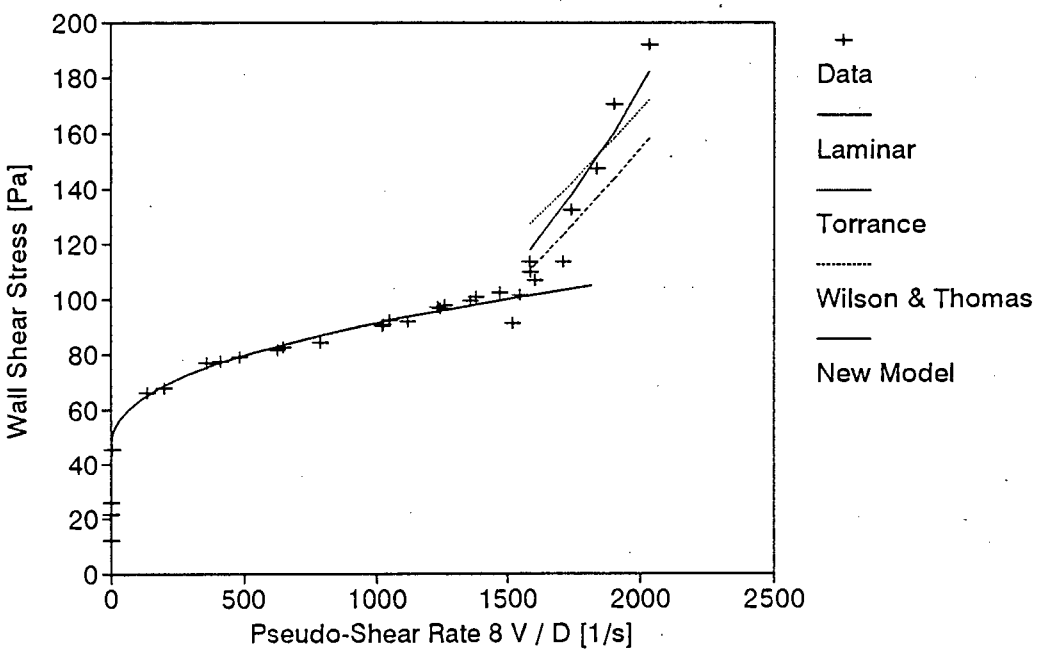

DATA FROM TEST	KBBM18
APPARATUS	
Facility	BBTV
Diameter	13 mm
Material	Kaolin
Operator	PTS
Supervisor	PTS

SLURRY PROPERTIES	
Solids Relative Density	2,4449
Slurry Relative Density	1,2559
Volumetric Concentration	17,7 %
Yield Stress	80,0 Pa
Fluid Consistency Index	2,2900 Pa s ^ n
Flow Behaviour Index	0,430
Representative Particle size	26 um

TURBULENT MODEL PERFORMANCE		
Model	Avg Err%	Avg LSE
Torrance	11,08	0,0171
Wilson and Thomas	17,57	0,0277
New Model	26,69	0,0415

Pseudo-Shear Diagram:KBBM18

Sm = 1,2559 : Diam = 13mm

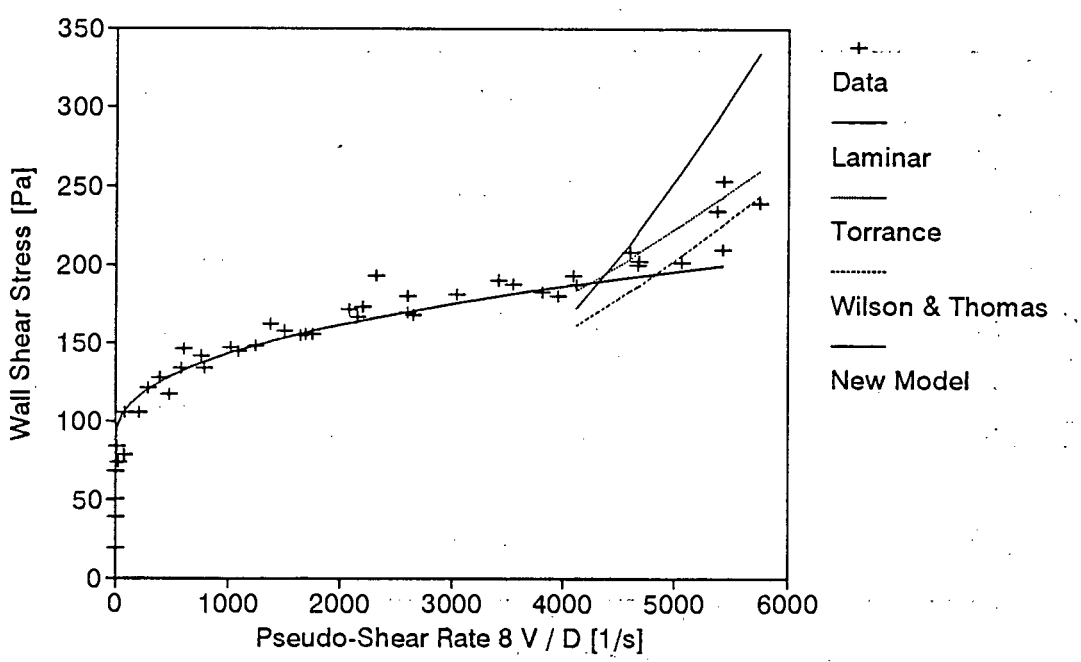

DATA FROM TEST	KBBL18
APPARATUS	
Facility	BBTV
Diameter	32 mm
Material	Kaolin
Operator	PTS
Supervisor	PTS

SLURRY PROPERTIES	
Solids Relative Density	2,4449
Slurry Relative Density	1,2559
Volumetric Concentration	17,7 %
Yield Stress	80,0 Pa
Fluid Consistency Index	2,2900 Pa s ^ n
Flow Behaviour Index	0,430
Representative Particle size	26 um

TURBULENT MODEL PERFORMANCE		
Model	Avg Err%	Avg LSE
Torrance	5,11	0,0179
Wilson and Thomas	13,63	0,0456
New Model	9,33	0,0441

Pseudo-Shear Diagram:KBBL18

Sm = 1,2559 : Diam = 32mm

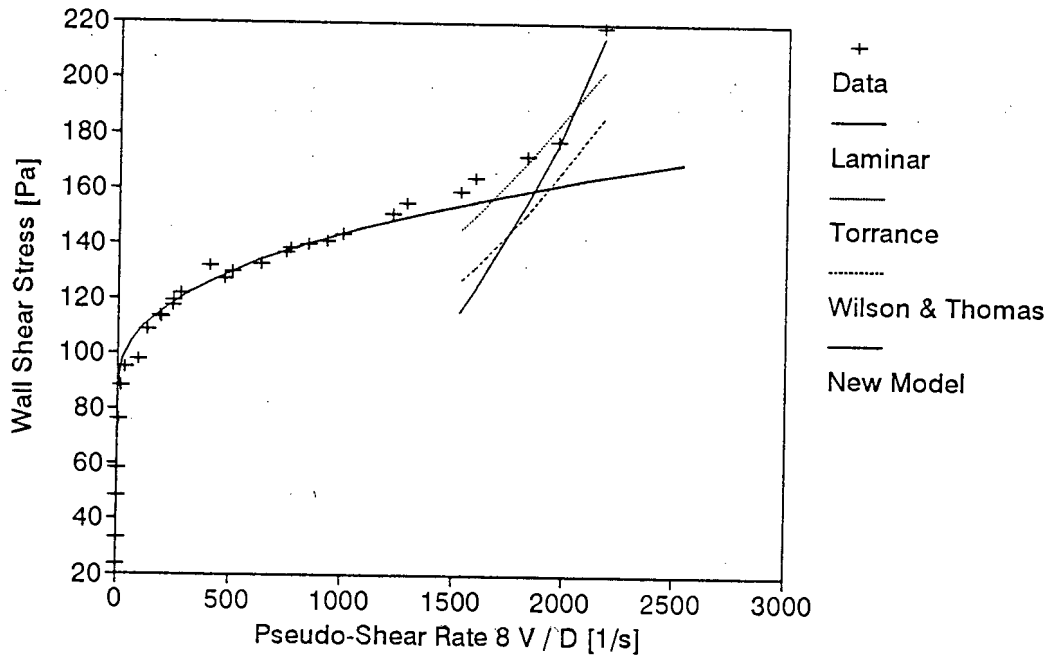

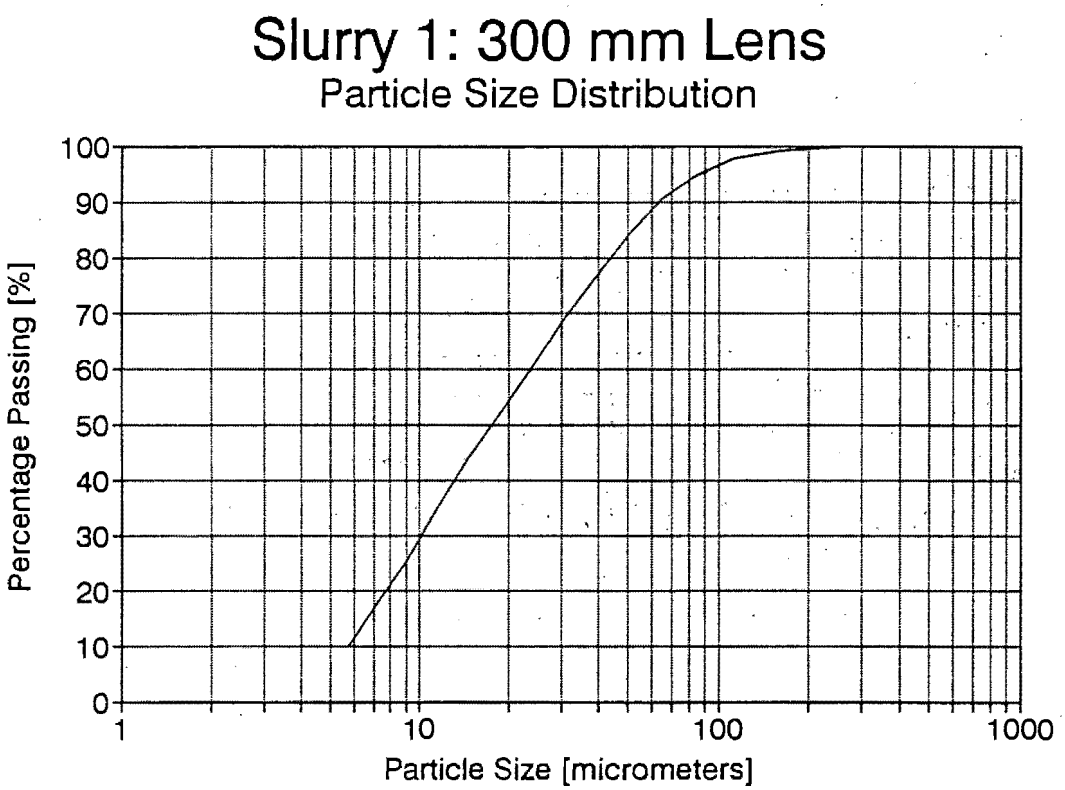
Slurry 1: 300 mm Lens
Particle Size Distribution
Percentage Passing [%]
100
90
80
70
60
50
40
30
20
10
0
1
10
100
1000
Particle Size [micrometers]

DATA FROM TEST	UBBM01
APPARATUS	
Facility	BBTV
Diameter	13 mm
Material	Slurry 1 (U)
Operator	PTS
Supervisor	PTS

SLURRY PROPERTIES	
Solids Relative Density	2,4449
Slurry Relative Density	1,3933
Volumetric Concentration	27,2 %
Yield Stress	17,0 Pa
Fluid Consistency Index	0,1800 Pa s ^ n
Flow Behaviour Index	0,740
Representative Particle size	50 um

TURBULENT MODEL PERFORMANCE		
Model	Avg Err%	Avg LSE
Torrance	37,38	0,0544
Wilson and Thomas	27,13	0,0419
New Model	32,51	0,0491

Pseudo-Shear Diagram:UBBM01

Sm = 1,3933 : Diam = 13mm

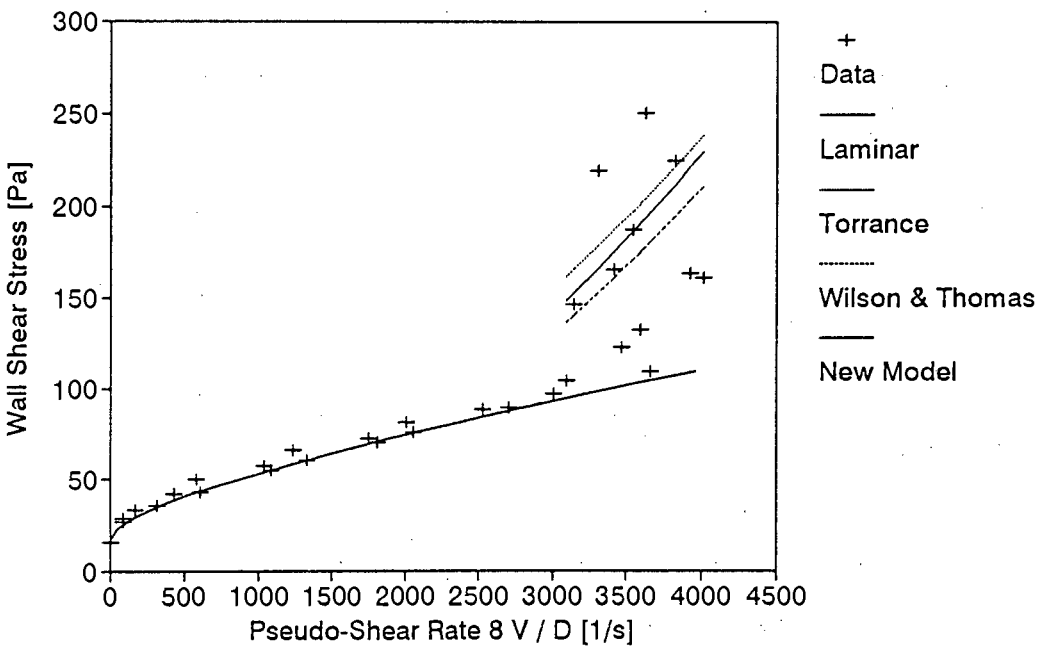

DATA FROM TEST	UBBL01
APPARATUS	
Facility	BBTV
Diameter	32 mm
Material	Slurry 1 (U)
Operator	PTS
Supervisor	PTS

SLURRY PROPERTIES	
Solids Relative Density	2,4449
Slurry Relative Density	1,3933
Volumetric Concentration	27,2 %
Yield Stress	17,0 Pa
Fluid Consistency Index	0,1800 Pa s ^ n
Flow Behaviour Index	0,740
Representative Particle size	50 um

TURBULENT MODEL PERFORMANCE		
Model	Avg Err%	Avg LSE
Torrance	5,83	0,0175
Wilson and Thomas	11,04	0,0239
New Model	6,93	0,0146

Pseudo-Shear Diagram:UBBL01

Sm = 1,3933 : Diam = 32mm

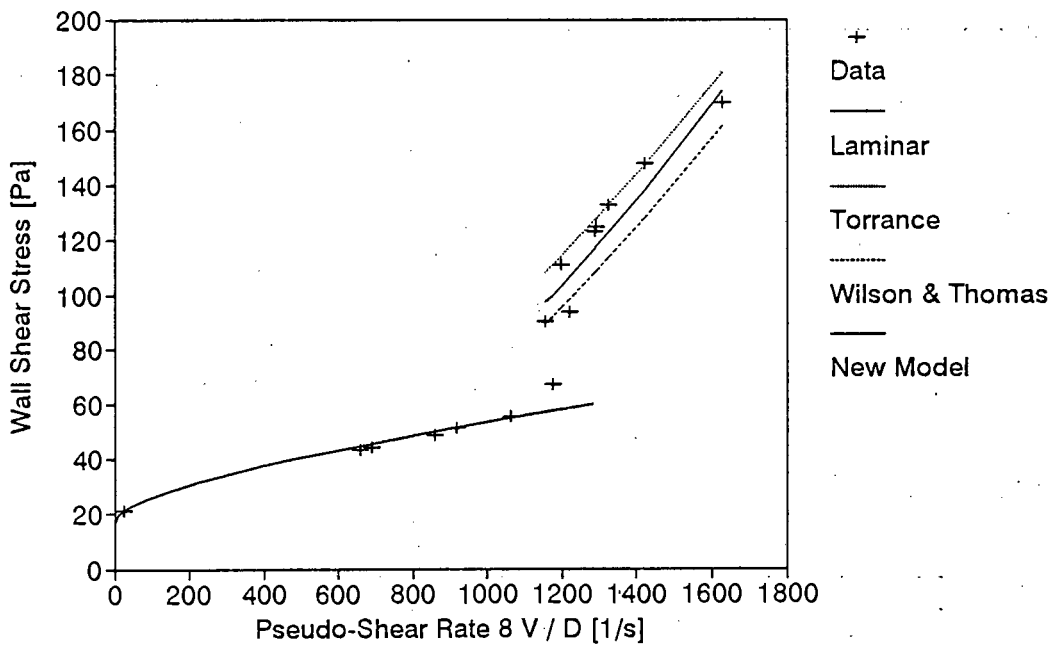

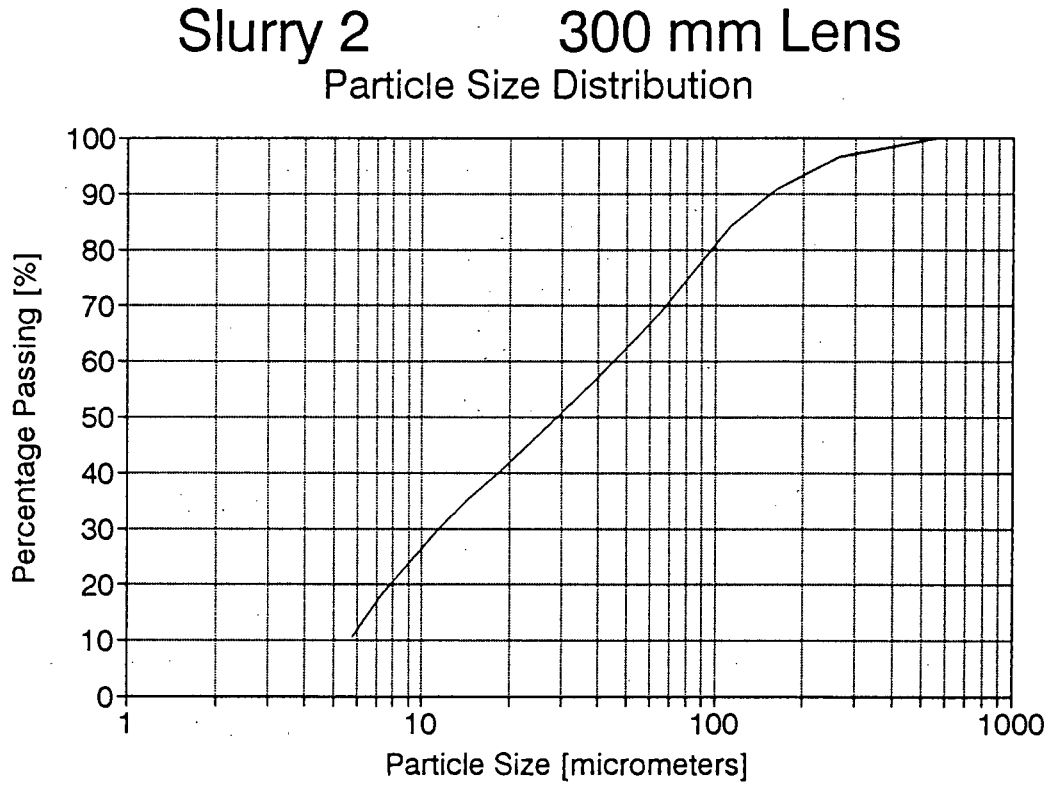
Slurry 2 300 mm Lens
Particle Size Distribution
Percentage Passing [%]
100
90
80
70
60
50
40
30
20
10
0
1
10
100
1000
Particle Size [micrometers]

DATA FROM TEST	UBBM02
APPARATUS	
Facility	BBTV
Diameter	13 mm
Material	Slurry 2 (U)
Operator	PTS
Supervisor	PTS

SLURRY PROPERTIES	
Solids Relative Density	2,7500
Slurry Relative Density	1,5004
Volumetric Concentration	28,6 %
Yield Stress	10,0 Pa
Fluid Consistency Index	0,1200 Pa s ^ n
Flow Behaviour Index	0,810
Representative Particle size	118 um

TURBULENT MODEL PERFORMANCE		
Model	Avg Err%	Avg LSE
Torrance	54,24	0,0867
Wilson and Thomas	37,03	0,0638
New Model	50,35	0,0828

Pseudo-Shear Diagram:UBBM02

Sm = 1,5004 : Diam = 13mm

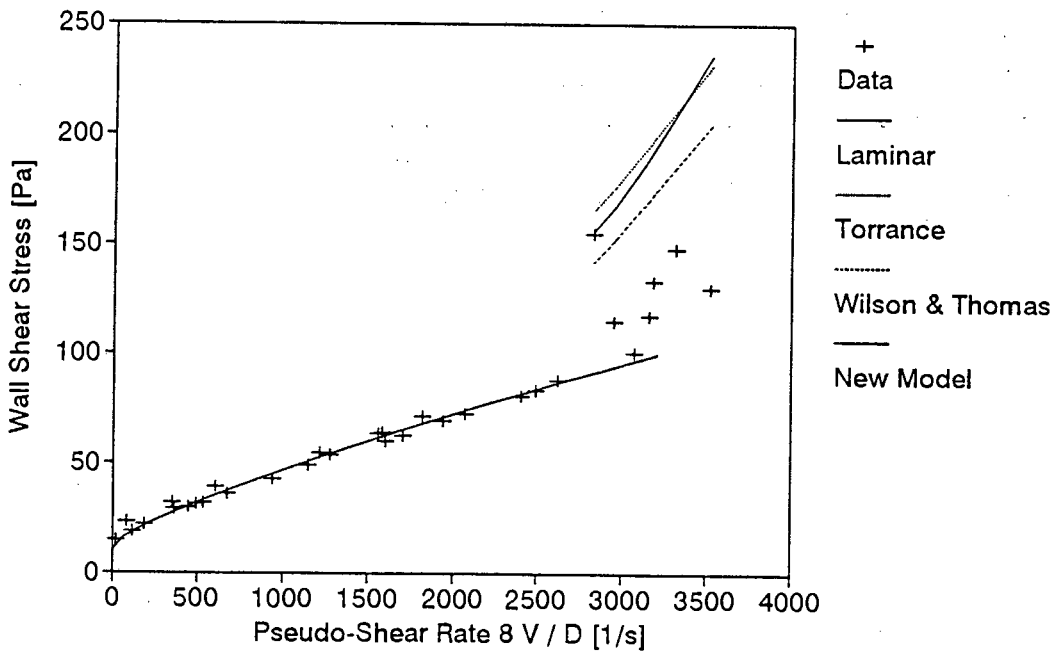

DATA FROM TEST	UBBL02
APPARATUS	
Facility	BBTV
Diameter	32 mm
Material	Slurry 2 (U)
Operator	PTS
Supervisor	PTS

SLURRY PROPERTIES	
Solids Relative Density	2,7500
Slurry Relative Density	1,5004
Volumetric Concentration	28,6 %
Yield Stress	10,0 Pa
Fluid Consistency Index	0,1200 Pa s ^ n
Flow Behaviour Index	0,810
Representative Particle size	118 um

TURBULENT MODEL PERFORMANCE		
Model	Avg Err%	Avg LSE
Torrance	13,30	0,0279
Wilson and Thomas	8,93	0,0182
New Model	9,80	0,0201

Pseudo-Shear Diagram:UBBL02

Sm = 1,5004 : Diam = 32mm

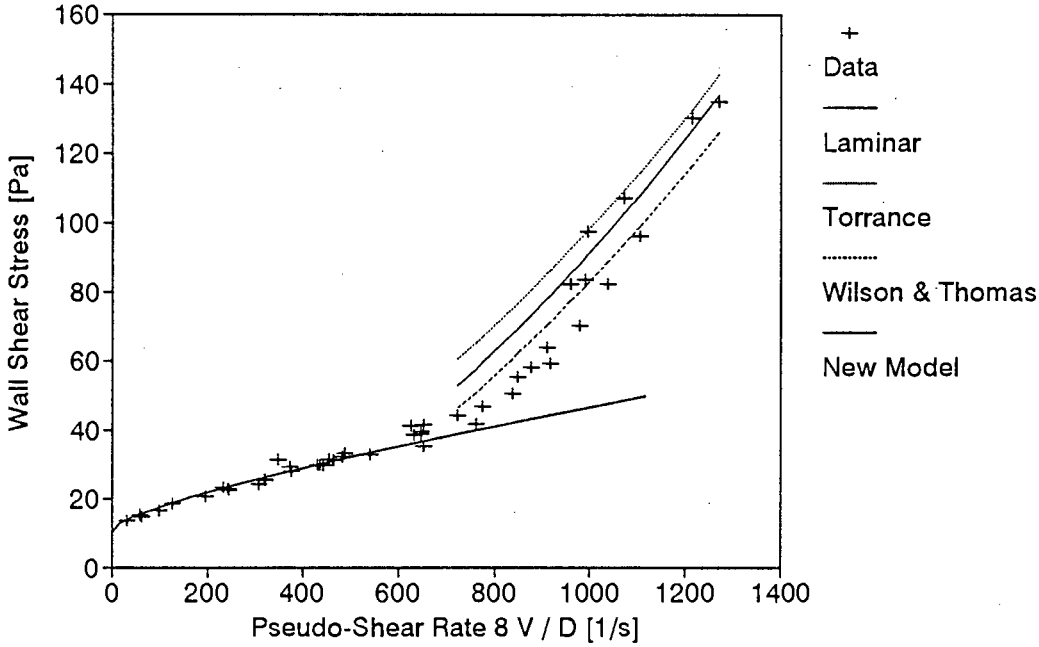

Belt Filtered Tailings: -500

Particle Size Distribution

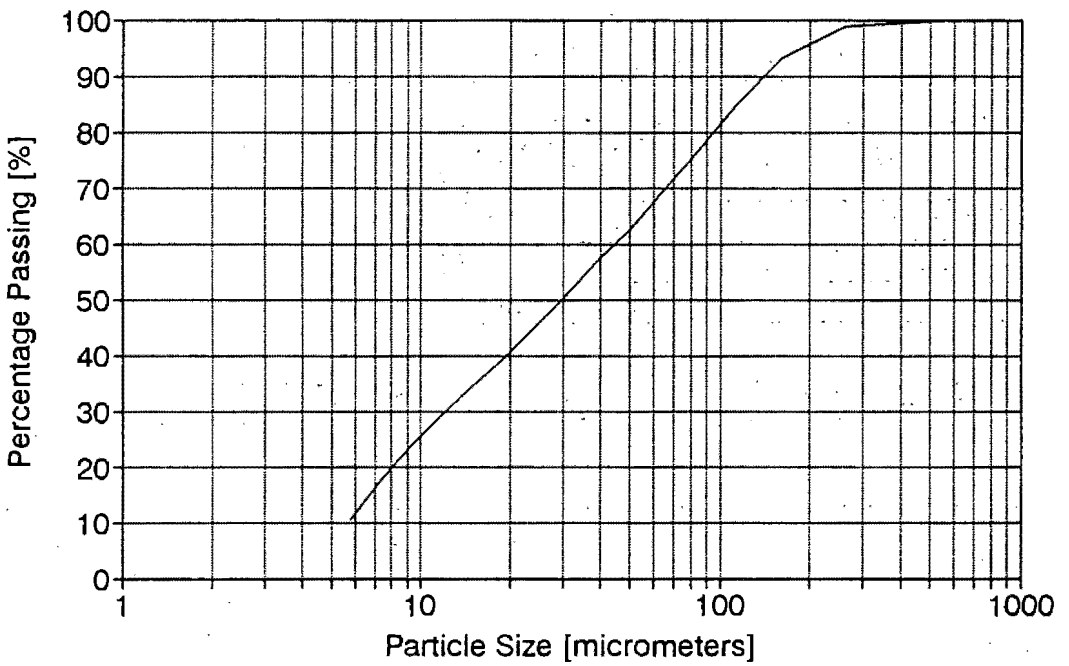

DATA FROM TEST	BBBL-500
APPARATUS	
Facility	BBTV
Diameter	33 mm
Material	Belt Filtered Tailings
Operator	RIGN
Supervisor	PTS

SLURRY PROPERTIES	
Solids Relative Density	2,7435
Slurry Relative Density	1,6512
Volumetric Concentration	37,4 %
Yield Stress	6,0 Pa
Fluid Consistency Index	0,0942 Pa s ^ n
Flow Behaviour Index	0,8309
Representative Particle size	113 um

TURBULENT MODEL PERFORMANCE		
Model	Avg Err%	Avg LSE
Torrance	8,69	0,0138
Wilson and Thomas	9,51	0,0107
New Model	6,36	0,0098

Pseudo-Shear Diagram:BBBL-500

Sm = 1,6512 : Diam = 33mm

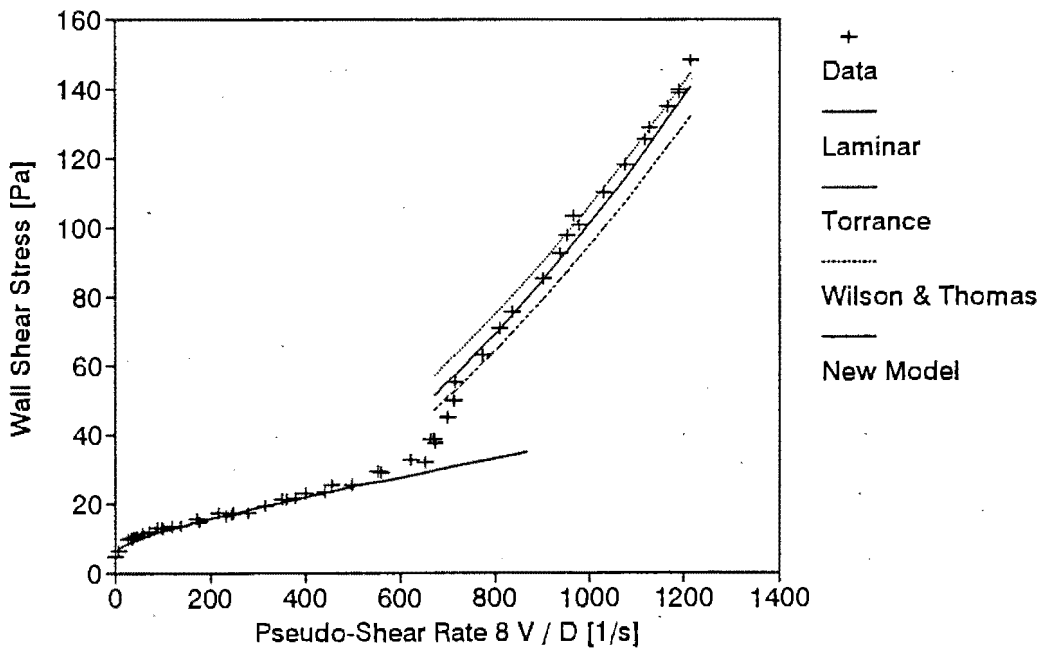

DATA FROM TEST	BBBM-500
APPARATUS	
Facility	BBTV
Diameter	13 mm
Material	Belt Filtered Tailings
Operator	RIGN
Supervisor	PTS

SLURRY PROPERTIES	
Solids Relative Density	2,7435
Slurry Relative Density	1,6500
Volumetric Concentration	37,3 %
Yield Stress	6,0 Pa
Fluid Consistency Index	0,0942 Pa s ^ n
Flow Behaviour Index	0,8309
Representative Particle size	113 um

TURBULENT MODEL PERFORMANCE		
Model	Avg Err%	Avg LSE
Torrance	5,83	0,0207
Wilson and Thomas	7,42	0,0274
New Model	4,23	0,0137

Pseudo-Shear Diagram:BBBM-500

Sm = 1,6500 : Diam = 13mm

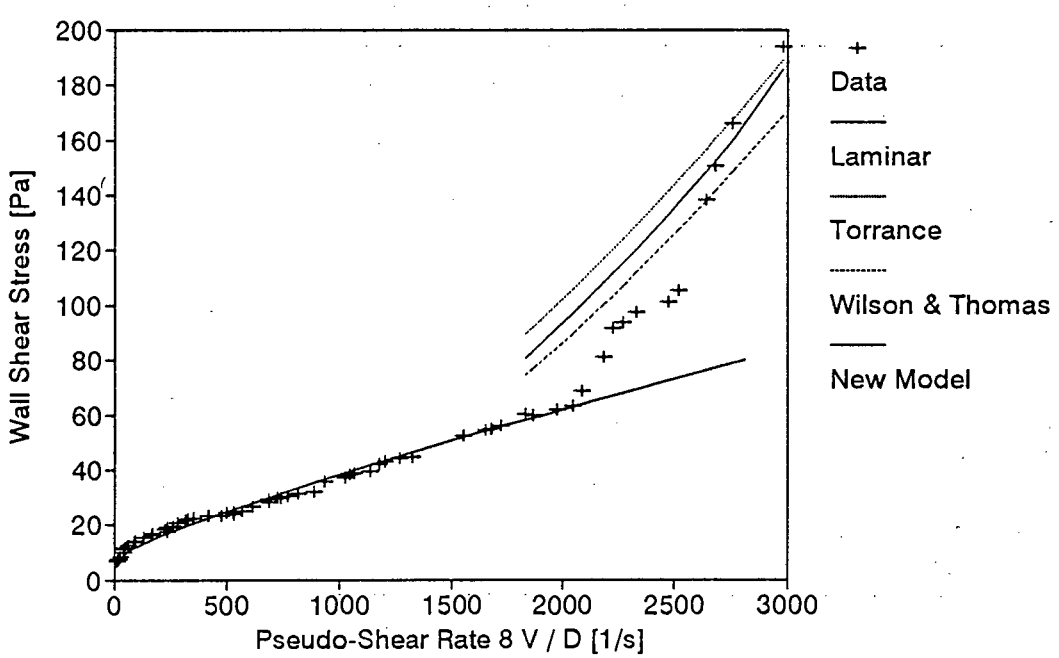

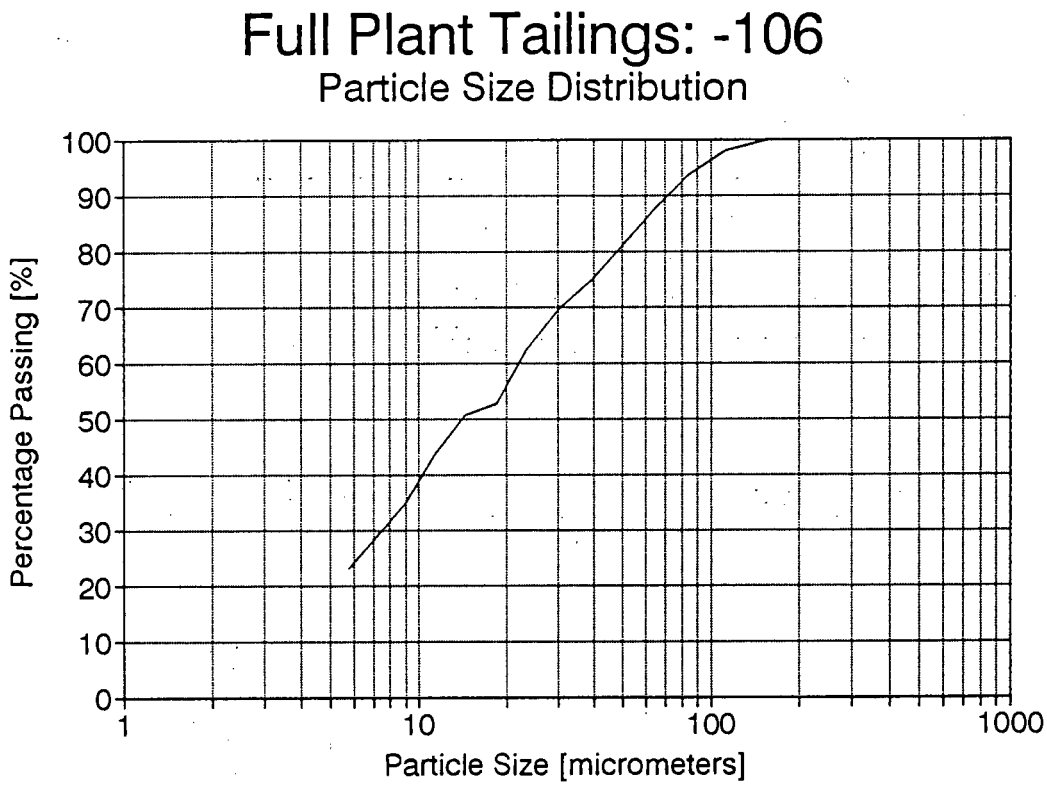
Full Plant Tailings: -106
Particle Size Distribution
Percentage Passing [%]
100
90
80
70
60
50
40
30
20
10
0
1
10
100
1000
Particle Size [micrometers]

DATA FROM TEST	FBBL-100
APPARATUS	
Facility	BBTV
Diameter	28 mm
Material	Full Plant Filt. Tailing
Operator	RIGN
Supervisor	PTS

SLURRY PROPERTIES	
Solids Relative Density	2,7468
Slurry Relative Density	1,5507
Volumetric Concentration	31,5 %
Yield Stress	5,0 Pa
Fluid Consistency Index	0,0269 Pa s ^ n
Flow Behaviour Index	0,8955
Representative Particle size	58 um

TURBULENT MODEL PERFORMANCE		
Model	Avg Err%	Avg LSE
Torrance	7,93	0,0136
Wilson and Thomas	5,62	0,0079
New Model	3,92	0,0076

Pseudo-Shear Diagram:FBBL-100

Sm = 1,5507 : Diam = 28mm

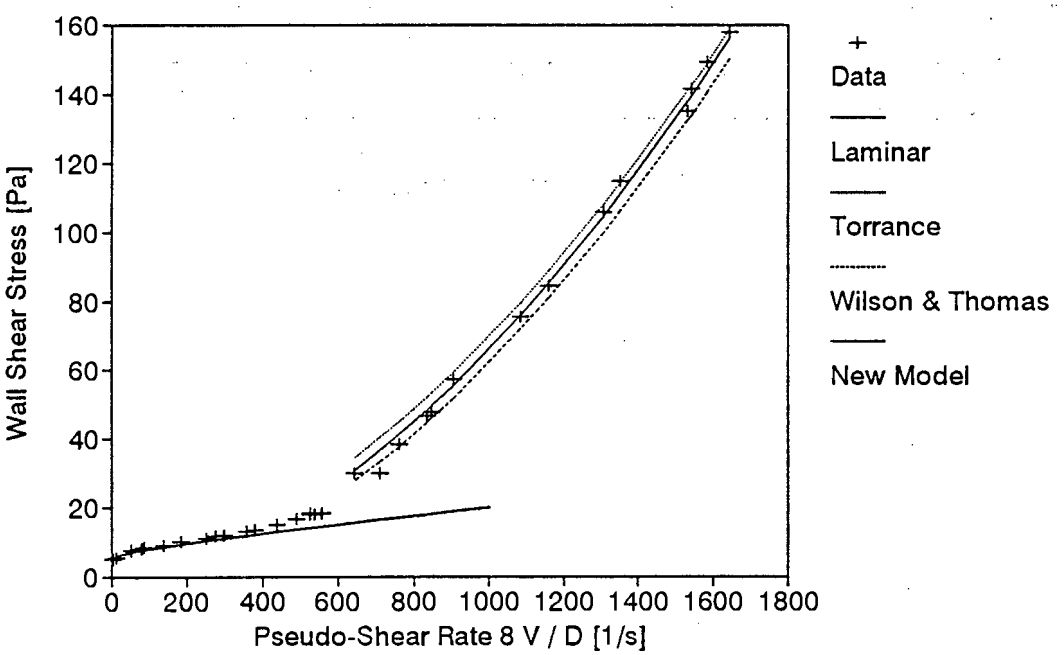

DATA FROM TEST	FBBM-100
APPARATUS	
Facility	BBTV
Diameter	13 mm
Material	Full Plant Filt. Tailing
Operator	RIGN
Supervisor	PTS

SLURRY PROPERTIES	
Solids Relative Density	2,7468
Slurry Relative Density	1,5507
Volumetric Concentration	31,5 %
Yield Stress	5,0 Pa
Fluid Consistency Index	0,0269 Pa s ^ n
Flow Behaviour Index	0,8955
Representative Particle size	58 um

TURBULENT MODEL PERFORMANCE		
Model	Avg Err%	Avg LSE
Torrance	9,60	0,0136
Wilson and Thomas	3,52	0,0059
New Model	6,04	0,0093

Pseudo-Shear Diagram:FBBM-100

Sm = 1,5507 : Diam = 13mm

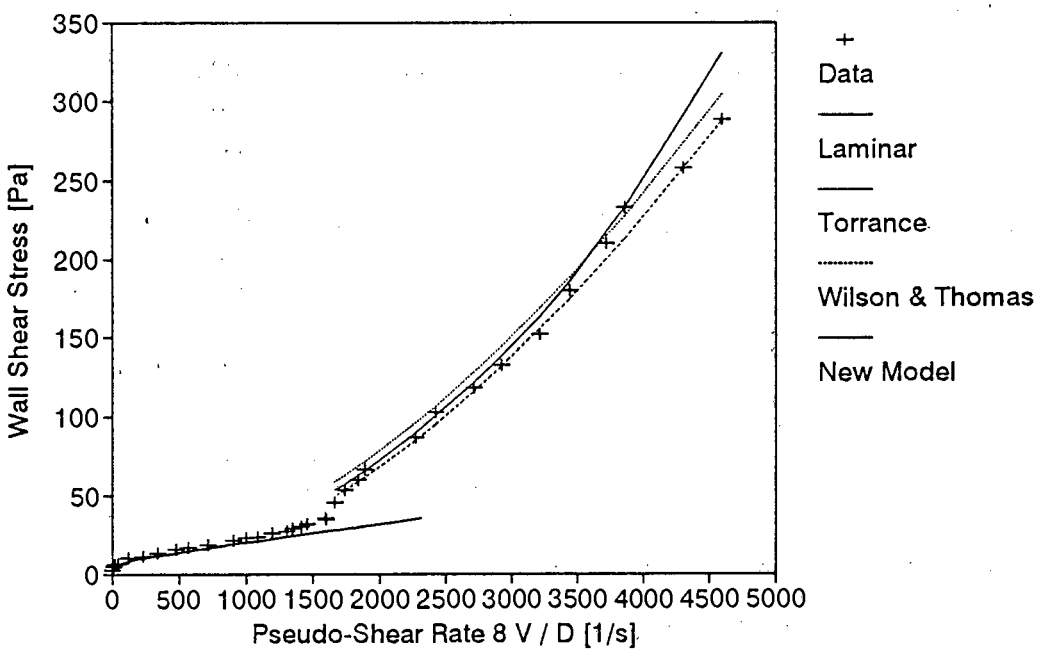

DATA FROM TEST	FBBS-100
APPARATUS	
Facility	BBTV
Diameter	4 mm
Material	Full plant Filt. tailings
Operator	RIGN
Supervisor	PTS

SLURRY PROPERTIES	
Solids Relative Density	2,7468
Slurry Relative Density	1,5507
Volumetric Concentration	31,5 %
Yield Stress	5,0 Pa
Fluid Consistency Index	0,0269 Pa s ^ n
Flow Behaviour Index	0,8955
Representative Particle size	58 um

TURBULENT MODEL PERFORMANCE		
Model	Avg Err%	Avg LSE
Torrance	19,99	0,0342
Wilson and Thomas	7,78	0,0166
New Model	24,27	0,0387

Pseudo-Shear Diagram:FBBS-100

Sm = 1,5507 : Diam = 4mm

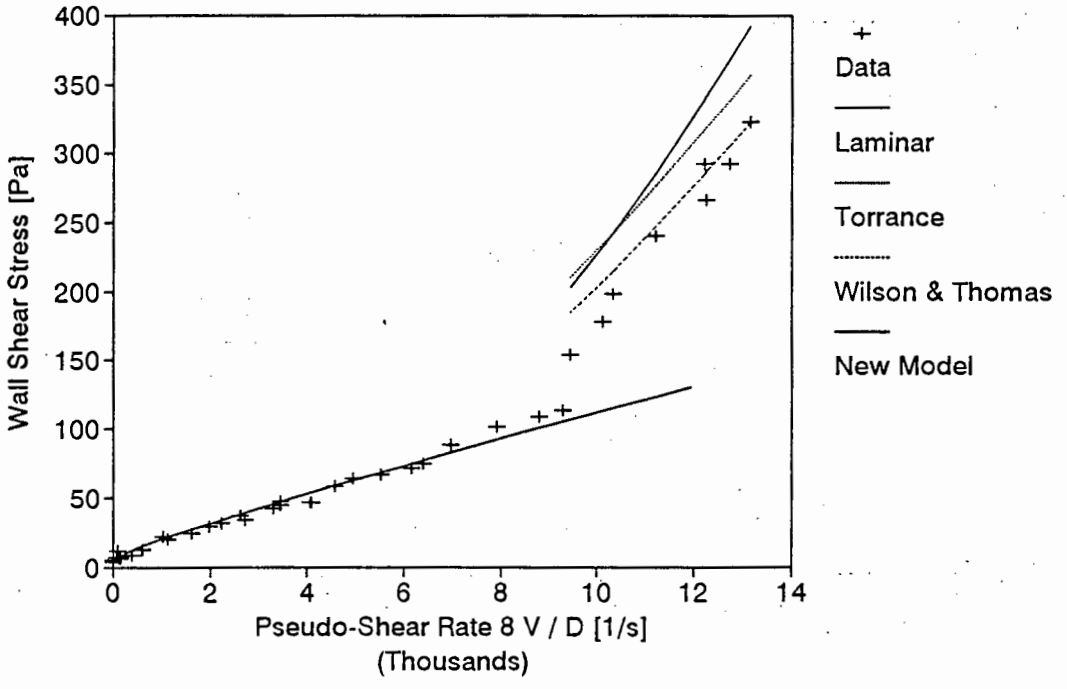

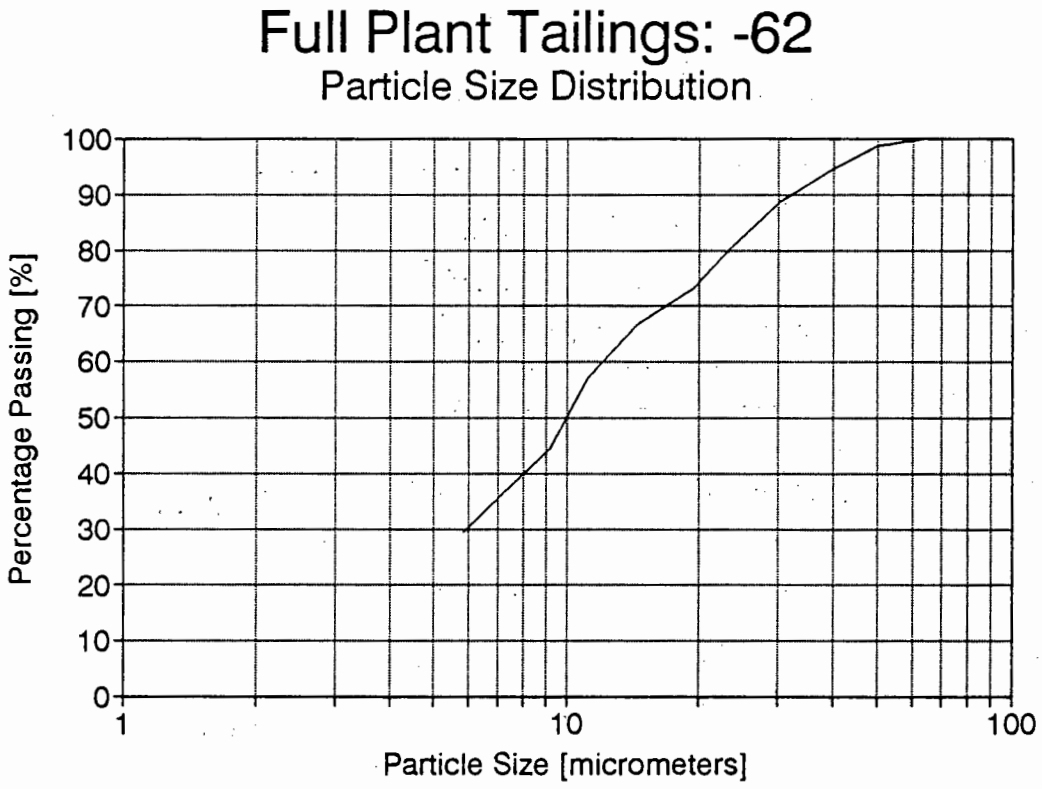
Full Plant Tailings: -62
Particle Size Distribution
Percentage Passing [%]
100
90
80
70
60
50
40
30
20
10
0
1
10
100
Particle Size [micrometers]

DATA FROM TEST	FBBL-62
APPARATUS	
Facility	BBTV
Diameter	28 mm
Material	Full Plant Filt. Tailing
Operator	RIGN
Supervisor	PTS

SLURRY PROPERTIES	
Solids Relative Density	2,7566
Slurry Relative Density	1,5144
Volumetric Concentration	29,3 %
Yield Stress	12,0 Pa
Fluid Consistency Index	0,0418 Pa s ^ n
Flow Behaviour Index	0,8902
Representative Particle size	27 um

TURBULENT MODEL PERFORMANCE		
Model	Avg Err%	Avg LSE
Torrance	26,08	0,0348
Wilson and Thomas	8,70	0,0131
New Model	14,83	0,0211

Pseudo-Shear Diagram:FBBL-62

Sm = 1,5144 : Diam = 28mm

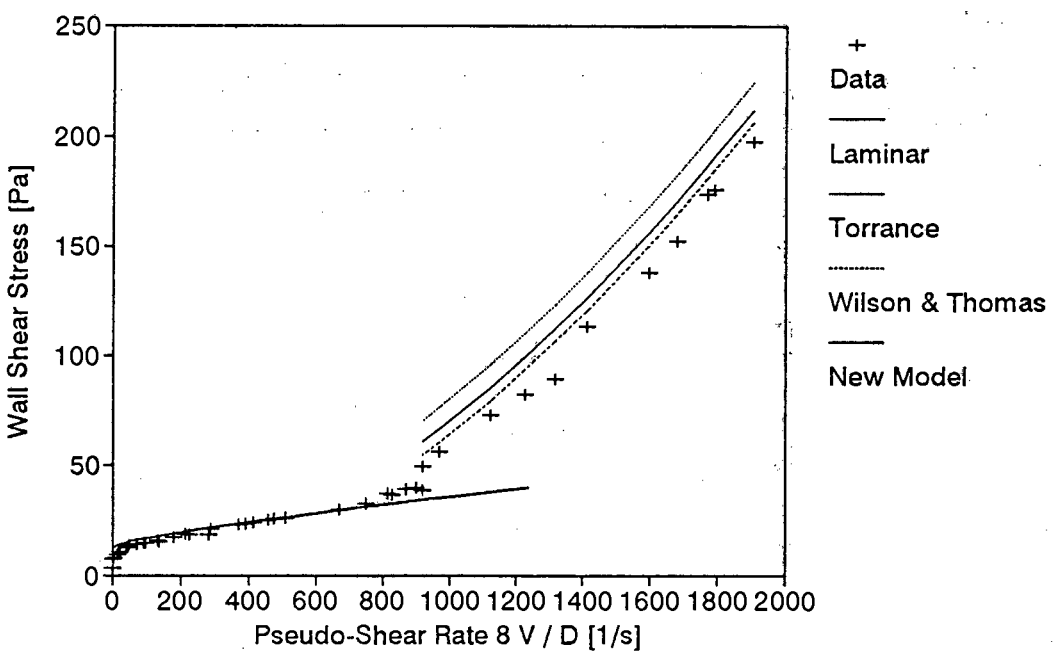

DATA FROM TEST	FBBM-62
APPARATUS	
Facility	BBTV
Diameter	13 mm
Material	Full Plant Filt. Tailing
Operator	RIGN
Supervisor	PTS

SLURRY PROPERTIES	
Solids Relative Density	2,7566
Slurry Relative Density	1,5144
Volumetric Concentration	29,3 %
Yield Stress	12,0 Pa
Fluid Consistency Index	0,0418 Pa s ^ n
Flow Behaviour Index	0,8902
Representative Particle size	27 um

TURBULENT MODEL PERFORMANCE		
Model	Avg Err%	Avg LSE
Torrance	22,69	0,0298
Wilson and Thomas	9,09	0,0147
New Model	12,80	0,0190

Pseudo-Shear Diagram:FBBM-62

Sm = 1,5144 : Diam = 13mm

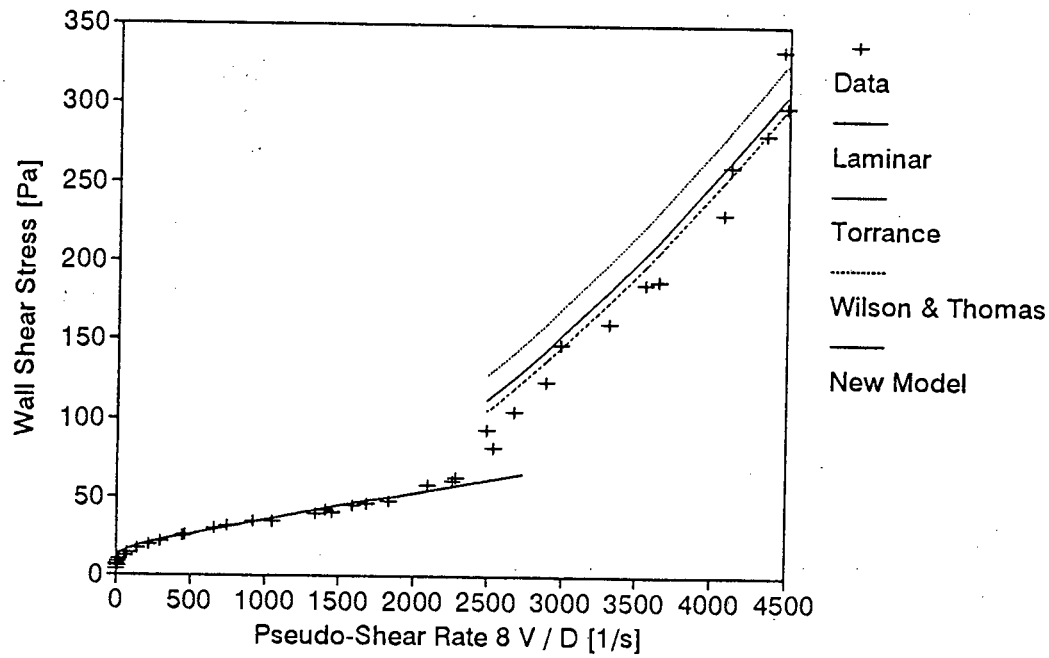

DATA FROM TEST	FBBS-62
APPARATUS	
Facility	BBTV
Diameter	4 mm
Material	Full Plant Filt. Tailing
Operator	RIGN
Supervisor	PTS

SLURRY PROPERTIES	
Solids Relative Density	2,7566
Slurry Relative Density	1,5144
Volumetric Concentration	29,3 %
Yield Stress	12,0 Pa
Fluid Consistency Index	0,0418 Pa s ^ n
Flow Behaviour Index	0,8902
Representative Particle size	27 um

TURBULENT MODEL PERFORMANCE		
Model	Avg Err%	Avg LSE
Torrance	74,39	0,1625
Wilson and Thomas	51,35	0,1225
New Model	57,21	0,1331

Pseudo-Shear Diagram:FBBS-62

Sm = 1,5144 : Diam = 4mm

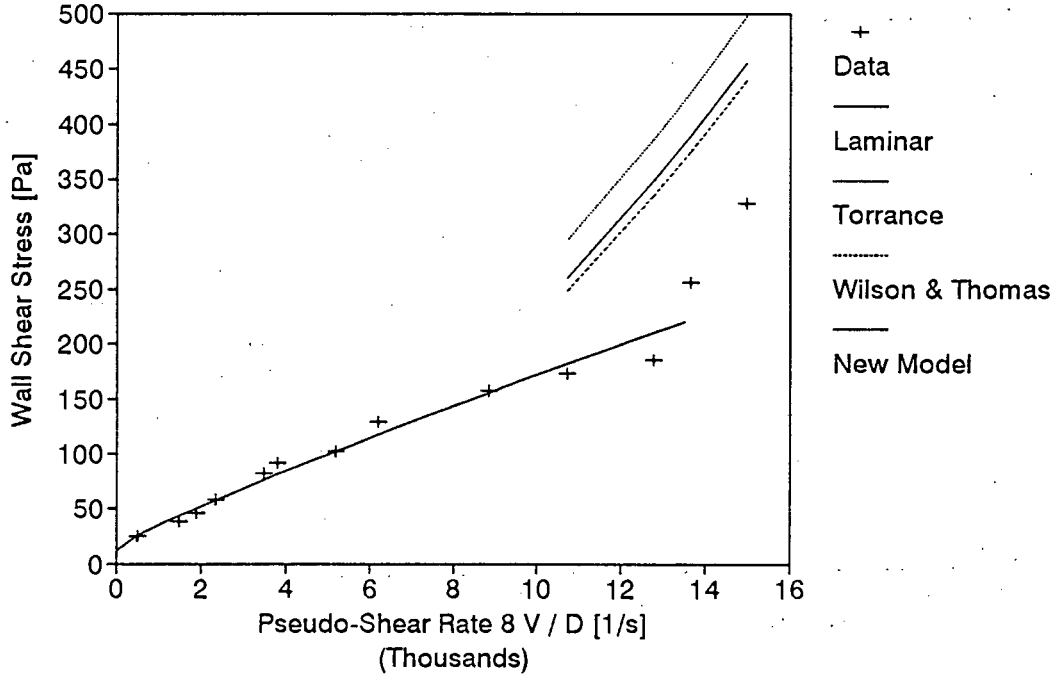

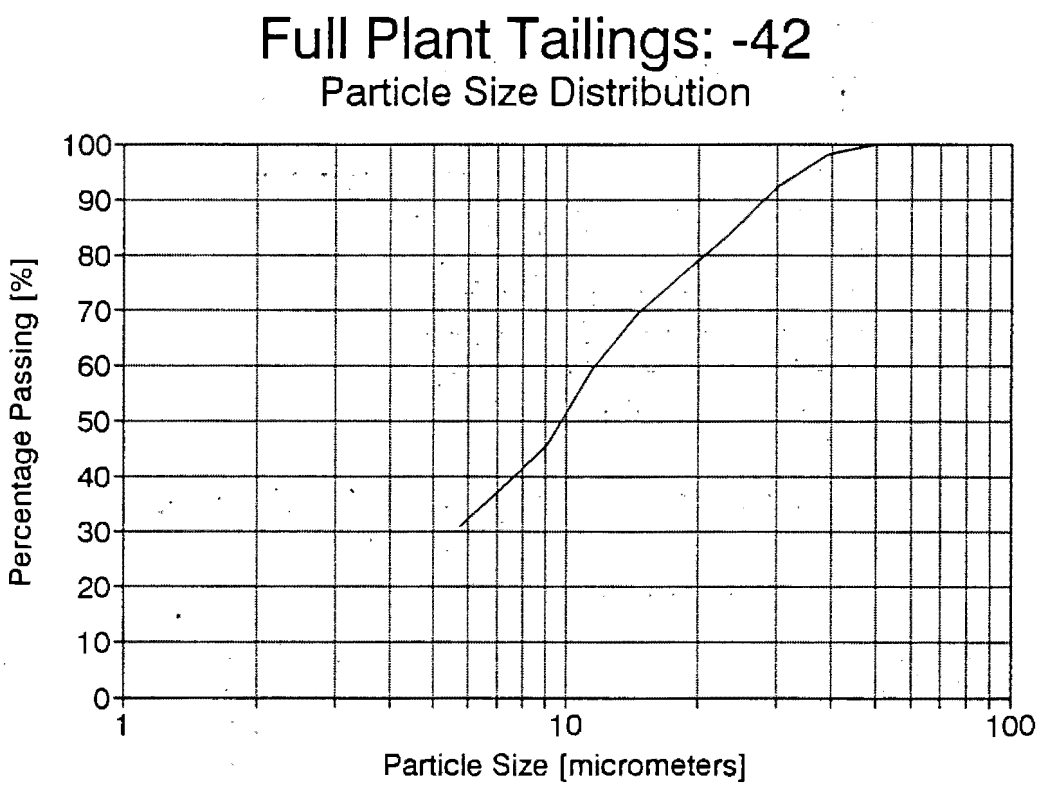
Full Plant Tailings: -42
Particle Size Distribution
Percentage Passing [%]
100
90
80
70
60
50
40
30
20
10
0
1
10
100
Particle Size [micrometers]

DATA FROM TEST	FBBL-42
APPARATUS	
Facility	BBTV
Diameter	28 mm
Material	Full Plant Filt. Tailing
Operator	RIGN
Supervisor	PTS

SLURRY PROPERTIES	
Solids Relative Density	2,7733
Slurry Relative Density	1,5013
Volumetric Concentration	28,3 %
Yield Stress	8,0 Pa
Fluid Consistency Index	0,0371 Pa s ^ n
Flow Behaviour Index	0,8791
Representative Particle size	24 um

TURBULENT MODEL PERFORMANCE		
Model	Avg Err%	Avg LSE
Torrance	7,92	0,0113
Wilson and Thomas	4,98	0,0071
New Model	3,75	0,0056

Pseudo-Shear Diagram:FBBL-42

Sm = 1,5013 : Diam = 28mm

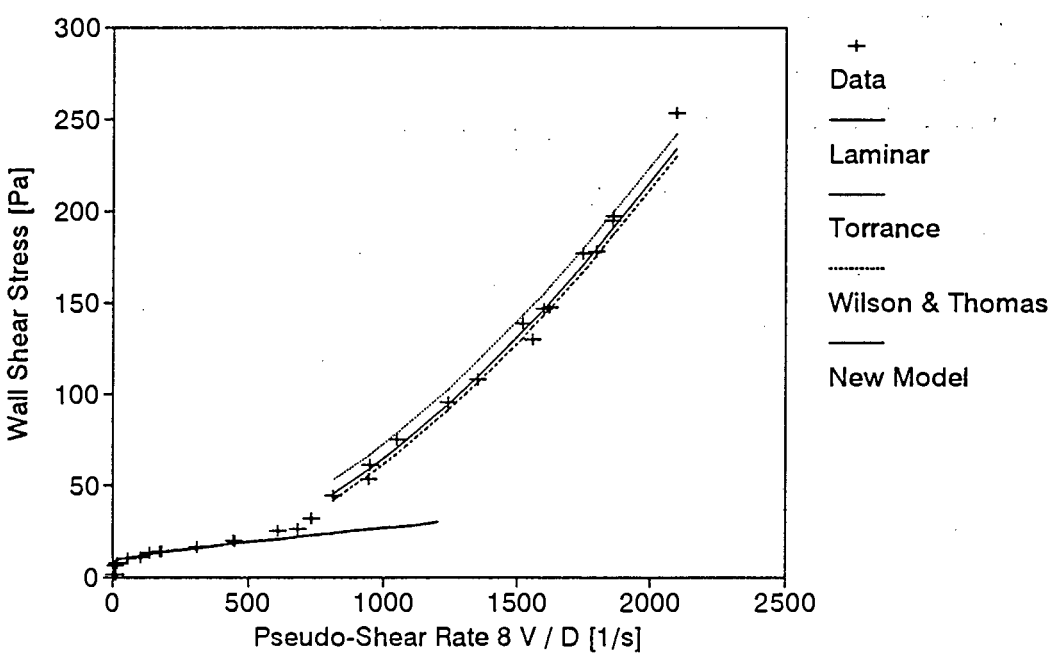

DATA FROM TEST	FBBM-42
APPARATUS	
Facility	BBTV
Diameter	13 mm
Material	Full Plant Filt. Tailing
Operator	RIGN
Supervisor	PTS

SLURRY PROPERTIES	
Solids Relative Density	2,7733
Slurry Relative Density	1,5013
Volumetric Concentration	28,3 %
Yield Stress	8,0 Pa
Fluid Consistency Index	0,0371 Pa s ^ n
Flow Behaviour Index	0,8791
Representative Particle size	24 um

TURBULENT MODEL PERFORMANCE		
Model	Avg Err%	Avg LSE
Torrance	10,10	0,0168
Wilson and Thomas	8,03	0,0116
New Model	7,34	0,0113

Pseudo-Shear Diagram:FBBM-42

Sm = 1,5013 : Diam = 13mm

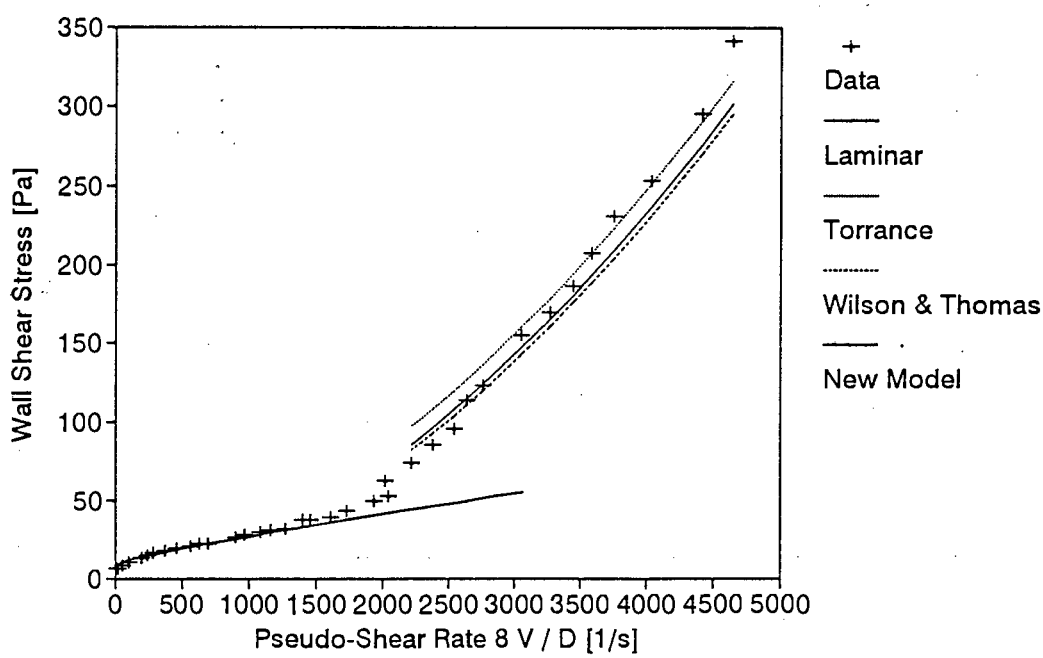

DATA FROM TEST	FBBS-42
APPARATUS	
Facility	BBTV
Diameter	4 mm
Material	Full Plant Filt. Tailing
Operator	RIGN
Supervisor	PTS

SLURRY PROPERTIES	
Solids Relative Density	2,7733
Slurry Relative Density	1,5013
Volumetric Concentration	28,3 %
Yield Stress	8,0 Pa
Fluid Consistency Index	0,0371 Pa s ^ n
Flow Behaviour Index	0,8791
Representative Particle size	24 um

TURBULENT MODEL PERFORMANCE		
Model	Avg Err%	Avg LSE
Torrance	47,03	0,0611
Wilson and Thomas	29,07	0,0425
New Model	33,46	0,0471

Pseudo-Shear Diagram:FBBS-42

Sm = 1,5013 : Diam = 4mm

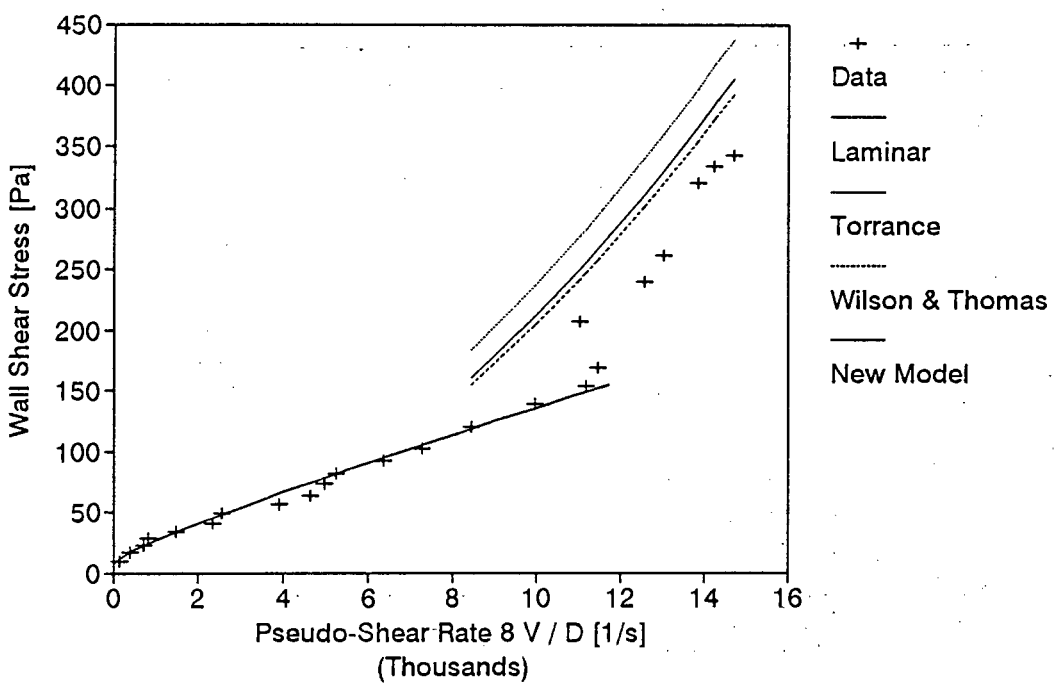

A.6 DETAILED PIPE TEST RESULTS II

The detailed pipe test results are presented in this section.

The rheology for each test was obtained from the correlation of the BBTV kaolin test results.

Kaolin : 2704

Particle Size Distribution

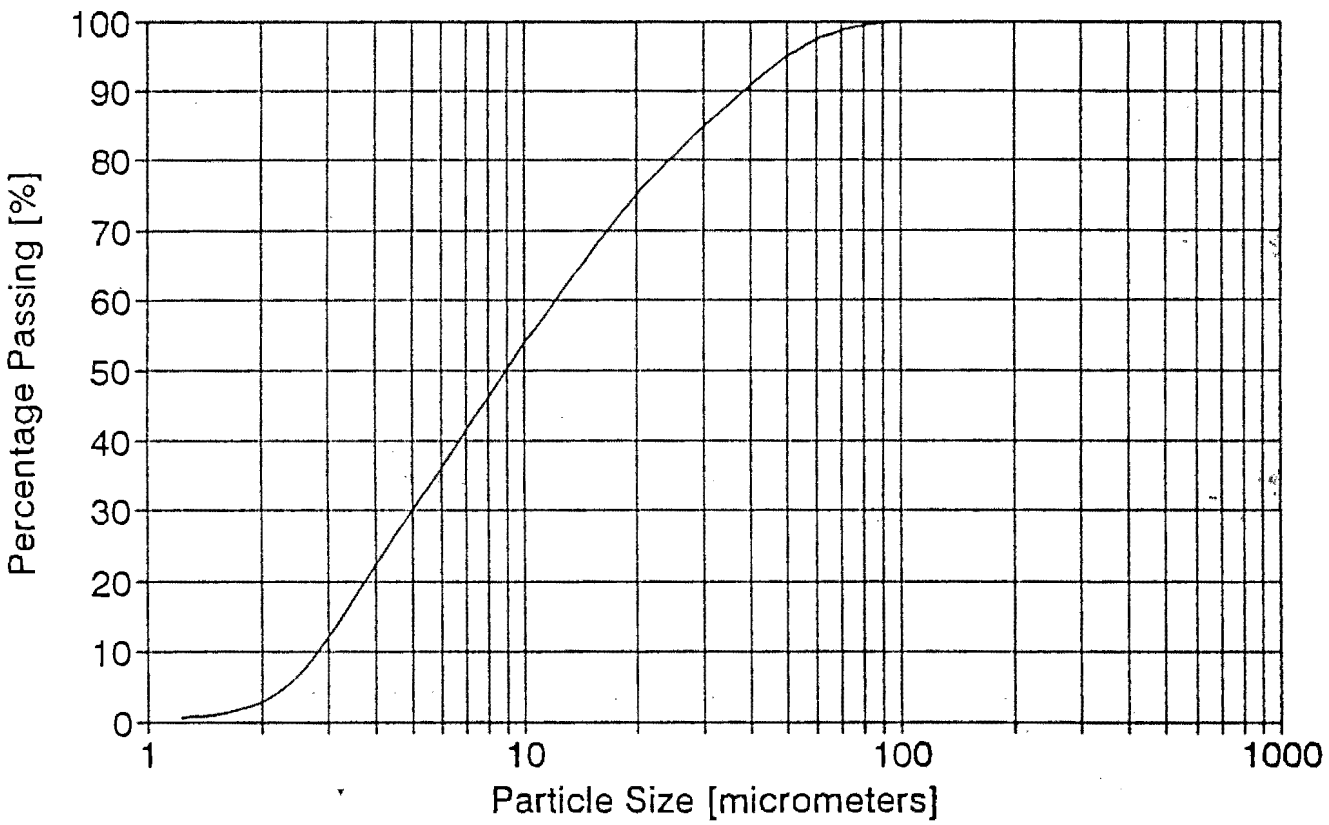

DATA FROM TEST	KERM1501
APPARATUS	
Facility	East Rig
Diameter	141 mm
Material	Kaolin
Operator	PTS
Supervisor	PTS

SLURRY PROPERTIES	
Solids Relative Density	2,4449
Slurry Relative Density	1,0488
Volumetric Concentration	3,4 %
Yield Stress	1,070 Pa
Fluid Consistency Index	0,0452 Pa s ^ n
Flow Behaviour Index	0,5890
Representative Particle size	32 um

TURBULENT MODEL PERFORMANCE		
Model	Avg %	Avg LSE
Torrance	13,33	0,0371
Wilson and Thomas	17,64	0,0338
New Model	5,34	0,0091

Pseudo-Shear Diagram: KERM1501

Sm = 1,0488 : Diam = 141 mm

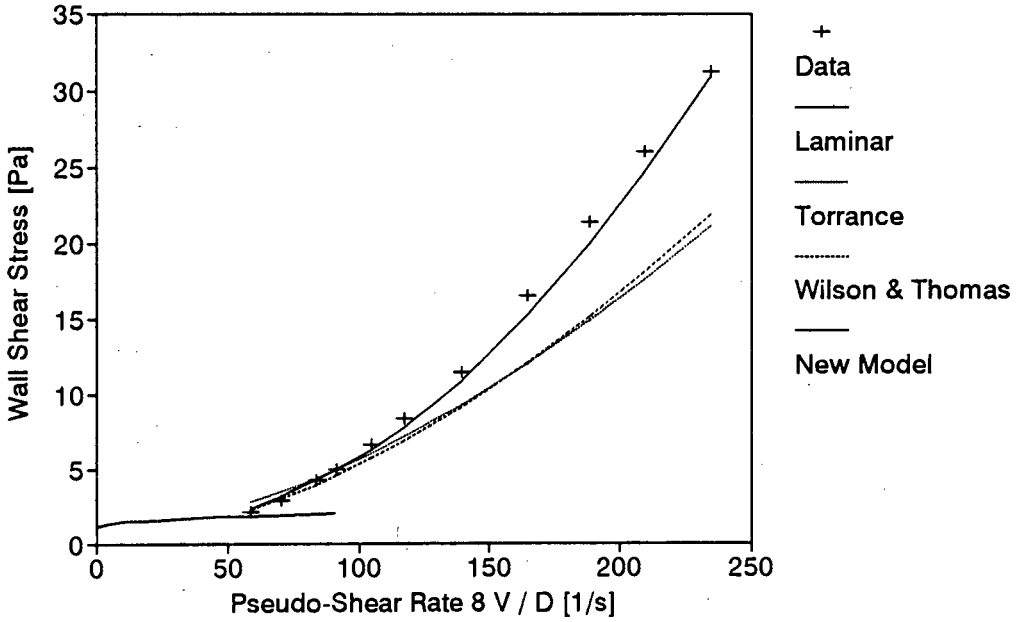

DATA FROM TEST	KERM1502
APPARATUS	
Facility	East Rig
Diameter	141 mm
Material	Kaolin
Operator	PTS
Supervisor	PTS

SLURRY PROPERTIES	
Solids Relative Density	2,4449
Slurry Relative Density	1,0306
Volumetric Concentration	2,1 %
Yield Stress	0,610 Pa
Fluid Consistency Index	0,0149 Pa s ^ n
Flow Behaviour Index	0,6840
Representative Particle size	32 um

TURBULENT MODEL PERFORMANCE		
Model	Avg %	Avg LSE
Torrance	13,33	0,0348
Wilson and Thomas	20,35	0,0351
New Model	5,67	0,0102

Pseudo-Shear Diagram: KERM1502

Sm = 1,0306 : Diam = 141 mm

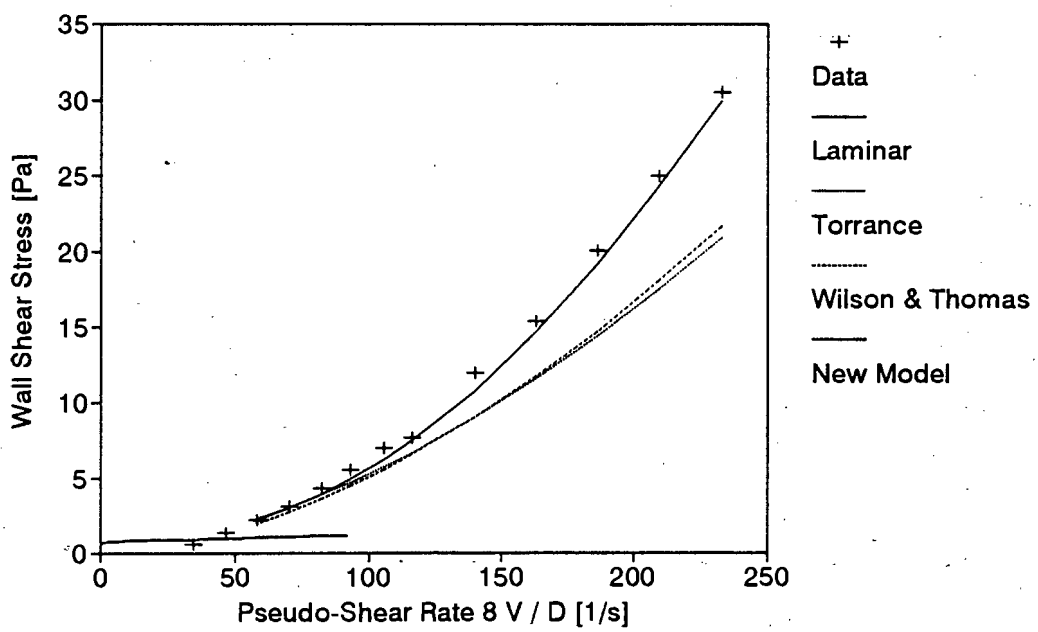

DATA FROM TEST	KERM1503
APPARATUS	
Facility	East Rig
Diameter	141 mm
Material	Kaolin
Operator	PTS
Supervisor	PTS

SLURRY PROPERTIES	
Solids Relative Density	2,4449
Slurry Relative Density	1,0617
Volumetric Concentration	4,3 %
Yield Stress	1,583 Pa
Fluid Consistency Index	0,0841 Pa s ^ n
Flow Behaviour Index	0,5455
Representative Particle size	32 um

TURBULENT MODEL PERFORMANCE		
Model	Avg %	Avg LSE
Torrance	13,33	0,0428
Wilson and Thomas	20,42	0,0402
New Model	9,22	0,0200

Pseudo-Shear Diagram: KERM1503

Sm = 1,0617 : Diam = 141 mm

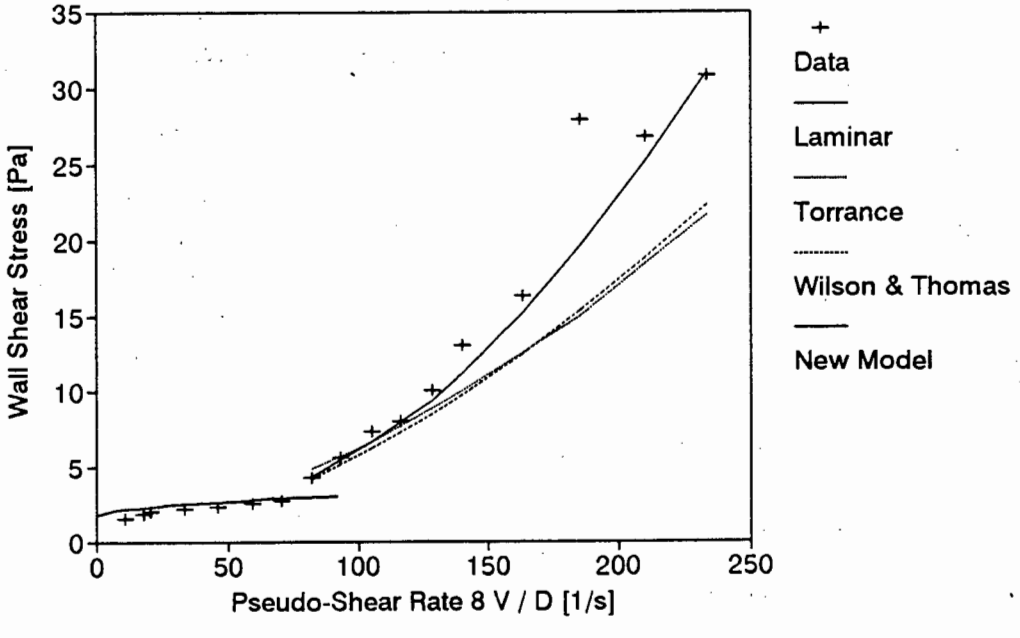

DATA FROM TEST	KERM1504
APPARATUS	
Facility	East Rig
Diameter	141 mm
Material	Kaolin
Operator	PTS
Supervisor	PTS

SLURRY PROPERTIES	
Solids Relative Density	2,4449
Slurry Relative Density	1,0853
Volumetric Concentration	5,9 %
Yield Stress	3,070 Pa
Fluid Consistency Index	0,1943 Pa s ^ n
Flow Behaviour Index	0,4994
Representative Particle size	32 um

TURBULENT MODEL PERFORMANCE		
Model	Avg %	Avg LSE
Torrance	13,33	0,0387
Wilson and Thomas	14,11	0,0345
New Model	7,40	0,0167

Pseudo-Shear Diagram: KERM1504

Sm = 1,0853 : Diam = 141 mm

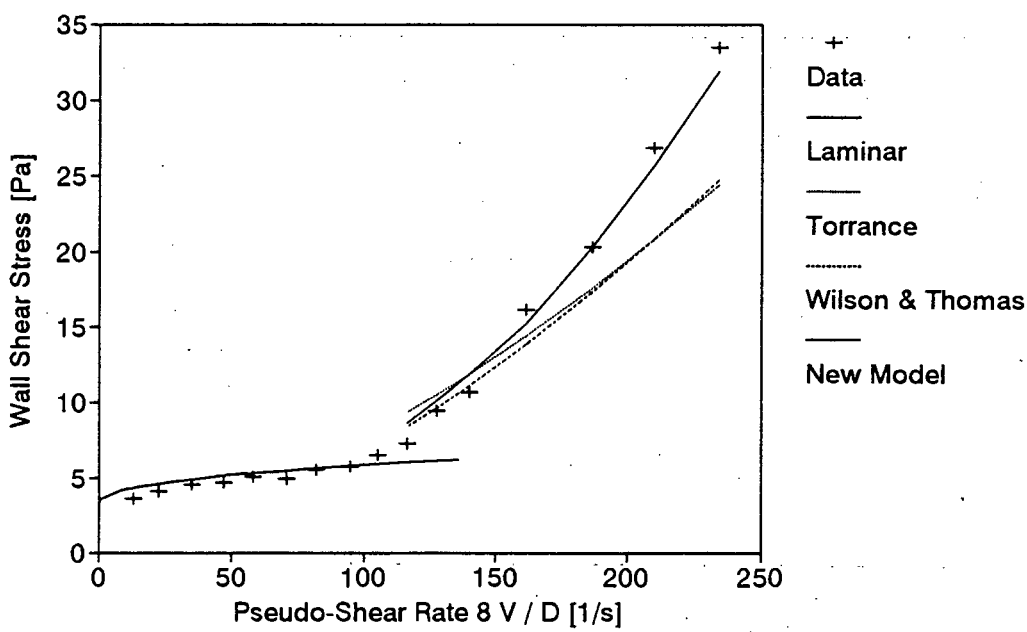

DATA FROM TEST	KERM1505
APPARATUS	
Facility	East Rig
Diameter	141 mm
Material	Kaolin
Operator	PTS
Supervisor	PTS

SLURRY PROPERTIES	
Solids Relative Density	2,4449
Slurry Relative Density	1,1128
Volumetric Concentration	7,8 %
Yield Stress	6,085 Pa
Fluid Consistency Index	0,3511 Pa s ^ n
Flow Behaviour Index	0,4809
Representative Particle size	32 um

TURBULENT MODEL PERFORMANCE		
Model	Avg %	Avg LSE
Torrance	13,33	0,0250
Wilson and Thomas	6,24	0,0233
New Model	2,92	0,0075

Pseudo-Shear Diagram: KERM1505

Sm = 1,1128 : Diam = 141 mm

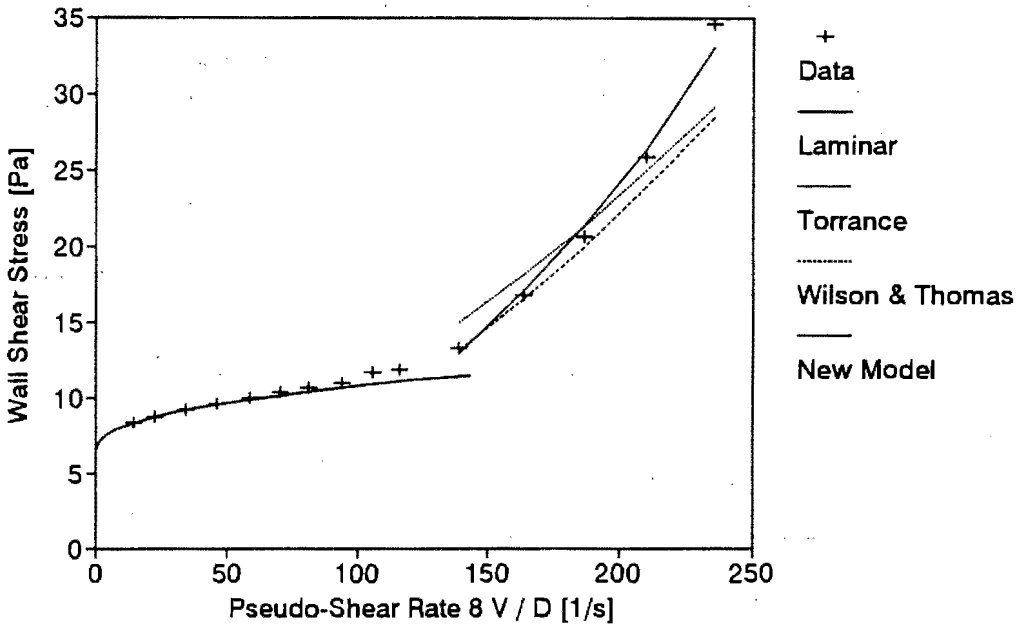

DATA FROM TEST	KERM1506
APPARATUS	
Facility	East Rig
Diameter	141 mm
Material	Kaolin
Operator	PTS
Supervisor	PTS

SLURRY PROPERTIES	
Solids Relative Density	2,4449
Slurry Relative Density	1,0690
Volumetric Concentration	4,8 %
Yield Stress	1,959 Pa
Fluid Consistency Index	0,1133 Pa s ^ n
Flow Behaviour Index	0,5273
Representative Particle size	32 um

TURBULENT MODEL PERFORMANCE		
Model	Avg %	Avg LSE
Torrance	13,33	0,0525
Wilson and Thomas	20,14	0,0499
New Model	6,77	0,0150

Pseudo-Shear Diagram: KERM1506

Sm = 1,0690 : Diam = 141 mm

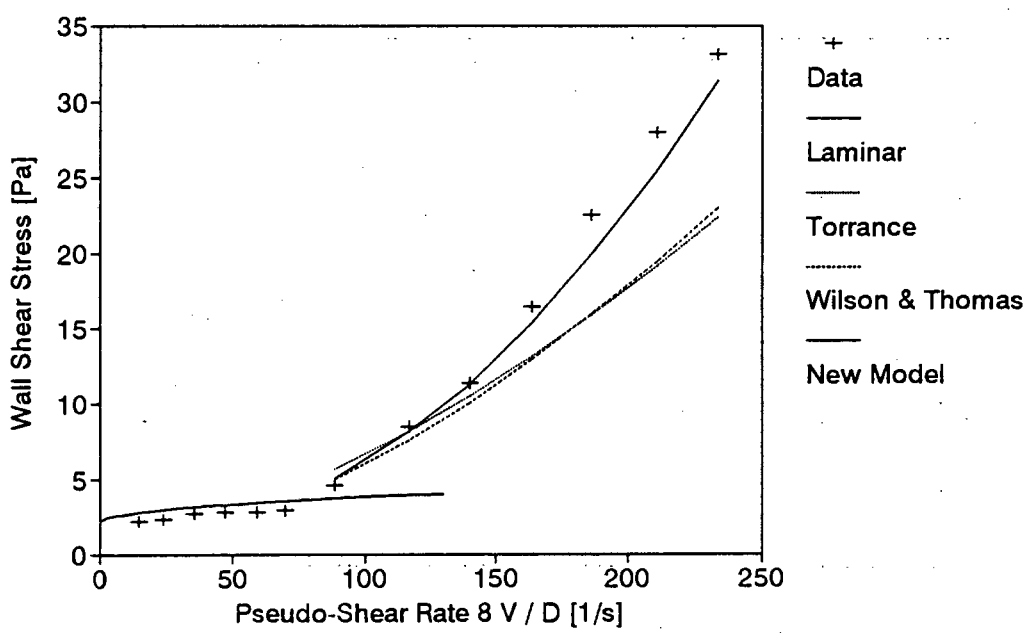

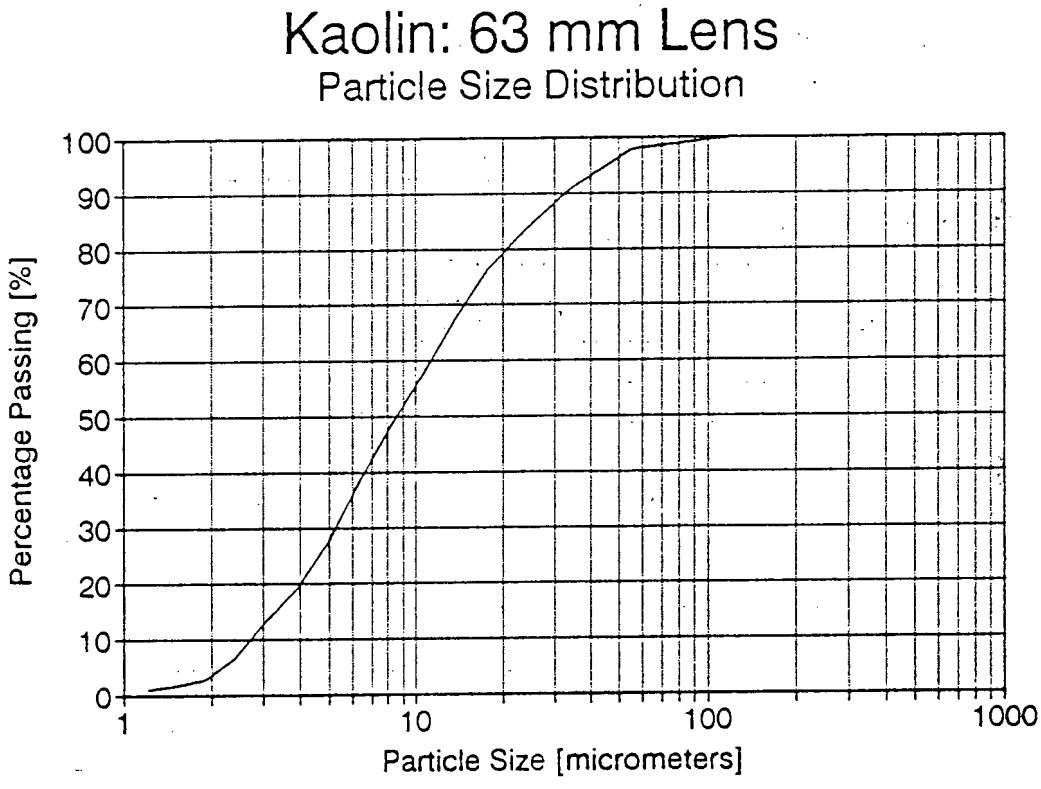
Kaolin: 63 mm Lens
Particle Size Distribution
Percentage Passing [%]
100
90
80
70
60
50
40
30
20
10
0
1
10
100
1000
Particle Size [micrometers]

DATA FROM TEST	KPIPE1
APPARATUS	
Facility	East Rig
Diameter	80 mm
Material	Kaolin
Operator	AWS
Supervisor	AWS

SLURRY PROPERTIES	
Solids Relative Density	2,440
Slurry Relative Density	1,0793
Volumetric Concentration	5,5 %
Yield Stress	2,634 Pa
Fluid Consistency Index	0,1639 Pa s^n
Flow Behaviour Index	0,5074
Representative Particle size	26 um

TURBULENT MODEL PERFORMANCE		
Model	Avg Err%	Avg LSE
Torrance	29,44	0,0630
Wilson and Thomas	28,69	0,0600
New Model	6,89	0,0186

Pseudo-Shear Diagram: KPIPE1

Sm = 1,0793 : Diam = 80 mm

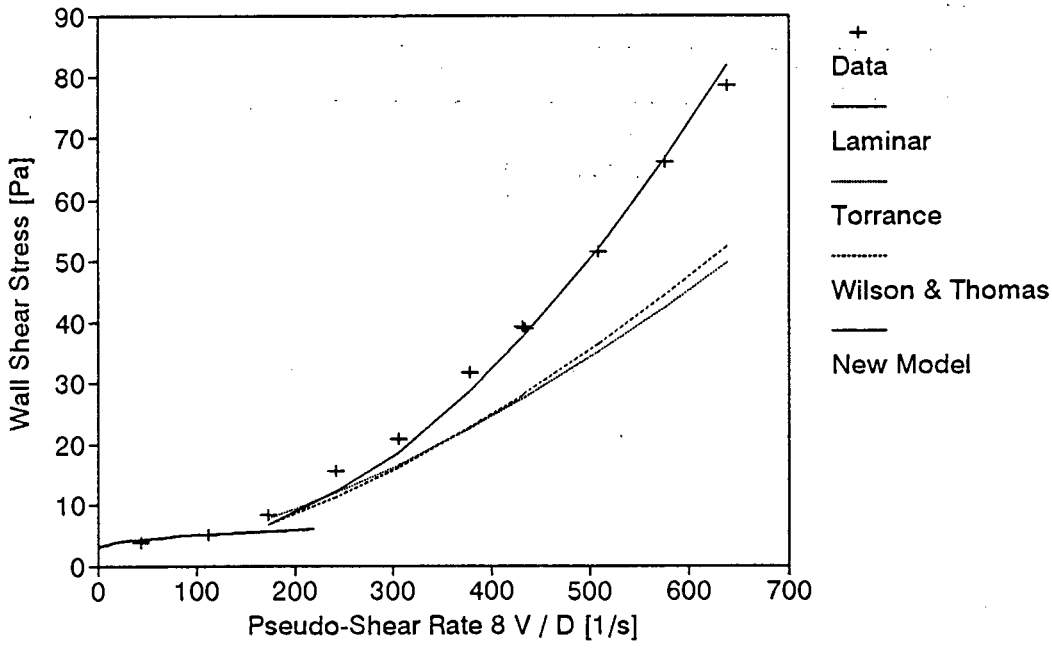

DATA FROM TEST	KPIPE2
APPARATUS	
Facility	East Rig
Diameter	80 mm
Material	Kaolin
Operator	AWS
Supervisor	AWS

SLURRY PROPERTIES	
Solids Relative Density	2,440
Slurry Relative Density	1,0803
Volumetric Concentration	5,6 %
Yield Stress	2,706 Pa
Fluid Consistency Index	0,1690 Pa s ^ n
Flow Behaviour Index	0,5058
Representative Particle size	26 um

TURBULENT MODEL PERFORMANCE		
Model	Avg Err%	Avg LSE
Torrance	25,39	0,0596
Wilson and Thomas	23,18	0,0543
New Model	3,22	0,0069

Pseudo-Shear Diagram: KPIPE2

Sm = 1,0803 : Diam = 80 mm

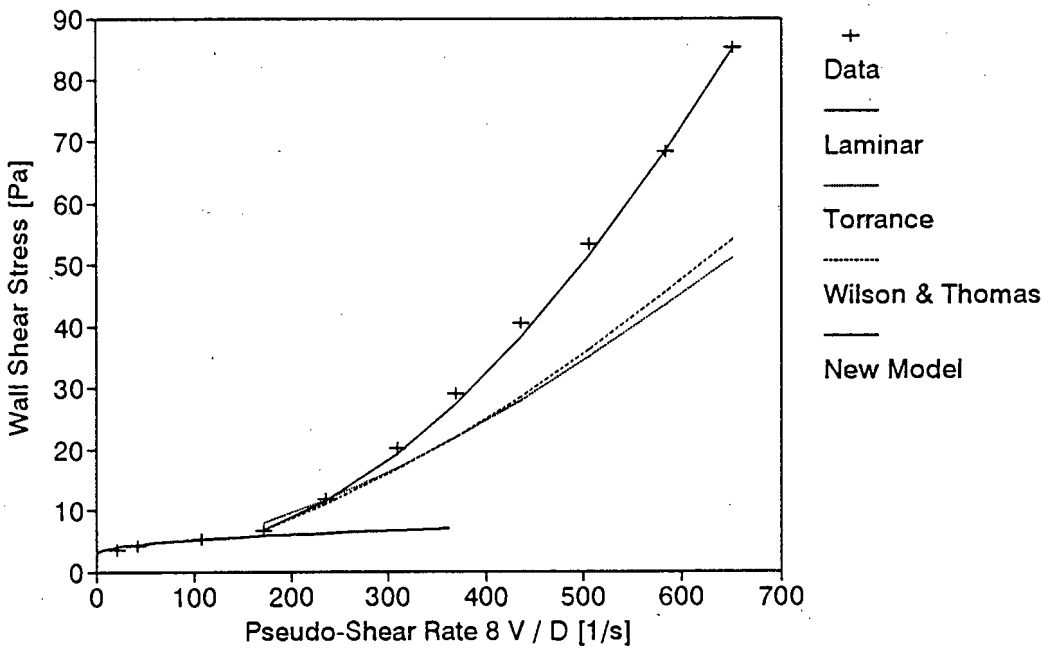

DATA FROM TEST	KPIPE3
APPARATUS	
Facility	East Rig
Diameter	139 mm
Material	Kaolin
Operator	AWS
Supervisor	AWS

SLURRY PROPERTIES	
Solids Relative Density	2,440
Slurry Relative Density	1,0748
Volumetric Concentration	5,2 %
Yield Stress	2,323 Pa
Fluid Consistency Index	0,1410 Pa s ^ n
Flow Behaviour Index	0,5151
Representative Particle size	26 um

TURBULENT MODEL PERFORMANCE		
Model	Avg Err%	Avg LSE
Torrance	23,12	0,0387
Wilson and Thomas	19,59	0,0337
New Model	3,79	0,0071

Pseudo-Shear Diagram: KPIPE3

Sm = 1,0748 : Diam = 139 mm

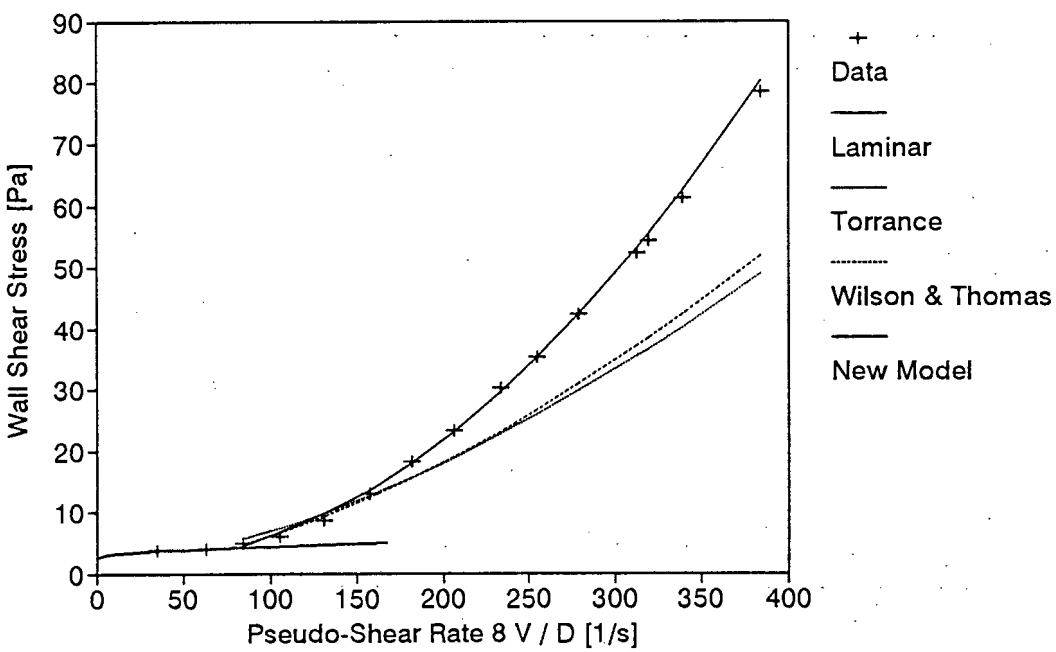

DATA FROM TEST	KPIPE4
APPARATUS	
Facility	East Rig
Diameter	139 mm
Material	Kaolin
Operator	AWS
Supervisor	AWS

SLURRY PROPERTIES	
Solids Relative Density	2,440
Slurry Relative Density	1,1160
Volumetric Concentration	8,1 %
Yield Stress	6,606 Pa
Fluid Consistency Index	0,3703 Pa s ^ n
Flow Behaviour Index	0,4804
Representative Particle size	26 um

TURBULENT MODEL PERFORMANCE		
Model	Avg Err%	Avg LSE
Torrance	15,64	0,0279
Wilson and Thomas	11,07	0,0235
New Model	3,24	0,0061

Pseudo-Shear Diagram: KPIPE4

Sm = 1,1160 : Diam = 139 mm

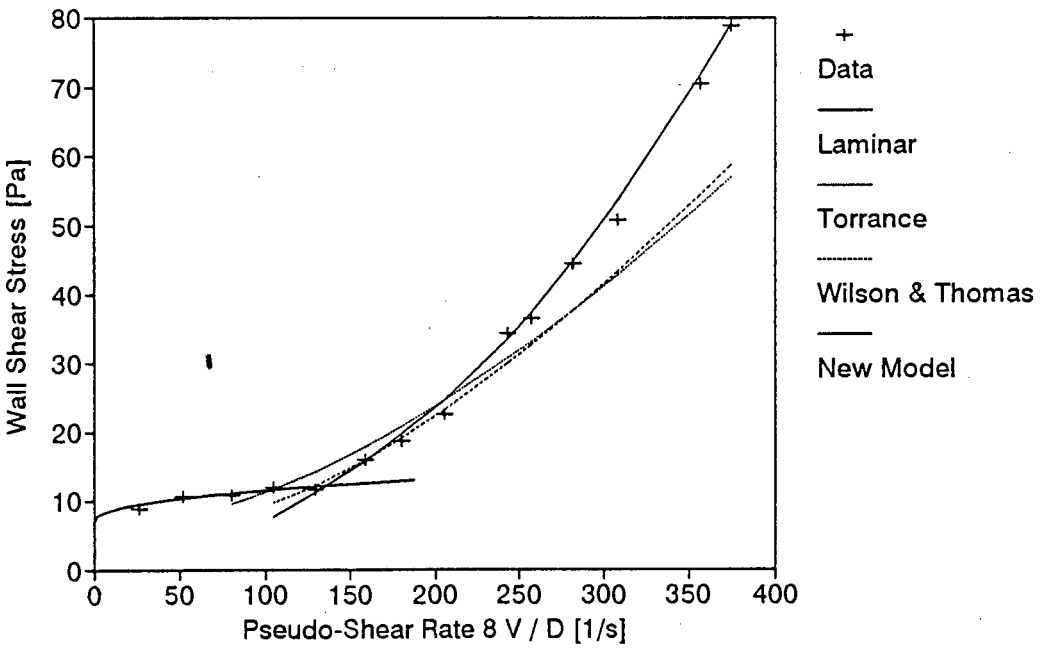

A.7 TESTS FROM THE LITERATURE

Two tests from the literature have been used (Xu *etal*, 1993 and Park *et al*, 1989). The rheology was obtained from the published data using the approach of Lazarus & Slatter (1988).

DATA FROM TEST	PARK1
APPARATUS	
Facility	Pipe Loop
Diameter	50,6 mm
Material	Hi Sil T-600 silica
Operator	}Park et al,
Supervisor	}1989

SLURRY PROPERTIES	
Solids Relative Density	1,3640
Slurry Relative Density	0,8310
Volumetric Concentration	3,4 %
Yield Stress	9,3 Pa
Fluid Consistency Index	0,0894 Pa s ^ n
Flow Behaviour Index	0,7254
Representative Particle size	45 um

TURBULENT MODEL PERFORMANCE		
Model	Avg Err%	Avg LSE
Torrance	13,45	0,0327
Wilson and Thomas	10,93	0,0266
New Model	5,29	0,0138

Pseudo-Shear Diagram:PARK1

Sm = 0,8310 : Diam = 51mm

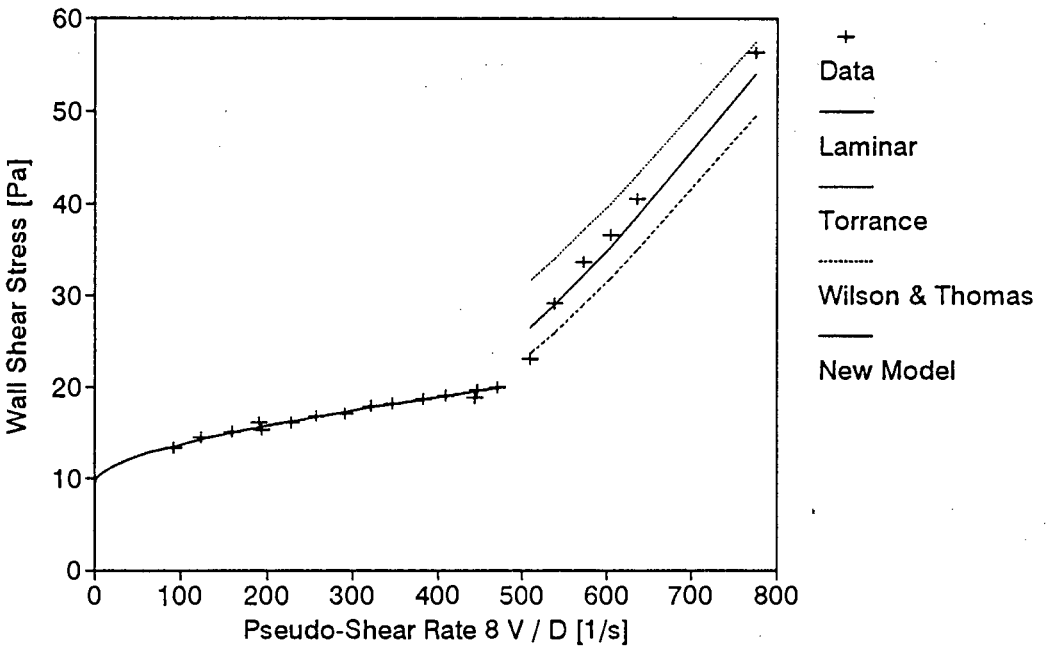

DATA FROM TEST	XU_17
APPARATUS	
Facility	Pipe Loop
Diameter	158 mm
Material	Kaolin
Operator	}Xu et al,
Supervisor	}1993

SLURRY PROPERTIES	
Solids Relative Density	2,4449
Slurry Relative Density	1,2456
Volumetric Concentration	17,0 %
Yield Stress	7,0 Pa
Fluid Consistency Index	0,2671 Pa s ^ n
Flow Behaviour Index	0,5880
Representative Particle size	22 um

TURBULENT MODEL PERFORMANCE		
Model	Avg Err%	Avg LSE
Torrance	17,56	0,0473
Wilson and Thomas	2,05	0,0078
New Model	5,44	0,0185

Pseudo-Shear Diagram:XU_17

Sm = 1,2456 : Diam = 158mm

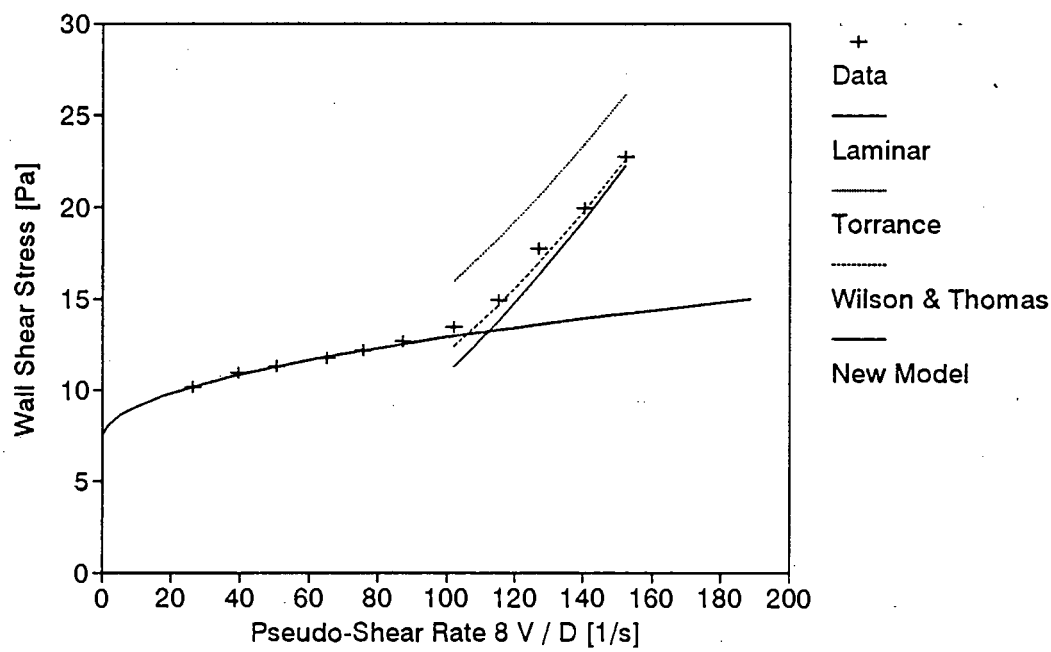

APPENDIX B

APPENDIX B

DIMENSIONAL ANALYSIS OF THE YIELD PSEUDOPLASTIC MODEL

The wall shear stress is a function of mixture density (ρ_m), mean velocity (V), pipe diameter (D), yield stress (τ_y), fluid consistency index (K) and flow behaviour index (n);

$$\tau_0 = \phi(\rho_m , V , D , \tau_y , K , n) \qquad \textbf{(B.1)}$$

Four dimensionless groups result (with appropriate constants from the literature):-

$$f = \frac{\tau_0}{\frac{1}{2} \rho_m V^2} \qquad \textit{(Fanning Friction Factor)} \qquad \textbf{(B.2)}$$

$$Y = \frac{\tau_y}{\rho_m V^2} \qquad \textit{(Yield Number)} \qquad \textbf{(B.3)}$$

$$Re_{nn} = \frac{8 \rho V^2}{K \left(\frac{8 V}{D}\right)^n} \qquad \textit{(Reynolds Number)} \qquad \textbf{(B.4)}$$

and **n** **(B.5)**

Eliminating V from equations B3 and B4 ;

$$He = \frac{D^2 \rho_m}{\tau_y} \left(\frac{\tau_y}{K} \right)^{\frac{2}{n}} \qquad \textit{(Hedström Number)} \qquad \textbf{(B.6)}$$

Therefore

$$f = \phi' \left(Re_{nn} , He , n \right) \qquad \textbf{(B.7)}$$

A Design Chart (Fig B 1) of friction factor vs Reynolds number with Hedström number as parameter can be plotted for each value of **n** using the equations from Chapter 2 in the main text. The equation of Torrance has been used to plot the turbulent flow line.

As can be seen, the transition from laminar to turbulent flow does not occur at a fixed value. Rather, a critical Reynolds number has to be determined for each design case.

This method tends to separate τ_y from the other rheological variables in the Reynolds number formulation and cannot be used to develop a simple, single transition criterion.

This design chart is only useful for laminar flow.

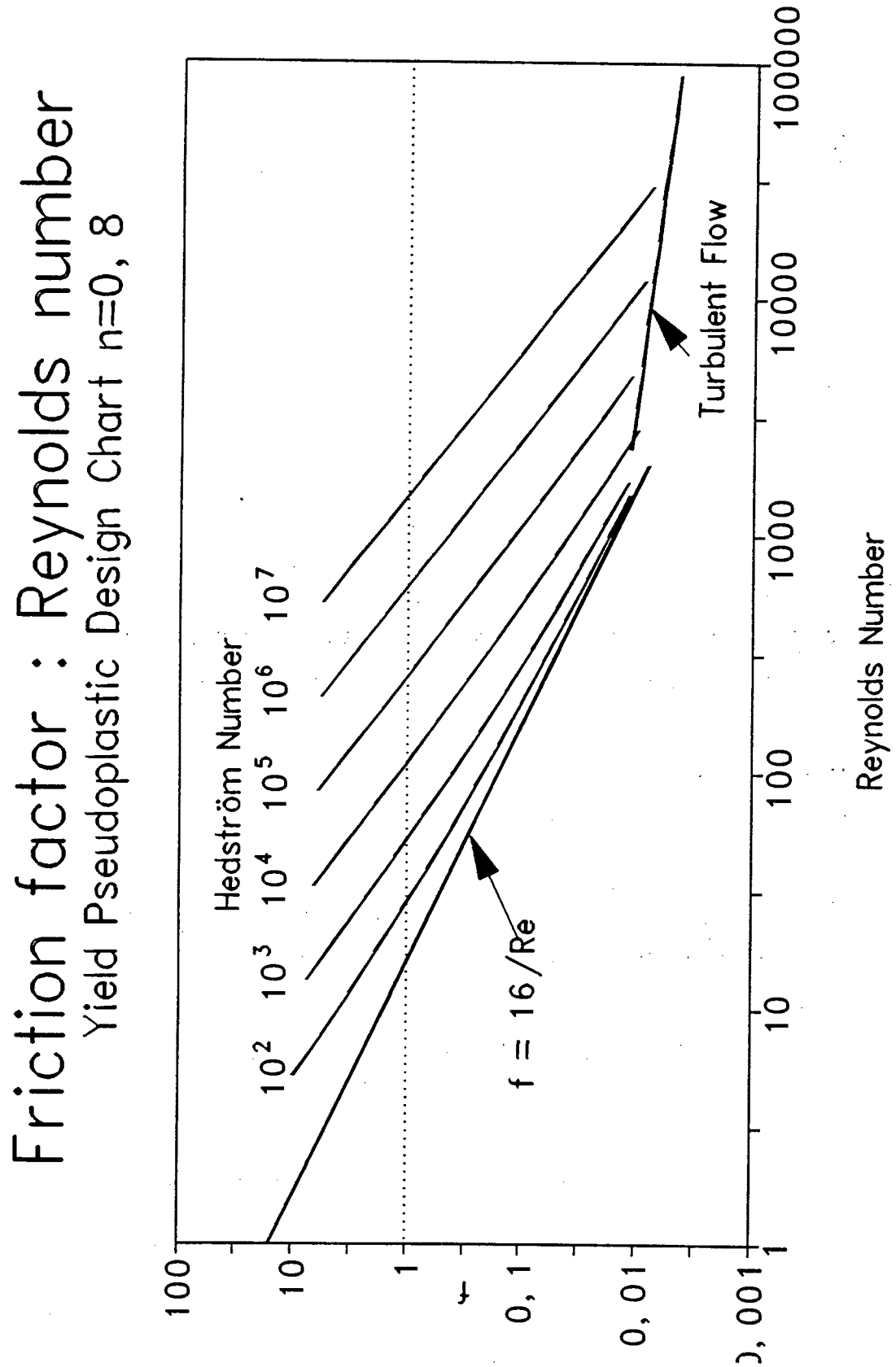

Figure B 1 : Yield Pseudoplastic Design Chart.

APPENDIX C

APPENDIX C

CASE STUDY

C.1 INTRODUCTION

The purpose of this case study is to introduce the original problem as it became evident to the Author.

The end goal was the design of a hydrotransport system to transport kaolin over a distance of several kilometers. The objective of this exercise was to predict the turbulent behaviour of kaolin slurry in a large diameter pipe (140mm). As the models of Torrance and Wilson & Thomas were to be used in the analysis, the rheology of the slurry was required.

Test work was performed in a large diameter pipe, to verify the analysis, and in the Balanced Beam Tube Viscometer (BBTV) so that the slurry rheology could be obtained.

C.2 METHODOLOGY

Slurry tests at seven concentrations were performed in the BBTV and the rheological characterisations performed. The rheological parameters were then correlated against the volumetric concentration, C_v, so that large scale pipe tests could be performed at any concentration in the range and a rheology would be available for the analysis.

Large scale pumped pipeline tests were then performed using the kaolin slurry in a 140mm diameter pipe.

C.3 EXPERIMENTAL TEST RESULTS AND ANALYSIS

Full test results are presented in Appendix A. The turbulent flow data was analysed using

the turbulent models of Torrance and Wilson & Thomas, as presented in Chapter 2 of the main text.

The large pipe tests and analyses are presented in Figures C 1 to 4.

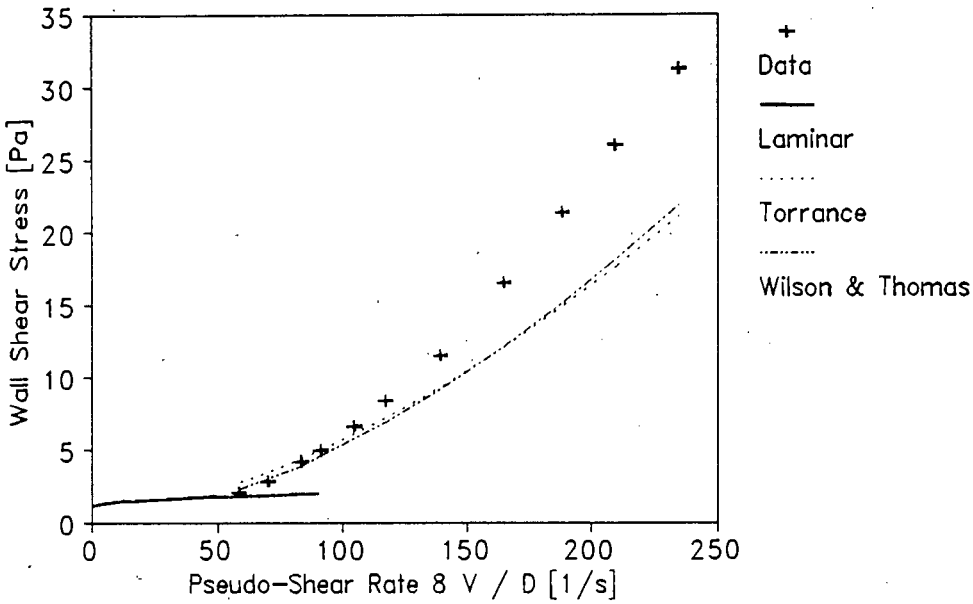

Figure C 1 : Test KERM1501 : S_m = 1,05 : D = 141mm : Kaolin.

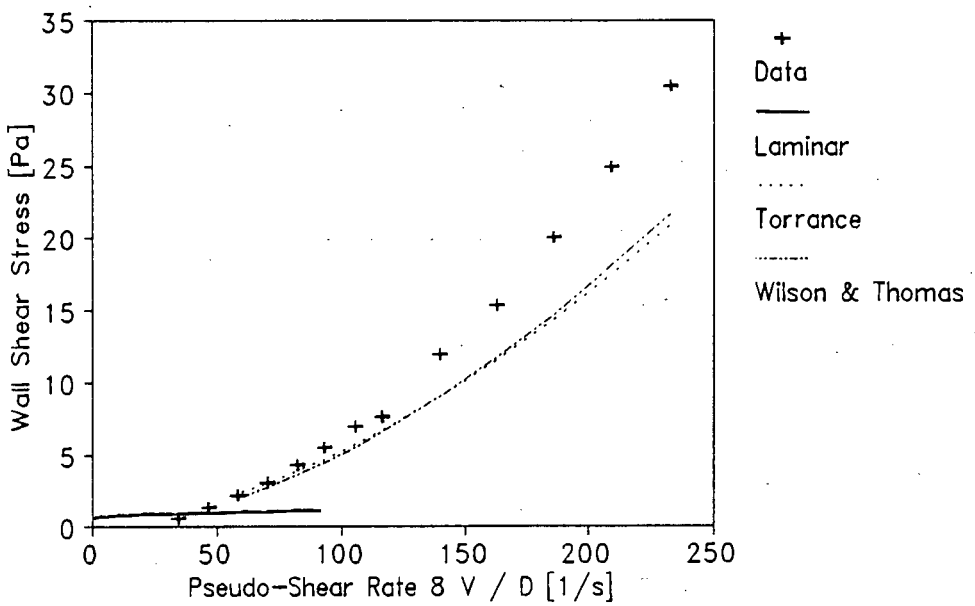

Figure C 2 : Test KERM1502 : S_m = 1,03 : D = 141mm : Kaolin.

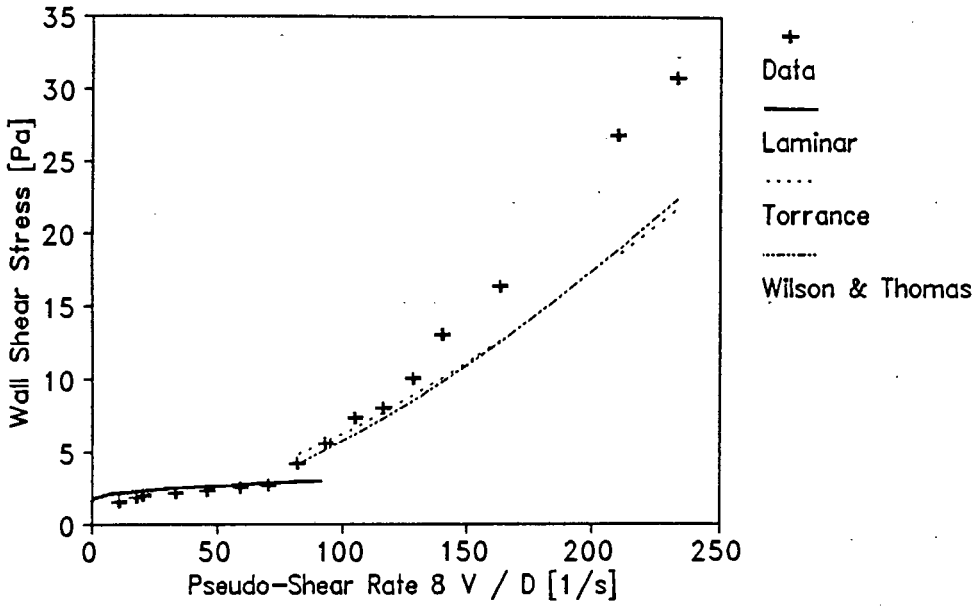

Figure C 3 : Test KERL1503 : S_m = 1,06 : D = 141mm : Kaolin.

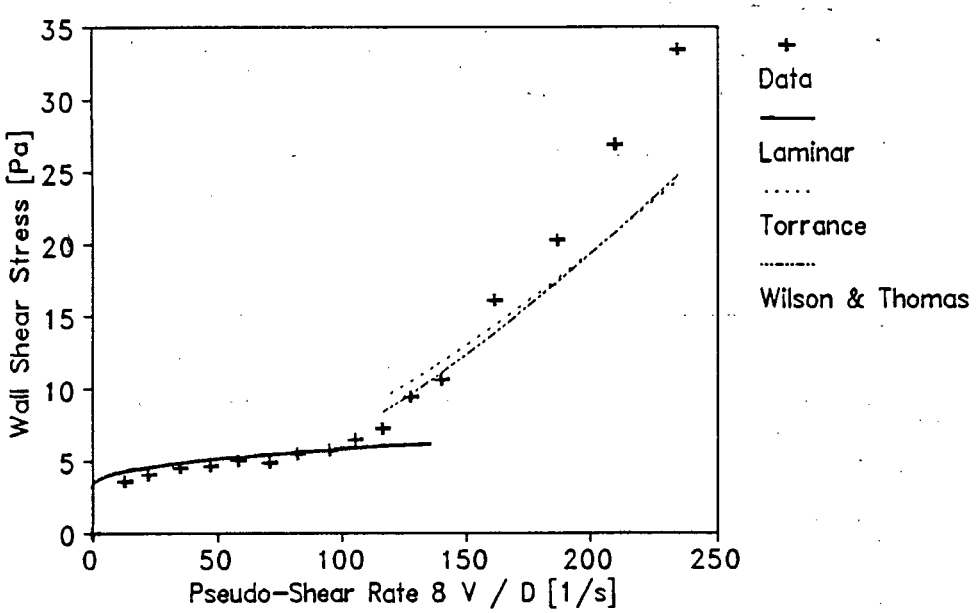

Figure C 4 : Test KERM1504 : S_m = 1,09 : D = 141mm : Kaolin.

C.4 CONCLUSIONS

These figures show that the errors in the turbulent flow analyses obtained in this way are unacceptable for design purposes.

APPENDIX D

APPENDIX D

RECOMMENDED DESIGN PROCEDURE - HEAD LOSS FOR STEADY FLOW OF NON-NEWTONIAN SLURRIES IN STRAIGHT CIRCULAR PIPES

D.1 INTRODUCTION

The recommended design procedure for determining the head loss for steady flow of non-Newtonian slurries in straight circular pipes, formulated in this thesis, is presented.

D.2 DETERMINATION OF SLURRY PROPERTIES

The relative density of the slurry and its particle size distribution are determined using the procedures described in Chapter 3. The d_{85} size is obtained from the particle size distribution.

Viscometer tests are performed on the slurry for the rheological characterisation. It is recommended that a tube viscometer be used. However, rotational viscometer test results may be used for preliminary design work. The rheological parameters τ_y, K and n are extracted using the approach of Lazarus & Slatter (1988).

D.3 INITIAL VALUES

The volumetric flow rate, Q, is usually determined from the dry solids mass flow rate

and the required slurry concentration. A trial pipe diameter, D, is also chosen.

D.4 REGIME DETERMINATION

The pipe Reynolds number Re_3 is calculated to determine whether the flow is laminar or turbulent.

Calculate the laminar flow wall shear stress, τ_0, using

$$\frac{32Q}{\pi D^3} = \frac{8V}{D} = \frac{4n}{K^{\frac{1}{n}} \tau_0^3} (\tau_0 - \tau_y)^{\frac{1+n}{n}} \left[\frac{(\tau_0-\tau_y)^2}{1+3n} + \frac{2\tau_y(\tau_0-\tau_y)}{1+2n} + \frac{\tau_y^2}{1+n} \right] , \qquad \textbf{(D.1)}$$

where $\tau_0 = D\Delta p/4L$ and $V=Q/A$.

The radius of the plug is

$$r_{plug} = \frac{\tau_y}{\tau_0} R , \qquad \textbf{(D.2)}$$

and the area of the annulus is

$$A_{ann} = \pi (R^2 - r_{ann}^2) . \qquad \textbf{(D.3)}$$

The sheared diameter, D_{shear}, is calculated using

$$D_{shear} = D - D_{plug} , \qquad \textbf{(D.4)}$$

where $D_{plug} = 2\, r_{plug}$. The corrected mean velocity in the annulus V_{ann} is then obtained from

$$V_{ann} = \frac{Q_{ann}}{A_{ann}} . \qquad \textbf{(D.5)}$$

Now calculate Re_3,

$$Re_3 = \frac{8 \rho V_{ann}^2}{\tau_y + K \left[\frac{8 V_{ann}}{D_{shear}} \right]^n} . \qquad \textbf{(D.6)}$$

If $Re_3 \leq 2100$, the flow is laminar, otherwise, the flow is turbulent.

D.5 LAMINAR FLOW HEAD LOSS

If the flow is laminar, the wall shear stress, τ_0, is determined using Equation (D.1) and the headloss is calculated from

$$\Delta H = \frac{4 L \tau_0}{D g \rho} . \qquad \textbf{(D.7)}$$

D.6 TURBULENT FLOW HEAD LOSS

The turbulent flow head loss depends on the roughness Reynolds number,

$$Re_r = \frac{8 \rho V_*^2}{\tau_y + K \left[\frac{8 V_*}{d_x} \right]^n} , \qquad \textbf{(D.8)}$$

where $V_* = \sqrt{(\tau_0/\rho)}$.

The representative roughness size, d_x, is taken as the greater of the 85th percentile passing particle size, d_{85} and pipeline hydraulic roughness, k.

If $Re_r \leq 3,32$ then the flow is smooth wall turbulent flow and the wall shear stress is calculated from

$$\frac{V}{V_*} = 2,5 \ln \left[\frac{R}{d_{85}}\right] + 2,5 \ln Re_r + 1,75 , \qquad \textbf{(D.9)}$$

If $Re_r > 3,32$ then the flow is fully developed rough turbulent flow and the wall shear stress is calculated from

$$\frac{V}{V_*} = 2,5 \ln \left[\frac{R}{d_{85}}\right] + 4,75 , \qquad \textbf{(D.10)}$$

or

$$\frac{1}{\sqrt{f}} = 4,07 \log \left[\frac{3,34\ D}{d_{85}}\right] , \qquad \textbf{(D.11)}$$

where $f = 2\tau_0/\rho V^2$.

The headloss is calculated using Equation (D.7).

It should be noted that the turbulent flow headloss calculation is implicit.

D.7 ITERATION AND OPTIMISATION

This process is repeated using different diameters, usually to suit a given pump curve or to optimize the cost of a pipeline system. The flow chart of the design procedure is shown in Figure D.1.

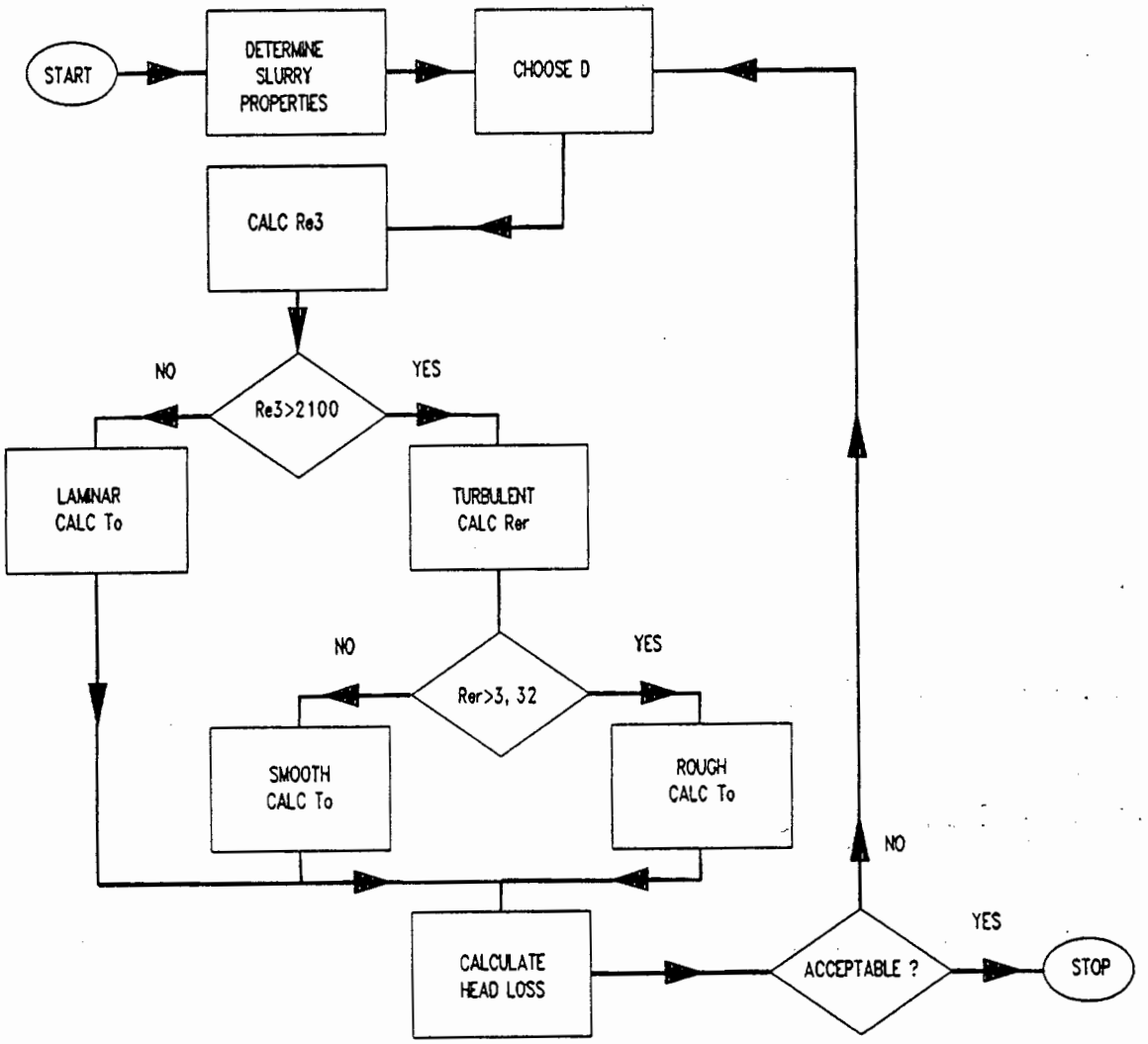

Figure D.1 : Flow Chart of the recommended design procedure.

D.8 NUMERICAL EXAMPLE

In this section the design procedure is illustrated using a numerical example. The values chosen are from the data point with the highest velocity in test KERM1501 shown in Appendix C.

D.8.1 Slurry Properties

Sm	τ_y [Pa]	K [Pa s^n]	n
1,049	1,070	0,04520	0,5890

The d_{85} particle size is determined from the particle size distribution graph as shown in Figure D.2.

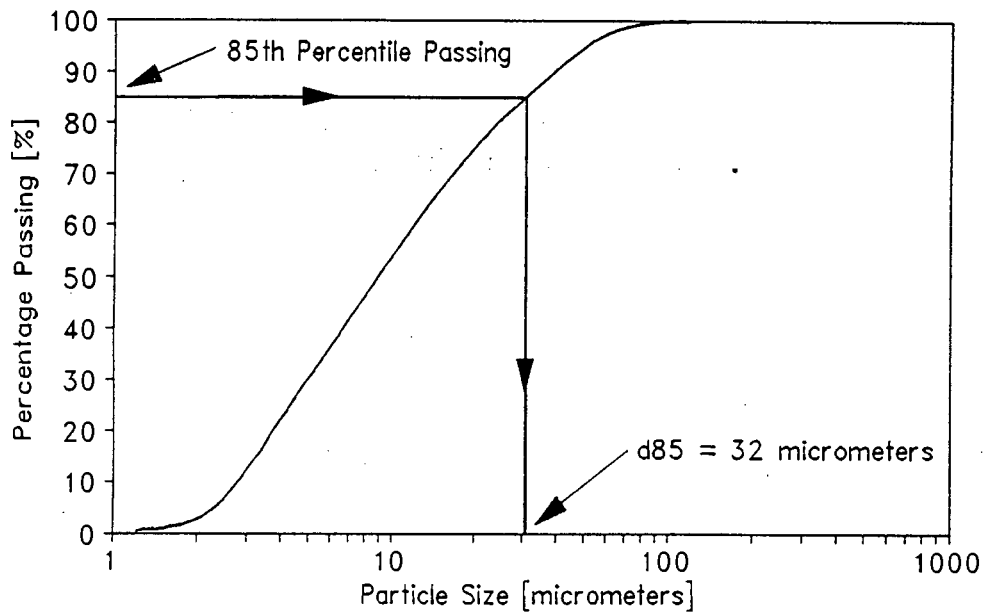

Figure D.2 : Particle size distribution for kaolin used in test KERM1501, showing the determination of the d_{85} size.

The d_{85} size for this slurry is 32 μm.

D.8.2 Pipeline Conditions

D = 0,1405 m

V = 4,122 m/s

D.8.3 Regime Determination

τ_o = 2,555 Pa

r_{plug} = 0,02942 m

A_{ann} = 0,01279 m^2

D_{shear} = 0,08167 m

V_{ann} = 3,789 m/s

Re_3 = 47350 > 2100, therefore the flow is turbulent.

D.8.4 Turbulent flow headloss

Re_r = 9,803 > 3,32, therefore the turbulent flow is rough.

τ_o = 30,98 Pa

The measured value was

$\tau_{o\ obs}$ = 31,26 Pa, giving an error of -1%.

D.9 GRAPHICAL PRESENTATION OF NEW MODEL

The above numerical example is shown in Figure D.3, together with the new model. The improvement obtained using the new model, compared to previous models, is shown clearly in this diagram.

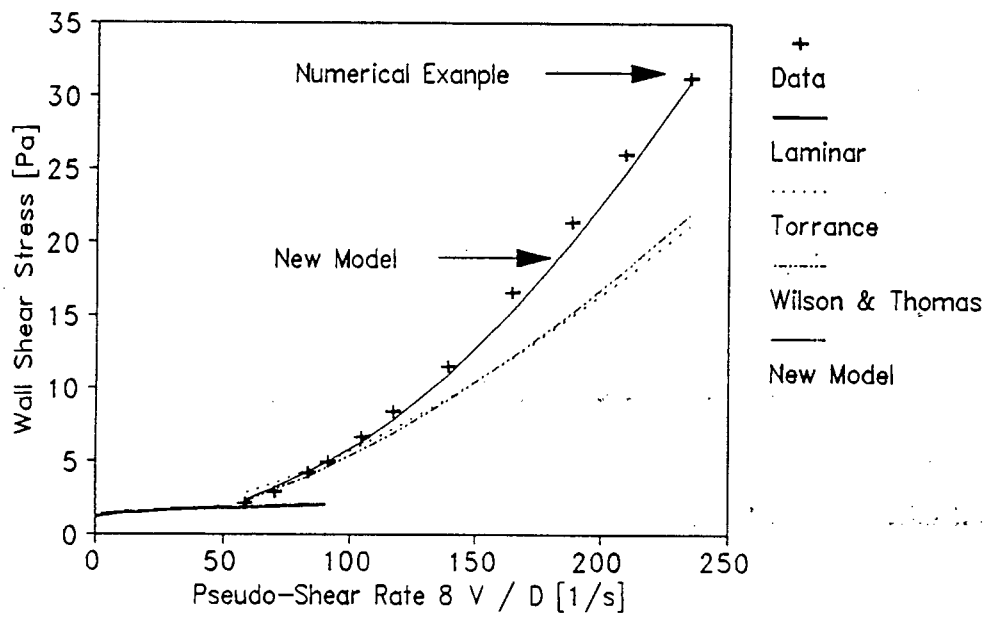

Figure D.3 : Graphical presentation of the new model showing the numerical example. Test KERM1501 : S_m = 1,05 : D = 141mm : Kaolin.